Synthesis and Characterization of Supramolecular Porphyrin and Porphyrazine Photonic Materials & Synthesis of a Covalent Base Pair of DNA

by

Kai Fan Cheng

A dissertation submitted to the Graduate Faculty in Chemistry in partial fulfillment of the requirements for the degree of Doctor of Philosophy, The City University of New York

2004

This manuscript has been read and accepted for the Graduate Faculty in Chemistry in satisfaction of the dissertation requirement for the degree of Doctor of Philosophy.

JUNE 21, 2004
Date

Prof. Charles Michael Drain
Chair of Examining Committee

JUNE 21, 2004
Date

Prof. Klaus Grohmann
Chair of Examining Committee

6/22/2004
Date

Prof. Gerald Koeppl
Executive Officer

Prof. Charles Michael Drain

Prof. Klaus Grohmann

Prof. Richard Franck

Prof. Maria C. Tamargo

Supervisory Committee

THE CITY UNIVERSITY OF NEW YORK

Abstract

Synthesis and Characterization of Supramolecular Porphyrin and Porphyrazine Photonic Materials & Synthesis of a Covalent Base Pair of DNA

by

Kai Fan Cheng

Advisors: Prof. Charles Michael Drain & Prof. Klaus Grohmann

Part A: Porphyrins Linked Directly to the 4,4' or 5,5' Positions of 2,2'- Bipyridine: A New Supramolecular Building Block and Switch

The synthesis and coordination chemistry of two porphyrin dimers linked either at the 5,5' or the 4,4' positions of 2,2' bipyridine is described. These compounds, which may serve as a molecular tectons for the constructions of a variety of supramolecular arrays of diverse function, reveal that the ground- and excited- state electronic communication between the chromophores is only moderately affected by the complexation state of the bipyridyl moiety. The nature of the metal ion chelated by the bipyridine only slightly perturbs the ground state spectra and differences observed in the excited state are largely ascribed to the heavy atom effect. This investigation also shows that conformational changes in structural subunits, in this case, induced by bipyridyl complexation of various metal ions, do not necessarily require reorganization supramolecular systems.

Part B: Hierarchical Self-assembly of Photonic Materials: Synthesis and Characterization of Porphyrazine-Porphyrazine Dimers and Porphyrazine-Porphyrin Tetramers

The 2,3-bis(dimethylamino or diamino)-7,8,12,13,17,18-hexakis(4-(tert-butyl)phenyl) porphyrazine has been prepared via mixed Linstead macrocyclization in good yield. The synthesis and coordination chemistry of the porphyrazine dimers via square planar metal ion linkers are described. The structures of the dimers were characterized by ^{1}H NMR, Electrospray and MALDI mass spectrometry. The photophysical profiles of the dimers were evaluated by means of absorption and emission spectroscopy. This investigation also shows that the supramolecular tetramers consisting of two different chromophores (porphyrazine and porphyrin) can be self-assembled in solution by coordinating the appropriate transition metal ions bearing multitopic ligands. These molecules will serve as part of a library of building blocks for the self-assembly of nanoscale photonic materials.

Part C: Synthesis and Characterization of a Covalent Base Pair of DNA

The molecular modeling techniques let Leslie E. Orgel and coworkers propose the design and synthesis of a covalent base with the hydrazone bond linker between two aromatic systems. They claimed the geometry of the covalent base pair is very close to that for the DNA double helix and suggested a double helix containing this covalent base pair should be stable. However, the synthesis of these analogues and starting materials is only heuristically outlined. These compounds are of general interest to research in the field of nucleic acid structure and the mechanisms of nucleic acid unwinding. We report a detailed synthesis of a similar analogue of the covalent base pair and expect similar biochemical properties to those reported by Orgel et al., which will be investigated by a cooperative biochemistry group.

Acknowledgments

I would like to take this opportunity to thank my mentors Prof. Klaus Grohmann and Prof. Charles Michael Drain for their helpful advise and kind guidance in my past five years doctoral studies. It is almost a decade in Hunter College since my first day enrolling in the undergraduate program. Chemistry department on the 13th floor of the north building already becomes my second family. I am very proud of the close relationships among the faculty and students in the family. Thank you to all members in the department for your kind help, encouragement, support and sharing.

I would also like to thank my committee members Prof. Richard Franck and Prof. Maria Tamargo. Without your participation, I would not finish my doctoral studies and get my thesis done on time. Also, I thank to Dr. Clifford Soll for his help with ESI-MS; Dr. Michael Blumenstein for his help with NMR and Miss Ngee Ai Thai for her valuable assistance in preparation of porphyrazine building blocks.

Finally, I deeply thank to my parents for their kind encouragement and unlimited support. Also, I thank to my lovely wife, Yin Ling Leung, and daughter, Christine Cheng, for their support, encouragement and considerateness. Thank you very much!!!

感謝父母對我的

無限關懷

及

無量支持

謝謝您們 !!!

Table of Contents

List of Figures

Part A

Part B

Appendix

List of Schemes

Part A

Part B

Part C

Abbreviations

NMR	Nuclear Magnetic Resonance
ESI-MS	Electrospray Ionization Mass Spectroscopy
MALDI	Matrix – Assisted Laser Desorption Ionization
M	Metal
OA_c	Acetate
TFA	Trifluroacetic Acid
TPP	5,10,15,20-Tetraphenylporphyrin
THF	Tetrahydrofuran
DDQ	2,3-Dichloro-5,6-dicyano-1,4-benzoquinone
Py	Porphyrin
Pz	Porphyrazine
Bpy	Bipyridine
BiPy	Biporphyrin

Part A:

Porphyrins Linked Directly to the 4,4' or 5,5' Positions of 2,2'- Bipyridine:

A New Supramolecular Building Block and Switch

A1.

Introduction

1.1. What are the porphyrins?

The word *porphyrin* comes from the ancient Greek word *porphura* meaning purple color, which immediately shows the most important physical property of porphyrins: their intense purple color.[1] From the chemistry point of view, porphyrins are an aromatic macrocycle, which are built up from four pyrrole subunits and four bridging carbons. The macrocycles contain a total of 22 conjugated π-electrons, 18 of which are incorporated into the delocalization pathway in accord with Hückel's [4n+2] rule for aromaticity (n=4).[2] The 18 π-electrons delocalization pathway (shown in bold in scheme 1.1.1.) can be discerned, and for this reason porphyrins are often considered to be the bridged [18] annulenes.[3] A recent theoretical study has shown that the aromatic properties of porphyrins are best described as 22 π-electrons delocalized system that utilize two of the nitrogen electron pairs (scheme 1.1.2.).[4]

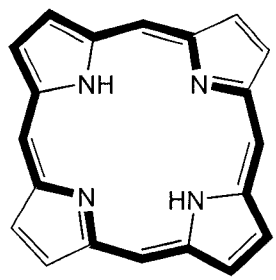

Porphyrin
4 pyrroles
4 bridging carbons

Scheme 1.1.1. The 18 π-electrons delocalization pathway of porphyrin.

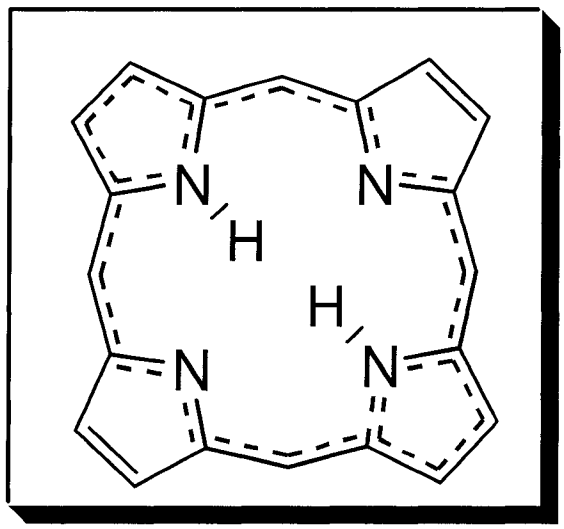

Scheme 1.1.2. The 22 π-electrons delocalization model of porphyrin involving 9 double bonds and 2 nitrogen electron pairs.

Free base porphyrins in solution consist of two rapidly interconverting tautomers **1a** and **1b**, together with minor contributions from less favored *cis* tautomers such as **1c** (scheme

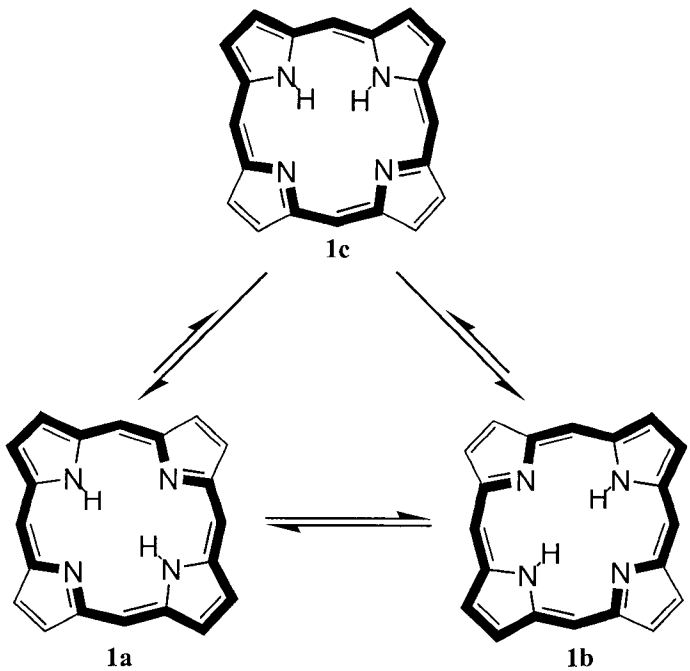

Scheme 1.1.3. The preferred pathway for the delocalization of the 18 π-electrons in free base porphyrins: 3 possible tautomers.[65]

1.1.3.). The mechanism of N-H migration between porphyrin *trans* tautomers is believed to proceed in a stepwise manner, via the less favored *cis* tautomers. The preferred pathway for the delocalization of the 18 π-electrons in free base porphyrins is believed to be as shown in scheme 1.1.3., and for metalloporphyrins and porphyrin dications as shown in scheme 1.1.4. Porphyrins can efficiently harvest light due to their strong absorption bands. They also have very characteristic electronic absorption spectra dominated by a B band (or 'Soret' band, after its discoverer) near 400 nm, followed by between two and four much weaker bands, called Q bands, situated between 480-700 nm. The proton NMR spectra for porphyrins are particularly diagnostic showing powerful diamagnetic ring currents with internal NH's shifted upfield to about –4 ppm while the externals *meso*-protons are generally downfield near +10 ppm.

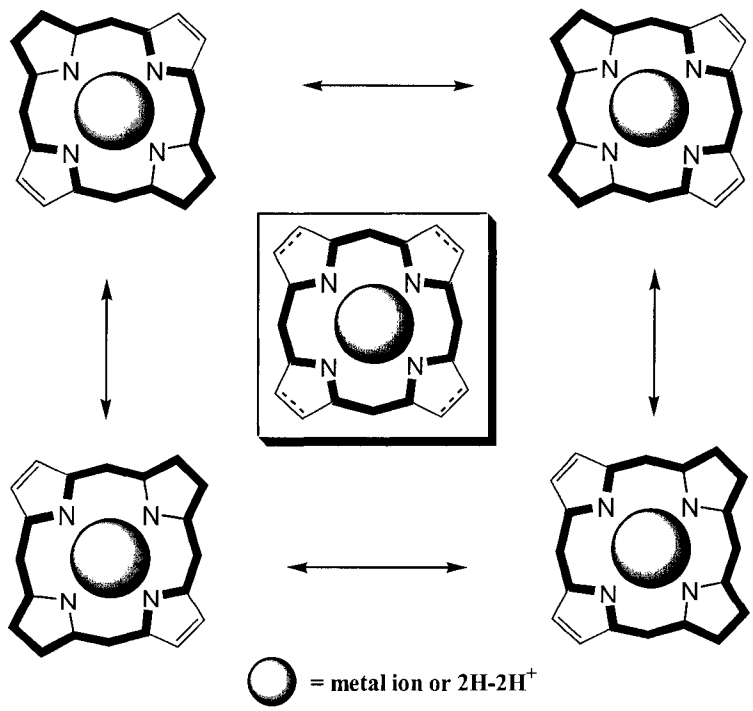

Scheme 1.1.4. The preferred pathway for the delocalization of the 18 π-electrons in metalloporphyrins and porphyrin dications.[65]

1.2. Nomenclature of the porphyrins

Since porphyrins are built up from four pyrrole subunits and four bridging carbons, in general, we refer the bridging carbons as *meso*-position while the carbon 2 of the pyrrole as α-position and the carbon 3 of the pyrrole as β-position (scheme 1.2.1.). It

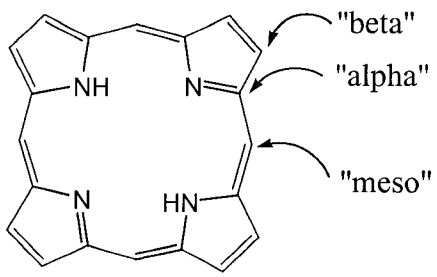

H_2Py

Scheme 1.2.1. Basic porphyrin structure.

was Hans Fischer who thought up the first system of nomenclature for porphyrin.[5] In his numbering system, the β-carbon was given a number 1 to 8; the α-carbon remained unnumbered and the *meso*-carbons were given a Greek lower case letter, α–δ (scheme 1.2.2.).

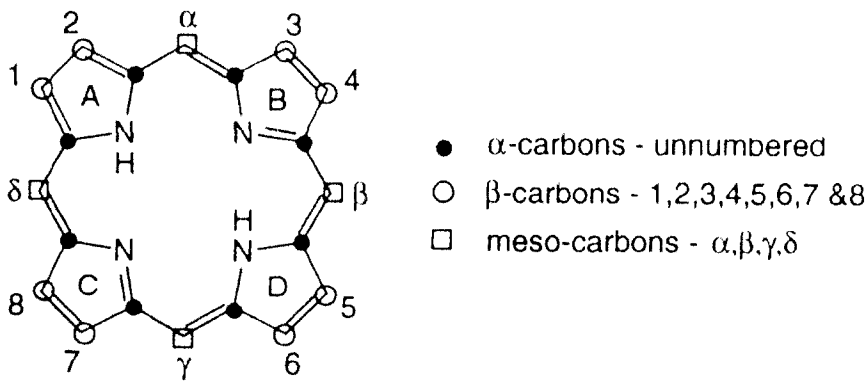

Scheme 1.2.2. Fischer's numbering system.[65]

The Fischer system is straightforward for naming simple porphyrins, but as the complexity of porphyrin derivatives increase, with different substituents on *β*- and/or *meso*- positions, the system becomes unwieldy and even contradictory. In 1979, a new and more systematic IUPAC nomenclature was introduced and finalized in 1987. The

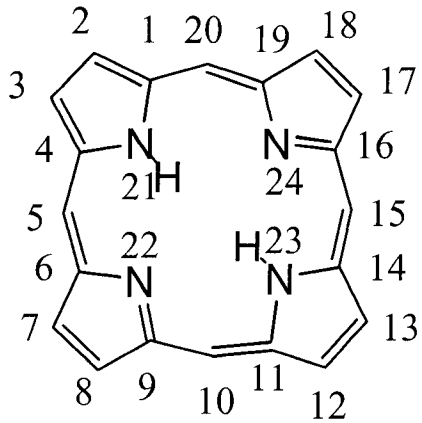

Scheme 1.2.3. IUPAC systematic nomenclature on macrocycle.[65]

IUPAC nomenclature numbered all atoms including the nitrogen atoms in the macrocycle (scheme 1.2.3.). The parent macrocycle is called *porphyrin* and the numbering of a substituted porphyrin depends on where on the macrocycle the principle groups are present.[6]

1.3. Landmarks in porphyrin synthesis

Although the macrocyclic structure of porphyrin was first proposed by Küster in 1912, nobody believed him at that time because such a large ring was though to be intrinsically unstable.[67] Until many years later, in 1929, Hans Fischer eventually came round to this structure and finally succeeded in synthesizing heme (the iron porphyrin in

hemoproteins) from pyrrolic starting materials.[7] Ten years later, in 1939, Ruthemund first reported the synthesis of the well-known TPP (5,10,15,20-tetraphenylporphyrin) in ~5% yield by mixing benzaldehyde and pyrrole in a sealed-tube in pyridine which was then heated at 150-200 °C for two days.[8] Alder improved the Ruthemund method in 1964 with the refluxing of aldehyde and pyrrole in propionic acid or acetic acid in open air. The yield ranged from 10% to 30%.[9, 47] In 1987, with the introduction of the Lindsey method[10], which had a broad impact on modern porphyrin synthesis. The Lindsey method is based on the MacDonald approach,[66] and allows for the synthesis of porphyrins bearing different sensitive functional groups among the *meso*-positions in yields ranging from 10% to 60%. Recently, Lash[11] and others[12] have revived the "3+1" approach and have demonstrated that this can be a superior methodology for porphyrin synthesis. Also, a new solvent free porphyrin synthesis method had been investigated in Drain's group[13] with yields 5-30%. These landmarks in porphyrin synthesis are shown in figure 1.3.1.

1912	Küster first proposed the macrocyclic structure of porphyrin[67]
1929	Hans Fischer first synthesized the iron porphyrin in hemoproteins[7]
1939	Ruthemund first synthesized the TPP in 5% yield[8]
1960	MacDonald method, 10-20% yield[66]
1964	Alder-Longo method, 10-30% yield[9,47]
1987	Lindsey method, 10-60% yield[10]
1995	"3+1" approach, 30-80% yield[11,12]
1996	Solvent free porphyrin synthesis method, 5-30% yield[13]

Figure 1.3.1. General landmarks in porphyrin synthesis.

1.4. Objectives of Our Research

With the rapidly developing field of molecular based materials, the preparation of supramolecular organic photonic devices is an important research area in view of both fundamental science and applications development.[14] The practical applications of supramolecular photonics[15] include solar energy conversion into electrical or chemical energy[16-20] and as components of nanoscaled devices.[14,21-23] Porphyrins are appealing subunits for materials[11-15] because they can efficiently harvest light due to their strong absorption bands, they are remarkably robust considering their rich photochemical and redox properties, and the variety of means to fine-tune these properties via peripheral substituent modifications or metal complexation. Since their discovery at the end of nineteenth century, bipyridines such as 2,2'-bipyridine (BiPy) and their coordination chemistry has been well studied for many of the same reasons.[15,29] The combination of porphyrins and BiPy techtons[30-33] continues to develop in the arena of molecular-scale information processing systems, such as in highly conjugated porphyrin-based assemblies.[34-36] Terpyridyl and similar ligands appended to porphyrins are of continuing interest in the formation of catenanes and other topologically complex structures, and there are a variety of other approaches to self-assembled porphyrin systems.[24,34-36] Certainly, one of the most exploited methods to assemble porphyrin arrays, layers, and crystals is to use pyridyl porphyrins and transition metals. The 60°, 120°, and 180° direction of the respective 2-, 3-, and 4- pyridyl nitrogens, combined with the various coordination geometries of transition metals, and the axial positions of metalo derivatives, can result in a very large number of porphyrinic materials – both discrete and polymeric.[24,36,37] Therefore, one of the central issues in supramolecular porphyrin

chemistry is the role of the pyridyl-metal-pyridyl linker in mediating electron and energy transfer among the chromophores.[38]

To develop new building blocks that also address the role of the linker in the photo physics of supramolecular porphyrin arrays, herein we report the synthesis, characterization, and functionality of 5,5'-bis-[5'-(10,15,20-tri-4-tert-butlyphenyl)porphyrinyl]-2,2'-bipyridine, **1,** wherein the porphyrins are appended 180^0 from each other in any conformation of the BiPy (scheme 1.4.1.). In this system the covalent bond between the 2 and 2' positions is conjugated to the 5,5' positions where the porphyrins are attached and the pyridyl nitrogens are not conjugated to the 5 positions. The spectral properties of this supramolecular techton are compared to 4,4'-bis[5'-(10,15,20-tri-4-tert-butylphenyl)porphyrinyl]-2,2'-bipyridine, **2**, wherein the relative angle between the porphyrin planes changes with the conformation of the BiPy moiety (scheme 1.4.1.).

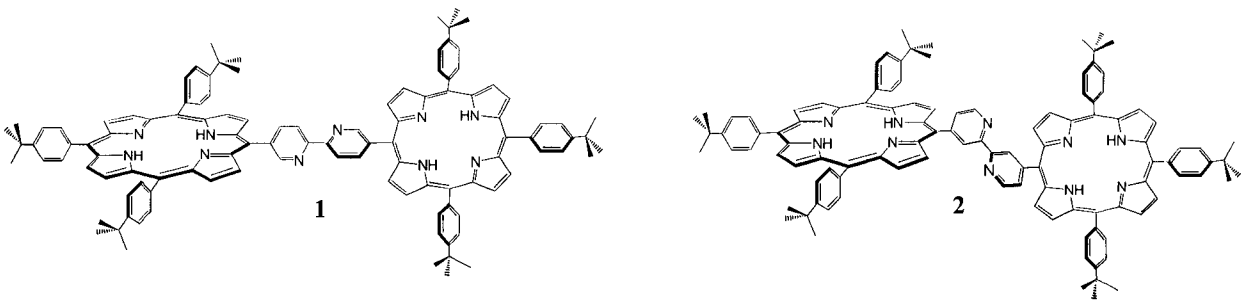

Scheme 1.4.1. Structure of 5,5'-bis-[5'-(10,15,20-tri-4-tert-butlyphenyl)porphyrinyl]-2,2'-bipyridine, **1** and 4,4'-bis[5'-(10,15,20-tri-4-tert-butylphenyl)porphyrinyl]-2,2'-bipyridine, **2**.

A meso alkyl derivative of **2** was reported earlier.[39] In contrast, the covalent bond in this latter system is not conjugated to the 4,4' position bearing the porphyrins, but the pyridyl nitrogens are. As in all meso aromatic porphyrin compounds, the dihedral angle between the porphyrin macrocycle and the meso pyridyl substituent is on average 90° and can vary between $\pm$ ~60° in solution. The orthogonality of the porphyrins to the pyridines minimizes conjugation; nevertheless, it is well known that the wavelength of the Q and B bands in the ground state electronic spectra of meso 4-pyridyl porphyrins are shifted by several nm upon pyridyl coordination to a variety of metal ions.[40,41] Also, metalation of the porphyrin significantly alters the basicity of the para pyridyl nitrogen. These are clear indications that there is significant electronic communication between the macrocycle and the pyridyl subunits.

The BiPy moiety is normally not planar, but adopts a planar conformation upon metal ion binding. The planar structure electronically couples, via conjugation, the two aromatic pyridine systems with the atomic orbitals of the metal contributing to varying degrees toward the overall molecular orbitals of the complex. As such, the complexation of a metal ion by the BiPy moiety results in increased electronic coupling between the two 5,5' attached chromophores because the BiPy becomes planar. Thus the bipyridyl moiety serves as a metal-gated switch to electronically couple the porphyrins (scheme 1.4.2.).

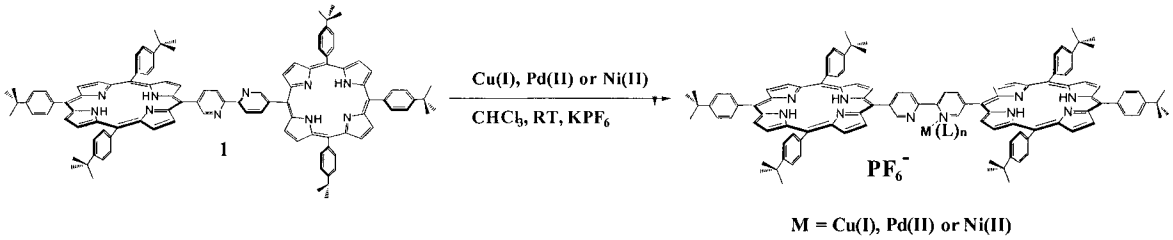

Scheme 1.4.2. BiPy moiety of compound **1** adopts a planar conformation upon metal ion binding.

When the BiPy unit of compound **2** binds a metal, the two porphyrins rotate from an average *anti*-like conformation to lock into a *syn*-like conformation so that they are on the same side of the BiPy and can serve as receptor to ditopic ligands of appropriate size and orientation (scheme 1.4.3.).

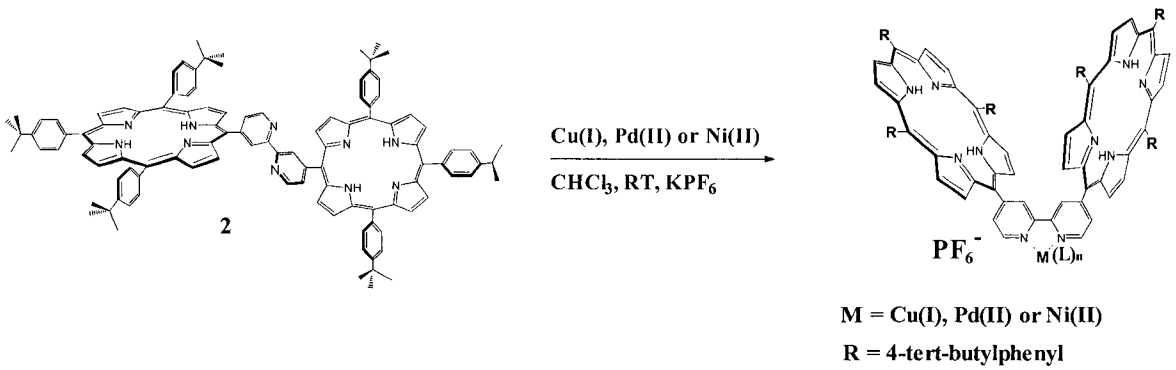

Scheme 1.4.3. Two porphyrins rotate from an average *anti*-like conformation to lock into a *syn*-like conformation when the BiPy unit of compound **2** binds a metal.

For **2** electronic communication is mediated also by the adoption of a planar structure by the BiPy, but the nitrogens in the chelate are conjugated to the point of attachment of the macrocycles.

The primary goals of the present work are to (1) compare the ground- and excited state spectra of these two structural isomers when the bipyridyl linker is coordinated to

various metal ions in order to gain insights into the role of this motif in the photophysical properties of supramolecular porphyrin arrays assembled by exocyclic coordination to metal ions, and (2) to design and characterize a new techton for the self-assembly of porphyrinic materials. To this end we have examined the electronic absorption and emission spectra of **1**, its zinc metalloporphyrin derivative, $\mathbf{Zn_2 1}$, and compared these results to those of **2**, and $\mathbf{Zn_2 2}$.

In most supramolecular systems, a conformational change in one of the structural elements results in a substantial change in the structure of the supermolecule[42-44] or even disassembly, as well demonstrated by techton **2** and its derivatives. Whereas in compound **1** the conformational changes resulting upon binding of a metal ion by the BiPy moiety leaves the structure of a supramolecular assembly intact. This latter feature is demonstrated by the observation that the structural integrity of a supramolecular square composed of two $\mathbf{Zn_2 1}$, and two 1,2,diazabicyclo[2,2,2]octane (DABCO) units (scheme 1.4.4.) remains intact even though the 2,2'-bipyridine moieties change conformation upon binding transition metals.

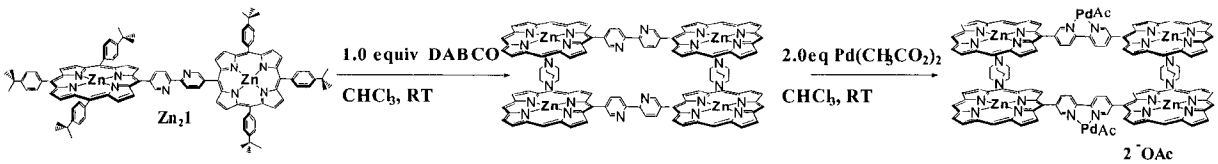

Scheme 1.4.4. The structural integrity of a supramolecular square composed of two $\mathbf{Zn_2 1}$, and two 1,2,diazabicyclo[2,2,2]octane (DABCO) units remains in tact even though the 2,2'-bipyridine moieties change conformation upon binding transition metals.

A2.

Results & Discussion

2.1. Synthesis

Compounds **1** and **2** were synthesized by mixed aldehyde condensations based on a modified Adler synthesis[9,47] in ~3% yield (scheme 2.1.1.) using the respective 2,2'-bipyridine-5,5'-dicarboxaldehyde and 2,2'-bipyridine-4,4'-dicarboxaldehyde.

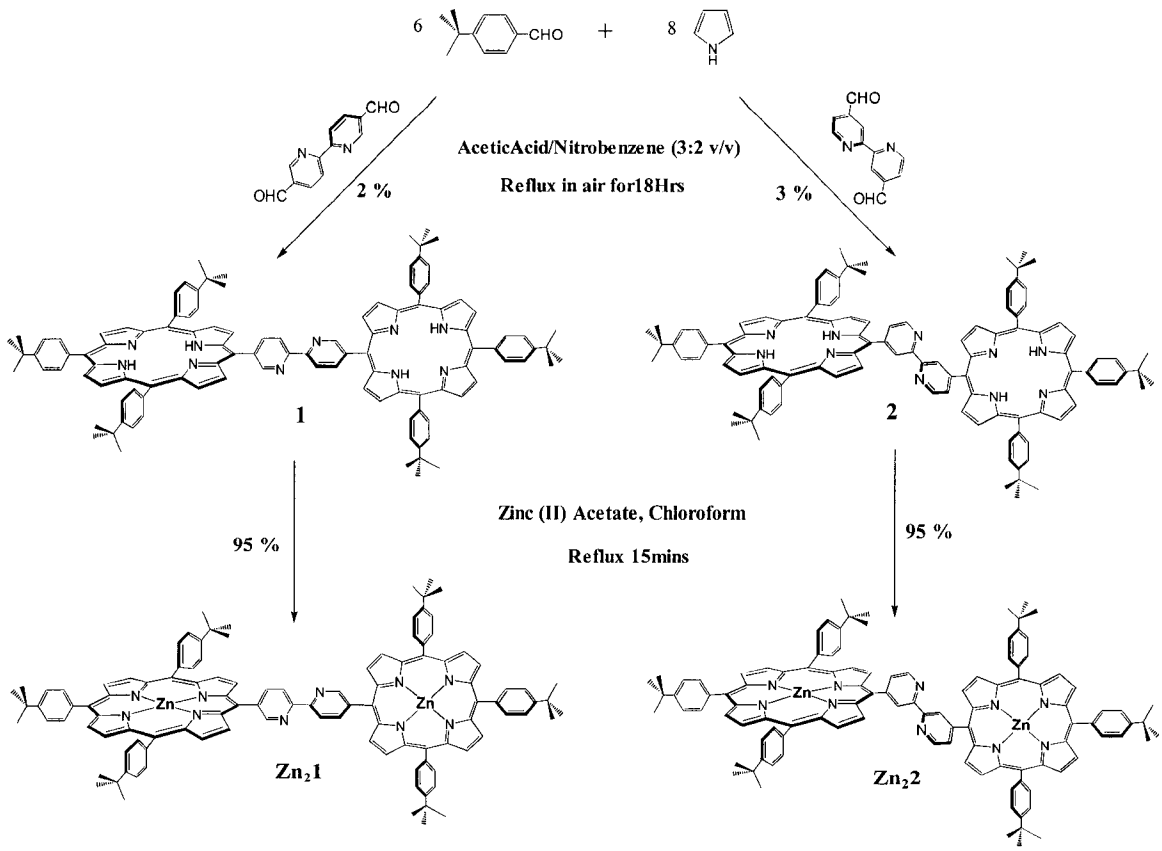

Scheme 2.1.1. Synthesis of compounds **1** and **2** via mixed aldehyde condensations based on a modified Adler method.

The directed synthesis of each using a MacDonald-type 2+2 coupling strategy of **3** and **4** (scheme 2.1.2.) was unsuccessful using a variety of reaction conditions with either the 4-*tert*-butlybenzaldehyde or the mesityl aldehyde.[48-52] While the precursors and their intermediates for both **1** and **2** were readily synthesized and characterized according to literature methods, these reaction sequences failed in the porphyinogen/porphyrin forming step as was observed earlier for a compound similar to **2** (scheme 2.1.3.).[39]

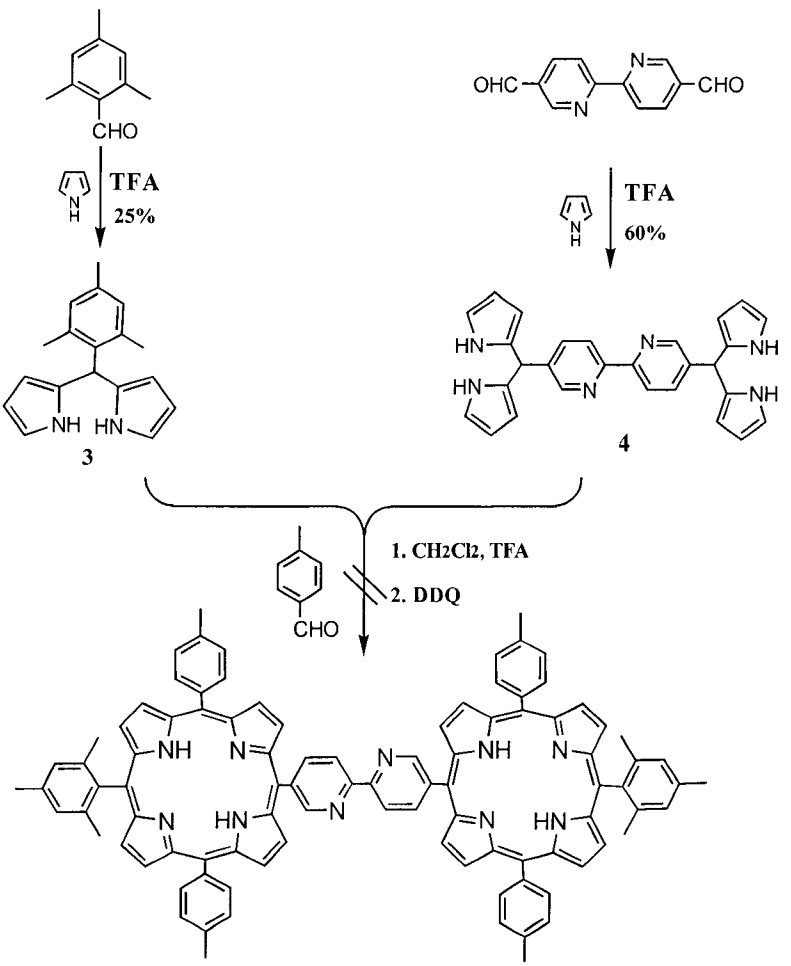

Scheme 2.1.2. Unsuccessful directed synthesis using a MacDonald-type 2+2 coupling strategy.

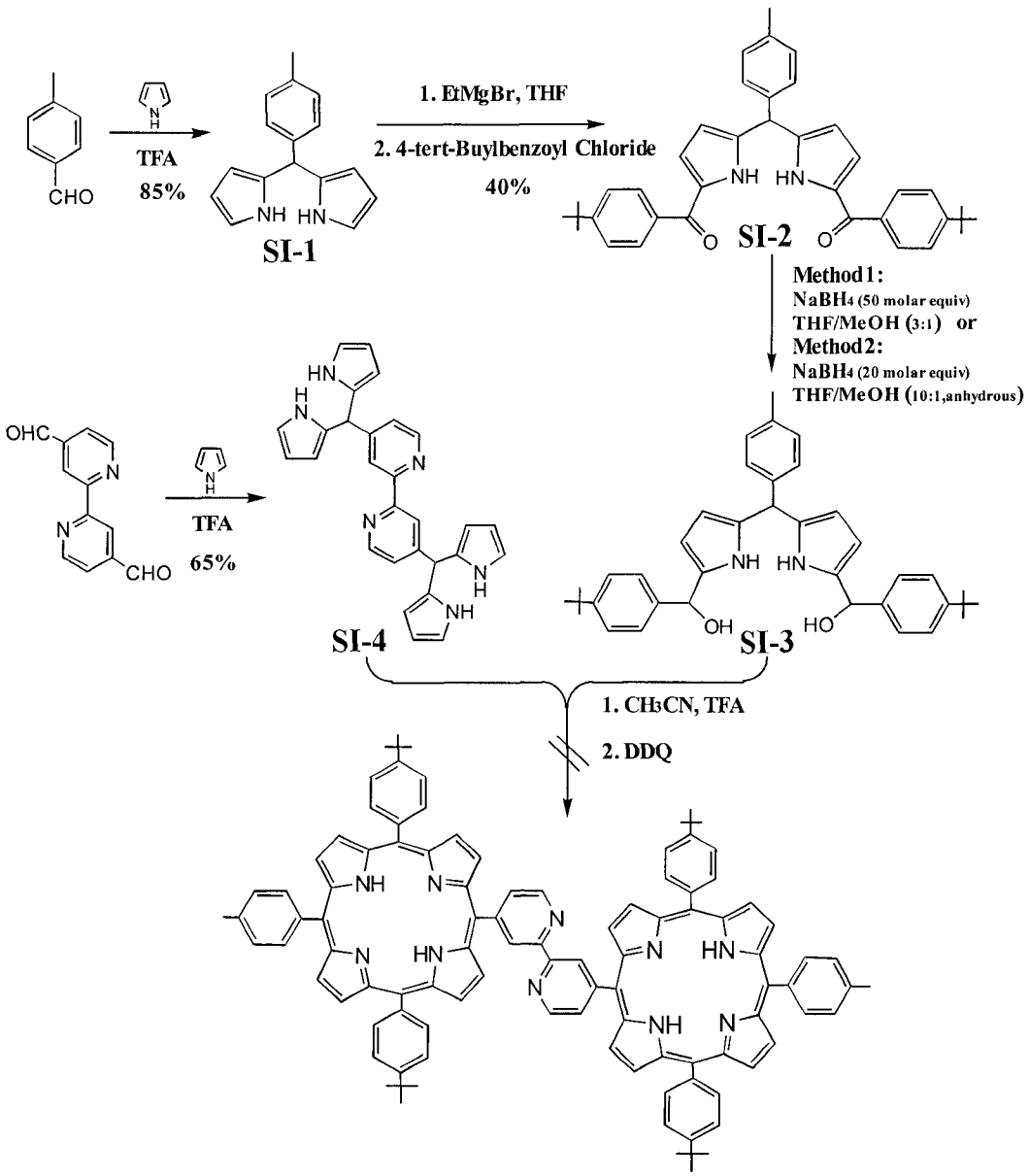

Scheme 2.1.3. Another unsuccessful directed synthesis of a compound similar to **2.**

The mesityl aldehydes are reported to minimize scrambling and increase the solubility (i.e. reactivity) of the intermediates, yet the synthesis of these derivatives also fails at the crucial porphyrin-forming step. The previous synthesis of a meso alkyl version of **2** involved the directed synthesis of a monopyridylporphyrin followed by a coupling reaction to form the pyridyl moiety.[39] Though more elegant from a synthetic point of view, this method for **2** is both more time consuming and the overall yield from the starting aldehydes is comparable (scheme 2.1.4.).

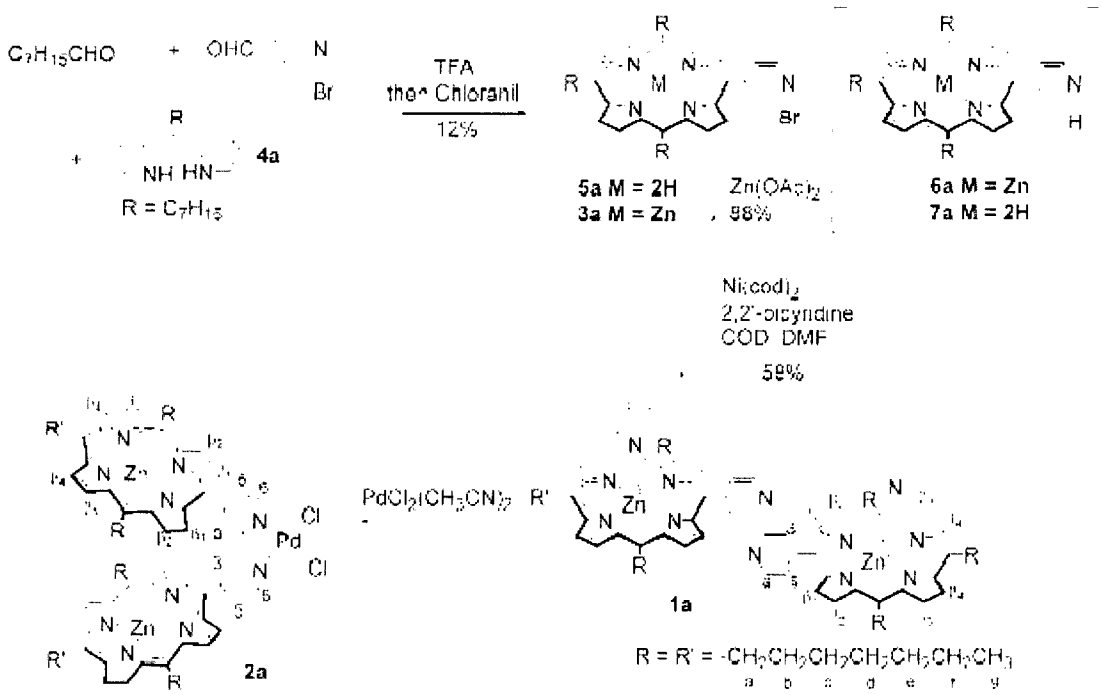

Scheme 2.1.4. The previous synthesis of a meso alkyl version of **2** involved the directed synthesis of a monopyridylporphyrin followed by a coupling reaction to form the pyridyl moiety.[39]

As noted with similar synthetic procedures that use the Adler method to make porphyrins bearing both heterocyclic and phenyl moieties, allowing the less reactive heterocyclic

aldehyde to react with the pyrroles for ~15 minutes before addition of the arylaldehyde significantly increases the yield of the porphyrins bearing the heterocyclic groups.[53,54] The yield from the Adler-based synthesis is somewhat less than the expected ~4% estimated from the statistical reaction of the aldehydes based on stoichiometry, and a 25% yield for each porphyrin. However, this is greatly ameliorated by the ease of scale-up of the one-step synthesis. We obtain only traces of porphyrin using the 5-step reaction sequence outlined in scheme 2.1.3 which would have an overall yield of ~2% had the two porphyrin-forming reaction occurred with 25% yields each.

2.2. Electronic Spectra

The two halves of free 2,2'-bipyridine are not coplanar, and the nitrogens generally point away from each other; therefore, there is little conjugation between the two pyridyl rings. Meso aryl groups on porphyrins are also non coplanar with the macrocycle but substitutions on the aryl ring are readily observed in the electronic spectra – indicating some degree of electronic coupling between the two. Therefore, we expected and observed, that the two free-base porphyrins of both compounds **1** and **2** linked by the free-base 2,2'-bipyridine are reasonably electronically isolated. There is a ~5 nm red shift and ~50% increase in FWHM of the Soret band of **1**, and for **2** the broadening is only ~25%, both vs. a monopyridylporphyrin analogue. These are somewhat greater than most simple substituent effects for porphyrinic systems (figure 2.2.1 & 2.2.2). The UV-visible spectrum indicates compound **1** has an increased proclivity to aggregate compared to **2**. Upon metal ion coordination the two pyridines of 2,2'-bipyridine become coplanar and the degree of conjugation between the halves

increases. The combination of the BiPy and the metal orbitals results in a system that allows greater electronic communication between the porphyrin chromophores. In **1** the 5 and 5' positions are conjugated to the covalent bond and not with the pyridyl nitrogens. Conversely for **2**, the nitrogens are conjugated to the point of attachment and the covalent bond is not.

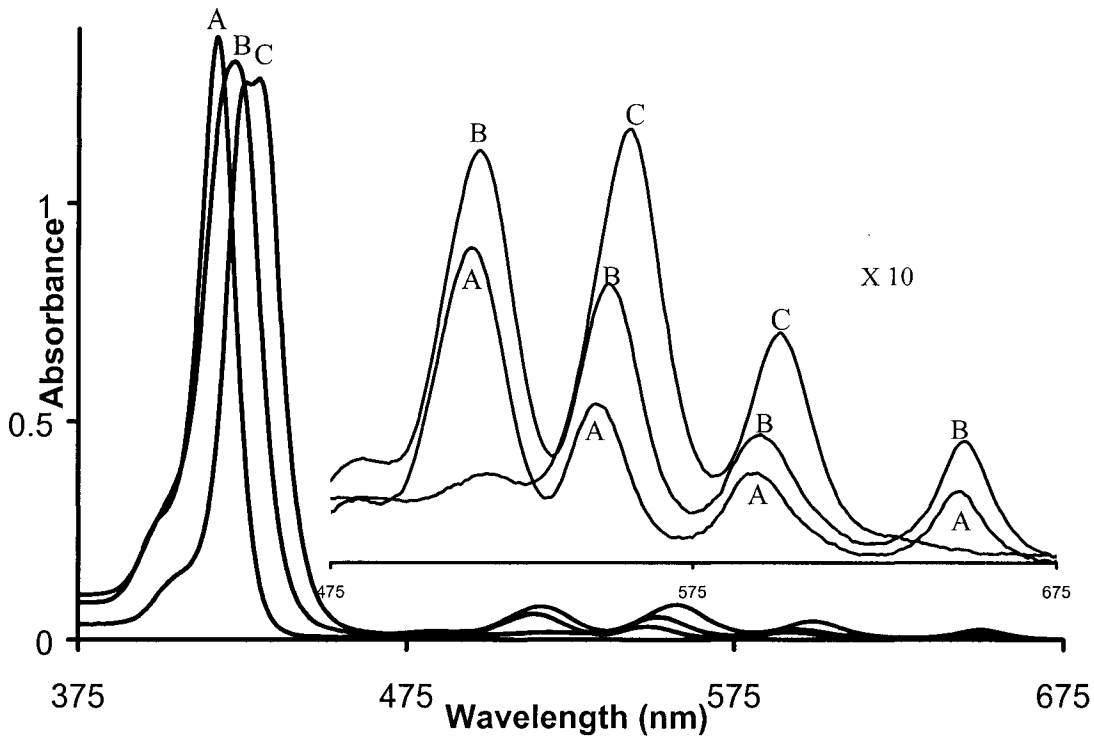

Figure 2.2.1. UV-Visible spectra of 5-(4-pyridyl)-10,15,20-tri(4-tert-butylphenyl)porphyrin (A), **1** (B), and Zn_2**1** (C) in 2-methyl-THF (4μM).

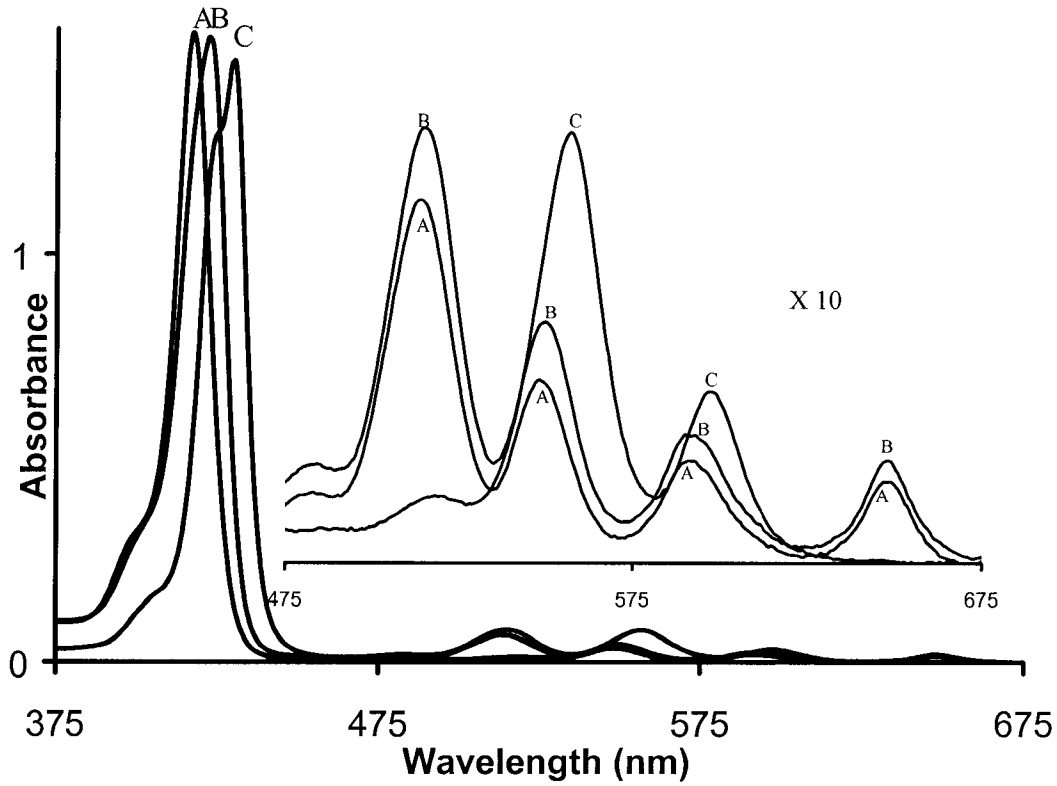

Figure 2.2.2. UV-Visible spectra of 5-(4-pyridyl)-10,15,20-tri(4-tert-butylphenyl)porphyrin (A), **2** (B), and Zn_2**2** (C) in 2-methyl-THF (4μM).

As expected, when the BiPy linker is coordinated by a variety of metal ions such as Cu(I) Ni(II), or Pd(II), is an increase in the electronic communication between the two porphyrins in **1** (figures 2.2.3 and 2.2.4) and **2** (Figure 2.2.5. and 2.2.6).

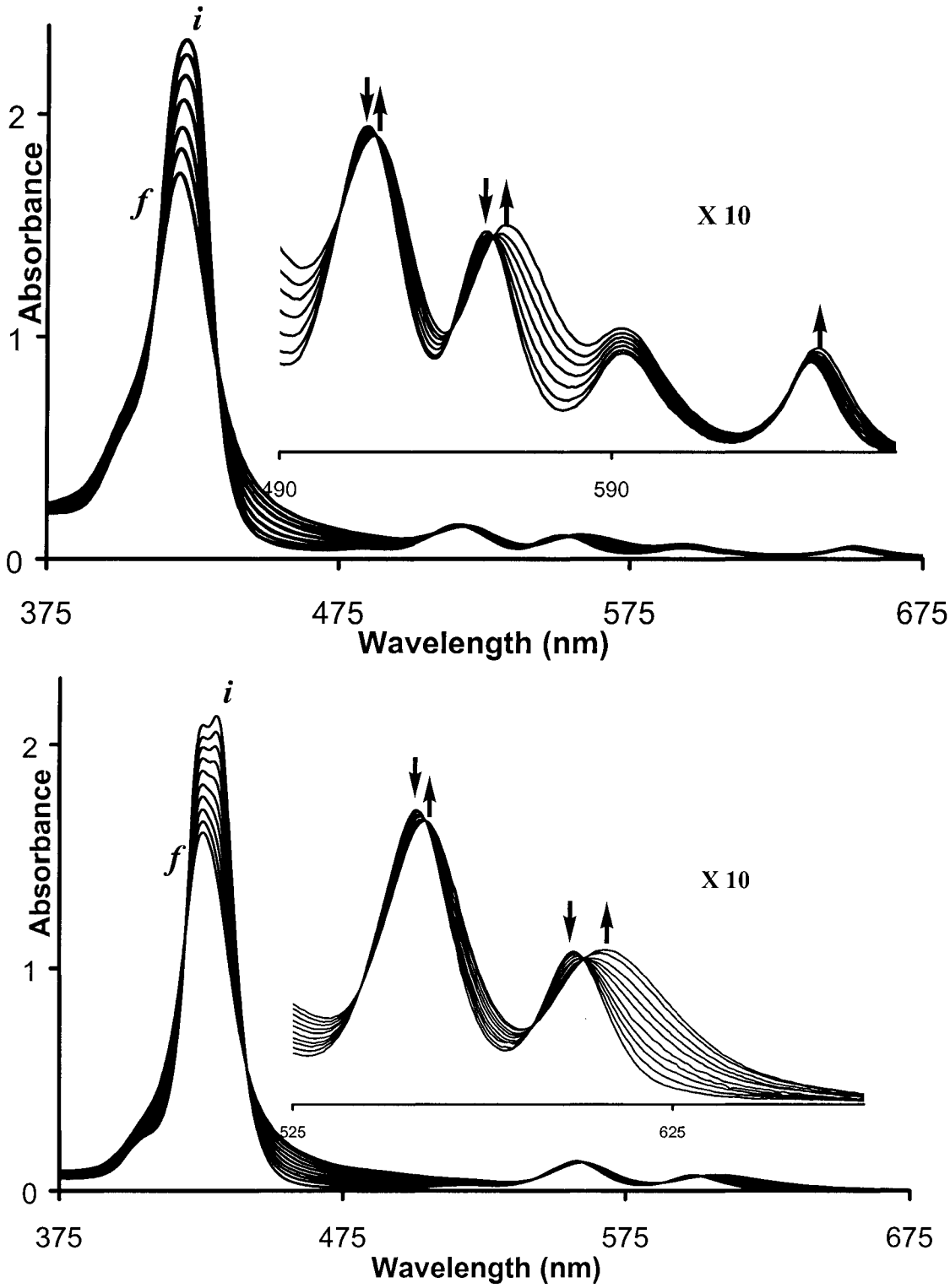

Figure 2.2.3. The UV-Visible spectra as one equivalent (in 6 ≤ 5μL aliquots) of Pd(II)Ac_2 is titrated into 3 mL of a 5μM solution of **1** (top) and Zn_2**1** (bottom) in 2-methyl-THF.

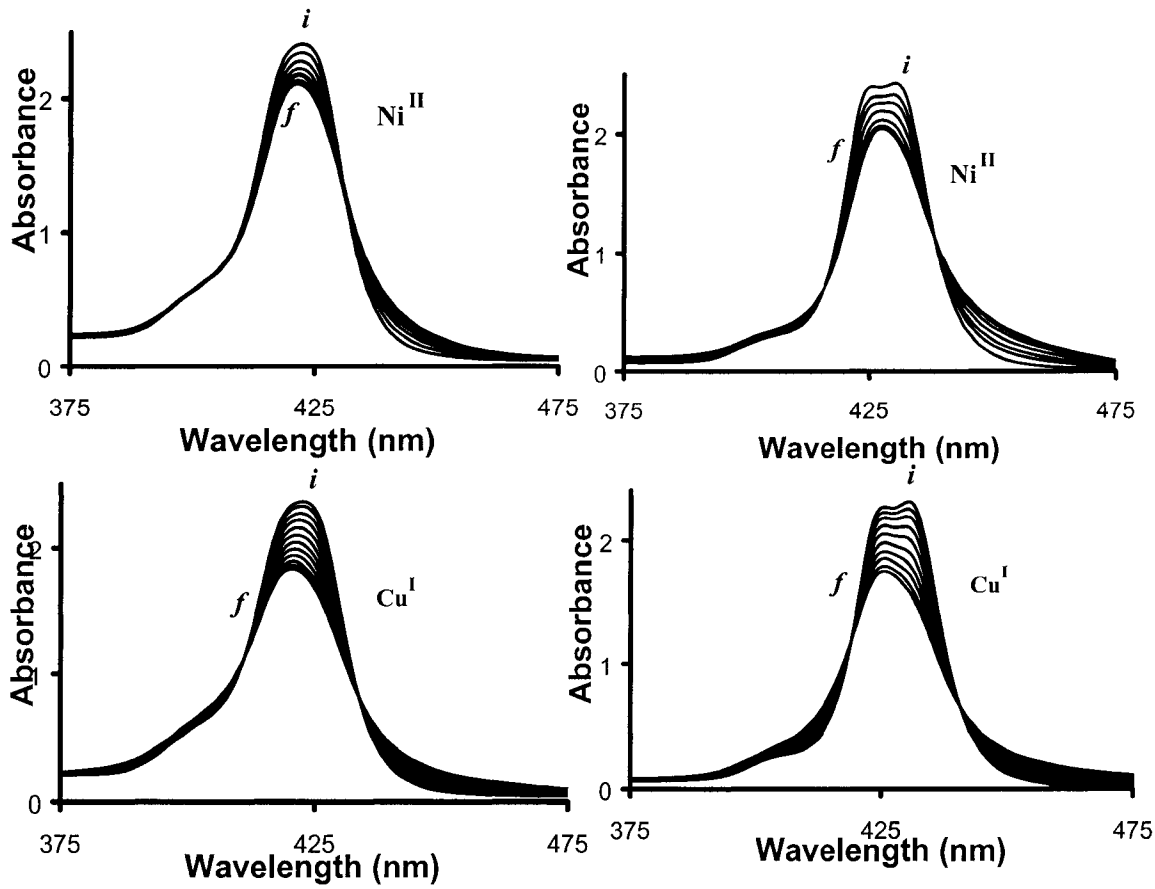

Figure 2.2.4. Soret region of the UV-Visible spectra as one equivalent (in 6 ≤ 5μL aliquots) of Ni(II)Ac_2 or Cu(I)ClO_4 is titrated into 3 mL of a 5μM solution of **1** (left) and Zn_2**1** (right) in 2-methyl-THF; i= initial, f= final.

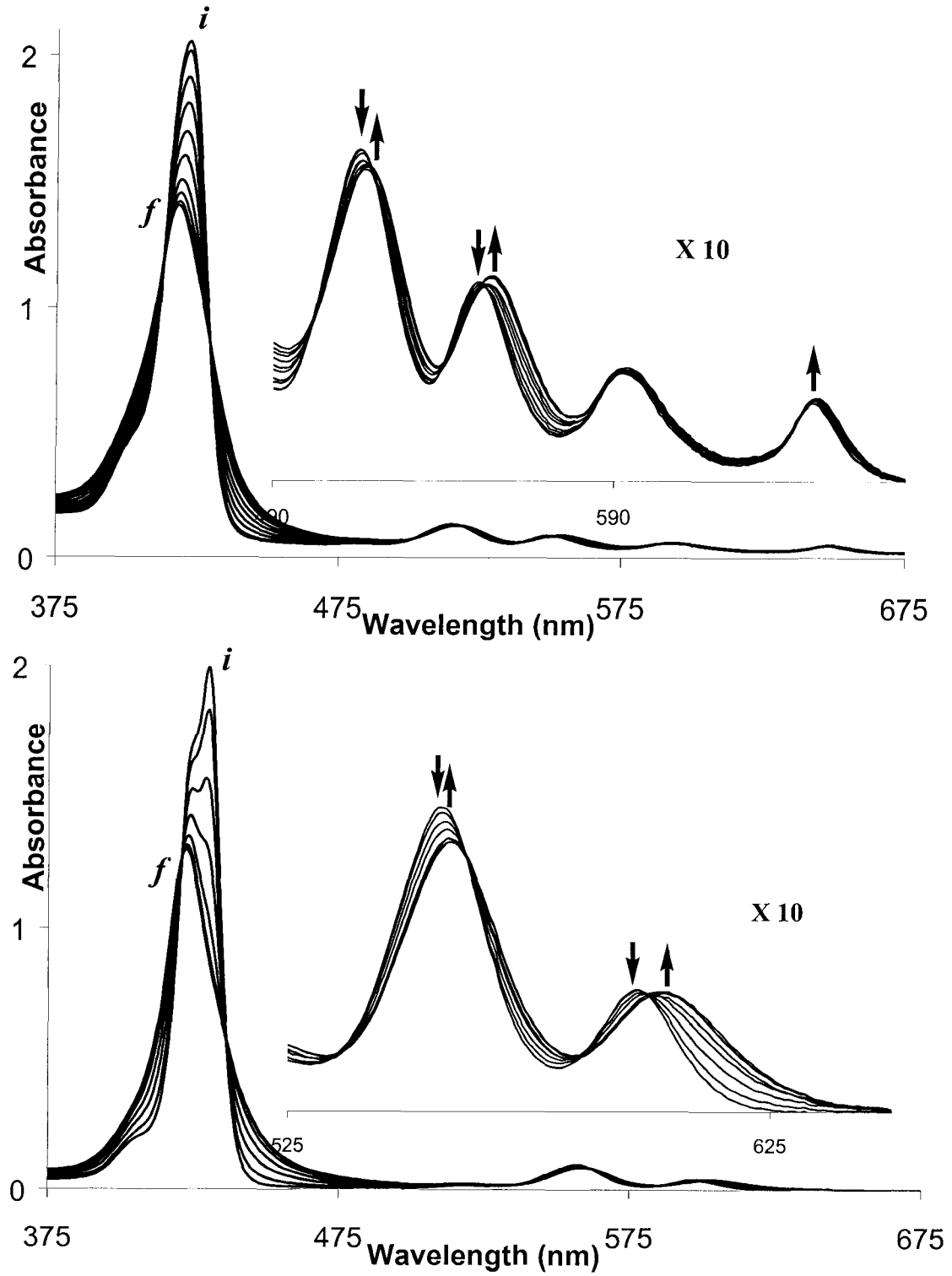

Figure 2.2.5. The UV-Visible spectra as one equivalent (in 6 ≤ 5μL aliquots) of Pd(II)Ac_2 is titrated into 3 mL of a 5μM solution of **2** (top) and Zn_2**2** (bottom) in 2-methyl-THF.

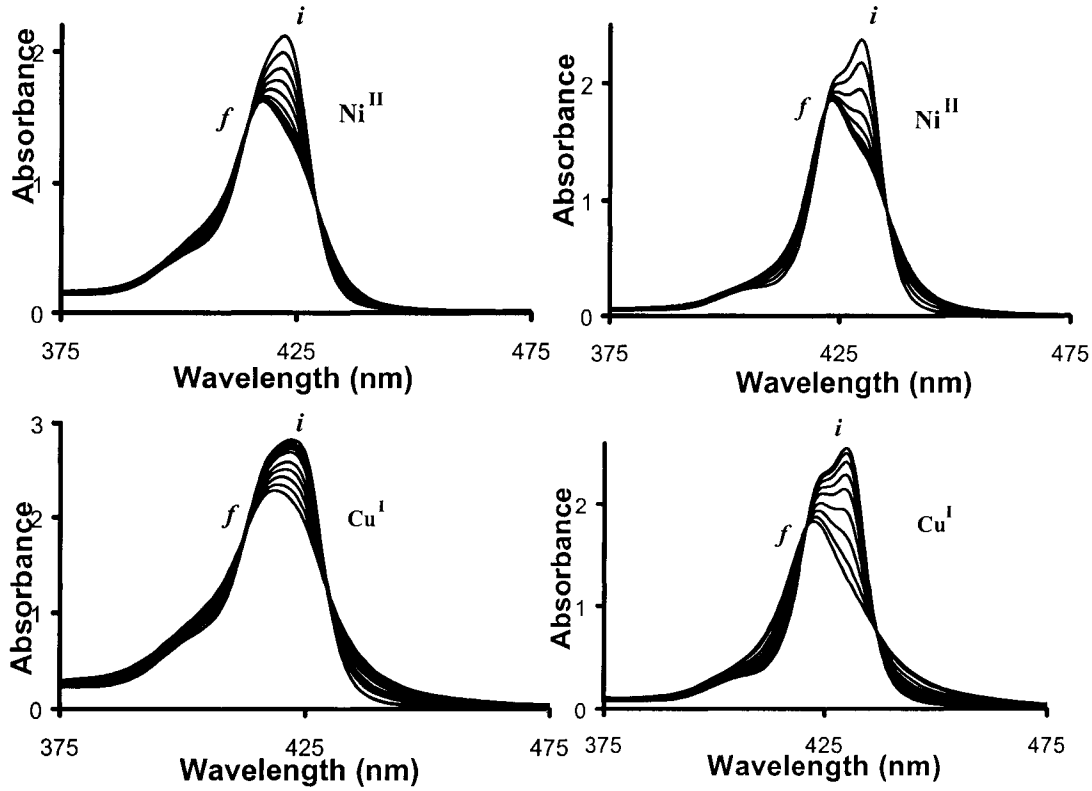

Figure 2.2.6. Soret region of the UV-Visible spectra as one equivalent (in 6 ≤ 5μL aliquots) of Ni(II)Ac_2 or Cu(I)ClO_4 is titrated into 3 mL of a 5μM solution of **2** (left) and Zn_2**2** (right) in 2-methyl-THF; i= initial, f= final.

For the Pd(II) adducts of **1** and **2** this is indicated by a ~2 nm blue shift and a further ~20% broadening of the Soret band, as well as red shifts in the Q bands (figure 2.2.3. and 2.2.5.). Several isosbestic points are found in the titration experiments for the free base compounds, indicating the formation of only one product. For comparison, a linear dimer formed from the coordination of two para pyridylporphyrins to Pd(II)Cl_2 results in a 2-3 nm red shift and a ~10% broadening of the Soret band.[40] Thus in addition to the substituent effects, the ground state electronic communication between chromophores is

mediated by both the covalent bond and by the BiPy chelated metal ion, though the effects are small.

Unexpectedly, when both of the porphyrins are metalated with zinc, the equilibrium between the free-base 2,2'-bipyridine conformations shifts such that a significant population of the co-planar form exists, as observed by the dual Soret bands in the optical spectra for Zn_2**1** (figure 2.2.1.), and to a different extent for Zn_2**2** (Figure 2.2.2.). The peak at 430nm is consistent with the known red-shift of porphyrin Soret bands upon Zn(II) coordination, and the 426nm band represents the fraction of molecules with the BiPy in a planar conformation. This latter observation also is consistent with the known increase in electron density on nitrogen(s) at the 4 of pyridyl porphyrins, as measured by coordination chemistry and basicity, upon zinc metalation.[40,41,53,54] This conclusion is also supported by the observation that when the Pd(II) species is titrated into a solution of Zn_2**1**, the 430nm band disappears, to yield a broad Soret band similar to the one found for the free base compounds upon coordination of this metal by the BiPy subunit. Again, the small red shift of the Zn_2**1** – Pd(II) complex is due to the zinc metalloporphyrin (figure 2.2.3. and 2.2.4.). Note that even at low concentrations of Zn_2**1**, the split Soret band remains, so this observation is not due to changes in the aggregation state. Note also that for **2** there is a ~3 nm blue shift of the Soret upon complexation of the same set of metal ions (figure 2.2.5. and 2.2.6.). When metal ions bind the BiPy of Zn_2**2** the split Soret band also evolves into a broader peak centered to the blue of Zn_2**2**. Thus, the largest contributor to the observed spectral shift is the locking-in of the planar conformation of the BiPy by metal ion binding, *vide infra*. The process of the formation of Zn_2**2**-Zn(II) complex also investigated by UV-vis titration experiment. In the

experiment, 5 μM **2** in $CHCl_3$ titrated with 3 equiv. $Zn(OAc)_2$ at 60 °C. It shows that 2.0 equiv. $Zn(OAc)_2$ gives Zn_2**2** and 3.0 equiv. $Zn(OAc)_2$ yields the Zn_2**2**-Zn(II) complex (figure 2.2.7.). The UV-vis λ_{max} values for all compounds are summarized in table 2.2.1..

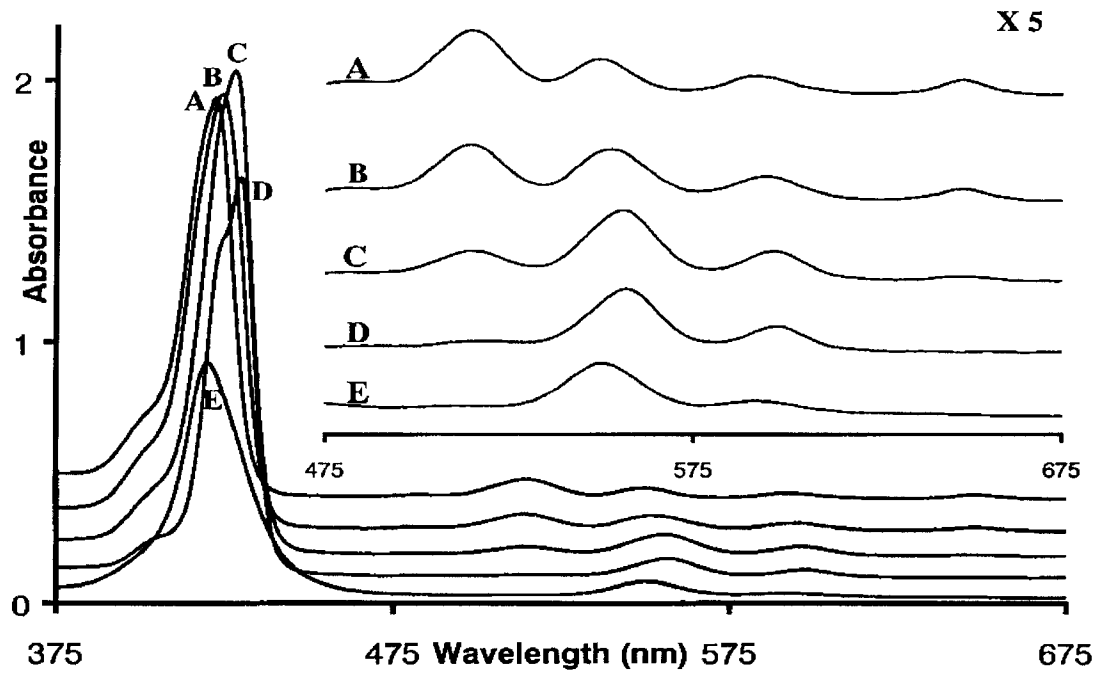

Figure 2.2.7. UV-visible spectra of 5 μM **2** in $CHCl_3$ titrated with 3 equiv. $Zn(OAc)_2$ at 60 °C. (A) **2**. (B) 1.5 equiv. $Zn(OAc)_2$. (C) 2.0 equiv. $Zn(OAc)_2$ to give Zn_2**2**. (D) 2.5 equiv. $Zn(OAc)_2$. (E) 3.0 equiv. $Zn(OAc)_2$ to yield the Zn_2**2**-Zn(II) complex.

Porphyrins and Complexes	Maximum Soret (nm)	Maxima Qs (nm)
MonoPyPorH2 (5 uM in 2-Methyl THF)	417	514, 548, 591, 648
1 (5 uM in 2-Methyl THF)	422	516, 552, 594, 650
Zn2 1 (5 uM in 2-Methyl THF)	426, 430	558, 599
Pd- 1 (5 uM in 2-Methyl THF)	420	518, 557, 593, 652
Cu- 1 (5 uM in 2-Methyl THF)	421	518, 555, 592, 651
Ni- 1 (5 uM in 2-Methyl THF)	421	517, 554, 594, 651
Pd- Zn2 1 (5 uM in 2-Methyl THF)	426	560, 607
Cu- Zn2 1 (5 uM in 2-Methyl THF)	426	560, 605
Ni- Zn2 1 (5 uM in 2-Methyl THF)	428	559, 603
Zn2 1 (70 uM in CHCl3)	428	559, 602
DABCO- Zn2 1 (70 uM in CHCl3)	426, 430	562, 606
DABCO-Pd- Zn2 1 (70 uM in CHCl3)	427	565, 618
2 (5 uM in 2-Methyl THF)	422	515, 550, 593, 648
Zn2 2 (5 uM in 2-Methyl THF)	425, 430	557, 597
Pd- 2 (5 uM in 2-Methyl THF)	418	518, 554, 593, 649
Cu- 2 (5 uM in 2-Methyl THF)	419	516, 553, 593, 648
Ni- 2 (5 uM in 2-Methyl THF)	418	516, 551, 592, 649
Pd- Zn2 2 (5 uM in 2-Methyl THF)	422	558, 600
Cu- Zn2 2 (5 uM in 2-Methyl THF)	422	559, 602
Ni- Zn2 2 (5 uM in 2-Methyl THF)	423	557, 599
Zn2 2 (70 uM in CHCl3)	429	555, 598
DABCO- Zn2 2 (70 uM in CHCl3)	424, 431	562, 604
DABCO-Pd- Zn2 2 (70 uM in CHCl3)	427	564, 610

Table 2.2.1. UV-vis λ_{max} values for all compounds.

The nature of the metal ion coordinated by the BiPy moiety for both **1** and **2** makes little difference in the ground state spectra as first row transition metals, second row metals, divalent, and univalent ions result in similar characteristic changes in the optical spectra with only subtle differences between them. The excited state spectra reveal several features that are worth noting. As expected for virtually any fluorophore, upon coordination of a metal ion by the BiPy moiety, the fluorescence emission spectra decrease in intensity relative to the parent compounds due to the heavy atom effect. Secondly, upon BiPy coordination to some metal ions, there are pronounced differences in the both the relative intensities and the energies of the emission bands relative to the unbound species. These differences likely arise from the different redox potentials of the different metal ions rather than enhanced electronic coupling of the chromophores, and may represent a means to fine-tune the excited state properties. The fluorescence emission and excitation spectra for **1**, Zn_2**1**, **2**, Zn_2**2** where the BiPy is complexed to Zn(II) or Pd(II) are essentially similar to the uncomplexed species, albeit with reduced intensity due to the heavy atom effect. This latter observation confirms the general conclusion that the conformational changes of the bisporphyrin BiPy compounds upon coordination to metal ions results in modest electronic coupling of the chromophores. The fluorescence emission and excitation spectra of **2** and **$Zn_2$2** are shown in figure 2.2.8..

These observations in the electronic spectra are consistent with the Gouterman four-orbital model (figure 2.2.9.).[55] For both **$Zn_2$1** and **$Zn_2$2**, the largest changes in terms of energetics are observed in the Q(0,0) bands which correspond to the lowest energy $^1(\pi, \pi^*)$ state. The highest occupied molecular orbitals of zinc porphyrins are a_2u and a_1u, and

the former has significant electron density at the *meso* positions (bearing the BiPy moiety) and the pyrrole nitrogens whereas the latter has electron density on the pyrrole α and β positions.

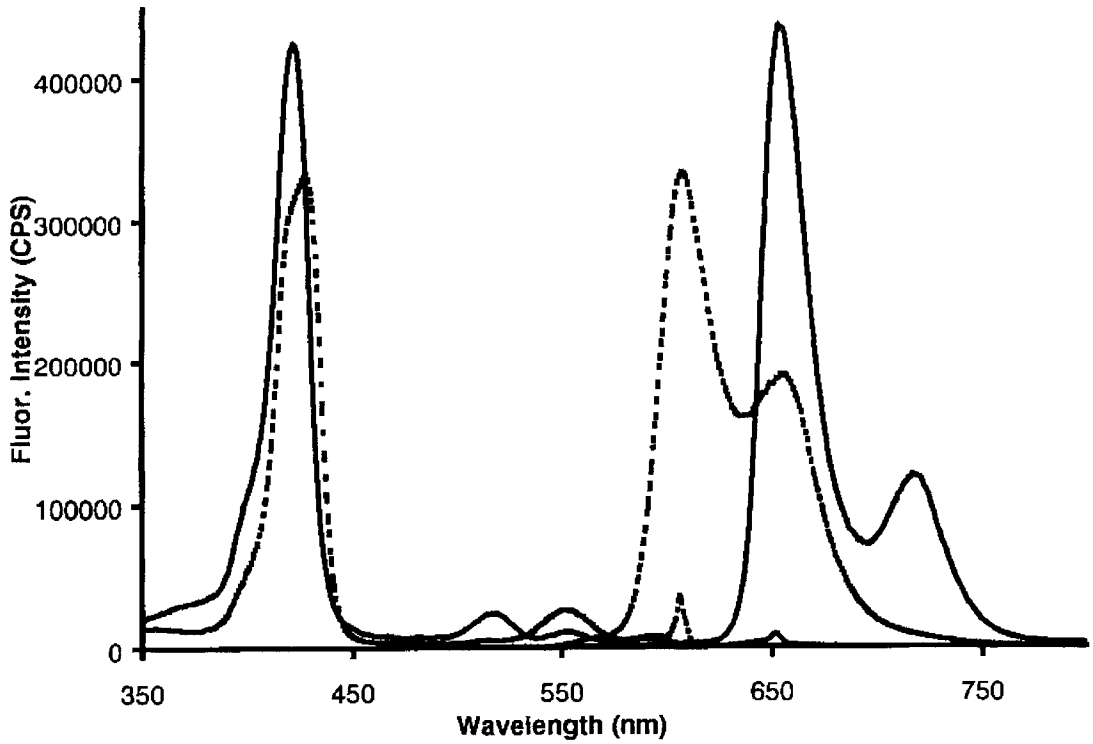

Figure 2.2.8. Fluorescence emission and excitation spectra of **2** (—) and Zn_2**2** (- - -) in $CHCl_3$ at RT. **2**: λex = 423 nm; λem = 655 nm. Zn_2**2**: λex = 429 nm; λem = 609 nm.

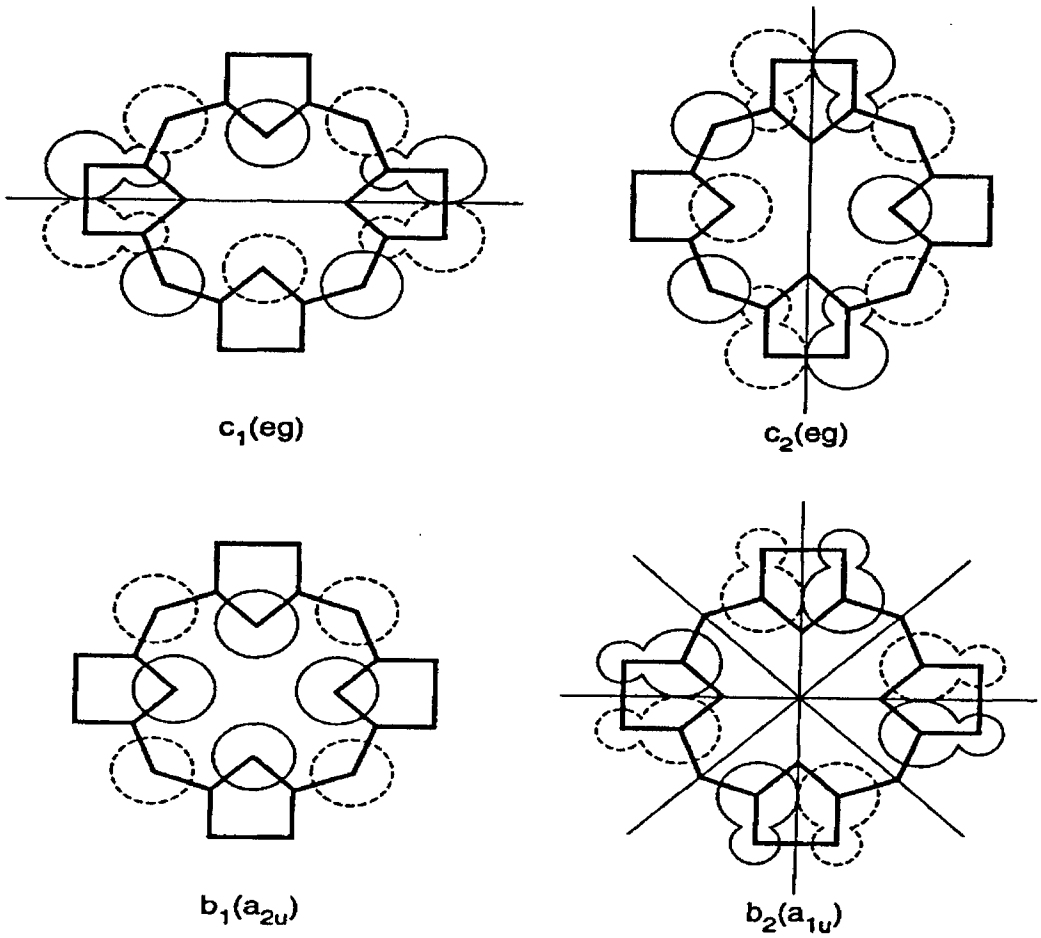

Figure 2.2.9. Porphyrin HOMOs b_1, b_2 and LUMOs c_1 and c_2 on the four orbital model. The orginal coefficients are proportional to the size of the circles. Solid or dashed circles indicate sign. Symmetry nodes are drawn in heavy lines.[65]

2.3. NMR Spectra

Chelation of $Pd(II)Ac_2$ by the 2,2'-BiPy subunit for both **1** and **2** was also examined by ^1H NMR titrations whereby 1.5 mg of **1** or **2** was dissolved in 1 ml $CDCl_3$ and the spectrum was taken of the initial solution and after each addition of 0.2 equivalents of $Pd(II)Ac_2$ dissolved in $CDCl_3$, were added (figure 2.3.1., 2.3.2. and 2.3.3.). The highly characteristic shift in the pyridyl protons upon coordination of a palladium ion indicates clean formation of the Pd adducts of **1** and **2**. For Zn_2**1** in 6:1 $CDCl_3$: THF-d_8 the singlet for the pyridyl 6H moves from 9.63 ppm to 9.25 ppm; the doublet for the pyridyl 3H moves from 9.13 ppm to 9.05 ppm; the doublet for the pyridyl 4H moves from 8.78 ppm to 8.65 ppm; the pyrrole doublet of doublets at 8.98 ppm (which arise from the pyrrole nearest the BiPy unit) change to complex multiplets at 9.00 ppm, and 8.75 ppm. The single pyrrole resonance from the outer pyrroles significantly broaden into three closely spaced peaks, and the 4-*tert*-butylphenyl CH_3 move from 1.59 ppm to 1.61 ppm. For **2** in $CDCl_3$, there are three distinguishable pyridyl proton peaks: a doublet of doublets (dd) at δ= 8.24, a doublet (d) at δ= 9.07, and a singlet (s) at δ= 9.64. As the solution is titrated, the pyridyl dd peak shifts downfield to δ= 8.44 while the other two peaks are shifted upfield to δ= 8.97 (d) and to δ= 8.77 (s), and all of the peaks broaden slightly. Significantly, the original two sets of phenyl proton doublets shift from one peak at δ= 8.18 to two peaks at δ= 8.05 and 7.91; and from one peak at δ= 7.78 to two peaks at δ= 7.71 and 7.61 and broaden significantly.

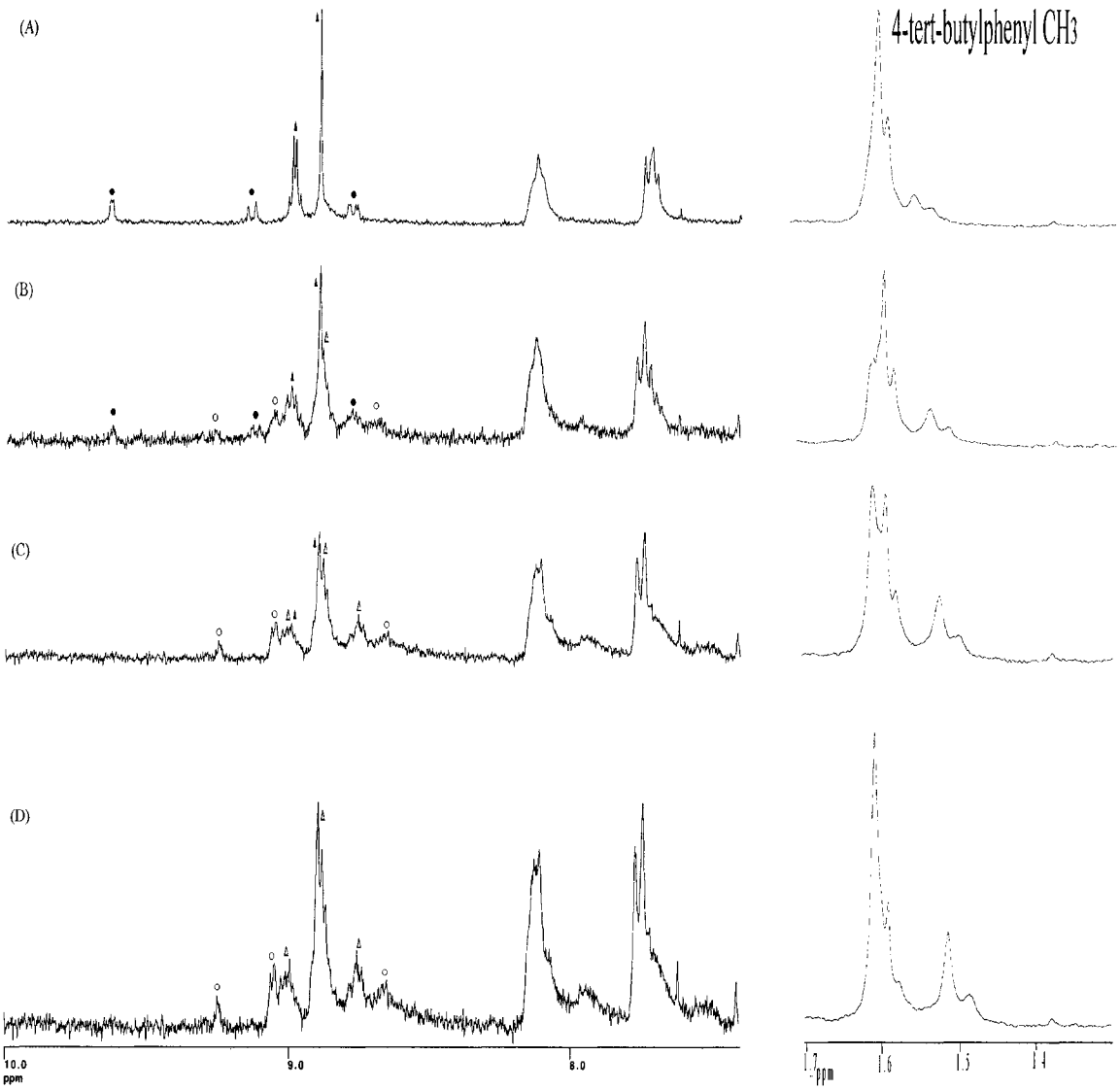

Figure 2.3.1. ^{1}H NMR titration of Zn_2**1** with $Pd(OAc)_2$ (300 MHz, $CDCl_3$/THF-d_8). (A) **2** (0.8 mM). (B) 0.5 equiv $Pd(CH_3CO_2)_2$. (C) 0.75 equiv $Pd(CH_3CO_2)_2$. (D) 1.0 equiv $Pd(CH_3CO_2)_2$. (●) Uncoordinated bipyridyl ^{1}H. (▲) Uncoordinated pyrrole-Hβ. (■) Uncoordinated 4-tert-butylphenyl ^{1}H. (○) Coordinated bipyridyl ^{1}H. (Δ) Coordinated pyrrole-Hβ. (□) Coordinated 4-tert-butylphenyl ^{1}H.

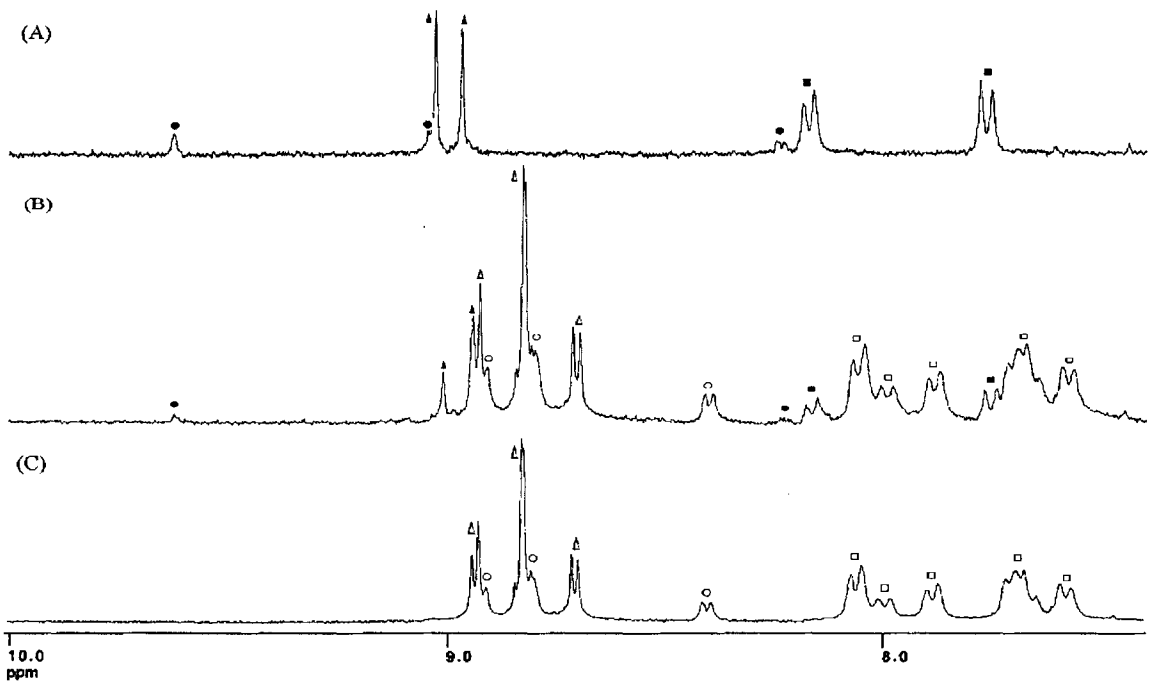

Figure 2.3.2 ^{1}H NMR titration of Zn_2**2** with $Pd(OAc)_2$ (300 MHz, $CDCl_3$/THF-d_8). (A) 2 (0.8 mM). (B) 0.75 equiv. $Pd(OAc)_2$. (C) 1.0 equiv. $Pd(OAc)_2$. (●) Zn_2**2** bipyridyl ^{1}H. (▲) Zn_2**2** pyrrole-Hβ. (■) Zn_2**2** 4-tert-butylphenyl ^{1}H. (○) Zn_2**2**·Pd(II) bipyridyl ^{1}H. (Δ) Zn_2**2**·Pd(II) pyrrole-Hβ. (□) Zn_2**2**·Pd(II) 4-tert-butylphenyl ^{1}H.

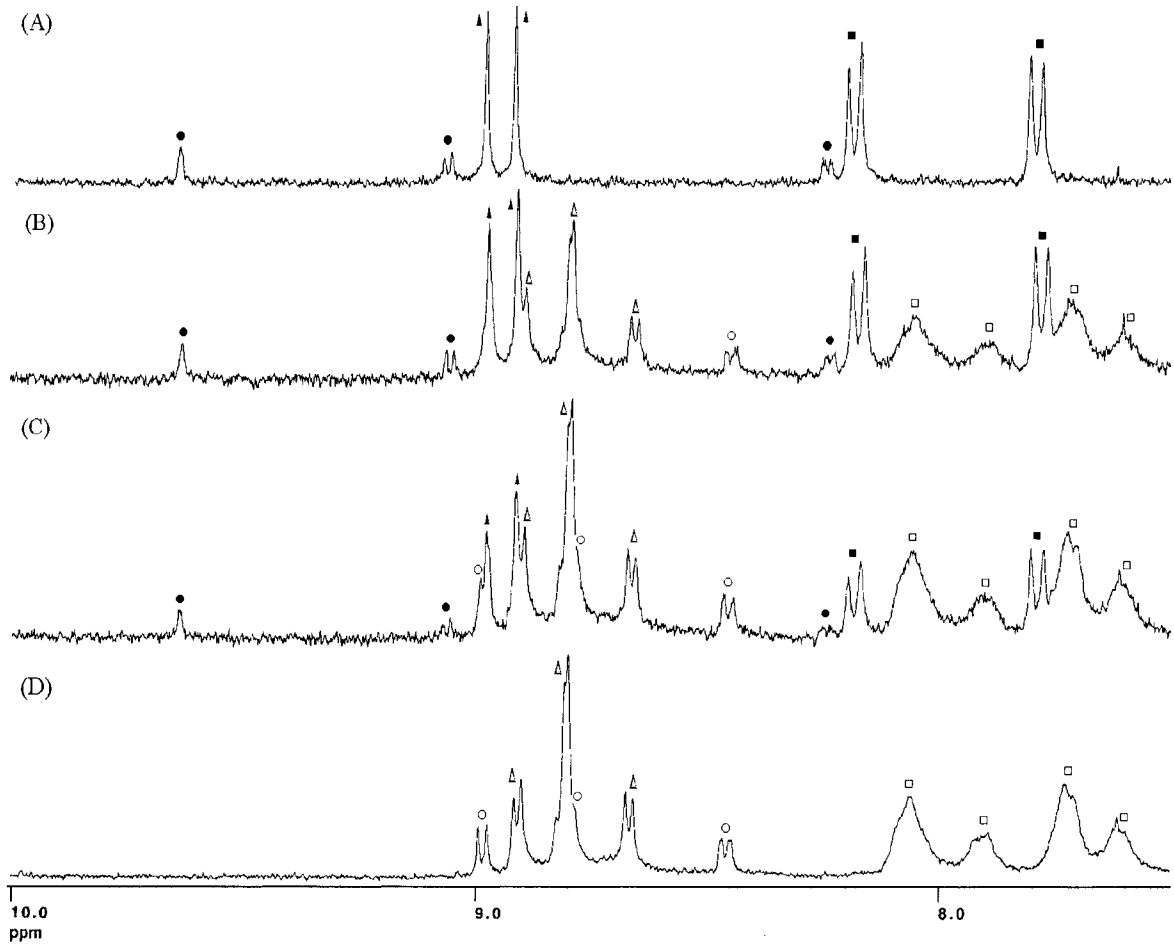

Figure 2.3.3. ^{1}H NMR titration of **2** with $Pd(OAc)_2$ (300 MHz, $CDCl_3$). (A) **2** (1 mM). (B) 0.5 equiv $Pd(CH_3CO_2)_2$. (C) 0.75 equiv $Pd(CH_3CO_2)_2$. (D) 1.0 equiv $Pd(CH_3CO_2)_2$. (●) Uncoordinated bipyridyl ^{1}H. (▲) Uncoordinated pyrrole-Hβ. (■) Uncoordinated 4-tert-butylphenyl ^{1}H. (○) Coordinated bipyridyl ^{1}H. (Δ) Coordinated pyrrole-Hβ. (□) Coordinated 4-tert-butylphenyl ^{1}H.

The changes in chemical shifts are consistent with those observed for other pyridylporphyrin complexes,[38,40,41] and the increased peak width is likely due to the increased rigidity of the system, and slight increase in molar mass. Significantly, the changes in chemical shift of the pyrrole protons for both **1** and **2** when the BiPy unit binds Pd(II) further indicates the substituent effects, but note that these changes in pyrrole chemical shift are about the same as those observed when two 5-(4-pyridyl)-10,15,20-tri-(4-tertbutylphenyl)porphyrins bind the same metal ion. Therefore the covalent bond between the pyridines in BiPy in **1**, and **2** has only minor effects on the ring current of the marcocycles. The predominant causes of the spectral changes are the metal ion and the conformational change of the BiPy induced by the metal ion binding.

2.4. Coordination Chemistry

The coordination chemistry of these two compounds has yet to be fully explored; however, the more than ample precedents in BiPy chemistry indicate that these will be good tectons for a variety of supramolecular arrays and polymers. Control of temperature, relative stoichiometry, and choice of metal ion allows one to design systems wherein these two compounds merely complex the metal ion, such as the work herein, or form higher ordered adducts (such as 2:1 or 3:1).[29] The structure of these complexes will be governed by the metal ion binding properties as well as the steric interactions of the porphyrins. For example, the tetrahedral coordination geometries of some metal ions such as Cu(I) and Zn(II) allow the formation of dimers of **1** or **2** bound together by the coordination of the BiPy moieties to the metal. In these cases the four chromophores are well separated (scheme 2.4.1.). The optical spectra of both of these simple coordination dimers are unremarkable such that neither dimer displays properties much different from the monomers coordinated by the same metal ion. The relative orientation of the porphyrins in coordination oligomers or arrays based on compounds **1** and **2** will be quite different. Coordination of the BiPy moiety of the 5,5' derivative to square planar metal ions will force the macrocycles to be cofacial thereby altering the photo physical properties, as exhibited by further blue shift in the Soret band.

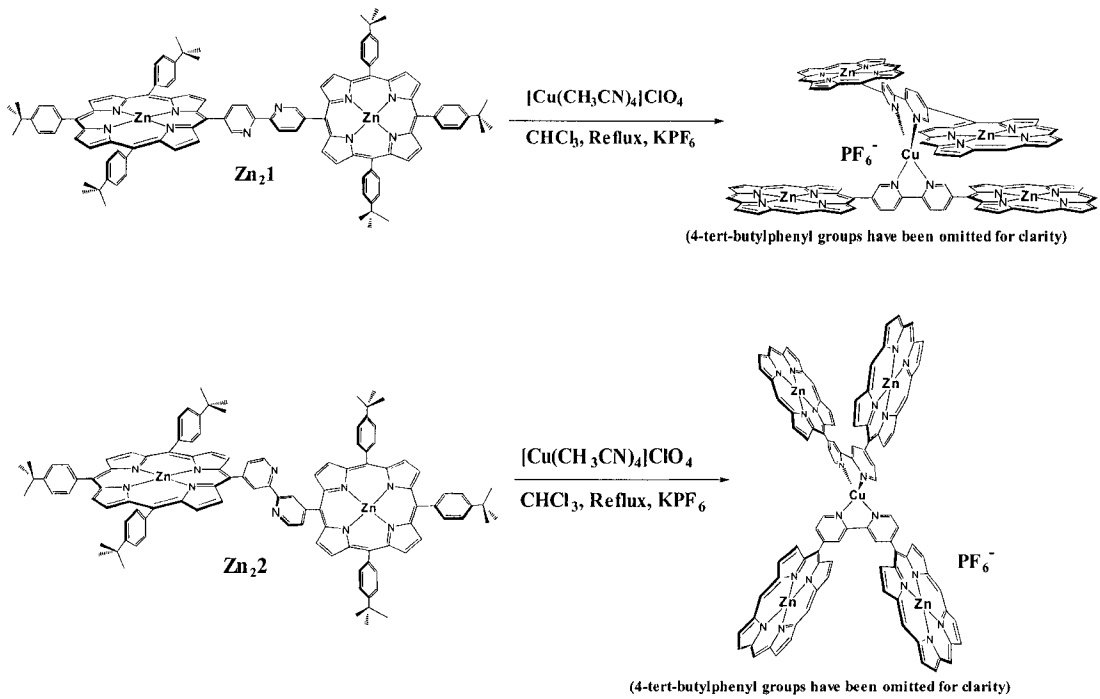

Scheme 2.4.1. Formation of dimers of $\mathbf{Zn_2 1}$ or $\mathbf{Zn_2 2}$ bound together by the coordination of the BiPy moieties to the copper metal.

The coordination of the 4,4' derivative to the square planar metals leave the chromophores separated and the photo physical properties are nearly indistinguishable from the simple monomer coordinated to the same metal ion. In principle these $\mathbf{Zn_2 1}$ or $\mathbf{Zn_2 2}$ can coordinate a metal such as Ru to yield hexaporphyrin arrays $(\mathbf{Zn_2 1})_3$Ru and $(\mathbf{Zn_2 2})_3$Ru. But the *meso* positions will be sterically crowded. Perhaps an alkyl chain on the *meso* positions will allow formation of such arrays.

2.5. Supramolecular Squares

Since the first publications on designed coordination squares[56] such as porphyrins[40] there has been numerous reports on the application of these concepts to the design of functional materials.[56] In all of the porphyrinic squares, and most supramolecular systems in general, a conformational change in the molecules that constitute the sides is either not possible because they are locked into place, or results in the dis-assembly of the supramolecular system, which may or may not re-assemble into a different structure.[43] Compound **1** and its metalloporphyrin derivatives; however, show that this is not a *priori* true. As a demonstration, it is possible to form a supramolecular square using two Zn_2**1** and two DABCO molecules (scheme 1.4.4.). At 70 μM in chloroform the supramolecular square is the predominant species according to well-established equillibria and exhibits the characteristic red-shift in the electronic spectra upon axial coordination of the zinc porphyrins by nitrogenous ligands[44] (figure 2.5.1.). In the process of forming the square the DABCO disrupts the aggregates of Zn_2**1** found at this concentration, and note that the Soret band of the final spectrum, '*f*' (peak maxima at 426nm, 430nm, 562nm, 606nm) is essentially identical to that of this compound at 5 μM, with one equivalent of piperidine. Note that the nominal Soret bands are essentially the same as that of unligated Zn_2**1**, but the Q bands are red shifted by ~5nm. A plot of ΔA vs. DABCO equivalents confirms the 1:1 stoichiometry. The porphyrins in each Zn_2**1** unit are now coplanar. This is in contrast to the 'average' coplanarity arising from the small oscillation about the pyridyl-porphyrin bonds when the BiPy unit in Zn_2**1** id bound by metal ions (peak maxima at 426nm, 560nm, 607nm). Then, as the Pd(II) species is titrated into the solution containing the square, there is a substantial red shift in the lowest

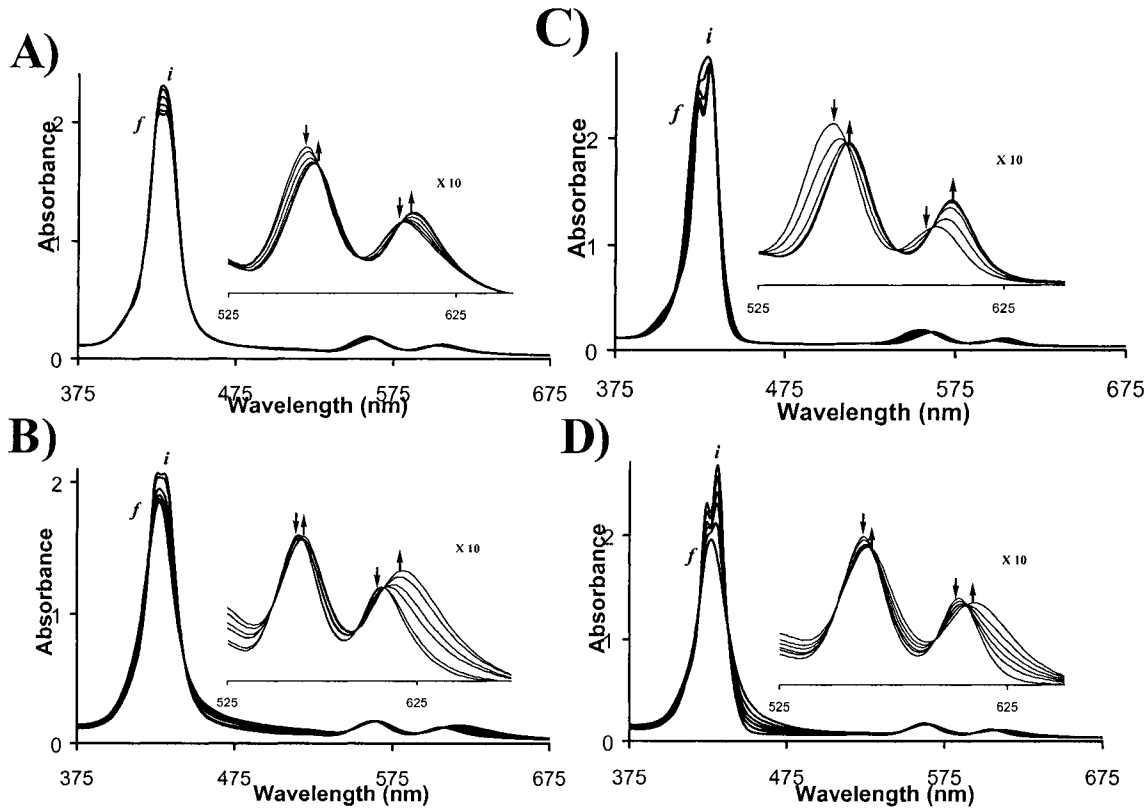

Figure 2.5.1. (A) The single broad Soret band in the UV-Visible spectra of Zn_2**1** (70 μM in chloroform, 1mm path length cuvette) indicates some aggregation, but disaggregation occurs as one equivalent of DABCO is titrated into the solution to form a supramolecular square (scheme 1.4.4). (B) The addition of one equivalent of Pd(II)Ac_2 per Zn_2**1** changes the conformation of the BiPy without changing the structure of the supermolecule. (C) Changes in the optical spectra are nearly complete after only ~0.5 equivalent of DABCO is added to Zn_2**2**, and (D) the addition of one equivalent of Pd(II)Ac_2 per Zn_2**2**.

energy Q band (12nm), a smaller shift in the intermediate Q band (3nm), and the red Soret band at 430nm disappears. The two BiPy unit are now locked into a planar conformation and the porphyrins in each subunit in the final structure are not only coplanar, but in register with the opposing subunit. This is further indication that the planar, metal-bound state of the BiPy is the main reason for the observed changes in the electronic spectra. On the other hand, with Zn_2**2** a plot of ΔA vs. DABCO equivalents indicates about half an equivalent of DABCO binds per Zn_2**2**. In this case the addition of the Pd(II) species shifts the Q bands to the red and there is a broadening of the Soret band (figure 2.5.1.).

The fluorescence of both the supramolecular square and the Zn_2**2**-DABCO complex is typical of axial binding of nitrogenous ligands to the Zn(II) centers.[58] As observed in other porphyrin assemblies mediated by Pd(II) coordination,[25,40,41] there are small red shifts in the emission spectra of Zn_2**1**·Pd(II) and Zn_2**2**·Pd(II) that reflect the observed shifts in the ground state spectra (figure 2.5.2. and 2.5.3.). However, note that when two Pd(II) bind to the square the fluorescence is quenched by ~50%, but when one Pd(II) binds to the Zn_2**2**-DABCO complex the emission is quenched by ~80%. This is consistent with other rigidly assembled porphyrin systems[27] and aggregates.[59]

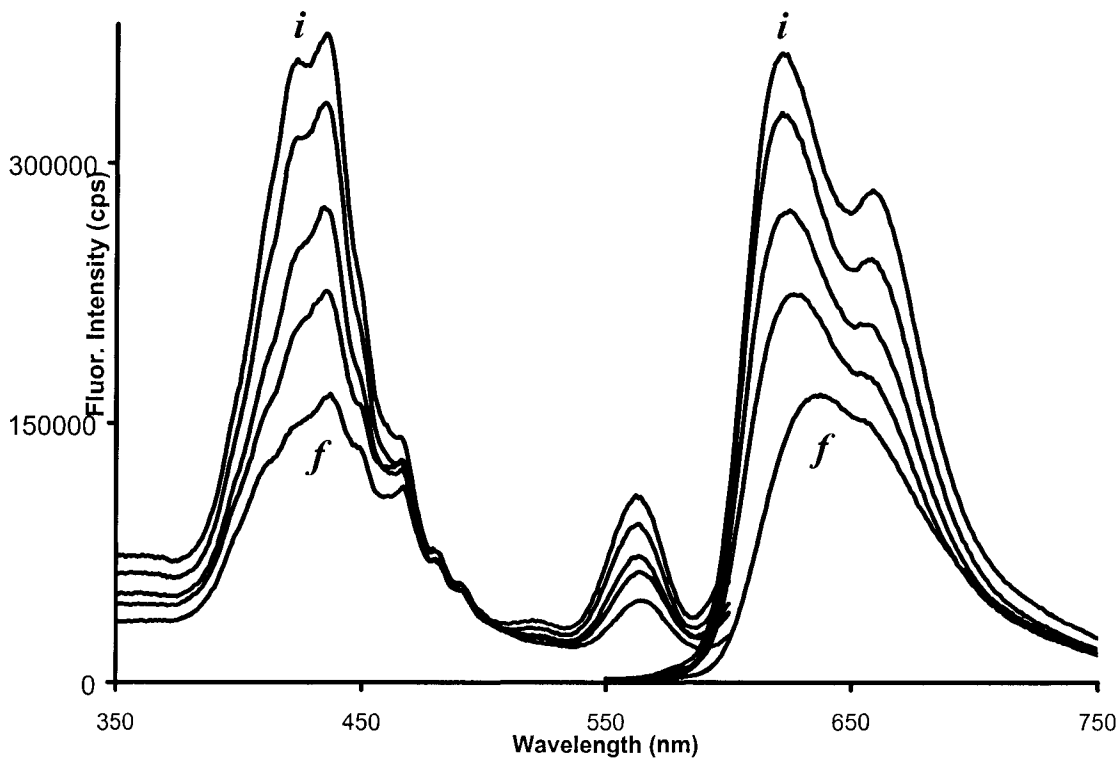

Figure 2.5.2. Fluorescence emission and excitation titration spectra of a supramolecular square composed of two Zn_2**1** and two DABCOs as 2 equiv. $Pd(II)(OAc)_2$ (1 Pd(II) per Zn_2**1**) are titrated into the solution in $CHCl_3$ at RT. λex = 429 nm; λem = 616 nm.

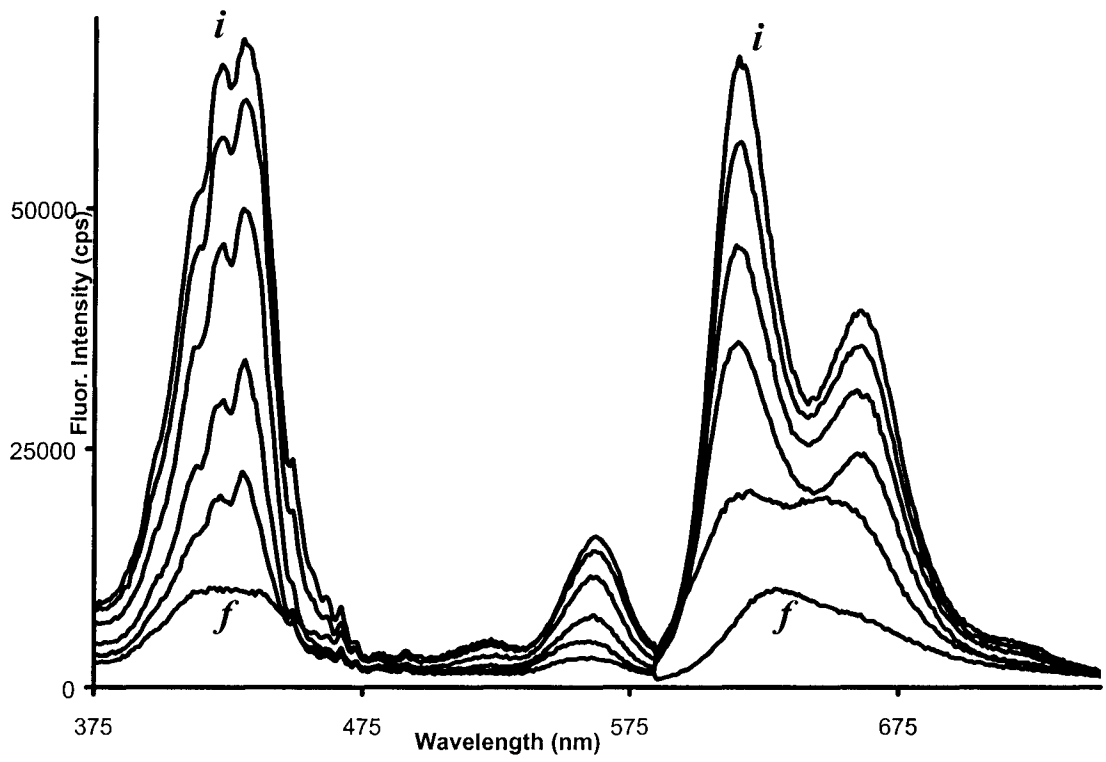

Figure 2.5.3. Fluorescence emission and excitation titration spectra of Zn_2**2** with DABCO titrated with 1 equiv. Pd(II)(OAc) in $CHCl_3$ at RT. λex = 424 nm; λem = 616 nm.

Taken together the absorption data indicate that the average coplanarity of the chromophores is not the predominant cause of the spectral shifts, but it is a combination of the planar conformation of the BiPy and the substituent effects caused by metal ion binding to the BiPy. The further red –shift of the electronic spectra of the supramolecular square is largely due to the highly rigid structure with the BiPy units locked into a planar conformation.

A3.

Conclusions

The new bis-porphyrin-2,2'-bipyridine system **1** and its Zn complex were synthesized and characterized by UV-Visible, NMR and ESI-MS. The rigid architectures of the molecules are in contrast to other porphyrin-bipyridine systems such as **2**, or similar derivatives.[26] When the BiPy subunit binds metal ions it becomes planar, and facilitates electron coupling between the chromophores of **1**, **2**, and their metalloporphyrin derivatives. These compounds (**1**, Zn_2**1**, **2** and Zn_2**2**) can serve as sensors for various metal ions with the sensitivity dictated by the binding constant of the BiPy for the given metal ion. In a second functional mode, these compounds can serve as an electronic switch gated by complexation and decomplexation of these ions. Initial studies comparing the ground and excited state spectra of supramolecular systems constructed from these compounds indicate that the spatial arrangement of the porphyrins further dictates the photophysical properties, as expected. Thus larger and more complex porphyrin arrays may be synthesized by coordinating the appropriate transition metal ions bearing multitopic ligands to the BiPy moiety.[36] These molecules will serve as part of a library of building blocks for the self-assembly of nano scaled photonic materials.[60-64]

Since the porphyrins only subtly alter the 2,2'-bipyridine metal ion binding properties, the well-established coordination chemistry of this subunit can be exploited. However, steric considerations may well prevent or complicate the formation of certain

bis- and tris- BiPy complexes that are well known in the literature, especially for **1** and its derivatives. Importantly, the results on the ladder complex of Zn_2**1** demonstrate that there is no *a priori* requirement that structural rearrangements or reorganization of supramolecular systems will result from structural changes in component molecules, even though these structural perturbations result in significantly different photophysical properties.

A4.

Experimental Section

4.1. Reagents and physical measurements

All solvents were distilled using standard methods. Silica gel (Baker, 60μm average particle size) and alumina (Fisher, 80-200 mesh) were used for column chromatography. The $CHCl_3$ was reagent grade and use directly. The methyl THF was of reagent grade and used as obtained. The THF was freshly distilled from Na and methanol was distilled from CaH_2. The other solvents were distilled either from CaH_2 or P_2O_5. 2,2'-bipyridine-4,4'-dicarboxaldehyde purchased from Aldrich Chem. Co. and 2,2'-bipyridine-5,5'-dicarboxaldehyde was prepared according to the literature.[45,46] Proton NMR spectroscopy was recorded on a Varian VXR-300 MHz instrument using chloroform-D solvent as internal reference. UV-visible spectra were recorded on a Varian Bio-100 spectrometer. Electrospray mass spectroscopy spectrum was performed on Hewlett-Packard HP-1100 LC/MS positive-ion mode.

In general for titration experiments, an aliquot of the solution containing the given metal ion was added to the porphyrin solution, the mixture was stirred at room temperature for ~15 minutes (for the Pd(II) compounds the mixture was heated to ~50 ^{0}C) and spectra were recorded at ~20 ^{0}C. Under the conditions described for the titrations, and consistent with known BiPy chemistry, plots of either absorption intensity or

chemical shifts versus mole ratio indicate a 1:1 stoichiometry of the porphyrin derivatives to the metal ion coordinated to the BiPy unit.

4.2. Synthesis of compounds

5,5'-bis-[5'-(10,15,20-tri-4-tert-butylphenyl)porphyrinyl]-2,2'-bipyridine (1). A mixture of 2,2'-bipyridine-5,5'-dicarboxaldehyde (25mg, 0.12mmol) and pyrrole (0.07mL, 0.96mmol) in a 15 mL solvent mixture of acetic acid and nitrobenzene (3:2 v/v) was refluxed for 15 min, then 4-tert-butylbenzaldehyde (0.12mL, 0.72mmol) was added to the reaction mixture. The final mixture was refluxed in air for 18 hr. at 140 °C. Then the excess solvent was removed by vacuum distillation. The crude dark solid was dissolved in chloroform and filtered through a pad of silica (5% EtOH in chloroform). The filtrate was concentrated, redissolved in $CHCl_3$, chromatographed (silica 37g, chloroform). The second purple band was collected. 4/5 solvent was removed and the crude product was crystallized with acetonitrile at 0 °C, affording a purple precipitate that was centrifuged and dried in vacuo (3.7mg, 2%). ^1H NMR (chloroform-d) δ 9.71 (d, J=2.5Hz, 2H, H6 in 2,2'-bipyridyl), 9.22 (d, J=8Hz, 2H, H3 in 2,2'-bipyridyl), 9.03 (d, J=5Hz, 4H, pyrrole-Hβ), 8.99 (d, J=5Hz, 4H, pyrrole-Hβ), 8.93 (s, 8H, pyrrole-Hβ), 8.87 (dd, J_1=2.5Hz, J_2=8Hz, 2H, H4 in 2,2'-bipyridyl), 8.19 (m, 12H, H2 in 4-tert-butylphenyl), 7.80 (m, 12H, H3 in 4-tert-butylphenyl), 1.65 (s, 54H, CH_3 in 4-tert-butylphenyl), -2.66 (br. s, 4H, inner-NH). UV-Vis (Methyl THF): λ_{max} = 422, 516, 552, 594, 650 nm. ESMS obsd 1566.8, calcd 1566.0 ($C_{110}H_{104}N_{10}$).

5,5'-bis-[5'-(10,15,20-tri-4-tert-butylphenyl)porphyrinatozinc(II)]-2,2'-bipyridine (Zn_2**1**). Bipyridine-Diporphyrin (**1**) (3.0mg, 1.9μmol) dissolved in 10mL $CHCl_3$. Then six drops of saturated $Zn(CH_3CO_2)_2$ in methanol was added to the solution. The resulting porphyrin solution was allowed to reflux for 15 min (the process was monitored by UV-Visible spectroscopy). The reaction was quenched by adding 10mL water and then the layers were separated. The organic layer was dried ($MgSO_4$), and concentrated to 1/5 of the volume. The resulting porphyrin solution was crystallized from acetonitrile at 0 °C to afford a reddish precipitate. The solid was centrifuged and dried in vacuo (3.1mg, 95%). ^1H NMR (chloroform-d / THF-d8) δ 9.63 (d, J=2.5Hz, 2H, H6 in 2,2'-bipyridyl), 9.14 (d, J=8Hz, 2H, H3 in 2,2'-bipyridyl), 8.99 (m, 8H, pyrrole-Hβ), 8.89 (s, 8H, pyrrole-Hβ), 8.78 (dd, J_1=2.5Hz, J_2=8Hz, 2H, H4 in 2,2'-bipyridyl), 8.13 (m, 12H, H2 in 4-tert-butylphenyl), 7.72 (m, 12H, H3 in 4-tert-butylphenyl), 1.59 (s, 36H, CH3 in 4-tert-butylphenyl), 1.58 (s, 18H, CH3 in 4-tert-butylphenyl). UV-Vis (Methyl THF): λ_{max} = 430, 558, 599 nm. ESMS obsd 1694.3, calcd 1693.0 ($C_{110}H_{100}N_{10}Zn_2$).

4,4'-bis-[5'-(10,15,20-tri-4-tert-butylphenyl)porphyrinyl]-2,2'-bipyridine (2). A sample of 2,2'-bipyridine-4,4'-dicarboxaldehyde (25mg, 0.12mmol) was treated identically as for **1**, affording 5.6 mg (3%) reddish purple solid. ^1H NMR (chloroform-d) δ 9.64 (s, 2H, H3 in 2,2'-bipyridyl), 9.07 (d, J=4.8Hz, 2H, H6 in 2,2'-bipyridyl), 8.98 (s, 8H, pyrrole-Hβ), 8.92 (s, 8H, pyrrole-Hβ), 8.24 (dd, J_1=1.4Hz, J_2=4.0Hz, 2H, H5 in 2,2'-bipyridyl), 8.18 (d, J=8.1Hz, 12H, H2 in 4-tert-butylphenyl), 7.78 (d, J=8.1Hz, 12H, H3 in 4-tert-butylphenyl), 1.63 (s, 54H, CH3 in 4-tert-butylphenyl), -2.68 (br. s, 4H, inner-NH). UV-Vis (Methyl THF): λ_{max} = 422, 515, 550, 593, 648 nm. ESMS obsd 1566.8, calcd 1566.0 ($C_{110}H_{104}N_{10}$).

4,4'-bis-[5'-(10,15,20-tri-4-tert-butylphenyl)porphyrinatozinc(II)]-2,2'-bipyridine (Zn_2**2**). A sample of Bipyridine-Diporphyrin (**2**) (5.0mg, 3.2μmol) was treated identically as for Zn2 **1**, affording 5.1mg (95%) of a reddish solid. ^{1}H NMR (chloroform-d) δ 9.63 (s, 2H, H3 in 2,2'-bipyridyl), 9.06 (d, J=4.8Hz, 2H, H6 in 2,2'-bipyridyl), 9.03 (s, 8H, pyrrole-Hβ), 8.97 (s, 8H, pyrrole-Hβ), 8.23 (dd, J_1=1.4Hz, J_2=4.0Hz, 2H, H5 in 2,2'-bipyridyl), 8.17 (d, J=8.1Hz, 12H, H2 in 4-tert-butylphenyl), 7.76 (d, J=8.1Hz, 12H, H3 in 4-tert-butylphenyl), 1.63 (s, 54H, CH3 in 4-tert-butylphenyl). UV-Vis (Methyl THF): λ_{max} = 430, 557, 597 nm. ESMS obsd 1694.3, calcd 1693.0 ($C_{110}H_{100}N_{10}Zn_2$).

5-Mesityldipyrromethane (**3**). A mixture of pyrrole (18.8mL, 271mmol) and mesitaldehyde (2mL, 13.5mmol) was flushed with nitrogen for 15 min and then treated with TFA (0.11mL, 2.5mmol), and the mixture was stirred under nitrogen at room temperature for 1 hour and then quenched with triethylamine (0.5 ml). 100mL toluene were added, and the organic phase was washed with brine (2 x 50mL) and dried ($MgSO_4$). The solvent was removed under vacuum to give a black oil. Vacuum distillation removed the pyrrole to yield a highly colored solid that was washed with ethyl acetate. The solvent was evaporated until a solid began to form. Then 50ml cyclohexanes were added to precipitate a yellow solid that was filtered and recrystallized from ethanol/water (10:1) giving the yellow crystal (0.88g, 25%). ^{1}H NMR (chloroform-d) δ 7.95 (br, 2H), 6.87 (s, 2H), 6.67 (m, 2H), 6.19 (m, 2H), 6.02 (m, 2H), 5.93 (s, 1H), 2.29 (s, 3H), 2.07 (s, 6H).

5,5'-Bis(2,2'-dipyrromethyl)-2,2'-bipyridine (**4**). A mixture of pyrrole (6.5mL, 94mmol) and 2,2'-bipyridine-5,5'-dicarboxaldehyde (200mg, 0.94mmol) was flushed

with nitrogen for 15 min and treated with TFA (0.06mL, 0.75mmol). The solution darkened, and the mixture was stirred for 15 min. 0.1N aqueous NaOH (20mL) and 20mL ethyl acetate was added, and the layers were separated. The organic layer was washed with water (2 x 20mL). The combined organic layers were washed with brine, dried ($MgSO_4$), and vacuum distillation removed the pyrrole. Precipitation from hexane/ CH_2Cl_2 gave a yellow solid, which was filtrated and dried in vacuo (0.25g, 60%). ^1H NMR (chloroform-d / DMSO-d_6) δ 9.20 (br, 4H), 8.40 (s, 2H), 8.16 (d, J=8Hz, 2H), 7.52 (dd, J1=2Hz, J2=8Hz, 2H), 6.61 (m, 4H), 5.99 (m, 4H), 5.77 (s, 4H), 5.45 (s, 2H).

5-(p-tolyl)dipyrromethane (SI-1). A mixture of pyrrole (27.8mL, 400mmol) and p-tolualdehyde (2.36mL, 20mmol) was flushed with nitrogen for 15 min and treated with TFA (0.15mL, 2mmol), and the mixture was stirred for 15 min. 0.1N aqueous NaOH (50mL) and 100mL CH_2Cl_2 were added, and the layers were separated. The organic layer was washed with water (2 x 50mL). The combined organic layers were washed with brine, dried ($MgSO_4$), and vacuum distillation removed the excess pyrrole. Column chromatography [silica 40g, cyclohexane/ethyl acetate/triethylamine (80:20:1)] a reddish brown solid and dried in vacuo (4.0g, 85%). ^1H NMR (chloroform-d) δ 7.92 (br, 2H), 7.12 (s, 4H), 6.69 (m, 2H), 6.16 (m, 2H), 5.93 (s, 2H), 5.45 (s, 1H), 2.35 (s, 3H).

1,9-Bis(4-tert-butylbenzoyl)-5-(p-tolyl)dipyrromethane (SI-2). A solution of EtMgBr (25mL, 25mmol) was added slowly to a stirred, tap-water-cooled flask containing a solution of 5-(p-tolyl)dipyrromethane (**SI-1**, 1.2g, 5mmol) in dry THF (10 mL) under nitrogen. The mixture was stirred for 30 min at room temperature. An exothermic reaction with gas evolution ensued. Then a solution of 4-tert-butylbenzoyl chloride (4.9mL, 25 mmol) in THF (10mL) was added over 15 min. The solution

darkened, and the mixture was stirred for additional 2 hr. The reaction was quenched by adding saturated aqueous NH_4Cl (50mL). CH_2Cl_2 (100mL) was then added. The layers were separated. The organic layer was washed with water (2 x 50mL). The combined organic layers were washed with brine, dried ($MgSO_4$). The solvent was removed under reduced pressure to afford reddish brown oil. The crude product was then purified by column chromatography [silica 100g, CH_2Cl_2/ ethyl acetate (20:1) to (5:1)]. The fractions containing the desired diacyl dipyrromethane were collected. Removal of solvent afforded a pale yellow solid (1.1g, 40%). ^1H NMR (chloroform-d) δ 11.59 (br, 2H), 7.77 (d, J=8.4Hz, 4H), 7.45 (d, J=8.4Hz, 4H), 7.42 (d, J=7.7Hz, 2H), 7.18 (d, J=7.7Hz, 2H), 6.66 (m, 2H), 6.04 (m, 2H), 5.75 (s, 1H), 2.40 (s, 3H), 1.39 (s, 18H).

Dipyrromethanediol (SI-3). A sample of $NaBH_4$ (36mmol, 50 mol equiv) was added in small portions over 25 min to a stirred solution of 1,9-Bis(4-tert-butylbenzoyl)-5-(p-tolyl)dipyrromethane (**SI-2**, 400mg, 0.72mmol) in THF/methanol (3:1, 20mL) in a round-bottomed flask open to the atmosphere. A significant evolution of gas occurred throughout the course of this reaction. The process of the reaction was monitored by TLC [hexane/ethyl acetate (1:1)]. After the reaction was complete (about 50 min), the reaction was quenched with 30mL water and extracted with CH_2Cl_2 (2 x 25mL). The organic phase was isolated, wash with water (2 x 25mL), and dried (Na_2CO_3). Removal of solvent afforded the dicarbinol as a pale red foamlike solid. The dicarbinol is extremely unstable in air, so it should be used immediately for the porphyrin synthesis.

4,4'-Bis(2,2'-dipyrromethyl)-2,2'-bipyridine (SI-4). A mixture of pyrrole (6.5mL, 94mmol) and 2,2'-bipyridine-4,4'-dicarboxaldehyde (200mg, 0.94mmol) was flushed with nitrogen for 15 min and treated with TFA (0.06mL, 0.75mmol). The

solution darkened, and the mixture was stirred for 15 min. 0.1N aqueous NaOH (20mL) and 20mL ethyl acetate was added, and the layers were separated. The organic layer was washed with water (2 x 20mL). The combined organic layers were washed with brine, dried ($MgSO_4$), and vacuum distillation removed the excess pyrrole. Precipitation from hexane/ CH_2Cl_2 gave a yellow solid, which was filtrated and dried in vacuo (0.27g, 65%). ^1H NMR (chloroform-d) δ 8.53 (d, J=4.8Hz, 2H), 8.30 (s, 2H), 8.15 (br, 4H), 7.14 (dd, J1=1.5Hz, J2=4.8Hz, 2H), 6.74 (m, 4H), 6.17 (m, 4H), 5.95 (s, 4H), 5.54 (s, 2H).

A5.

Appendix

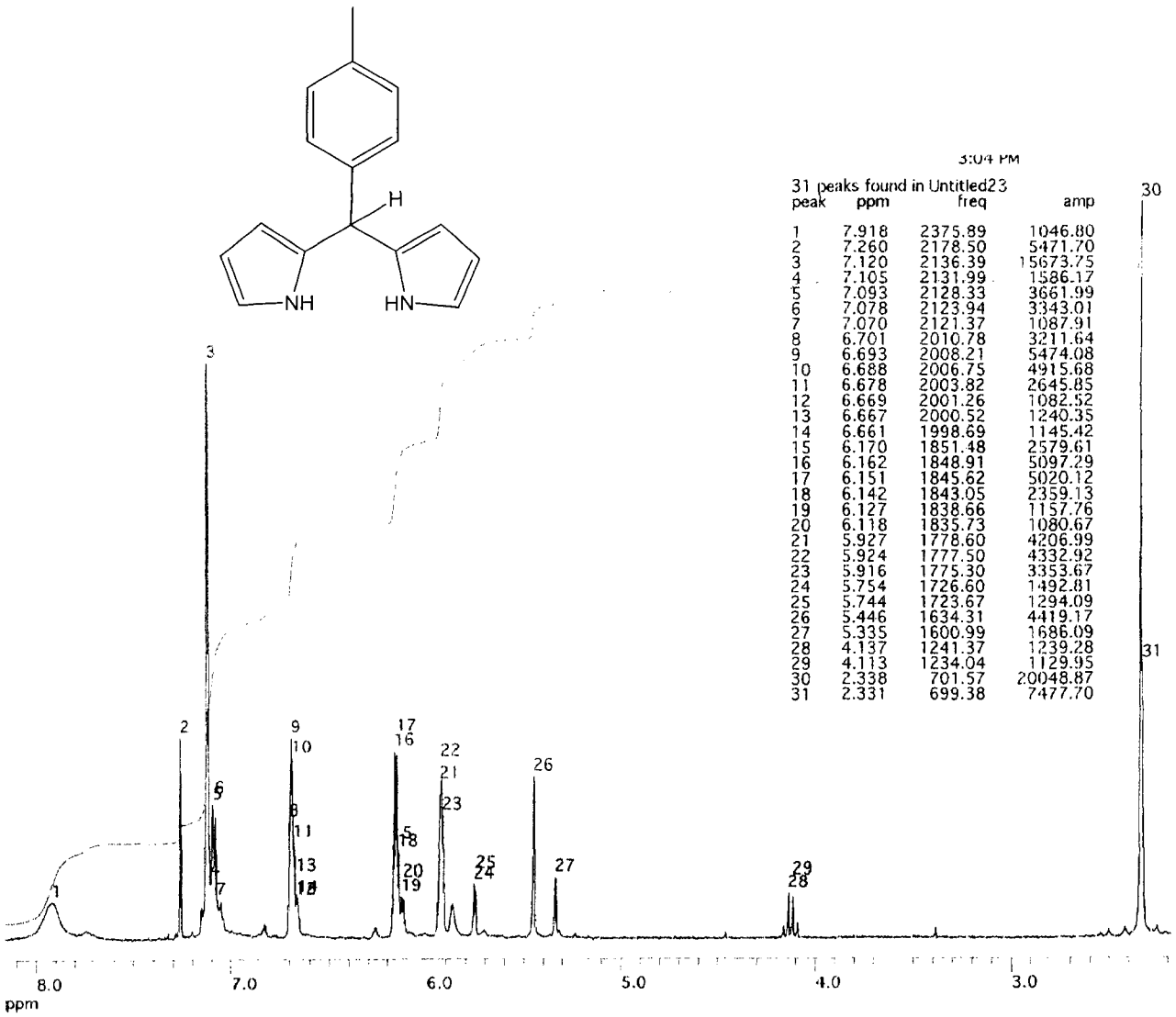

Figure A1. ^{1}H NMR (300 MHz, $CDCl_3$) of 5-(p-tolyl)dipyrromethane (SI-1).

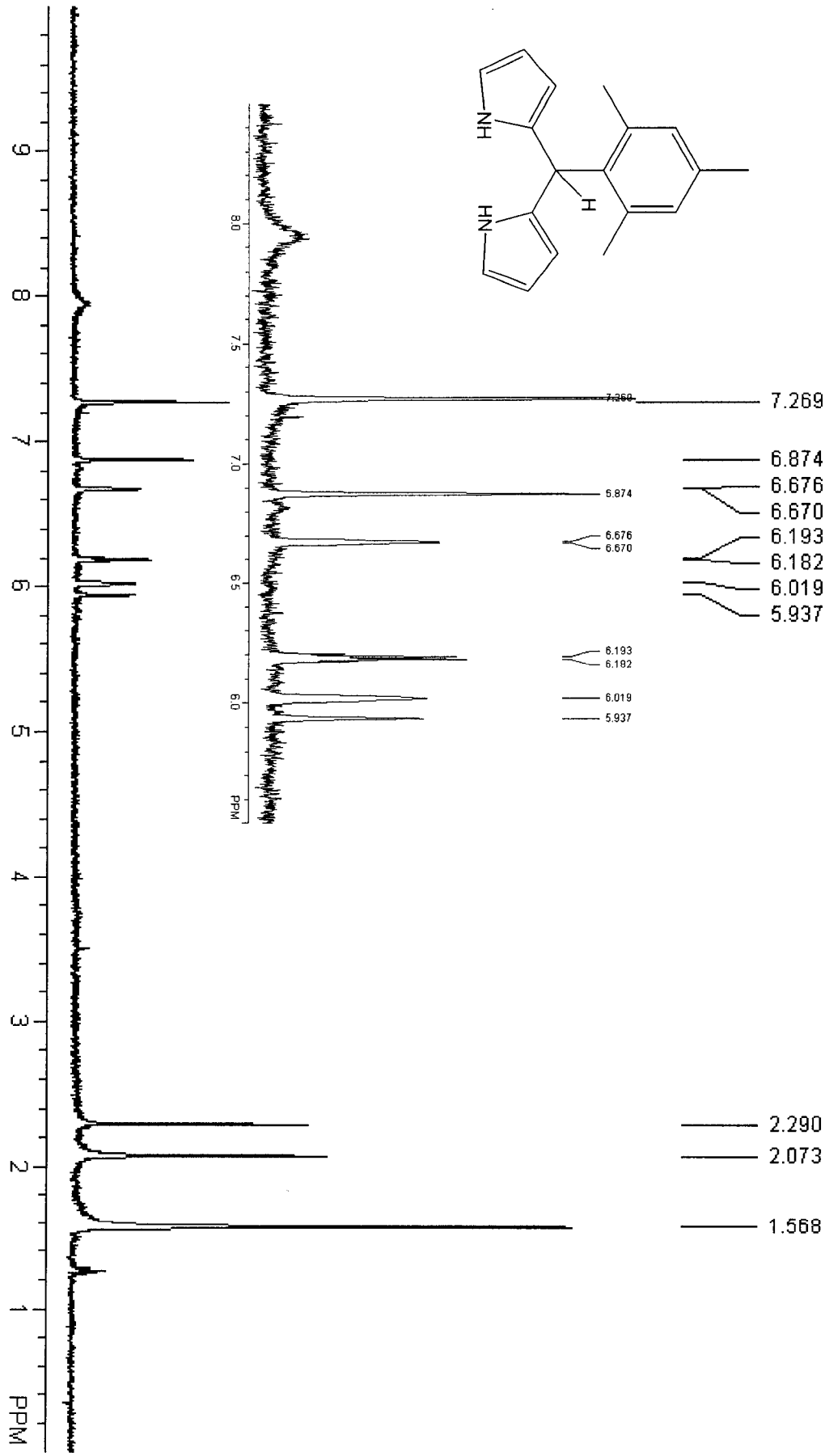

Figure A2. ^{1}H NMR (300 MHz, $CDCl_3$) of 5-Mesityldipyrromethane (3).

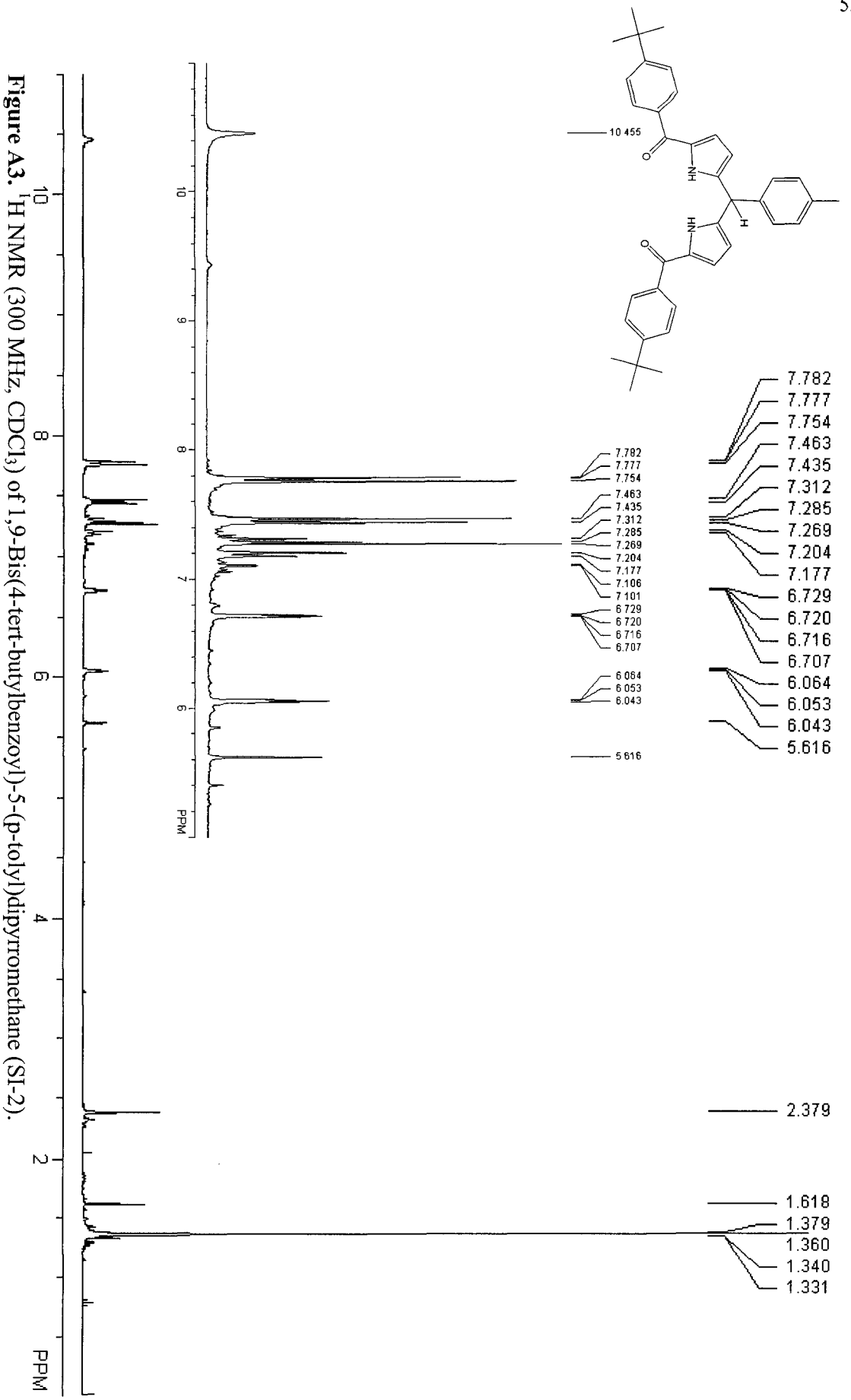

Figure A3. ^{1}H NMR (300 MHz, $CDCl_3$) of 1,9-Bis(4-tert-butylbenzoyl)-5-(p-tolyl)dipyrromethane (SI-2).

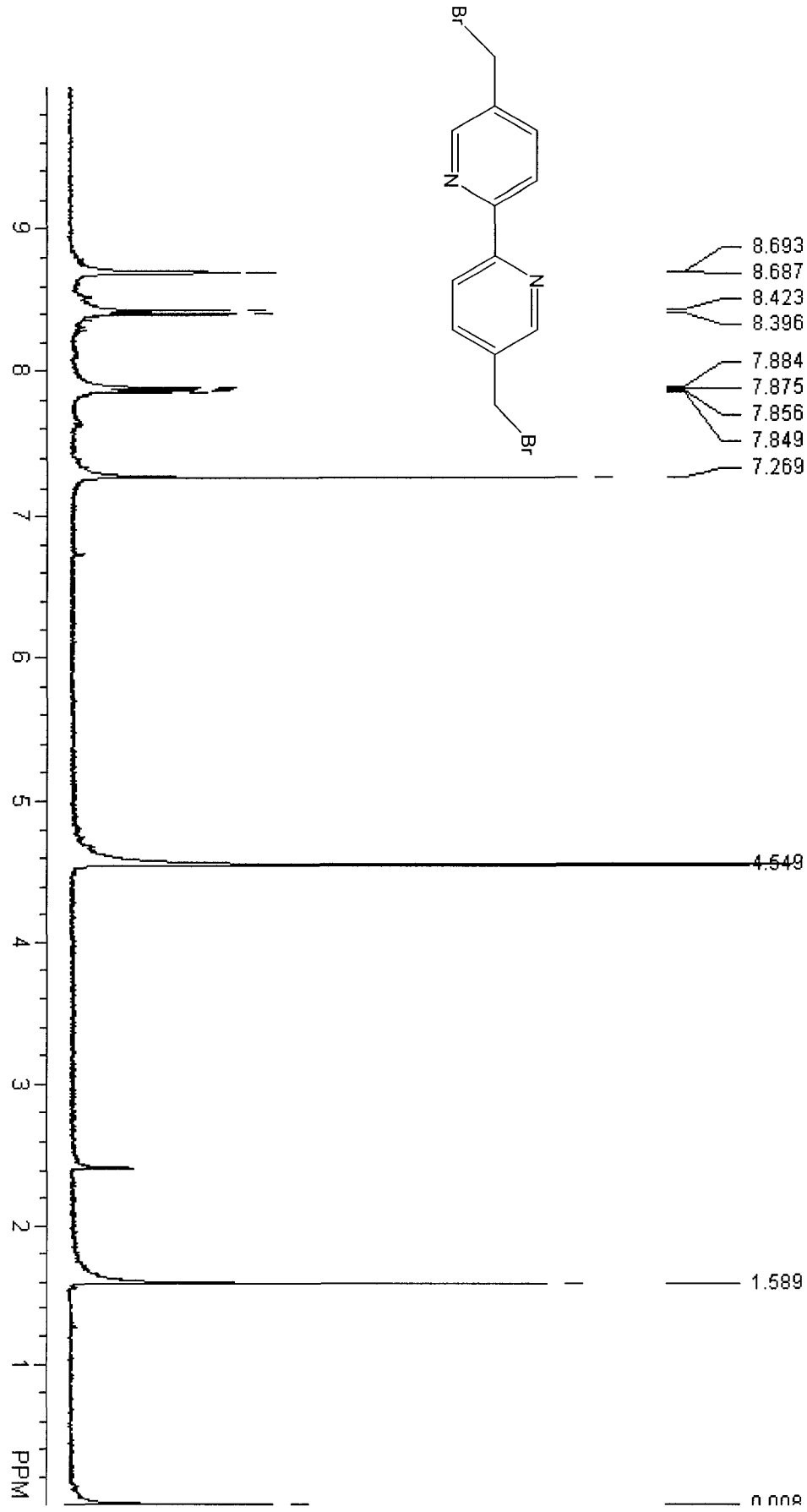

Figure A4. ^{1}H NMR (300 MHz, $CDCl_3$) of 5,5'-bromomethyl-2,2'-bipyridine.

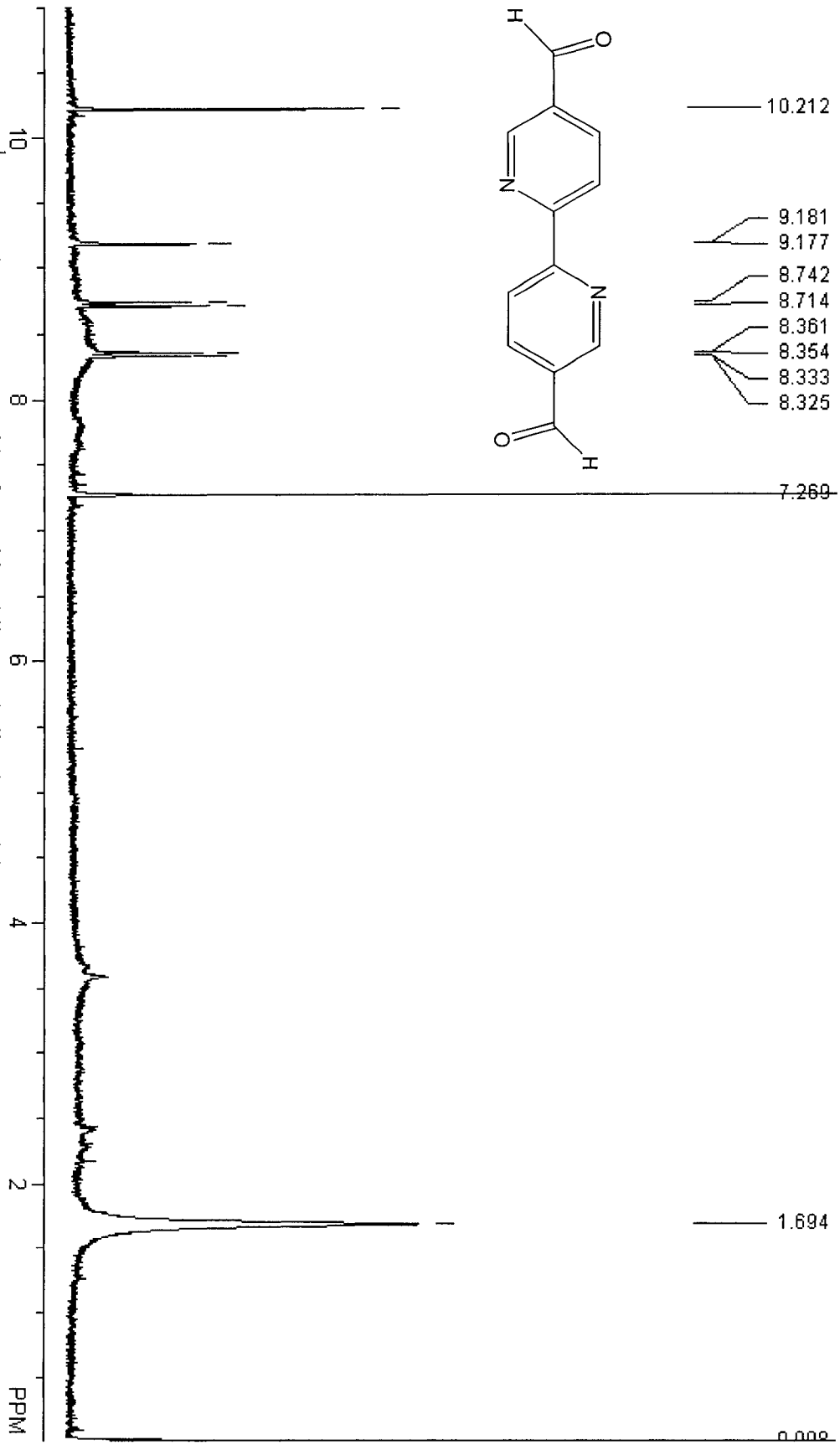

Figure A5. ^{1}H NMR (300 MHz, $CDCl_3$) of 2,2'-bipyridine-5,5'-dicarboxaldehyde.

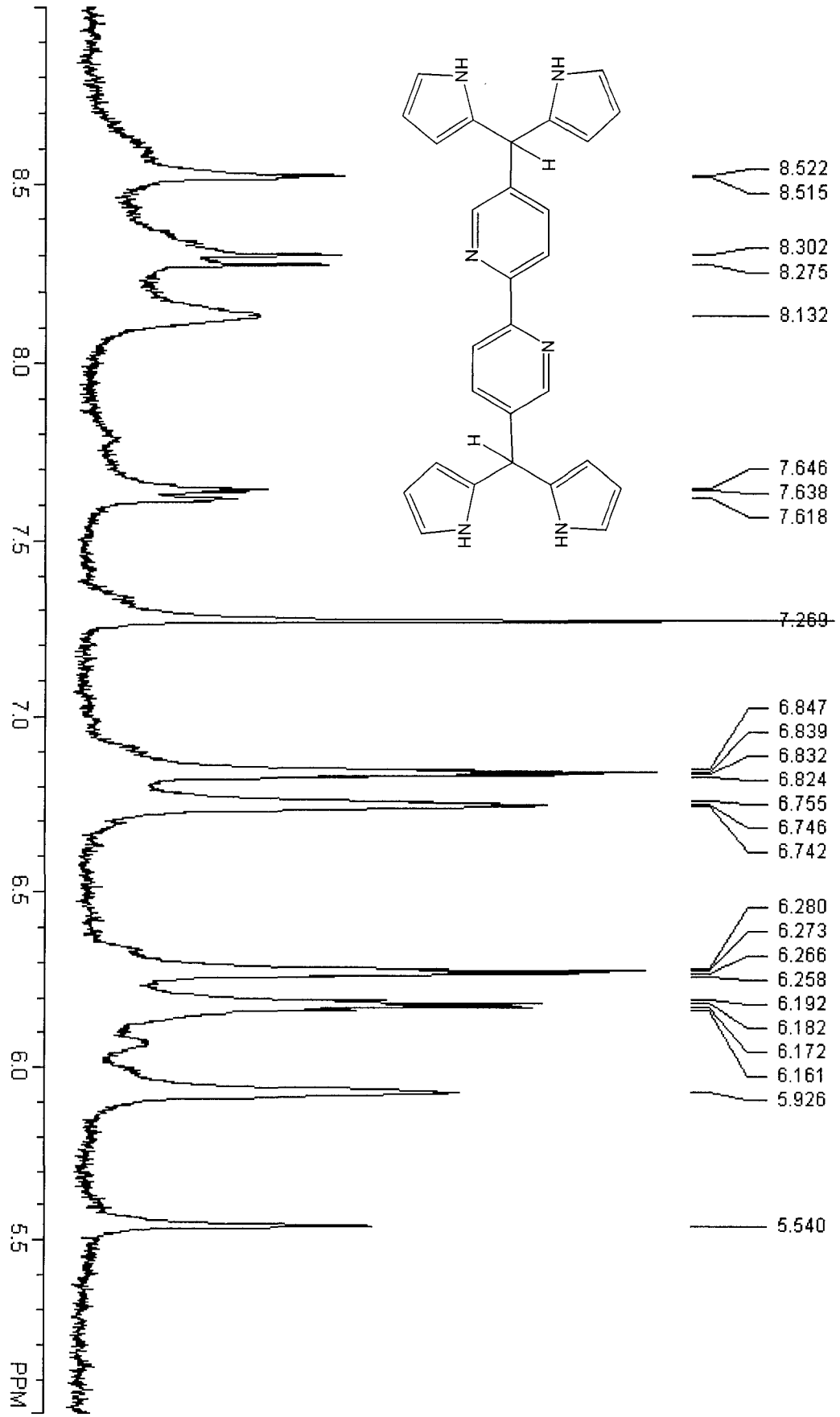

Figure A6. ^{1}H NMR (300 MHz, $CDCl_3$) of 5,5'-Bis(2,2'-dipyrromethyl)-2,2'-bipyridine (4).

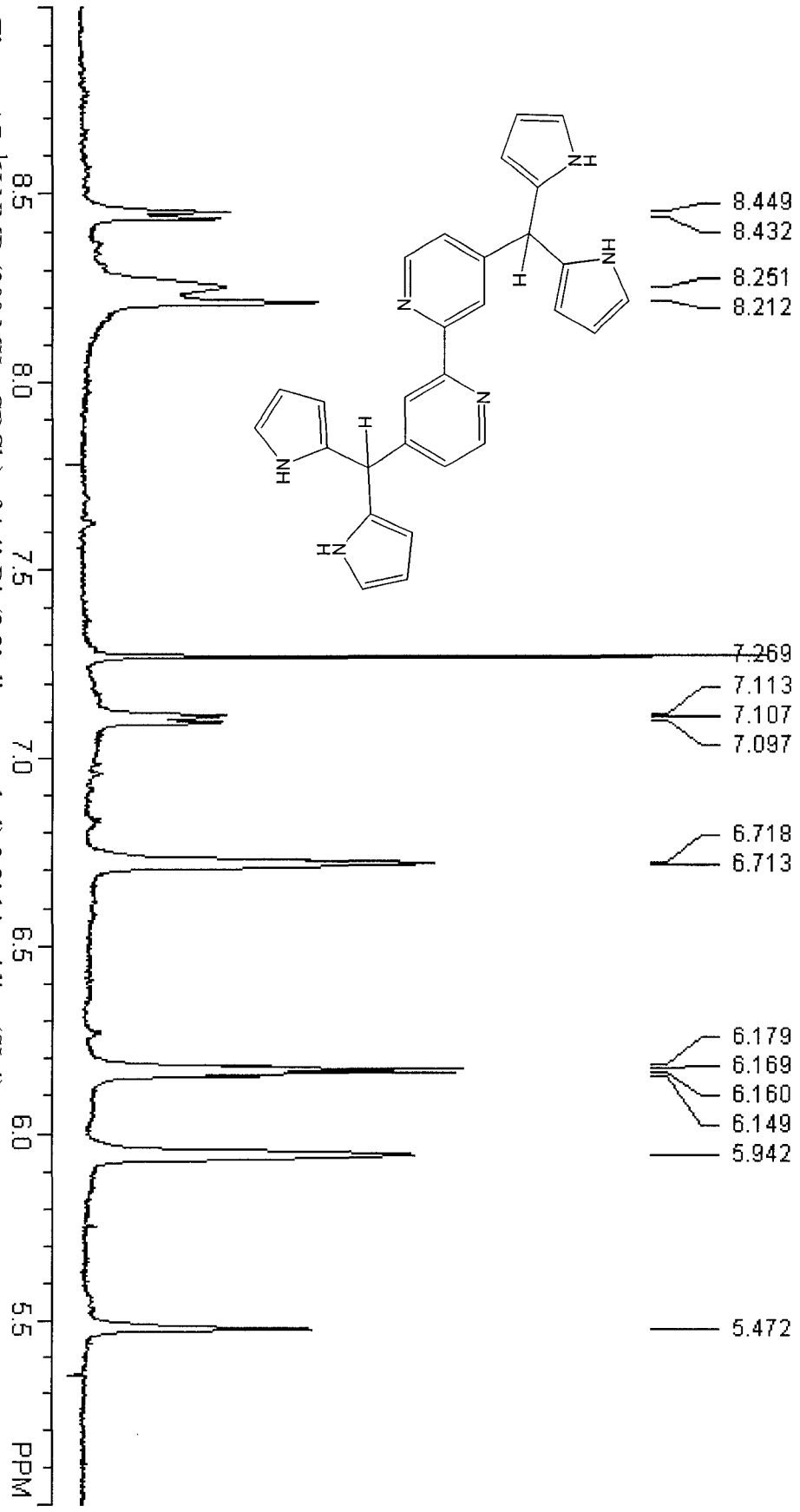

Figure A7. ^{1}H NMR (300 MHz, $CDCl_3$) of 4,4'-Bis(2,2'-dipyrromethyl)-2,2'-bipyridine (SI-4).

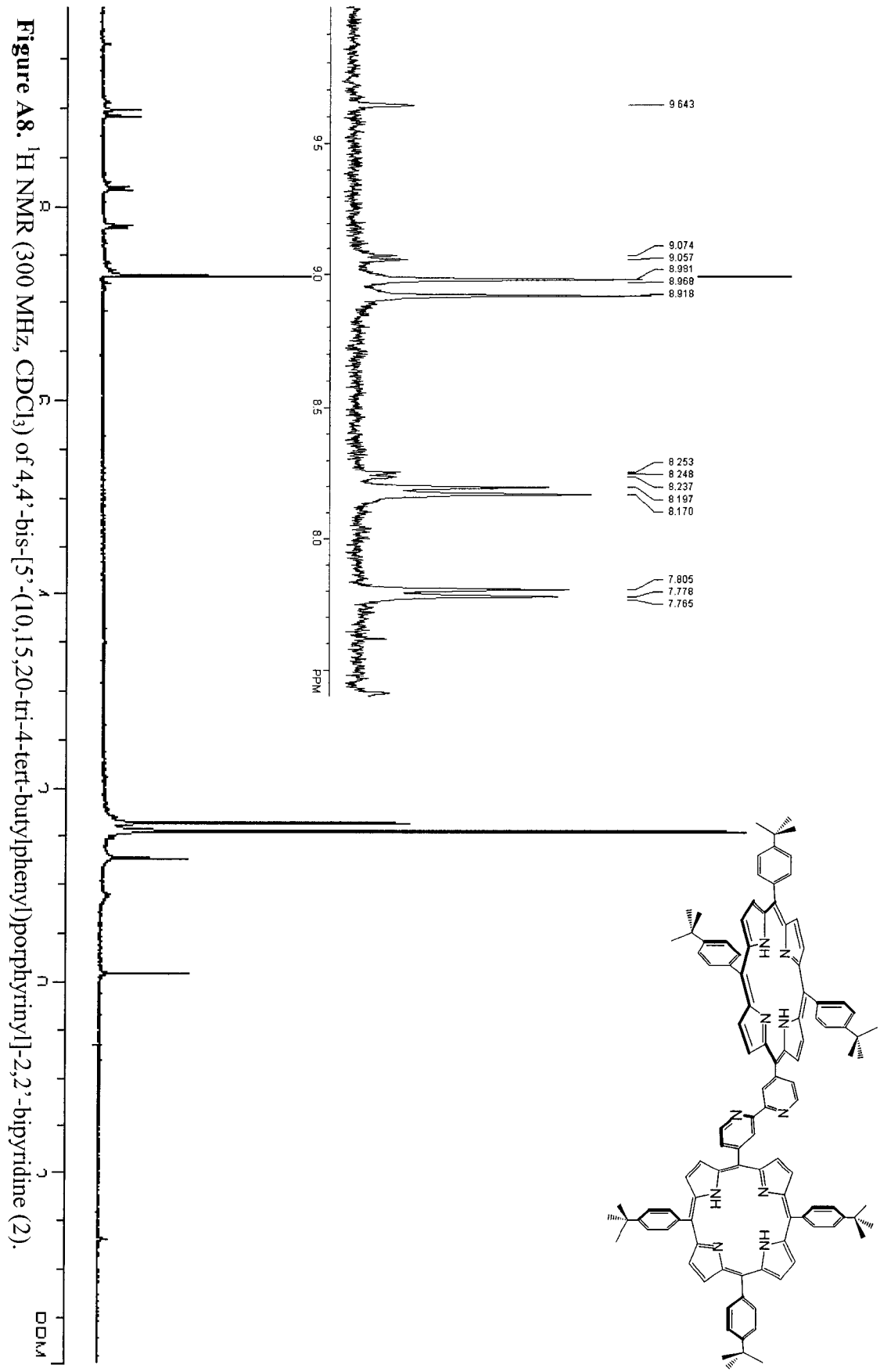

Figure A8. ^{1}H NMR (300 MHz, $CDCl_3$) of 4,4'-bis-[5'-(10,15,20-tri-4-tert-butylphenyl)porphyrinyl]-2,2'-bipyridine (2).

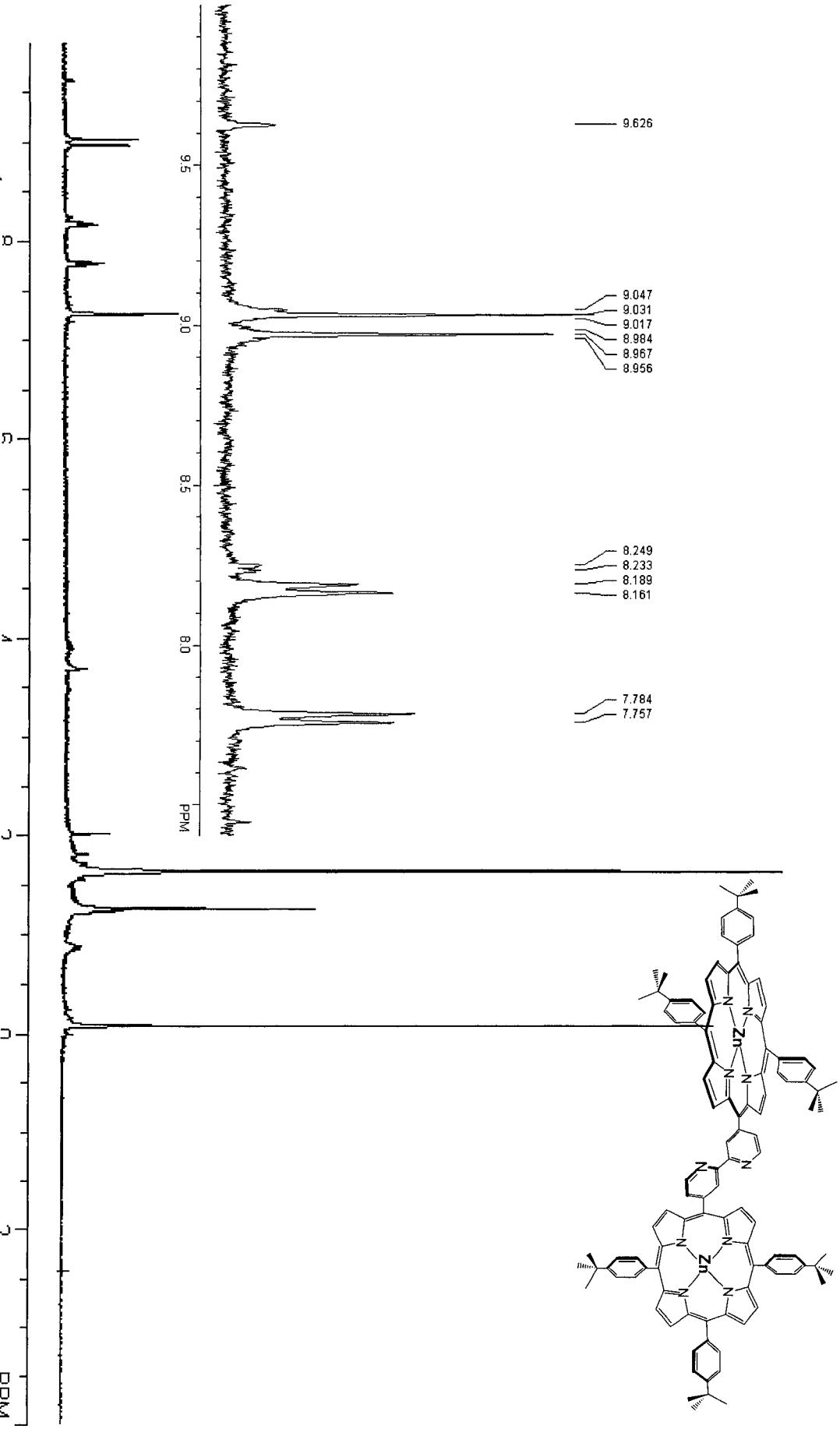

Figure A9. ^{1}H NMR (300 MHz, $CDCl_3$) of 4,4'-bis-[5'-(10,15,20-tri-4-tert-butylphenyl)porphyrinatozinc(II)]-2,2'-bipyridine ($Zn_2$2).

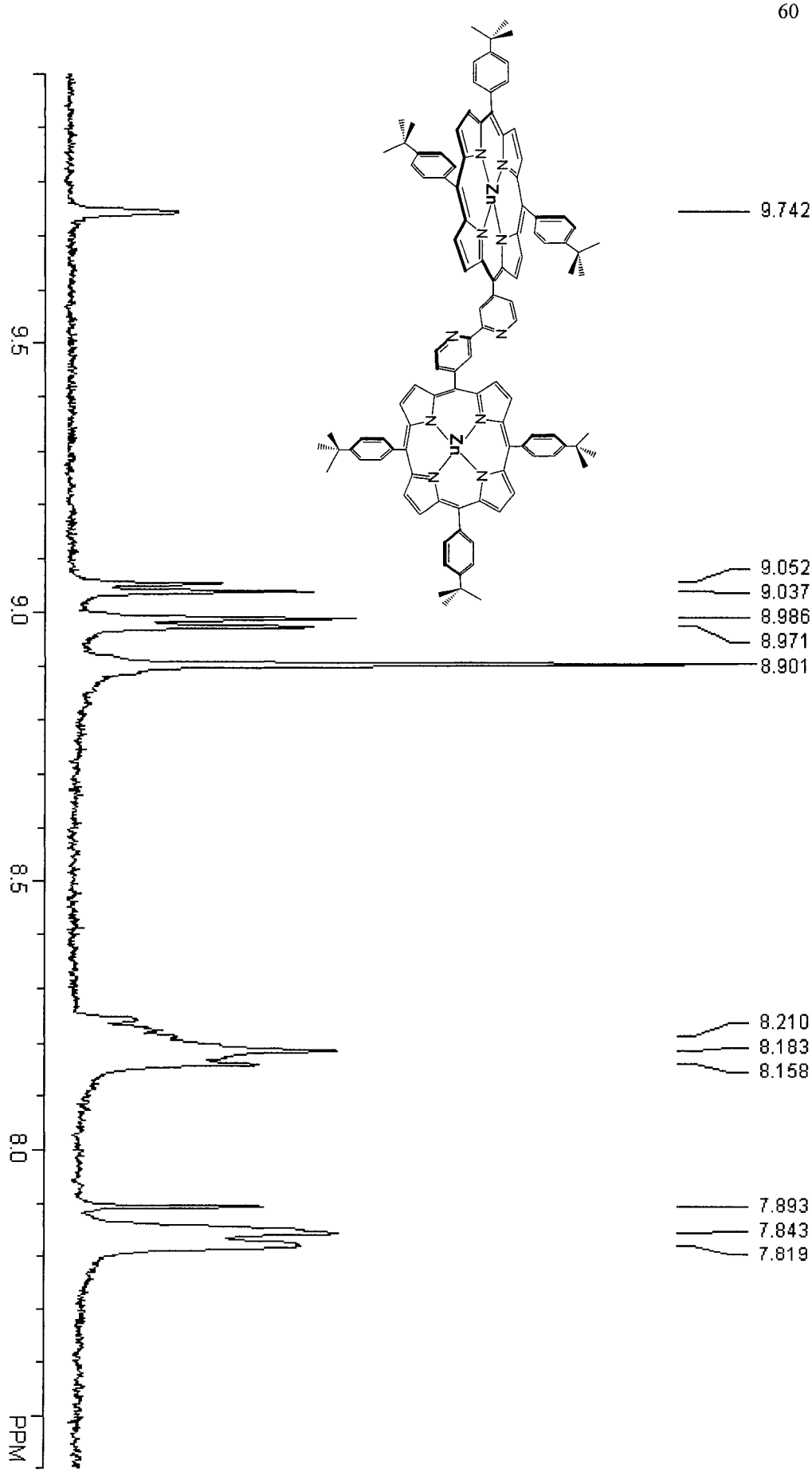

Figure A10. ^{1}H NMR (300 MHz, THF-d_8) of 4,4'-bis-[5'-(10,15,20-tri-4-tert-butylphenyl)porphyrinatozinc(II)]-2,2'-bipyridine ($Zn_2$2).

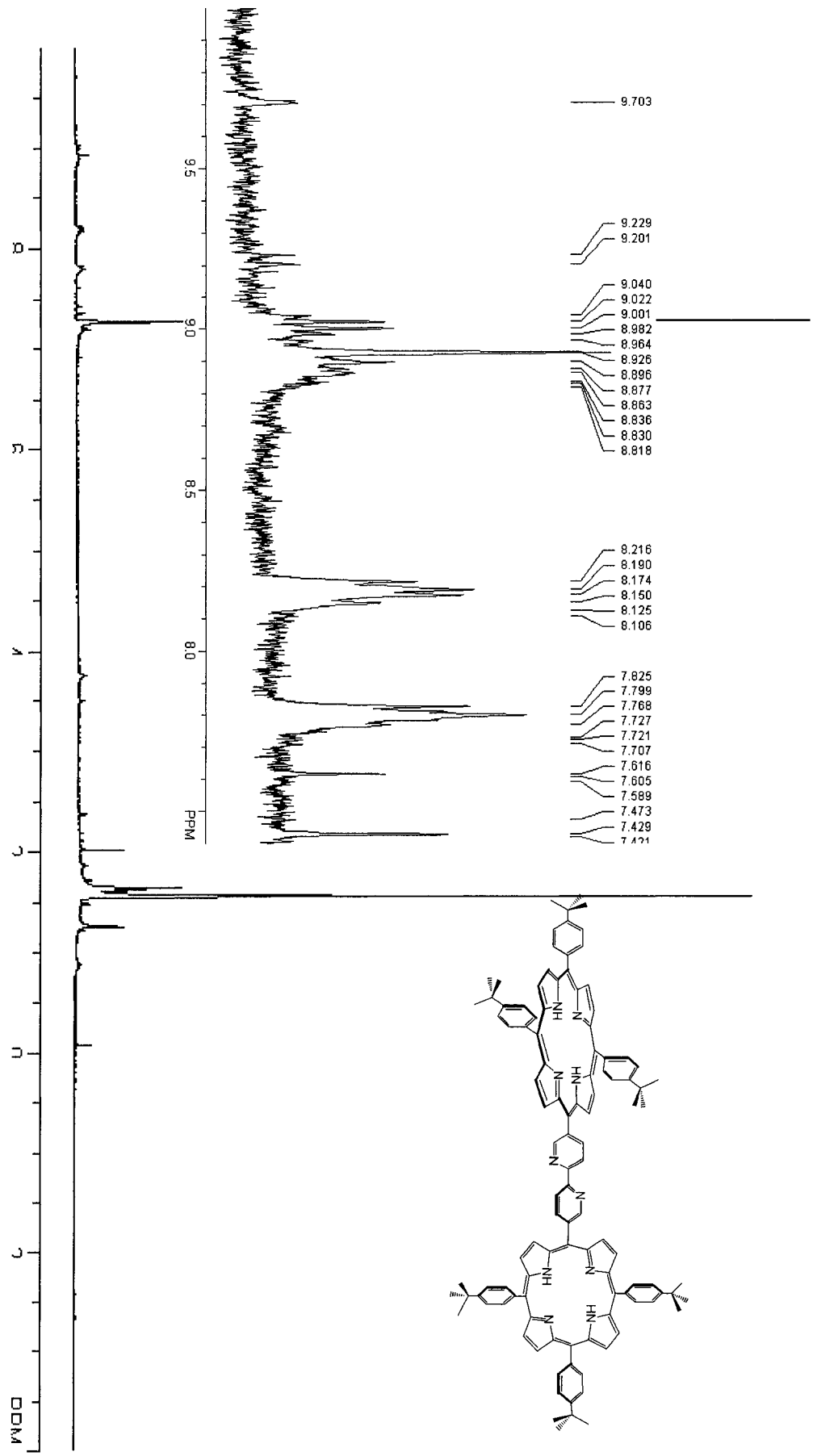

Figure A11. ^{1}H NMR (300 MHz, $CDCl_3$) of 5,5'-bis-[5'-(10,15,20-tri-4-tert-butylphenyl)porphyrinyl]-2,2'-bipyridine (1).

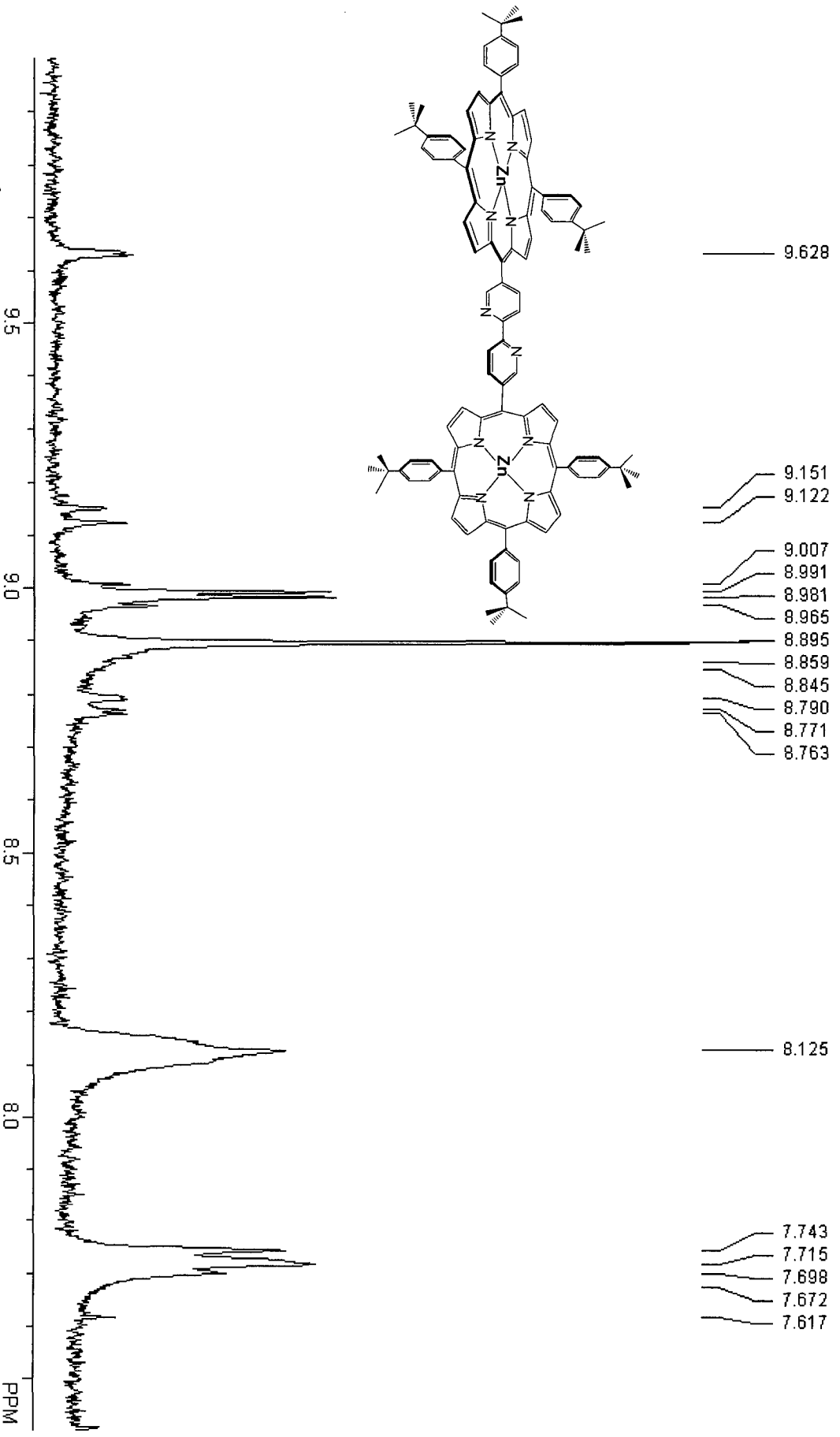

Figure A12. ^{1}H NMR (300 MHz, $CDCl_3$ / THF-d_8) of 5,5'-bis-[5'-(10,15,20-tri-4-tert-butylphenyl)porphyrinatozinc(II)]-2,2'-bipyridine ($Zn_2$1).

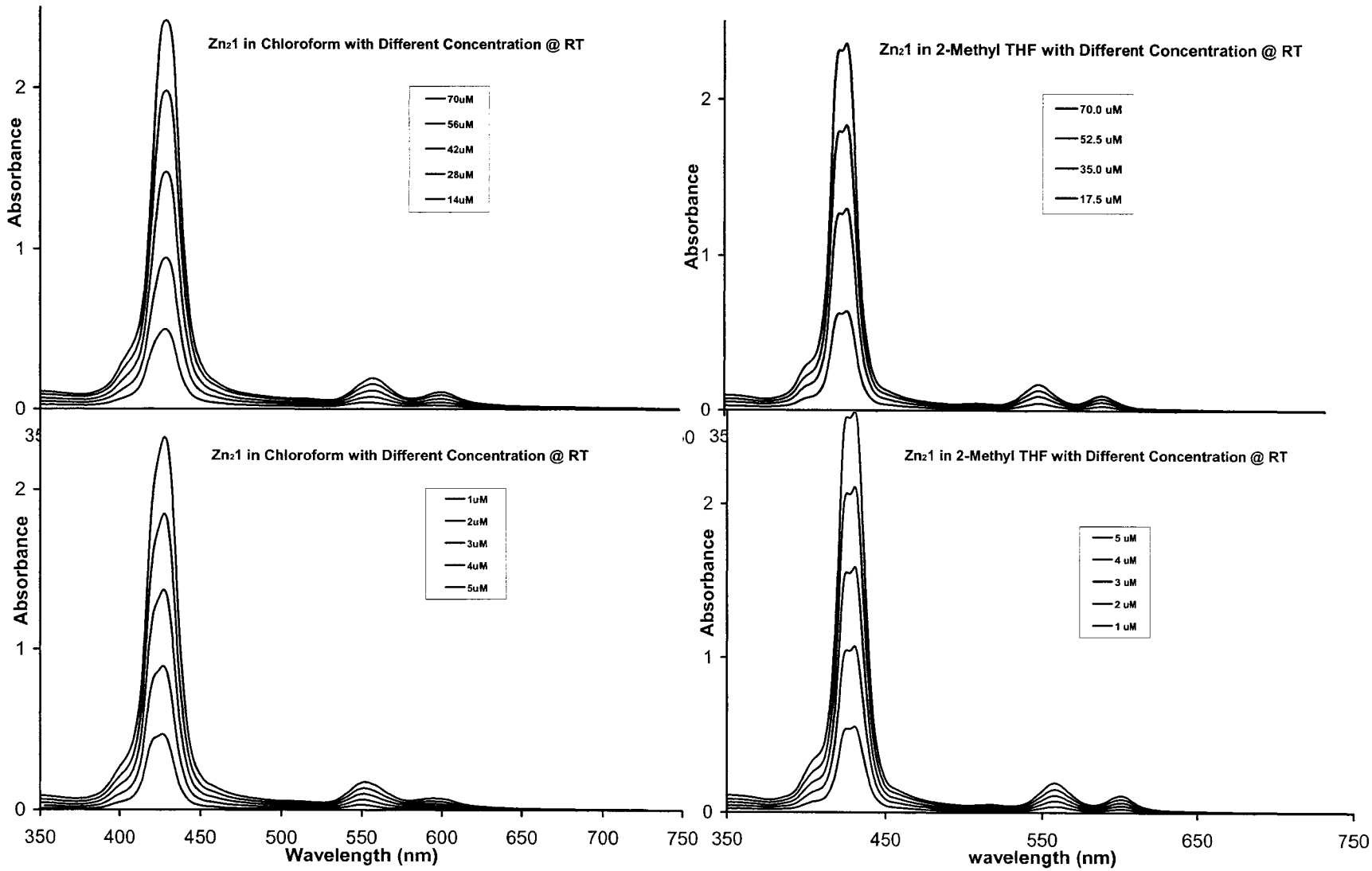

Figure A13. Dilution experiments show **Zn_21** forming aggregate in chloroform solution (~56 μM) but not in 2-methyl THF solution. Top spectra use a 1mm path cells and bottom use 1cm path cells.

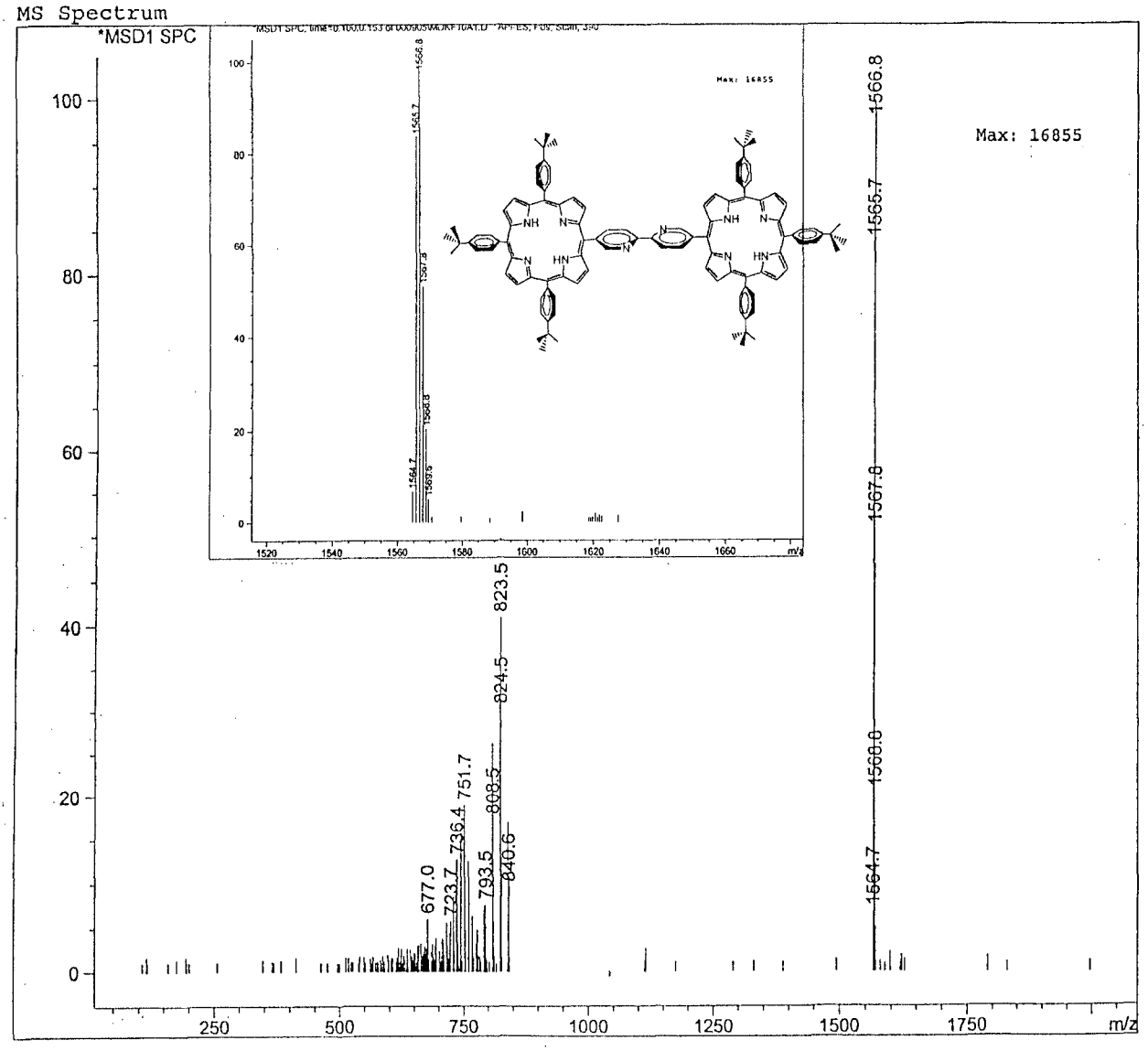

Figure A14. ESI-MS of 5,5'-bis-[5'-(10,15,20-tri-4-tert-butylphenyl)porphyrinyl]-2,2'-bipyridine (1).

A6.

Bibliography

(1) The Oxford English Dictionary, Vol. XII. 2nd Ed., Clarendon Press, Oxford **1989**, pp. 138-140.

(2) (a) Hückel, W. *Z. Phys.* **1931**, *70*, 204. (b) Hückel, W. *Z. Phys.* **1932**, *76*, 628. (c) Hückel, W. *Z. Electrochem.* **1937**, *9*, 725.

(3) (a) Vogel, E.; Haas, W.; Knipp, B.; Lex, J.; Schmickler, H. *Angew. Chem. Int. Ed. Engl.* **1998**, *27*, 406. (b) Lash, T. D. In the *Macmillan Encyclopedia of Chemistry*; Lagowski, J. J., Ed.; Simon and Schuster Macmillan: New York, **1997**, Vol. 3, pp. 1239-1245.

(4) Cyranski, M. K.; Krygowski, T. M.; Wisiorowski, M.; Hommes, N. J. R. van E.; Schleyer, P. von R. *Angew. Chem. Int. Ed. Engl.* **1998**, *37*, 177.

(5) Fischer, H.; Orth, H. *Die Chemie des pyrrols*, **1934-1940** Vols I-III, Akad. Verlagsges., Leipzig.

(6) For a thorough exposition of porphyrin nomenclature, see *Pur ε Appl. Chem.*, **1987**, *59*, 779.

(7) Fischer, H.; Walach, B. *Justus Liebigs Ann. Chem.* **1926**, *450*, 164.

(8) Rothemund, P.; Menotti, A. R. *J. Am. Chem. Soc.* **1941**, *63*, 267-270.

(9) Adler, A. D.; Longo, F. R.; Shergalis, W. *J. Am. Chem. Soc.* **1964**, *86*, 3145-3149.

(10) (a) Lindsey, J. S.; Schreiman, I. C.; Hsu, H. C.; Kearney, P. C.; Marguerettaz, A. M. *J. Org. Chem.* **1987**, *52*, 827-836. (b) Lindsey, J. S.; MacCrum, K. A.; Tyhonas, J. S.; Chuang, Y.-Y. *J. Org. Chem.* **1994**, *59*, 579-587. (c) Ravikanth, M.; Achim, C.; Tyhonas, J. S.; Munck, E.; Lindsey, J. S. *J. Porphyrins and Phthalocyanines* **1997**, *1*, 1385-1394.

(11) (a) Lash, T. D. *Angew. Chem. Int. Ed. Engl.* **1995**, *34*, 2533. (b) Lash, T. D. *J. Porphyrins and Phthalocyanines* **1997**, *1*, 29. (c) Lash, T. D.; Chandrasekar, P.; Osuma, A. T.; Chaney, S. T.; Spence, J. D. *J. Org. Chem.* **1998**, *63*, 8455.

(12) (a) Boudif, A.; Momenteau, M. *J. Chem. Soc. Perkin Trans. I* **1996**, 1235. (b) Boudif, A.; Momenteau, M. *J. Chem. Soc. Chem. Commun.* **1994**, 2069. (c) Nguyen, L.T.; Senge, M. O.; Smith, R. M. *J. Org. Chem.* **1996**, *61*, 998. (d) Heo, P.-Y.; Shin, K.; Lee, C.-H. *Tetrahedron Lett.* **1996**, *37*, 197. (e) Lee, C.-H.; Kim, H.-J. *Tetrahedron Lett.* **1997**, *38*, 3935. (f) Kai, S.; Suzuki, M.; Masaki, Y. *Tetrahedron Lett.* **1998**, *39*, 4063.

(13) Drain, C. M.; Gong, X. *Chem. Commun.* **1997**, 2117-2118.

(14) Alivisatos, A. P.; Barbara, P.F.; Castleman, A. W.; Chang, J.; Dixon, D. A.; Klein, M.L.; McLendon, G. L.; Miller, J. S.; Ratner, M. A.; Rossky, P. J.; Stupp, S. I.; Thompson, M. E. *Adv. Mater.* **1998**, *10*, 1297-1336.

(15) Kalyanasundaram, K.; Grätzel, M. *Coord. Chem. Rev.* **1998**, *177*, 347-414.

(16) Fungo, F.; Otero, L. A.; Sereno, L.; Silber, J. J.; Durantini, E. N. *J. Mater. Chem.* **2000**, *10*, 645-650.

(17) Goossens, A.; Schaafsma, T. J.; Wienke, J. *J. Phys. Chem. B* **1999**, *103*, 2702-2708.

(18) Gust, D.; Moore, T. A.; Moore, A. L. *Acc. Chem. Res.* **2001**, *34*, 40-48.

(19) Milgrom, L. R. *J. Chem. Soc. Perkin Trans. 1* **1984**, 1483-1487.

(20) Wasielewski, M. R.; Wiederrecht, G. P.; Svec, W. A.; Niemcyzk, M. P. *Solar Energy Materials and Solar Cells* **1995**, *38*, 127-134.

(21) Dagani, R. *Chem. Engin. News* **1998**, *76*, 35-46.

(22) Dagani, R. *Chem. Engin. News* **1998**, *76*, 70-78.

(23) Dagani, R. *Chem. Engin. News* **2000**, *78*, 1-19.

(24) Burrell, A.; Officer, D.; Plieger, P.; Reid, D. *Chem. Rev.* **2001**, *101*, 2751-2796.

(25) Milic, T. N.; Chi, N.; Yablon, D. G.; Flynn, G. W.; Batteas, J. D.; Drain, C. M. *Angew. Chem. Int. Ed.* **2002**, *41*, 2117-2119.

(26) Drain, C. M. *Proc. Natl. Acad. Sci., USA* **2002**, *99*, 5178-5182.

(27) Drain, C. M.; Batteas, J. D.; Flynn, G. W.; Milic, T.; Chi, N.; Yablon, D. G.; Sommers, H. *Proc. Natl. Acad. Sci., USA* **2002**, *99*, 6498-6502.

(28) Drain, C. M.; Mauzerall, D. *Biochemistry and Bioenergetics.* **1990**, *24*, 263-268.

(29) Kaes, C.; Katz, A.; Hosseini, M. W. *Chem. Rev.* **2000**, *100*, 3553-3590.

(30) Goldberg, I. *Chem. Eur. J.* **2000**, *6*, 3863-3870.

(31) Diskin-Posner, Y.; Dahal, S,; Goldberg, I. *Angew Chem. Int. Ed.* **2000**, *39*, 1228-1292.

(32) Kumar, R. K.; Balasubramanian, S.; Goldberg, I. *Inorg. Chem.* **1998**, *37*, 541-552.

(33) Kumar, R. K.; Diskin-Posner, Y.; Goldberg, I. *J. Incl. Phenom. Marcocyclic Chem.* **2000**, *37*, 219-230.

(34) Harriman, A.; Sauvage, J.-P. *Chem. Soc. Rev.* **1996**, 41-46.

(35) Collinson, S. R.; Bruce, D. W. In *Transition Metals in Supramolecular Chemistry*; Sauvage, J. P., Ed.; John Wiley & Sons Ltd., 1999, pp 285-368.

(36) Chambron, J.-C.; Heitz, V.; Sauvage, J.-P. In *The Porphyrin Handbook*; Kadish, K. M., Smith, K. M., Guilard, R., Eds.; Academic Press: New York, 2000; Vol. 6, pp 1-42.

(37) Kosal, M. E.; Chou, J.-H.; Nalwa, H. S.; Rakow, N. A.; Suslick, K. S. *Applications of porphyrins and metalloporphyrins to materials chemistry*; Academic Press: New York, 2000; Vol. 6.

(38) Prodi, A.; Keleverlaan, C. J.; Indelli, M. T.; Scandola, F.; Alessio, E.; Iengo, E. *Inorg. Chem.* **2001**, *40*, 3498-3504.

(39) Tomohiro, Y.; Satake, A.; Kobuke, Y. *J. Org. Chem.* **2001**, *66*, 8442-8446.

(40) Drain, C. M.; Lehn, J.-M. *Chem. Commun.* **1994**, 2313-2315.

(41) Drain, C. M.; Nifiatis, F.; Vasenko, A.; Batteas, J. *Angew. Chem. Int. Ed.* **1998**, *37*, 2344-2347.

(42) Lehn, J.-M. *Chem. Eur. J.* **2000**, *6*, 2097-2102.

(43) Funeriu, D. P.; Lehn, J.-M.; Fromm, K. M.; Fenske, D. *Chem. Eur. J.* **2000**, *6*, 2103-2111.

(44) Linke, M.; Chambron, J.-C.; Heitz, V.; Sauvage, J.-P.; Semetey, V. *Chem. Commun.* **1998**, 2469-2470.

(45) Ebmeyer, F.; Vogtle, F. *Chem. Ber.* **1989**, *122*, 1725-1727.

(46) Al-Sayah, M. H.; Salameh, A. S. *Arabian J. Sci. Engineering* **2000**, *25*, 67-70.

(47) Adler, A. D.; Longo. F. R.; Finarelli, J. D.; Goldmacher, J.; Assour, J.; Korsakoff, L. *J. Org. Chem.* **1967**, *32*, 476.

(48) Rao, P. D.; Dhanalekshmi, S.; Littler, B. J.; Lindsey, J. S. *J. Org. Chem.* **2000**, *65*, 7323-7344.

(49) Gryko, D.; Lindsey, J. S. *J. Org. Chem.* **2000**, *65*, 2249-2252.

(50) Geier, G. R.; Littler, B. J.; Lindsey, J. S. *J. Chem. Soc., Perkin Trans. 2* **2001**, *2*, 701-711.

(51) Lindsey, J. S.; Lee, C.; Miller, M. A.; Littler, B. J.; Kim, H.; Cho, W. *J. Org. Chem.* **1999**, *64*, 7890-7901.

(52) Littler, B. J.; Lindsey, J. S.; Miller, M. A.; Hung, C. H.; Wagner, R. W.; O'Shea, D. F.; Boyle, P. D. *J. Org. Chem.* **1999**, *64*, 1391-1396.

(53) Shi, X.; Barkigia, K. M.; Fajer, J.; Drain, C. M. *J. Org. Chem.* **2001**, *66*, 6513-6522.

(54) Drain, C. M.; Shi, X.; Milic, T.; Nifiatis, F. *Chem. Coummun.* **2001**, 287-288.

(55) Gouterman, M. *The Porphyrins*; Dolphin, D., Ed.; Acadermic Press: New York, **1978**; Vol. 3, pp. 1-165.

(56) (a) Melinda, H. K.; Kurt, D. B.; Joseph, T. H. *Coord. Chem. Rev.* **2000**, *205*, 201-228. (b) Fujita, M.; Yazaki, J.; Ogura, K. *J. Am. Chem. Soc.* **1990**, *112*, 5645-5647.

(57) Anderson, H. L. *Inorg. Chem.* **1994**, *33*, 972-981.

(58) Taylor, P. N.; Anderson, H. L. *J. Am. Chem. Soc.* **1999**, *121*, 11538-11545.

(59) Xu, W.; Guo, H.; Akins, D. L. *J. Phys. Chem. B* **2001**, *105*, 1543-1546.

(60) Abrahams, B. F.; Hoskins, B. F.; Michall, D. M.; Robson, R. *Nature* **1994**, *369*, 727-729.

(61) Burrell, A. K.; Officer, D. L.; Reid, D. C. W. *Angew. Chem. Int. Ed.* **1995**, *34*, 900-902.

(62) Iengo, E.; Zangrando, E.; Minatel, R.; Alessio, E. *J. Am. Chem. Soc.* **2002**, *124*, 1003-1013.

(63) Lindsey, J. S.; Prathapan, S.; Johnson, T. E.; Wagner, R. W. *Tetrahedron* **1994**, *50*, 8941-8968.

(64) Prathapan, S.; Johnson, T. E.; Lindsey, J. S. *J. Am. Chem. Soc.* **1993**, *115*, 7519-7520.

(65) Milgrom, L. R. *The Colours of Life: An Introduction to the Chemistry of Porphyrins and Related Compounds*; Oxford University Press: New York, 1997.

(66) Arsenault, G. P.; Bullock, E.; MacDonald, S. F. *J. Am. Chem. Soc.* **1960**, *82*, 4384-4389.

(67) Küster, W. *Hoppe-Seyler's Z. Physiol. Chem.* **1912**, *82*, 463.

Part B:

Hierarchical Self-assembly of Photonic Materials: Synthesis and Characterization of Porphyrazine-Porphyrazine Dimers and Porphyrazine-Porphyrin Tetramers

B1.

Introduction

1.1. What are the porphyrazines?

Porphyrazines, a member of teraazaporphyrins where the *meso* positions are nitrogens, have received considerably less attention since their first synthesis almost fifty years ago (scheme 1.1.1.).[1] The recent renaissance in porphyrazine chemistry is largely due to new synthetic strategies and the introduction of efficient syntheses of soluble derivatives pioneered by the Hoffman – Barret Team.[2-7] The electron rich

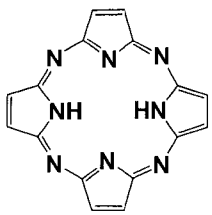

Porphyrazine

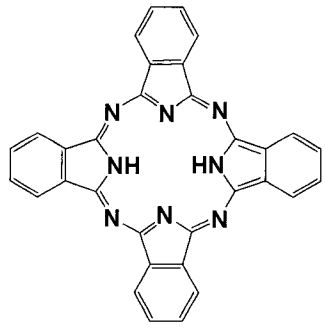

Phthalocyanine

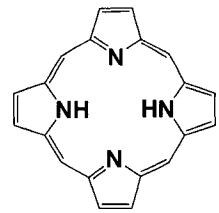

Porphyrin

Scheme 1.1.1. Structure of porphyrazine, phthalocyanine and porphyrin.

porphyrazines have substantially different photophysical and chemical properties, and these properties may make them suitable for a diverse array of materials. Porphyrins and porphyrazines coordinate an extensive range of metal ions within their central cavities. In contrast to porphyrins, *meso*-substitution of nitrogen in tetraazaporphyrins modulates the electronic character of the macrocycle. Combining the electronic character and extended π-system of porphyrazines with peripheral metal coordination permits the preparation of a wide variety of multimetallic complexes and serves as a logical building block for supramolecular chemistry. Combination with porphyrin derivatives, for example, results in arrays consisting of two different chromophores.[8-10]

1.2 Porphyrazines synthesis

Porphyrazines are built up from four pyrrole subunits and four bridging nitrogens. Similar to the porphyrin aromatic core, the aromatic macrocycle is ruled by Hückel [4n+2] for aromaticity.[11-13] Similar to the metallophthalocyanine synthesis, the unsubstituted metallo parent Pz macrocycle was generally synthesized by template reaction involving four maleic dinitrile molecules and a divalent metal ion.[1] The low solubility and yield of the parent macrocycle together with the instability of the unsubstituted maleic dinitrile starting materials inhibited the development of the porphyrazine chemistry. However, the Hoffman-Barret Team found that the peripherally substituted porphyrazines are more soluble and convenient than the parent molecule, and can be made using stable di-substituted maleic dinitriles in the template reaction.[2-7,14] By applying the Linstead magnesium alkoxide templated macrocyclization reaction in a refluxing alcohol solvent, a variety of porphyrazines have been synthesized in good yield with substituents on the eight pyrrole positions.[15] To enhance the solubility of the macrocycle and permit the chromatographic separation of the dye mixtures, a nonpolar long alkyl or 4-*tert*-butylphenyl groups are often used. The disubstituted maleic dinitriles become the pyrroles and so each pyrrole bears the same substituent on each β position. Similar to the mixed aldehydes porphyrin synthesis, the crossover macrocyclization of equimolar quantities of two different maleonitrile derivatives produce a mixture of six Pz macrocycle molecules, where the pyrroles bear different moieties. For two different maleic dinitriles A and B the six compounds are: AAAA, BBBB, AAAB, BBBA, AABB, ABAB in terms of pyrrole subunits. The yield of each isomer is weighted by the reaction

conditions and the structure of the maleonitrile derivatives. Presumably, steric hindrance reduces the formation of the cis isomers.

1.3 Electronic absorption spectroscopy of porphyrazines

Pz optical spectra are somewhat analogous to porphyrin spectra. The electronic absorption spectra of all porphyrazine derivatives have two main bands: an intense B (Soret) band (π-π^*) at $\lambda < 400$ nm and a Q band (π-π^*) at $\lambda > 600$ nm, for the parent metallomacrocycle, there are more Q absorption bands in lower symmetry macrocycle such as free base Pz (D_{2h}) than the higher symmetry metalloporphyrazine such as Ni(Pz) (D_{4h}). These observations in the electronic spectra are consisted with the Gouterman four-orbital model.[16] In a D_{4h}-synmetric marcocycle, the lowest unoccupied molecular orbital (LUMO) is a doubly degenerate e_g. The B and Q bands of the marcocycle are assigned to the transitions from two highest occupied molecular orbitals ($HOMO_s$) (a_{1u}, a_{2u}) into the e_g. In a lower symmetric macrocycle such as H_2(Pz) (D_{2h}), the observed splitting of the Q bands are caused by the reduction of the degeneracy of the $LUMO_s$ (e_g) and results in the splitting of Q into Q_x and Q_y bands at about 710 cm^{-1}.[17,18] The symmetrically substituted porphyrazines such as octakis(dimethylamino) porphyrazine shows a Soret band at 334nm and two broad peaks at 522 and 705 nm.[6] Compared with the parent macrocycle, these absorption peaks are larger broader, and red shifted due to the n-π^* transitions of the lone pairs electrons on the dimethylamino nitrogens to the aromatic macrocycle core. The peak at 522nm is assigned as the n-π^* transition of the

meso nitrogens into the plane of the macrocycle core and 705nm is the π-π^* transition Q bands.[6,19]

For unsymmetricly substituted porphyrazines, the introduction of heteratoms to the periphery of these macrocycles also results in adding n-π^* transitions which either broaden the Q band or add additional absorbance bands to the electronic spectra. The absorption patterns depend on the geometries of the substituted groups and are predicted by the Gouterman four-orbital model.[16] For the Ni[Pz(a:b_3)] system, the point group is C_{2v}, so the splitting profile of the Q bands is expected to reflect the change in symmetry from D_{4h} (Ni[Pz(a_4)] system) to C_{2v} with non-degenerated e_g. In the case of Ni[Pz(a_2:b_2)] system, there are two isomers (cis and trans), and the patterns of the electronic spectra are totally different. The trans isomers have a D_{2h} point group with two different substituents in the "x" and "y" direction in the aromatic core, which splits the two $LUMO_s$ (e_g) further apart and results in large splitting of the Q bands. Typically the splitting of the Q bands is about four time larger than free base porphyrazines.[18,20] On the other hand, the C_{2v} symmetry of cis isomers show only one Q band because the substituents along the "x" and "y" directions in the macrocycle are the same in the four-orbital picture. So, the $LUMO_s$ are accidentally degenerate and give rise to a single observed Q band. When the cis isomers are de-metallated to cis free base porphyrazines, the splitting of the Q bands will be recovered since the symmetry is changed from D_{4h} to D_{2h}.[18,20]

1.4 Porphyrazine multimers

Porphyrazine multimers are not well studied and investigated. Although a variety peripherally functionalized porphyrazines have been prepared and can be considered as logical building blocks for the elaboration of dimers, trimers and higher order oligomers via exocyclic metal ion coordination chemistry, there are few examples of porphyrazine dimers reported in the literature. A trinuclear porphyrazine dimer was reported by Hoffman et al (scheme 1.4.1.).[14] The dimer was synthesized by nickel ion chleation by two porphyrazinedithiolates. The optical spectrum of the

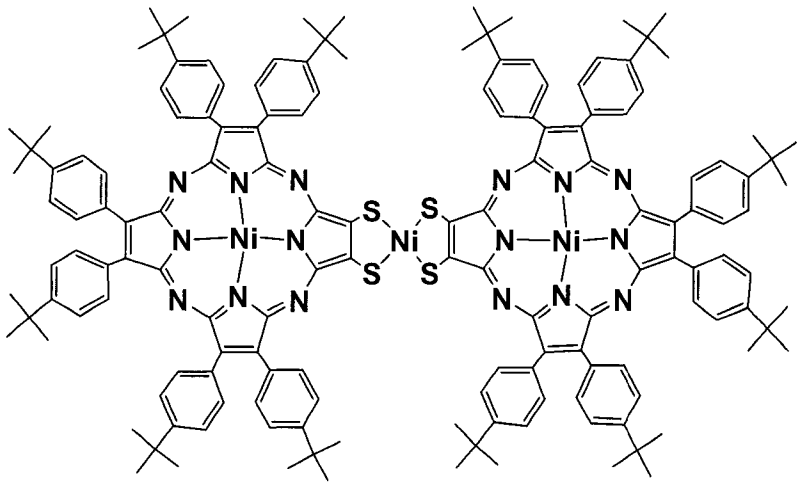

Scheme 1.4.1. The reported trinuclear porphyrazine dimer.[14]

unsymmetrically substituted porphyrazinedithiolates shows a typical B band at 340-350 nm and Q bands at 640-680nm, which can be assigned as the electron transitions from two $HOMO_s$ (a_{1u} and a_{2u}) into LUMO (e_g). The additional weak peak at about 450nm is assigned as the n-π^* transitions of the lone pairs *meso* nitrogens into the plane of the macrocycle core.[14] In contrast, the dimer shows Q

bands that are broad with a larger splitting (about 790cm^{-1}) and are red-shifted. These changes are caused by enhancement electronic coupling between two the porphyrazine macrocycles with introduction of the rigid [S_2NiS_2] spacer. Similar red-shifts and broadening of the Q bands are also observed in other porphyrinoid systems such as conjugated porphyrin dimers[21,22] and phthalocyanine dimers.[23,24]

1.5 Objectives of our research

The aim of our research is to use porphyrazines as the building block for the self-assembly of supramolecular arrays consisting of two different chromophores via metal ion coordination. In order to design supramolecular arrays, multi-component crystals, or aggregates, one must have a basic understanding of the relative coordination energetics and kinetics of the ligands on the two chromophores to the metal ions of choice. For example, it has been well established that the nature of the marcocycle can have profound effects on the basicity of the *meso* pyridyl groups.[25] Previous work in our laboratory has shown that the self-assembly of rigid supramolecular arrays require well-defined, geometrically rigid, building block precursors. For example, to assemble a planar-tape containing four chromophores, two of 5, 10 bis(4-pyridyl)porphyrins, and two of 5, 10, 15, 20 tetra(4-pyridyl)porphyrins are stitched together with six *cis*-platinum(II) dichlorides(scheme 1.5.1.).[26-29] The dispersity of such polymeric materials depends on the thermodynamics of the intermolecular interactions. The number of chromophores in the tape, therefore, depends on the energetics, and there is a distribution of products in topologically open systems such as these tapes.[30,31]

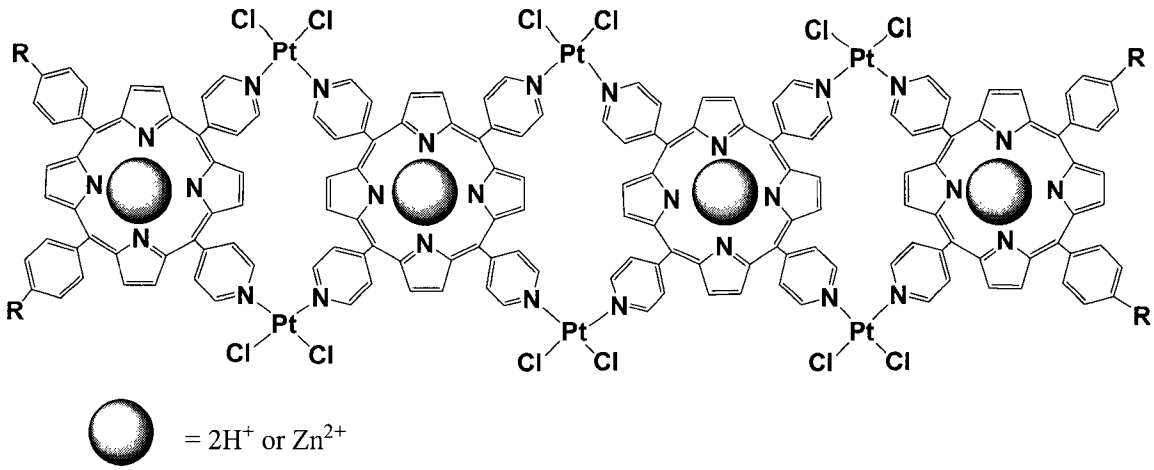

Scheme 1.5.1. Structure of planar-tapes containing four chromophores.[26-29]

For 2-dimensional structures, the obvious first step in this venture is to investigate the exocyclic coordination of [2,3-bis(dimethylamino)-7,8,12,13,17,18-hexakis (4-*tert*-butylphenyl)porphyrazine, **1**, to an equivalent of $Pd(OAc_2)_2$ [or the Pt derivative] to form an array, **2**, (scheme 1.5.2). Also the assembly of a [2,3,7,8-tetrakis(dimethylamino)-12,13,17,18-tetrakis(4-*tert*-butylphenyl)porphyrazine, **3**, to an equivalent of $Pd(OAc_2)_2$ [or the Pt derivative] to form a square tetramer, **4**, (scheme 1.2.2.). For the structures consisting of two different chromophores, one array could result from a mixture of equal amounts of the dimethylaminoporphyrazine, **1**, and the 5, 10-bis(4-pyridyl)-15,20-bis(4-tertbutylphenyl) porphyrin to an equivalent of $Pd(OAc_2)_2$ [or the Pt derivative] to form a tetramer, **5**, (scheme 1.5.3). The ratio of the possible products (porphyrin tape, porphyrazine dimer, porphyrazine-porphyrin tetramer and etc.) will indicate the relative strengths of the coordination bonds. If they are not substantially different, attempts to make 2-dimensional higher order structures

will result in statistical mixtures. To construct a given array or to design and synthesize supramolecular arrays that have both chromophores in pre-defined geometries, a sequence of reactions can be used. The porphyrazine-porphyrin tetramer, **5**, can be prepared with two different methods: (1) by dechlorination of the bisporphyrin Pt-planar tape, **6**, with silver perchlorate and then this is reacted with [2,3-bis(dimethylamino)-7,8,12,13,17,18-hexakis(4-*tert*-butylphenyl) porphyrazine, **1**, to form the tetramer; (2) by forming the porphyrazine-platinum monomer, dechlorination, and then forming the porphyrin tape (scheme 1.5.4.). A porphyrazine-porphyrin heptamer may be synthesized with a similar strategy: Formation of a Pt-planar tape through the coordination of exocyclic pyridyl groups on two different porphyrins to four trans platinum dichlorides, dechlorination the tape with silver perchlorate, and subsequent reaction with [2,3,7,8- tetrakis(dimethylamino) 12,13,17,18-tetrakis(4-*tert*-butylphenyl)porphyrazine to form the heptamer (figure B25). This latter example, though it illustrates the strategy, is not part of the present work.

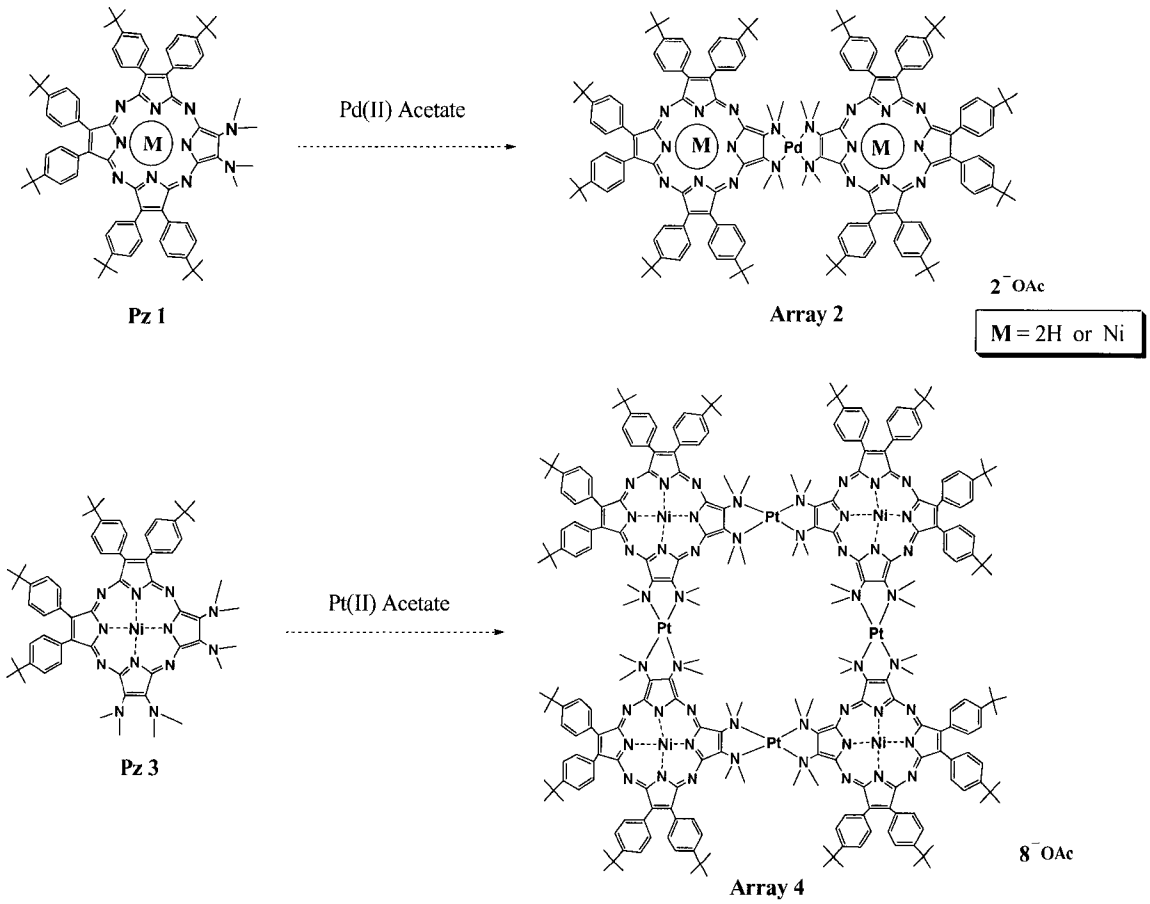

Scheme 1.5.2. Formation of a dimer and tetramer by mixing porphyrazines to an equivalent of $Pd(OAc_2)_2$ [or the Pt derivative].

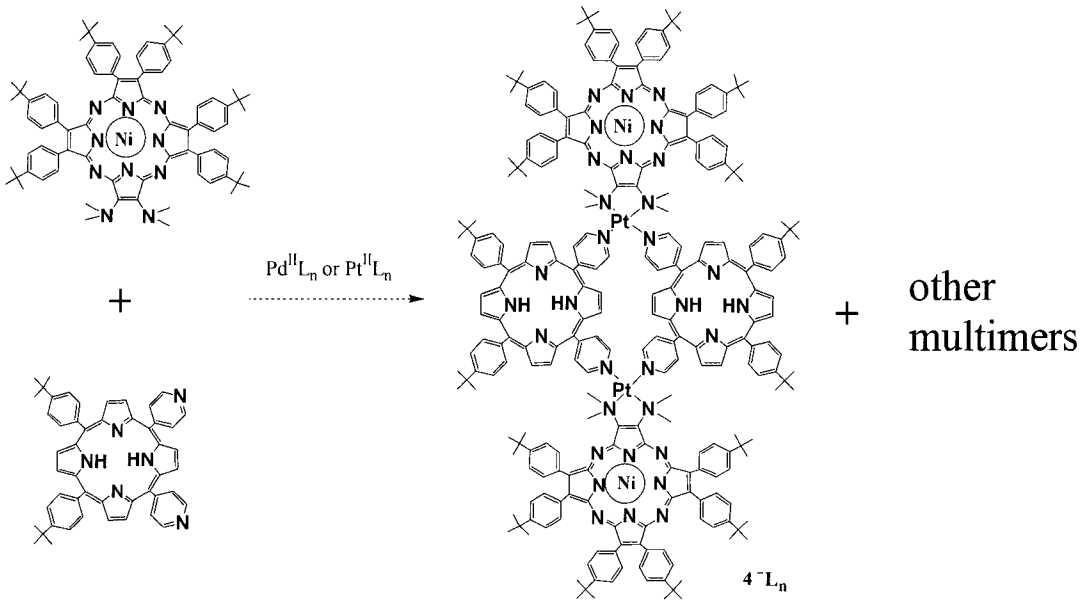

Scheme 1.5.3. Mixing equal amount of the dimethylaminoporphyrazine and the 5, 10 bis(4-pyridyl)porphyrin to an equivalent of $Pd(OAc_2)_2$ [or the Pt derivative] to form a tetramer consisting of two different chromophores. The yield of the array is detected by the various coordination bands, and this mode of assembly results in a mixture of products.

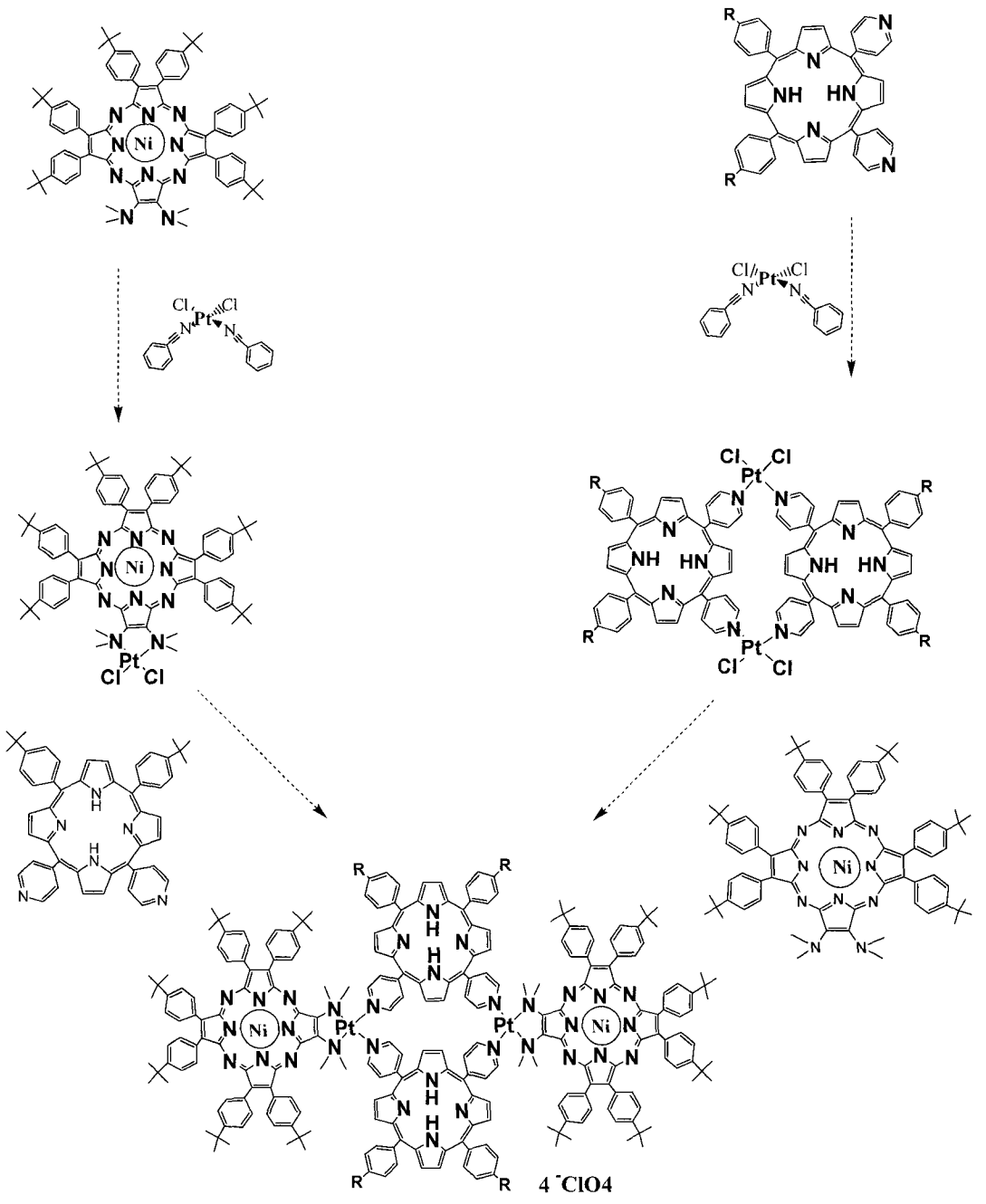

R = 4-tolyl or 4-*tert*-butylphenyl

Scheme 1.5.4. Formation of the porphyrazine-porphyrin tetramer via a sequence of reactions.

Again, our systematic apporach will be to make and understand the chemistry of the dimers, then the tetramers, and then these results will be used in the design of higher ordered structures and materials. The reactions will be investigated by UV/Vis spectroscopy, NMR and ESI-MS under different conditions.

1.6 Abbreviation of compounds

ABBREVIATION	STRUCTURE	FORMULA	UV-vis λ_{max} (nm)
1A	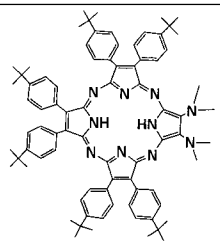	$C_{80}H_{92}N_{10}$	(Chloroform) 363, 450, 636, 669, 738
1A·$PdAc_2$	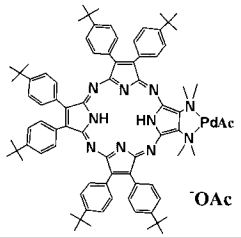	$C_{84}H_{98}N_{10}O_4Pd$	(Chloroform) 352, 489, 603, 660,737
1A·$PdCl_2$	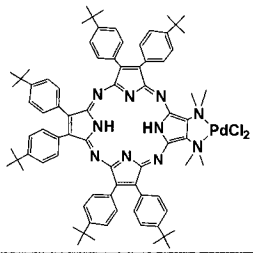	$C_{80}H_{92}Cl_2N_{10}Pd$	(Toluene) 369, 489, 603, 660, 716
1A·$PtCl_2$	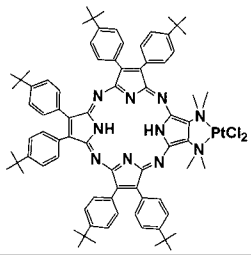	$C_{80}H_{92}Cl_2N_{10}Pt$	(Toluene) 368, 490, 604, 660, 733
1B	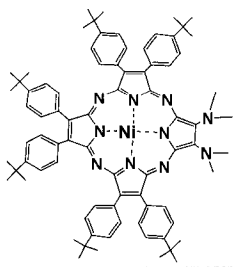	$C_{80}H_{90}N_{10}Ni$	(Chloroform) 343, 457, 622, 670, 696

1B·$PdAc_2$	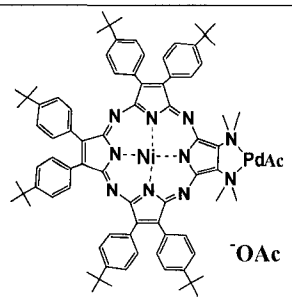	$C_{84}H_{96}N_{10}O_4NiPd$	(Chloroform) 344, 455, 573, 622, 720
2A	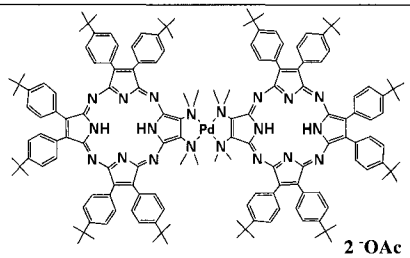	$C_{164}H_{190}N_{20}O_4Pd$	(Chloroform) 323, 420, 478, 602, 669, 701, 742, 779 (Toluene) 326, 428, 468, 591, 637, 671, 707, 736, 776
2B	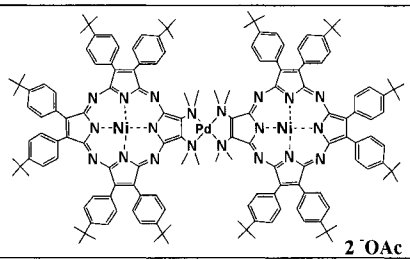	$C_{164}H_{186}N_{20}O_4Ni_2Pd$	(Chloroform) 312, 418, 487, 639, 702, 733 (Toluene) 313, 428, 482, 637, 709, 735
2C	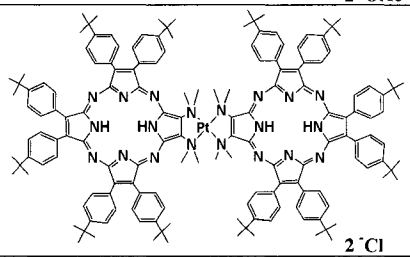	$C_{160}H_{184}Cl_2N_{20}Pt$	(Toluene) 343, 365, 468, 588, 621, 680
2D	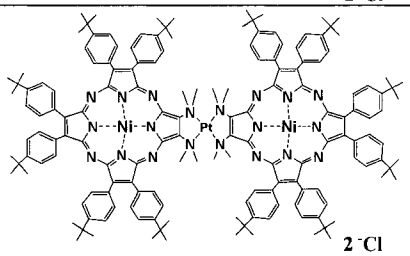	$C_{160}H_{180}Cl_2N_{20}Ni_2Pt$	(Toluene) 345, 427, 460, 630, 686
3A	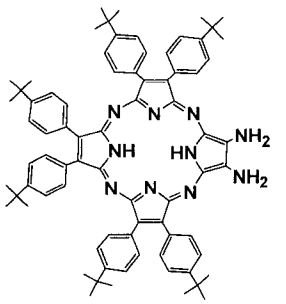	$C_{76}H_{84}N_{10}$	(Toluene) 366, 466, 560, 623, 669

3A·$PdCl_2$	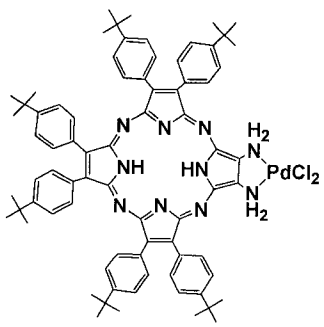	$C_{76}H_{84}Cl_2N_{10}Pd$	(Toluene) 364, 474, 609, 671, 727
4A	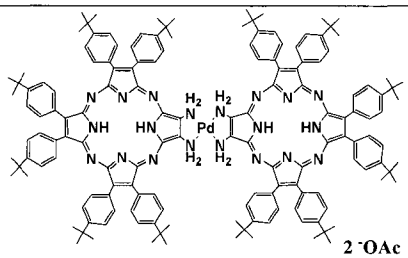	$C_{156}H_{174}N_{20}O_4Pd$	(Toluene) 364, 460, 591, 673, 730
5A	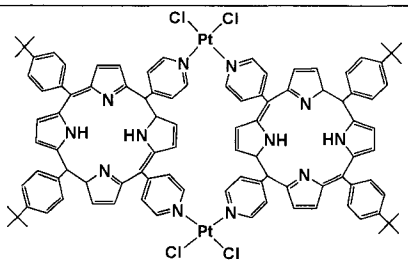	$C_{100}H_{96}Cl_4N_{12}Pt_2$	(Toluene) 423, 516, 552, 591, 646
5B	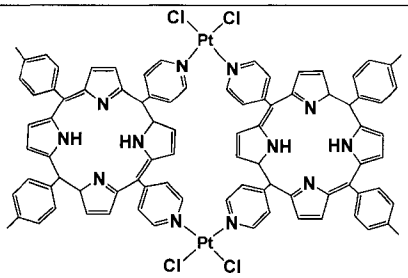	$C_{88}H_{72}Cl_4N_{12}Pt_2$	(Toluene) 422, 516, 551, 591, 647
6A	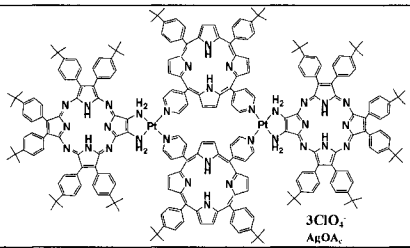	$C_{254}H_{259}AgCl_3N_{32}O_{14}Pt_2^{+}$	(Toluene) 372, 425, 518, 555, 593, 646, 700, 742
7A	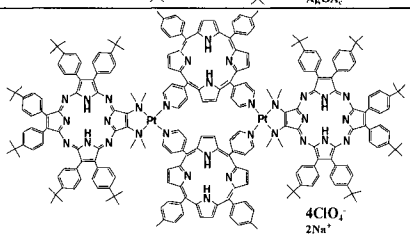	$C_{248}H_{248}Cl_4N_{32}Na_2O_{16}Pt_2^{2+}$	(Toluene) 367, 421, 516, 553, 583, 645, 671, 740

B2.

Results & Discussion

2.1. Synthesis

Porphyrin building blocks were prepared by the mixed aldehyde condensations based on the Adler[32,33] synthesis in ~25-30% isolated yield for all the porphyrins (scheme 2.1.1.). Using a mixture of two different aldehydes,

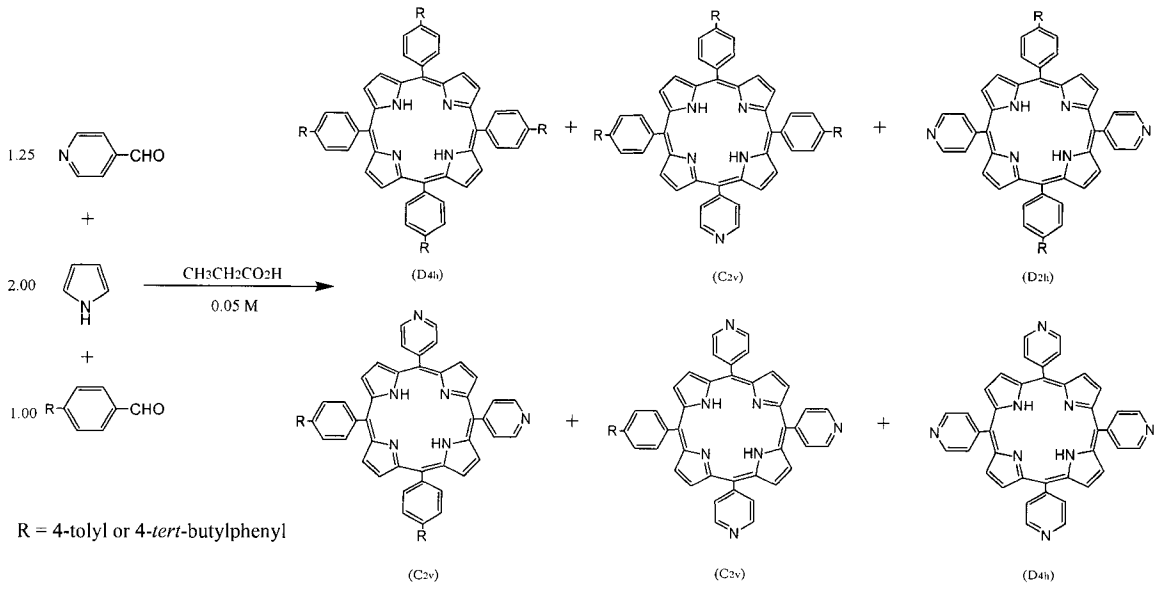

Scheme 2.1.1. Synthesis of porphyrin building blocks. The point groups do not include the pyrrole NH as they tautomerize on the NMR time scale; but they should be included in MO calculations for electronic spectra.[33]

4-pyridinecarboxaldehyde and 4-tolylbenzaldehyde (or 4-*tert*-butylbenzaldehyde), results in a mixture of six porphyrins in yields that are weighted by the reactivity, the solubility, and the relative amounts of the aldehydes.[34-38] All the porphyrins are readily characterized by the ^{1}H NMR spectra in the aromatic region, especially by the pyrrole β-H.

Porphyrazine building blocks were prepared from the corresponding heteroatom functionalized maleonitriles using a Linstead magnesium alkoxide templated macrocyclization reaction in a refluxing alcohol solvent.[18,39] In each case, the magnesium ion template was removed under acidic conditions and replaced with a diamagnetic ion, Ni(II), or kept as the free base (scheme 2.1.2.). Similar to the mixed aldehydes porphyrin synthesis, a mixture of two different maleonitriles will result in a mixture of six porphyrazines. The relative yield of each porphyrazine also weighted by the reactivity, the solubility, and the relative amounts of the maleonitriles. In order to examine the coordination chemistry of these porphyrazines through binding of metal ion by the peripheral ligating groups, a *bis*(dimethylamino)maleonitrile was introduced. *Bis*(dimethylamino)maleonitrile was prepared from the commercially available diaminomaleonitrile (DAMN) in ~54% yield according to the literature (scheme 2.1.3.). The mixture of cis /trans *bis*(dimethylamino)maleonitrile can be re-equilibrated to obtain more of the desired cis isomer.[40] Introducing more polar heteroatom peripheral groups onto the porphyrazine usually tends to lower the marcocyclic solubility, which would result in the difficulty making higher-order arrays soluble enough for study. The problem was solved by the Hoffman – Barrett team by designing a dinitrile

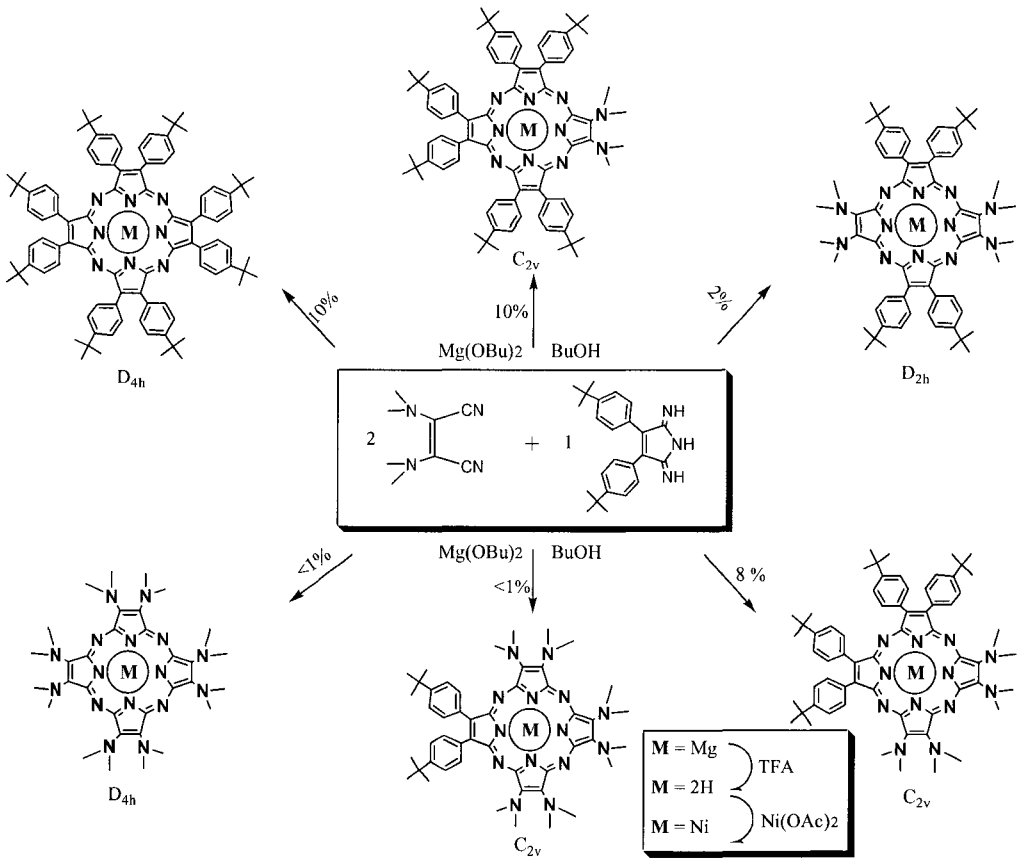

Scheme 2.1.2. Synthesis of porphyrazine building blocks.[41] The point groups assigned for the metallo Pz.

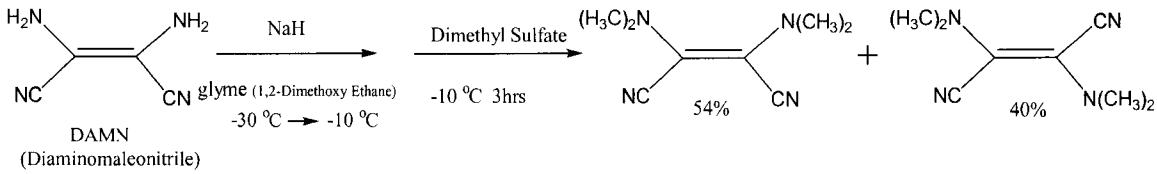

Scheme 2.1.3. Synthesis of *Bis*(dimethylamino)maleonitrile.[40]

functionalized with a noncoordinating component that would help solubilize the porphyrazine but remain compatible with the strategy established for the synthesis of the unsymmetrical marcocyles.[14] By the fact that the *tert*-butylphenyl substituents would enhance the solubility of most chromophores, the 3,4-bis(4-*tert*-butylphenyl)pyrroline-2,5-di-imine was selected as the nonpolar coreactant. The activation of the fumaronitrile yields the corresponding pyrrolinediimine which is more stable and cyclizes quite quickly in refluxing *n*-butanol without decomposition.[42] The 3,4-bis(4-*tert*-butylphenyl)pyrroline-2,5-di-imine was synthesized according to the literature procedures[14] and all the intermediates were readily characterized by ^{1}H NMR spectra (scheme 2.1.4.).

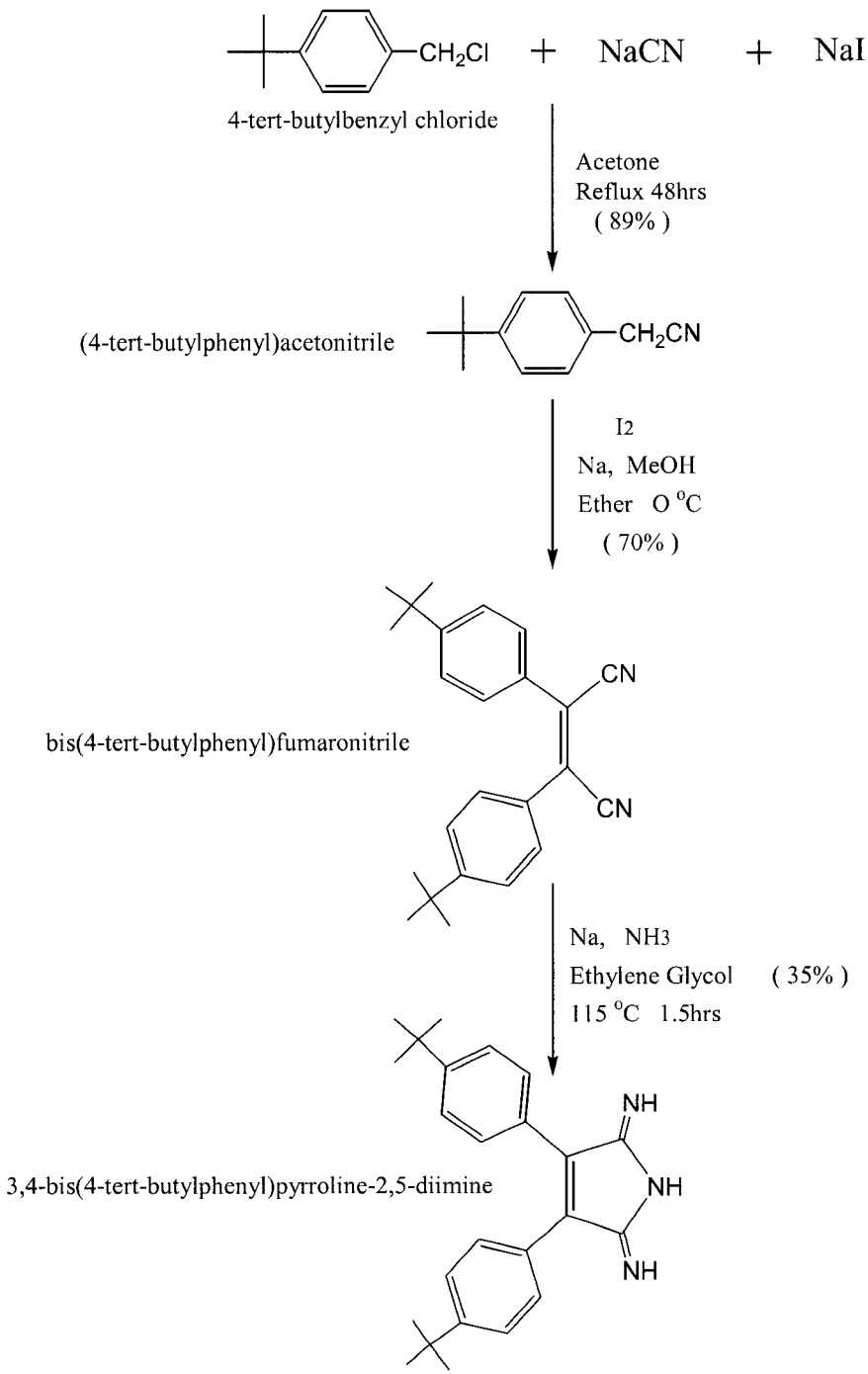

Scheme 2.1.4. Synthesis of 3,4-bis(4-*tert*-butylphenyl)pyrroline-2,5-di-imine.[14]

2.2. First generation porphyrazine – porphyrazine dimer

Dimer, **2**, was prepared from [2,3-bis(dimethylamino)-7,8,12,13,17,18-hexakis (4-*tert*-butylphenyl)porphyrazine, **1A**, [or Ni(II) porphyrazine, **1B**] to an equivalent of $Pd(OAc_2)_2$. The reaction is slow in that the mixture, after 24 hrs stirring at 60 ^{0}C, only gave ~40% of dimer together with the starting porphyrazine (~10%) and a Pd(II) coordinated monomer (~40%) (scheme 2.2.1.). The reaction mixture was separated and purified by silica gel column chromatography. The dimer and monomer were characterized by UV-Visible spectra (figure 2.2.1) and ^{1}H NMR spectra (figure 2.2.2.).

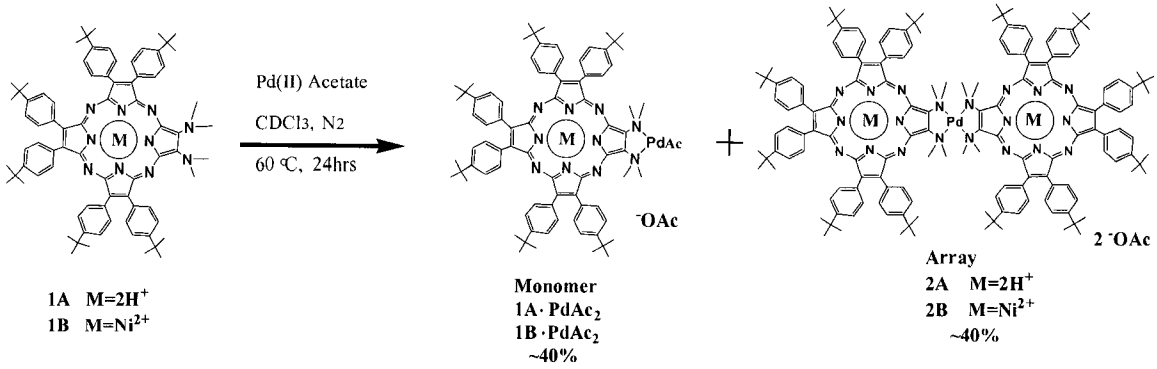

Scheme 2.2.1. Synthesis of the first generation Pd(II) coupled porphyrazine dimer.

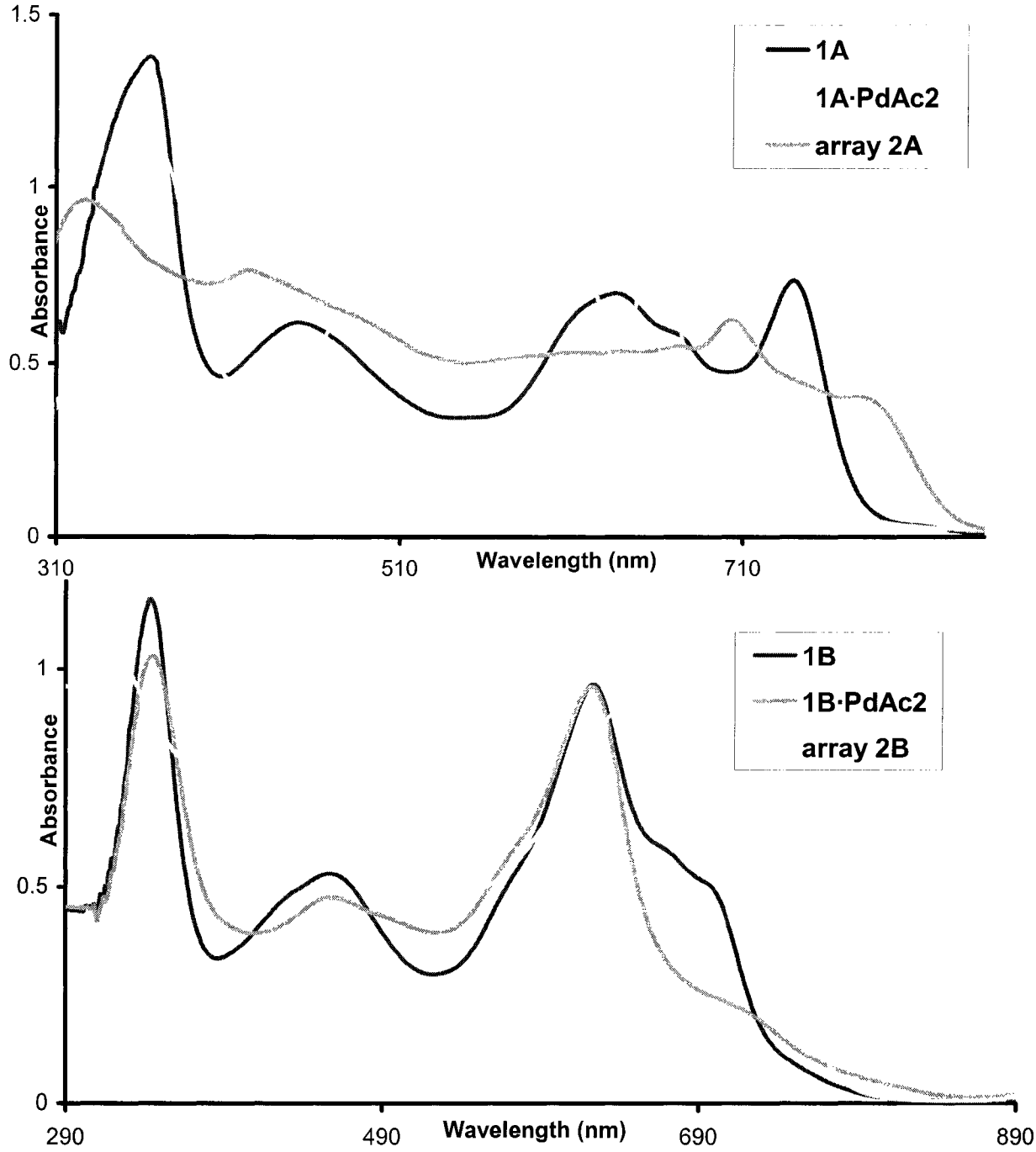

Figure 2.2.1 (Top) UV-vis spectra of free base [2,3-bis(dimethylamino)-7,8,12,13,17,18-hexakis(4-*tert*-butylphenyl)porphyrazine **1A**, its palladium monomer **1A**·$PdAc_2$ and dimer **2A** in chloroform (15μM) at room temperature. (Bottom) UV-vis spectra of Ni(II) [2,3-bis(dimethylamino)-7,8,12,13,17,18-hexakis(4-*tert*-butylphenyl)porphyrazine **1B**, its palladium monomer **1B**·$PdAc_2$ and dimer **2B** in chloroform (15μM) at room temperature.

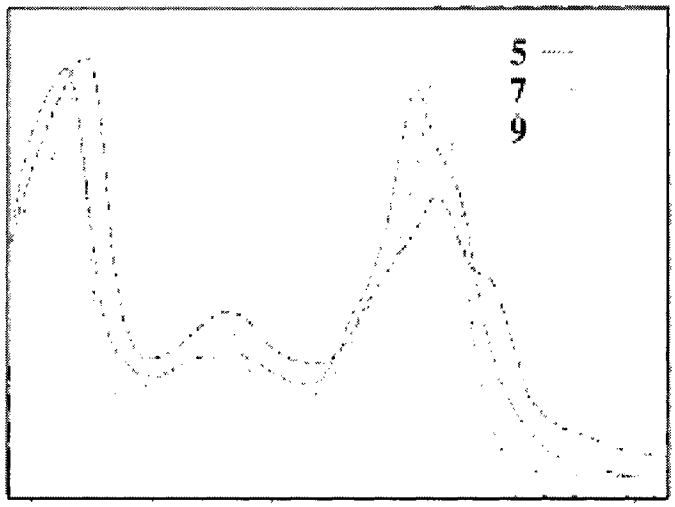

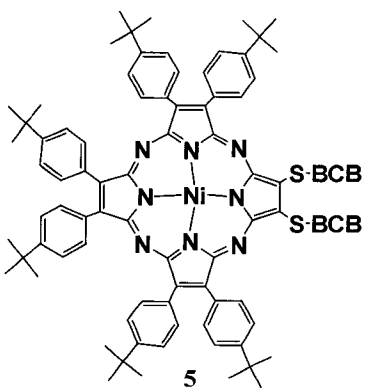

5

BCB = 4-[(butyloxy)carbonyl]benzyl

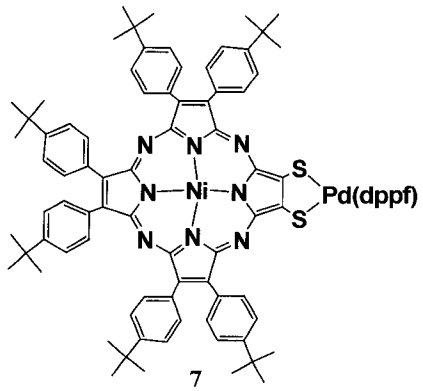

7

dppf = (1,1'-Diphenylphosphino)ferrocene

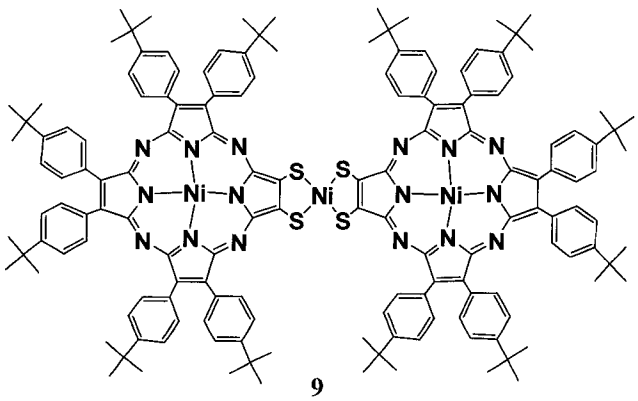

9

Figure 2.2.2. The optical absorption spectra of reported BCB-protected porphyrazine **5**, porphyrazine complex **7**, and porphyrazine dimer **9** in CH_2Cl_2.[14]

The interpretations of the observed UV-visible spectra discussed below are based on the models of Gouterman for porphyrin molecular orbitals,[16] and by Kasha's model for the electronic coupling of chromophore such as porphyrins.[43] Analogously to porphyrins, the electronic absorption spectra of all porphyrazine derivatives have two main bands: an intense B (Soret) band (π-π^*) at $\lambda < 400$ nm and a Q band (π-π^*) at $\lambda > 600$ nm. The coordination of a metal to the central cavity of the Pz **1B** increases the symmetry of the core from D_{2h} to D_{4h}, so a reduction of Q-band splitting is observed. Since the dimethyl amino groups are attached and the lone pair conjugated to the marcocycle, the Q bands are red-shifted and broadened (figure 2.2.1). The peripheral coordination of the dimethylamino substituents to a metal ion has a large effect on the electronic spectra of the aromatic macrocycle. The observed absorption spectra of **1A**·$PdAc_2$ and **1B**·$PdAc_2$ show blue-shifted Q bands that are dramatically sharpened (figure 2.2.1). The blue-shift and sharpening of the Q bands is largely due to the lost of n-π^* transitions from the heteroatoms of the dimethyl amino groups to the porphyrazines π system. These changes arise because the lone pair electrons of the heteroatoms are coordinated to the metal ion, which diminishes their coupling to the aromatic macrocycle.[6,44] The formation of the Pd(II) or Pt(II) linked dimers creates a direct link between the chromphores that extends the conjugation. Thus a red-shift and broadening of the optical bands is expected and observed for both **2A** and **2B**. The metallo Pz dimer **2B** has transition dipole arising only from the asymmetric disposition of the dimethyl amino groups. Thus the spectra for **2B** should have similar numbers of optical transitions as is observed. On the other hand, dimer **2A** has transition dipoles arising from both the dimethylamino groups and the pyrrole NH on each Pz. As in the free base porphyrins and the free base **1A**, the increased

numbers of optical transitions in the dimer **2A** arise from the various coupling of these dipoles. So, **1A**, **1A**·$PdAc_2$ are expected and observed to have the same numbers of bands but at different energies due to the electronic effects of Pd(II) coordination by the dimethylamino groups. The Pz are strongly coupled in dimer **2A**, as evidenced by the increased number of electronic absorption bands that arise from coupling the various transitions dipoles on each Pz. The optical absorption of **1B**, **1B**·$PdAc_2$, and array **2B** are similar to the reported porphyrazine analogue **5**, **7**, and **9** (figure 2.2.2).

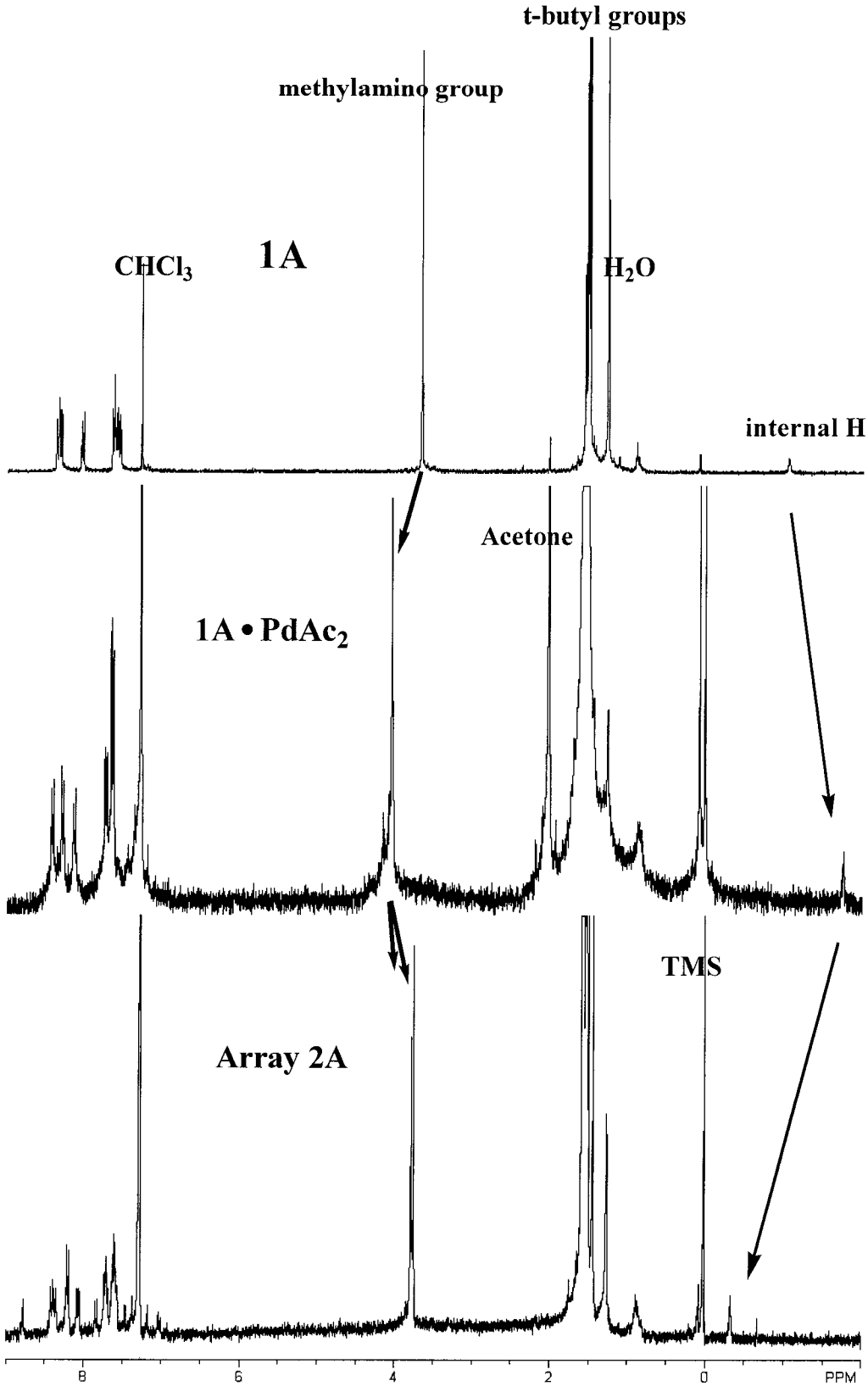

Figure 2.2.3. ^{1}H NMR spectra of free base [2,3-bis(dimethylamino)-7,8,12,13,17,18-hexakis(4-(*tert*-butyl)phenyl)porphyrazine, its palladium monomer and dimer. Arrows indicate the chemical shift changes in the methylamino groups and internal H from **1A** to array **2A**.

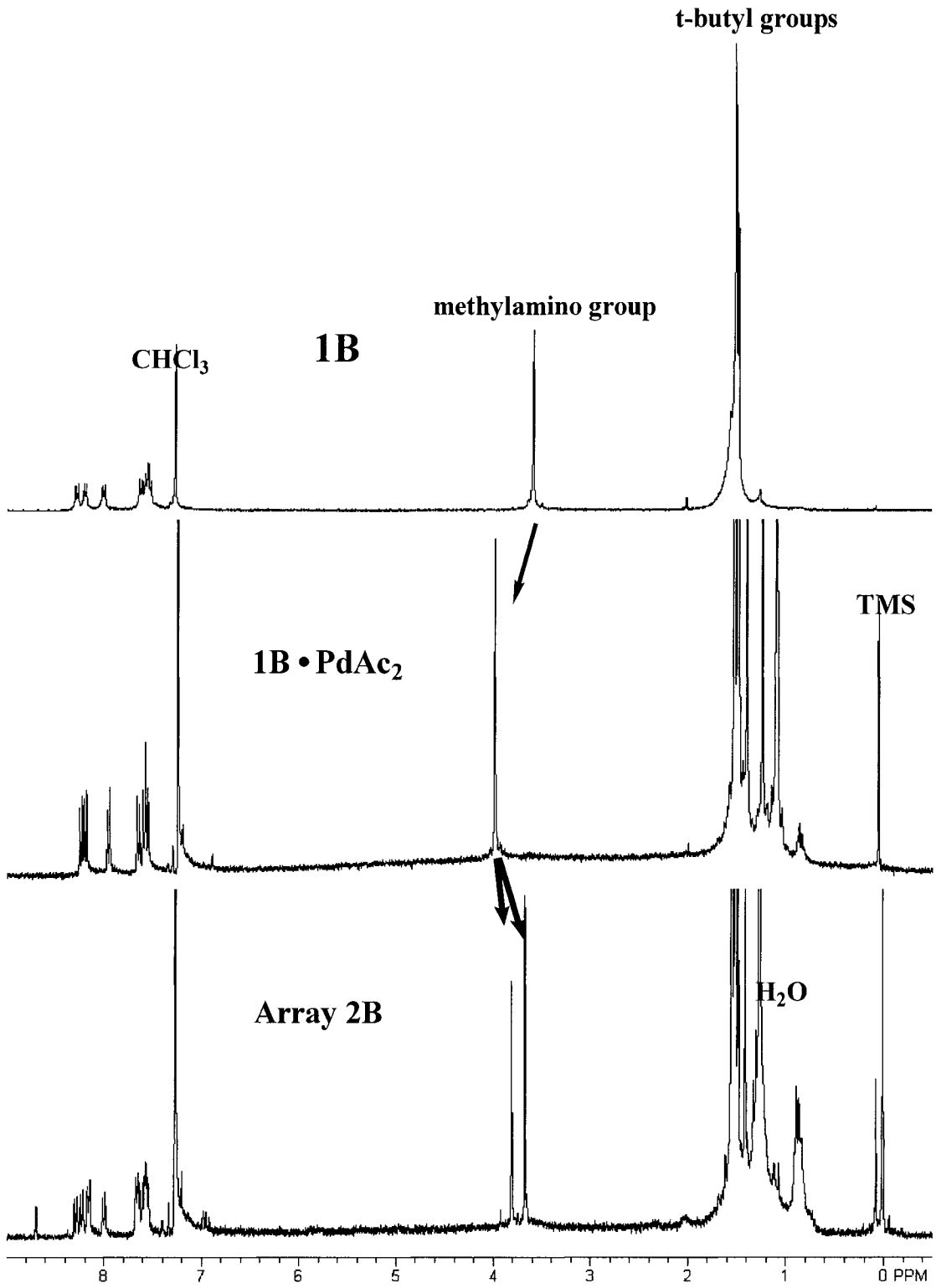

Figure 2.2.4. ^{1}H NMR spectra of nickellic [2,3-bis(dimethylamino)-7,8,12,13,17,18-hexakis(4-(*tert*-butyl)phenyl)porphyrazine, its palladium monomer and dimer. Arrows indicate the chemical shift changes for the methylamino groups from **1B** to array **2B**.

^{1}H NMR spectra of the dimers, monomers and the parent porphyrazines gave more structural detail among these complexes (figure 2.2.3. and 2.2.4.). The diagnostic peak of the methylamino groups directly indicates the mutual chelation of a palladium ion to the porphyrazine. For the free base porphyrazine, the ^{1}H NMR methylamino peak is 3.68ppm using chloroform-D as internal reference. The methylamino peak of the monomer downfield shifts from 3.68ppm to 4.05ppm upon palladium ion chelation (**1A**·$PdAc_2$). On the other hand, the methylamino peak of the dimer also downfield shifts but splits into two peaks (from 3.68ppm into 3.78 and 3.75 ppm). The inner- NH of the porphyrazines also shift. The large shift of the pyrrole NH resonances is an indication of the changes in ring current in the dimer that is caused by the coupling of the aromatic macrocycles. For the Ni(II) porphyrazine, **1B**, the methylamino peak of the monomer downfield shifts from 3.60ppm to 4.01ppm upon palladium ion chelation. Similar to the free base array **2A**, the methylamino peak of the dimer **2B** downfield shifts and splits from 3.60ppm into 3.81ppm and 3.67ppm and they are integrated to 1:1 in the ^{1}H NMR spectrum. The explanation for the splitting of the methylamino peak in the two dimers is that there is a twisted square planar geometry of the Pd(II) ions in the rigid dimer systems **2A** and **2B** due to the steric hindrance among the methylamino groups. In a perfect square planar, the methylamino groups on the same side of Pd(II) ion should adopt a totally eclipsed conformation which will result a single methylamino peak in ^{1}H NMR spectrum. However, when the square planar is twisted, the methylamino groups are distorted to avoid an eclipsed conformation. So, there are two sets of methylamino groups with different electronic environment in the rigid dimer systems **2A** and **2B**. This explanation is further supported by a simple molecular dynamics calculation using PC

model. To simplify the calculations, the chromophores were replaced by the pyrrole rings (figure 2.2.5.). The results of the calculations show that the monomers have an equivalent methylamino groups but the dimers have two sets of the methylamino groups: one towards the Pz macrocycle ring and one towards Pd(II) ion center.

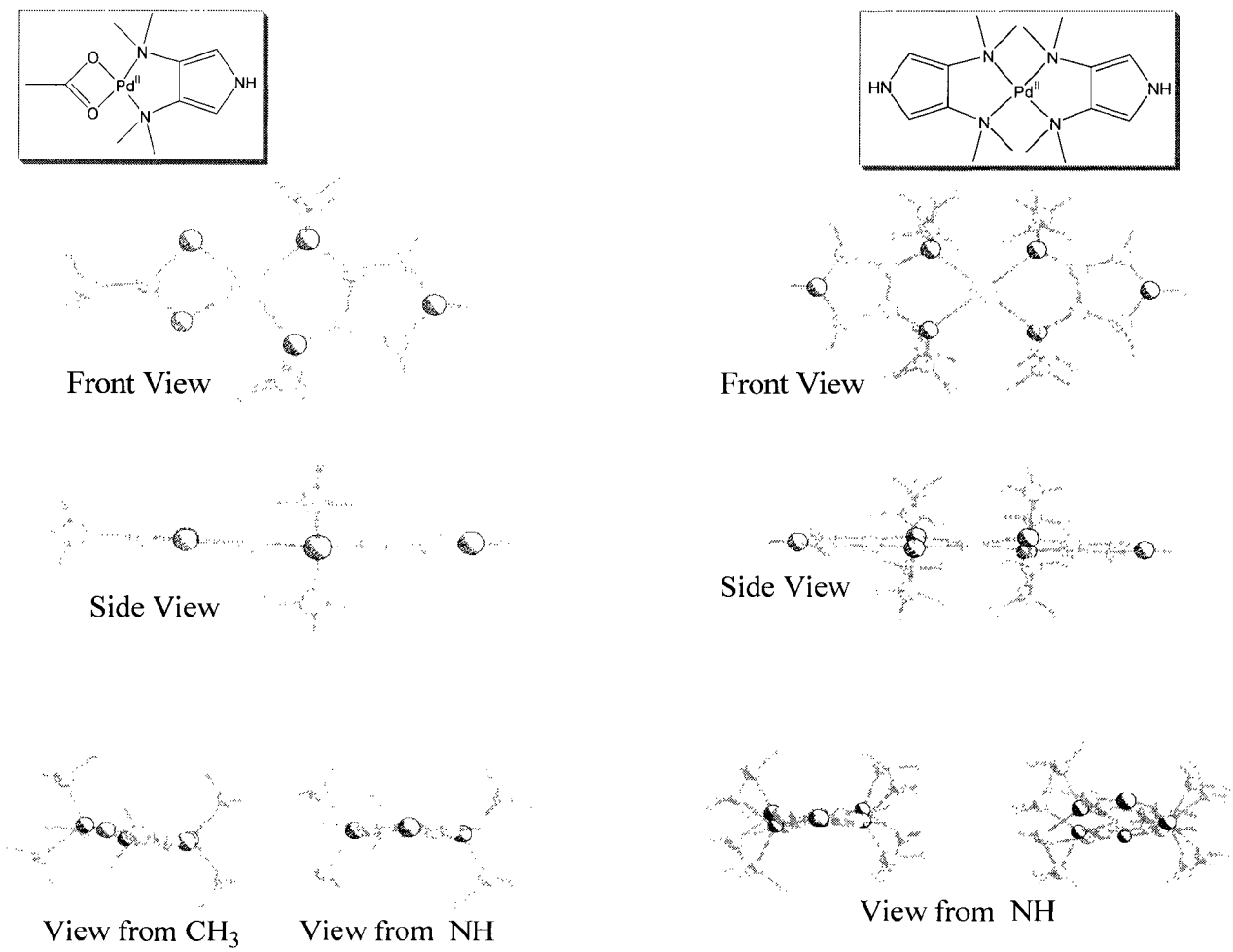

Figure 2.2.5. Simple molecular calculation in PC model on the ligand binding sites of the monomer and dimer. (For simplification the chromophores were replaced by the pyrrole rings)

To further illustrate the structure of the dimer, we performed a sequence of reactions to synthesize the dimer and then compared the ^{1}H NMR data to the products generated from stoichiometric mixture of one equivalent of the Pd complex to two of **1A** or **1B**. In this sequence of reactions, the **1B**·$PdCl_2$ was first generated and purified by reacting the Ni(II) porphyrazine **1B** with an equivalent bis(benzonitrile)dichloro-palladium(II). The monomer was then dechlorinated with silver perchlorate to form **1B**·$Pd(ClO_4^-)_2$. The **1B**·$Pd(ClO_4^-)_2$ intermediate was allowed to react with an other equivalent of **1B** to form array **2B** (scheme 2.2.6.). ^{1}H NMR spectra of the result **2B** dimer are identical to the purified product generated from the stoichiometric reaction, indicating that they are the same compounds. Attempts to get an ESI-MS on array **2A** or **2B** always results in decomposition of the complexes.

Alternatively, the Pz dimer **2D** $\{[(NiPz)_2Pt^{2+}](Cl^-)_2\}$ can be formed using $PtCl_2Bz_2$ with the following procedure. One equivalent of $PtCl_2Bz_2$ is complexed by the dimethylamino groups of **1B** in a refluxing solution of chlorobenzene and DMF (3:1 v/v) for 10 hours under nitrogen. The monomer (NiPz)PtCl2 was purified by silica gel column chromatography and precipitated from acetonitrile in 60% yield. The pure monomer in dry toluene was dechlorinated with silver perchlorate to form **1B**·$Pt(ClO_4^-)_2$. The **1B**·$Pt(ClO_4^-)_2$ intermediate was allowed to react with an other equivalent of **1B** to form array **2D** in 40% yield. A similar method is used to make array **2C** containing free base Pz complex. The advantage of using Pt as the linking ion is that it tends to form stronger coordination bonds to the nitrogen ligands, thus resulting in more robust self-assembled arrays, since both palladium and platinum are square planar metals and display similar coordination chemistry, we expect similar chemical properties and the corresponding

assemblies to have similar photophysical properties. In fact, the UV-vis spectra (figure 2.2.7.) and ^{1}H NMR (figure B11and B12) **1A**·$PdCl_2$ and **1A**·$PtCl_2$ are almost identical to each other, and the UV-vis spectra (figure 2.2.8.) and ^{1}H NMR (figure B18and B19) of array **2B** and **2D** are similar to each other. Electrospray mass spectroscopy spectra of the array **2D** in positive-ion mode shows the molecular weight of the dimer $(NiPz)_2Pt^{2+}Cl^-$ (figure 2.2.9.).

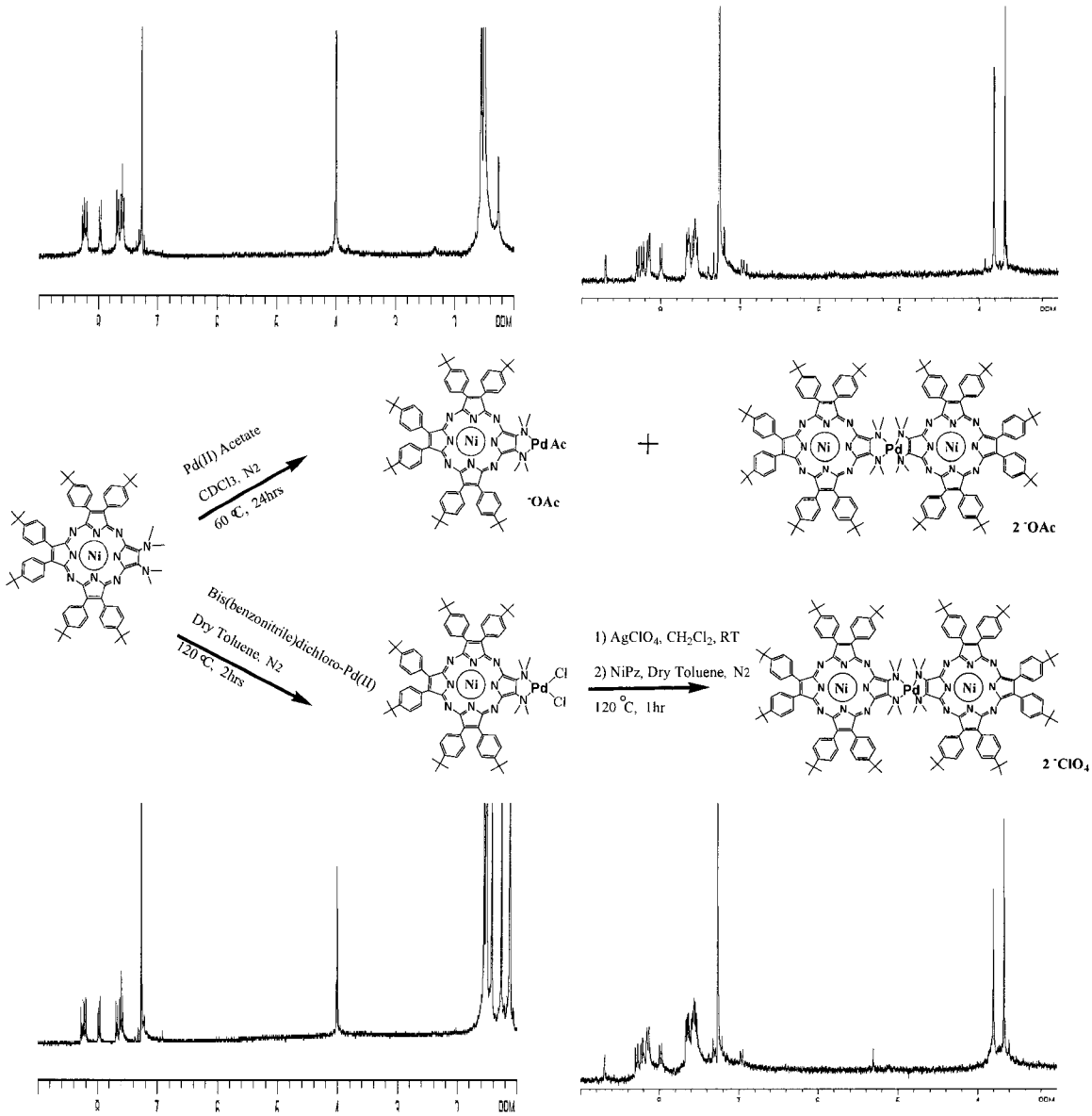

Figure 2.2.6. Formation of the Ni(II) porphyrazine palladium monomer **1B**·$PdAc_2$ and dimer **2B** via two different methods. ^1H NMR spectra indicating the products are the same compounds.

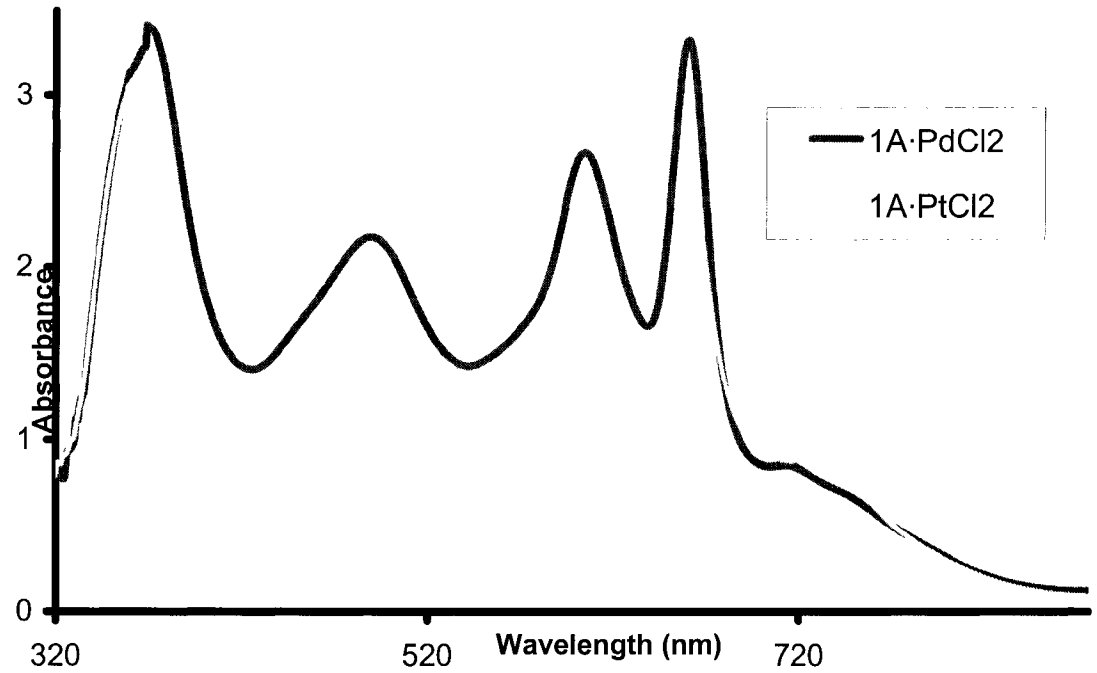

Figure 2.2.7. UV-vis spectra of **1A**·$PdCl_2$ and **1A**·$PtCl_2$ in toluene.

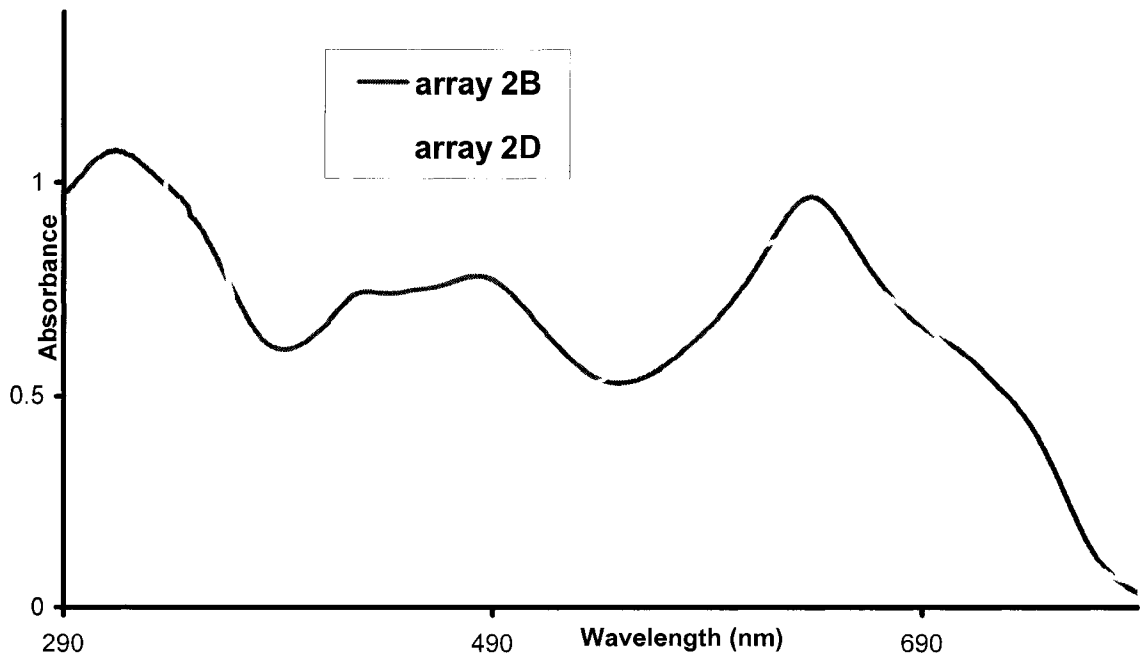

Figure 2.2.8. UV-vis spectra of array **2B** and **2D** in toluene.

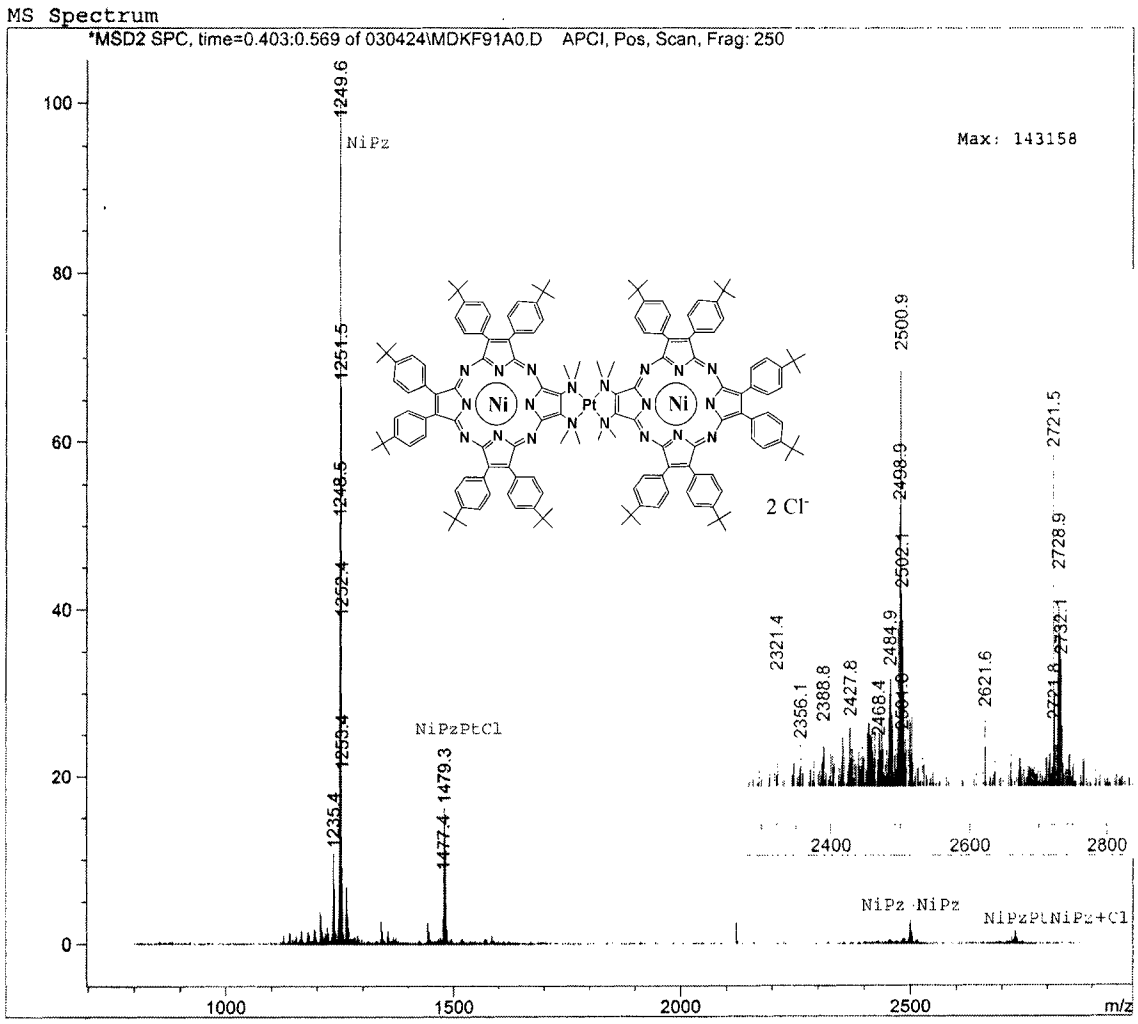

Figure 2.2.9. Electrospray mass spectroscopy spectra of the dimer **2D** in positive-ion mode shown the molecular weight of the dimer 2729 (**2D** – Cl^-). **1B** = 1249; **1B**•$PtCl^+$ = 1479; $(\mathbf{1B})_2$ = 2500.

2.3. Second generation porphyrazine – porphyrazine dimer

The first generation of the porphyrazine – porphyrazine dimers have a disadvantage in that self-assembly is inhibited by the steric hindrance among the dimethyl amino groups. As a result, the self-assembling reaction requires long reaction times and high temperatures (refluxing chloroform or toluene) and still yields are disappointing. To overcome this problem, we introduce the free amino porphyrazine building block [2,3-bis(diamino)-7,8,12,13,17,18-hexakis (4-*tert*-butylphenyl)porphyrazine]. In this case, the streic hindrance among the amino groups is minimized and we expect cleaner self-assembly at lower temperatures. Synthesis of the 2,3-bis(diamino)-7,8,12,13,17,18-hexakis (4-*tert*-butylphenyl)porphyrazine is achieved by the reductive deselenation of the monoselenodiazole-Pz using modifications of the conditions reported by Ercolani and co-workers.[45] The monoselenodiazole-Pz was synthesized through the mixed Linstead marcocylization of 3,4-dicyano-1,2,5-selenodiazole with 0.5 equivalent 3,4-bis(4-*tert*-butylphenyl)pyrroline-2,5-diimine in the presence of magnesium butoxide gave the isolated product in 15% yield (scheme 2.3.1.). Again, the magnesium ion template was removed under acidic conditions and replaced with a representative diamagnetic ion, Ni(II), or kept in the free base form. The free amino-Pz is not stable at room temperature. When a solution containing the free amino-Pz is exposed to light in air at room temperature for 30 minutes, the solution changes from blue to purple. The UV-vis spectra shows that it forms a new intense peak at 725nm (figure 2.3.1). There are several tautomers possible with the free amine groups attached directly to the pyrrole.

Also, it is likely that the product of the photo reaction in air is an oxidation of at least one of the amine to imine (scheme 2.3.2.). There are other possible products too, such as the formation of a ketone (scheme 2.3.3.). The long wavelength absorption (725nm) is typical of this type of oxidation of pyrrole to the bis keto variety on porphyrins, so is likely the oxidation product in the present case.

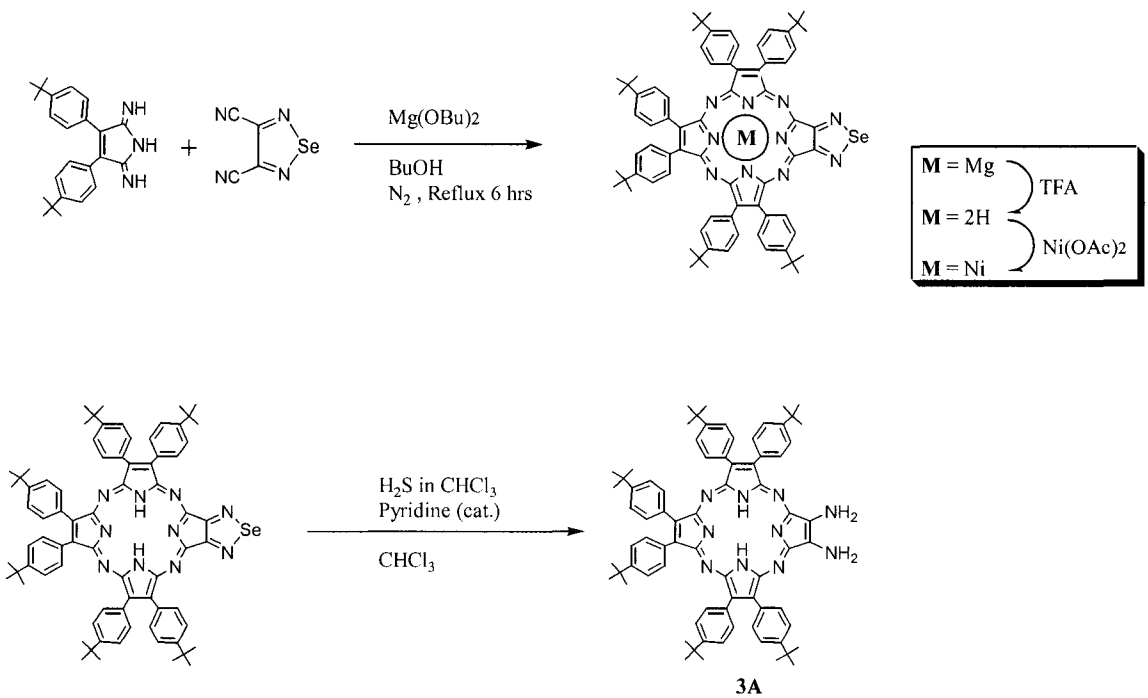

Scheme 2.3.1. Synthesis of the 2,3-bis(diamino)-7,8,12,13,17,18-hexakis (4-*tert*-butylphenyl) porphyrazine by the reductive deselenation of the monoselenodiazole-Pz.[45]

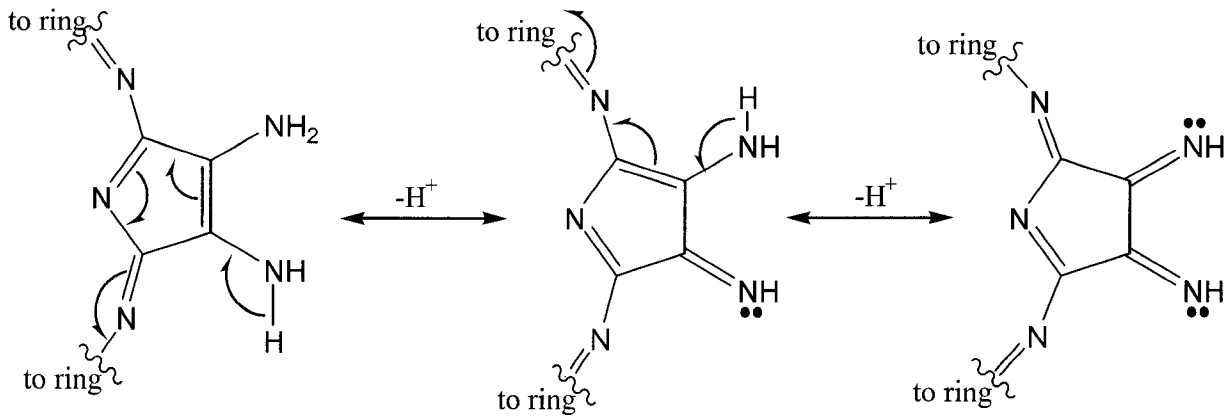

Scheme 2.3.2. The formation of the imines on the pyrrole free amino groups via tautomerization.

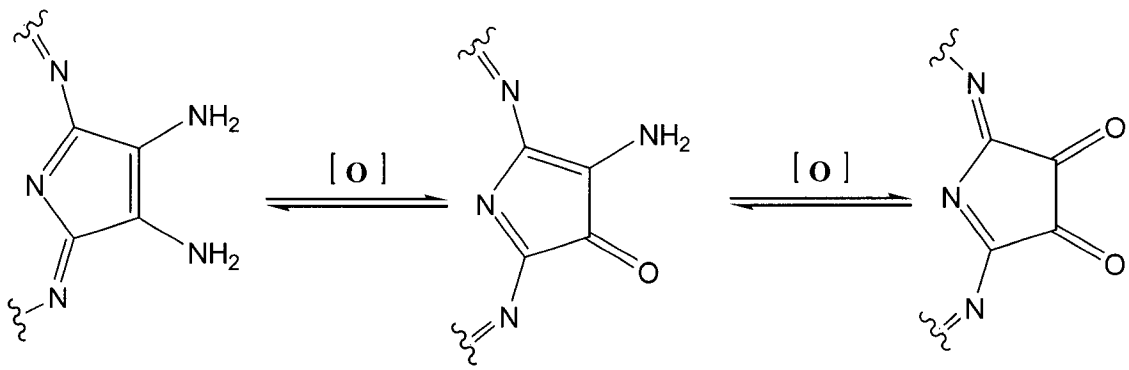

Scheme 2.3.3. The likely formation of the ketone on the pyrrole free amino group via photo reaction in air.

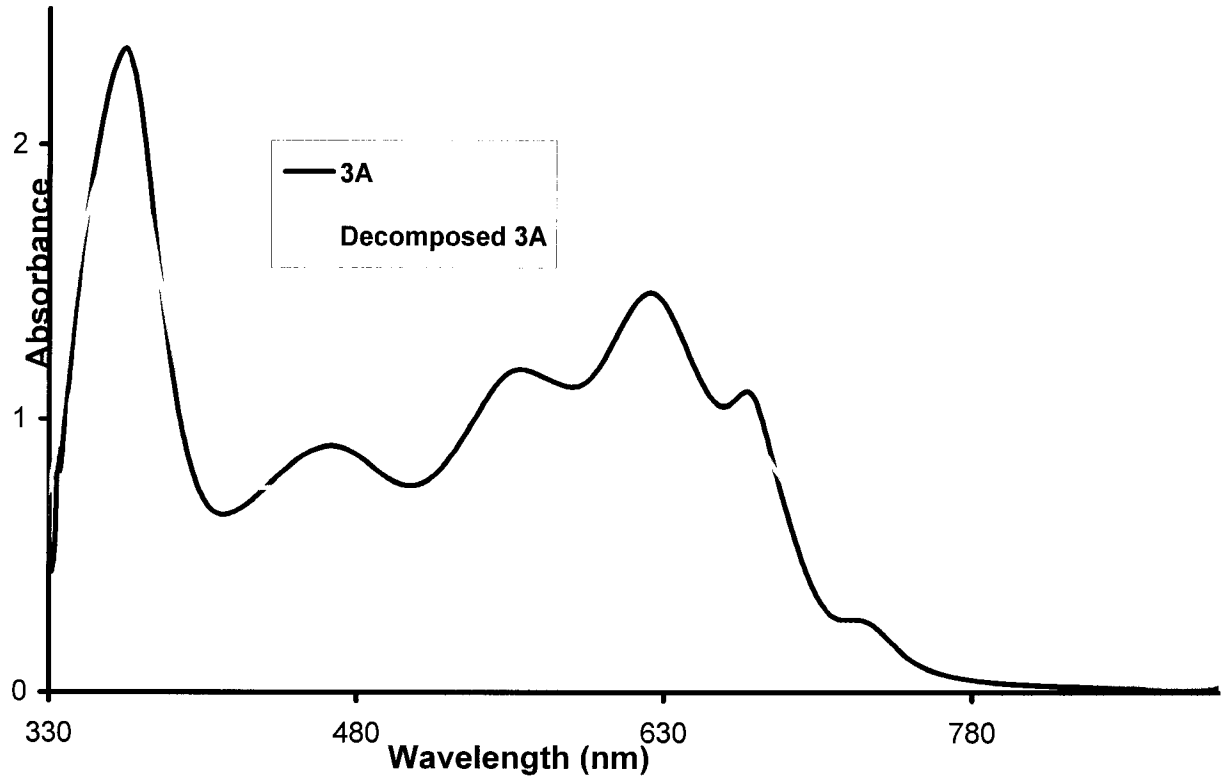

Figure 2.3.1. The UV-vis spectra of 2,3-bis(diamino)-7,8,12,13,17,18-hexakis (4-*tert*-butylphenyl) porphyrazine, **3A** (50μM in toluene) and the same solution after exposing to light in air for 30 minutes at room temperature.

The excocylic coordination of the second generation monomer was prepared from [2,3-bis(diamino)-7,8,12,13,17,18-hexakis(4-*tert*-butylphenyl)porphyrazine, **3A**, and an equivalent of bis(benzonitrile)dichloro-palladium(II) to form **3A**·$PdCl_2$. The dimer **4A** was prepared from same building block with 0.5 equivalent $Pd(OAc_2)_2$ (scheme 2.3.4.). The UV-visible spectrum of **3A**·$PdCl_2$ is similar to the first generation monomer **1A**·$PdCl_2$, but now the reaction is completed within 15mins in toluene at room temperature (figure 2.3.2.). The significantly enhanced metal chelation by the free amines on **3A** means that the dimer **4A** can be formed and is stable at much lower

concentrations. This is an advantage over the first generation dimers **2A** and **2B**. The enhanced ability of the free amino Pz to coordinate metal ions by geminal amines indicate that the investigation of the self-assembly of porphyrazine-porphyrazine dimers in solution at room temperature is now feasible. The formation of the dimer was monitored by UV-vis spectroscopy in toluene at room temperature. In the titration experiment, an aliquot of the solution containing 0.5 equivalent $Pd(OAc_2)_2$ was added to the porphyrazine **3A** solution (50μM in toluene), the mixture was stirred at room temperature ~10min, and spectra were recorded at ~20 °C (figure 2.3.3.). The UV-vis spectra indicate the electronic communication between the two porphyrazines mediated by the coordinated square planar metal. The highest energy peak blue shifts about 4nm, and two Q bands at 556nm and 621nm collapse to give a new broad peak at 588nm, and the lowest energy Q band red shifts from 669nm to 673nm. Also, there are several isosbestic points in the titration spectra, indicating the formation of only one product.

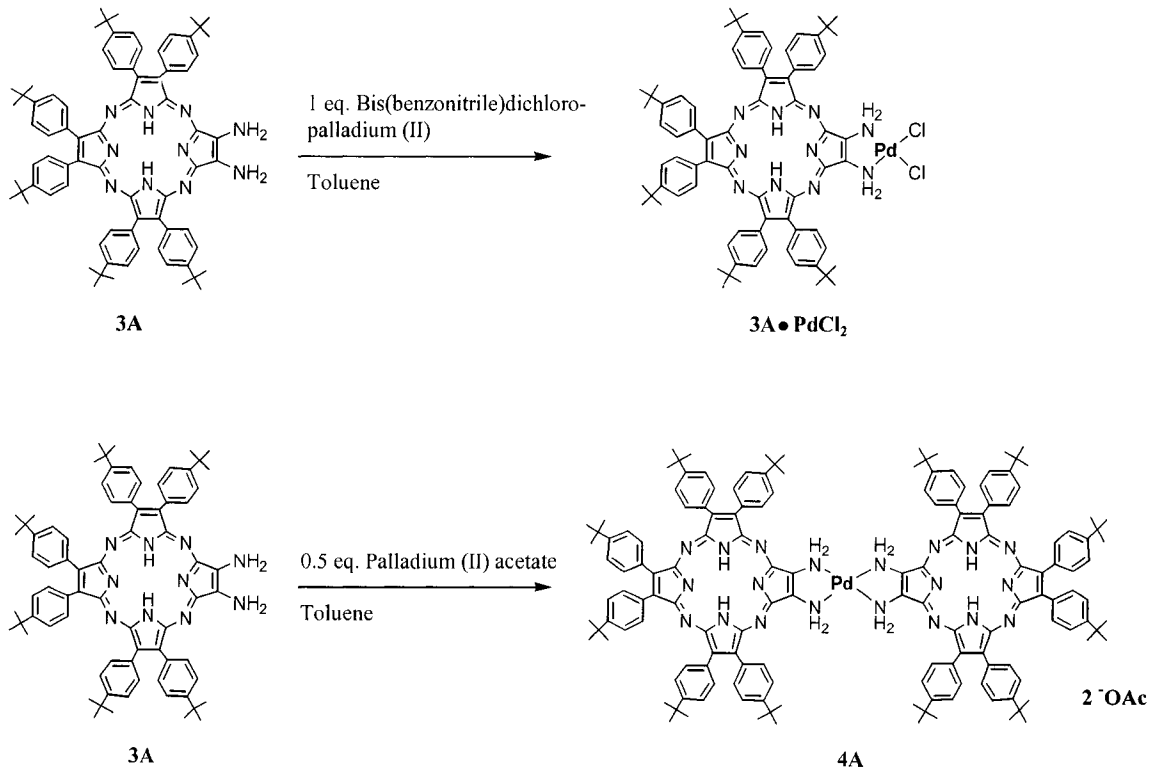

Scheme 2.3.4. Coordination of [2,3-bis(diamino)-7,8,12,13,17,18-hexakis (4-*tert*-butylphenyl)porphyrazine **3A** by Pd(II) and formation of the dimer.

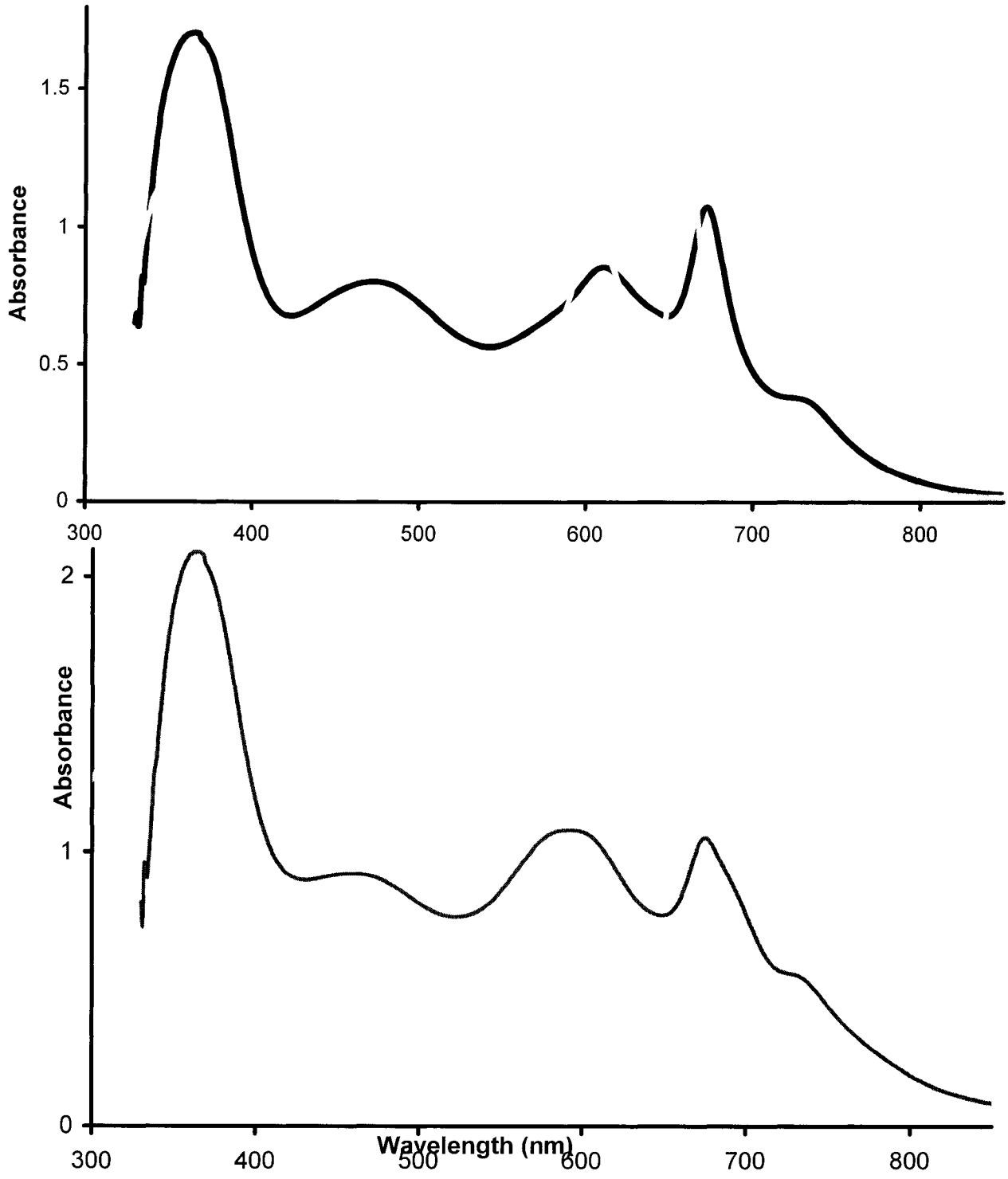

Figure 2.3.2. (Top)The UV-visible spectrum of the **3A**·$PdCl_2$ (black) compared to **1A**·$PdCl_2$ (gray) in toluene. (Bottom) The UV-visible spectrum of the **4A** (black) compared to **2A** (gray) in toluene.

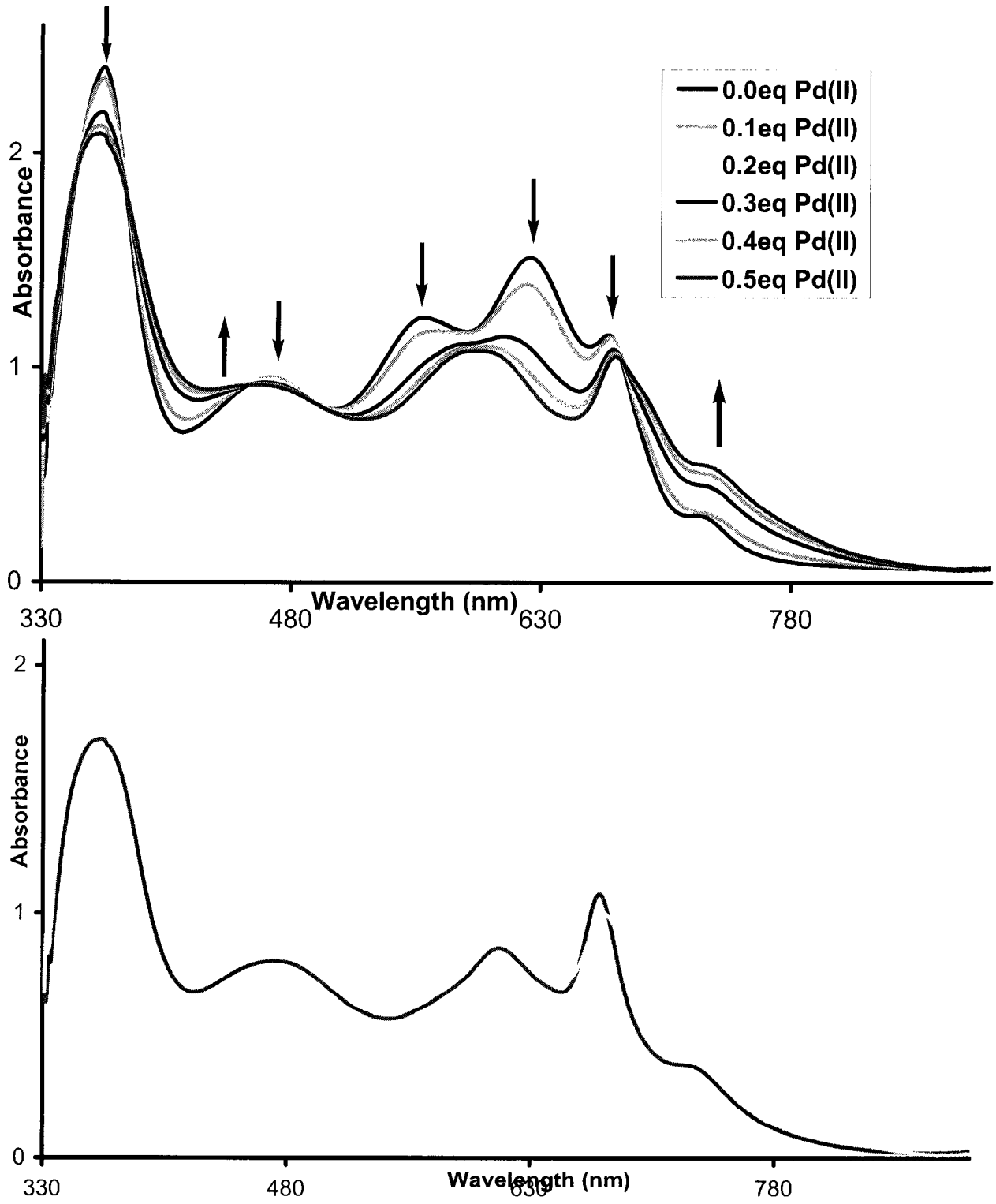

Figure 2.3.3. (Top) Formation of the dimer **4A** was investigated by titration experiments, aliquots of a solution containing the 0.5 equivalent $Pd(OAc_2)_2$ were added to the porphyrazine solution (50μM in toluene), the mixture was stirred at room temperature for ~10min, and spectra were recorded at ~20 °C. (Bottom) The UV-visible spectrum of the **3A**·$PdCl_2$ (black) compared to the dimer **4A** (gray) in toluene.

The conclusions about the formation of Pz dimers are as following:

(1) Although the assembly process is inefficient, the formation of Pz dimers by coordination of exocyclic dimethylamino groups to square planar metals Pd(II) or Pt(II) can be accomplished and the products characterized by ^{1}H NMR, UV-vis, and ESI-MS for the more robust Pt-linked dimer **2C**.

(2) The stronger and more facile coordination of free amino groups to Pd or Pt can be exploited to form these types of dimers; though the starting Pz is more labile. These second generation dimers are also readily characterized and exhibit somewhat different optical spectra.

(3) The free base porphyrazines **1A** emission is at 732nm when excited at 453nm, monomers **1A**·PdX_2 (X=Ac or Cl) emit at 732nm when excited at 490nm and **1A**·$PtCl_2$ also emits at 732nm when excited at 493nm. An overall 40-60% quenching in the emission is observed due to the heavy atom effect.[14] Similarly to the porphyrins, the Ni(II) complexes are non-luminescent. The free base dimer **2A** luminesces at 738nm but the Pd(II) or Pt(II) quences the luminescence by about 60%. The array **4A** emission is at 745nm when excited at 596nm.

(4) These photophysical properties are consistent with the thiol dimer reported earlier.[14,41]

2.4. Porphyrazine – porphyrin tetramer

The porphyrazine-porphyrin tetramer **6A** was prepared by dechlorination of the Pt-planar tape, **5A**, with silver perchlorate and then reacted with two equivalents **3A** in toluene at room temperature (~23 ^{0}C) for 24 hrs (scheme 2.4.1.). The Pt tape was formed

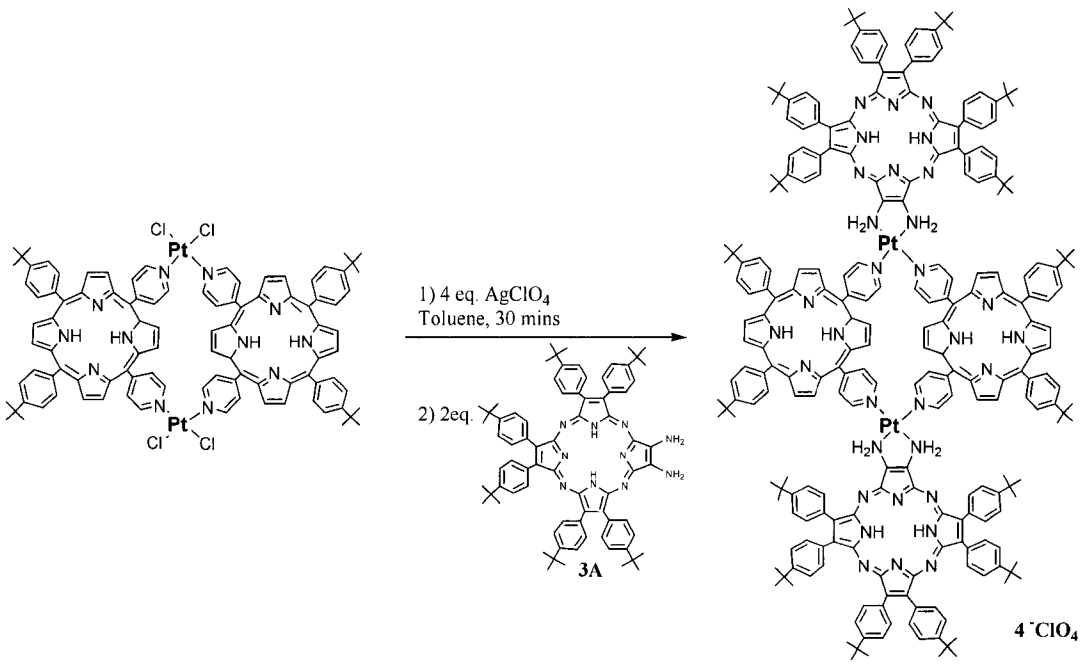

Scheme 2.4.1. Synthesis of the porphyrazine-porphyrin tetramer **6A**.

through the coordination of two equivalents 5, 10- bis(4-pyridyl) 15,20,-bis(4-*tert*-butylphenyl)porphyrin to two trans platinum dichloride in toluene with concentration of 10 μM in boiling toluene for 24hrs in the dark (scheme 2.4.2.).[28]

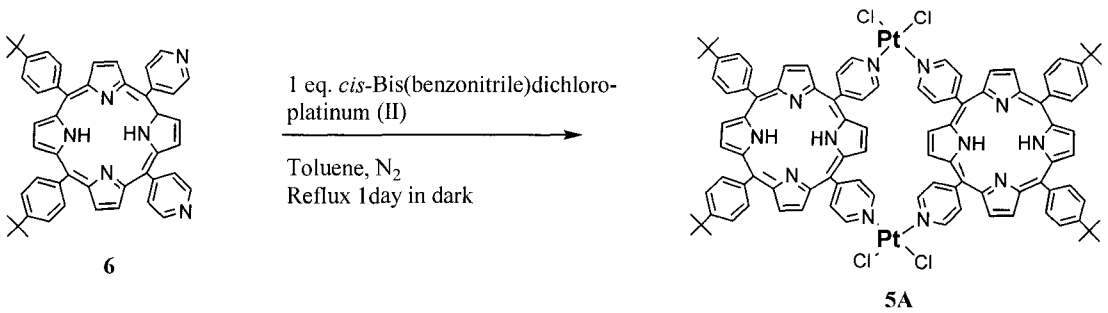

6

5A

Scheme 2.4.2. Formation of the Pt-planar tape.[28]

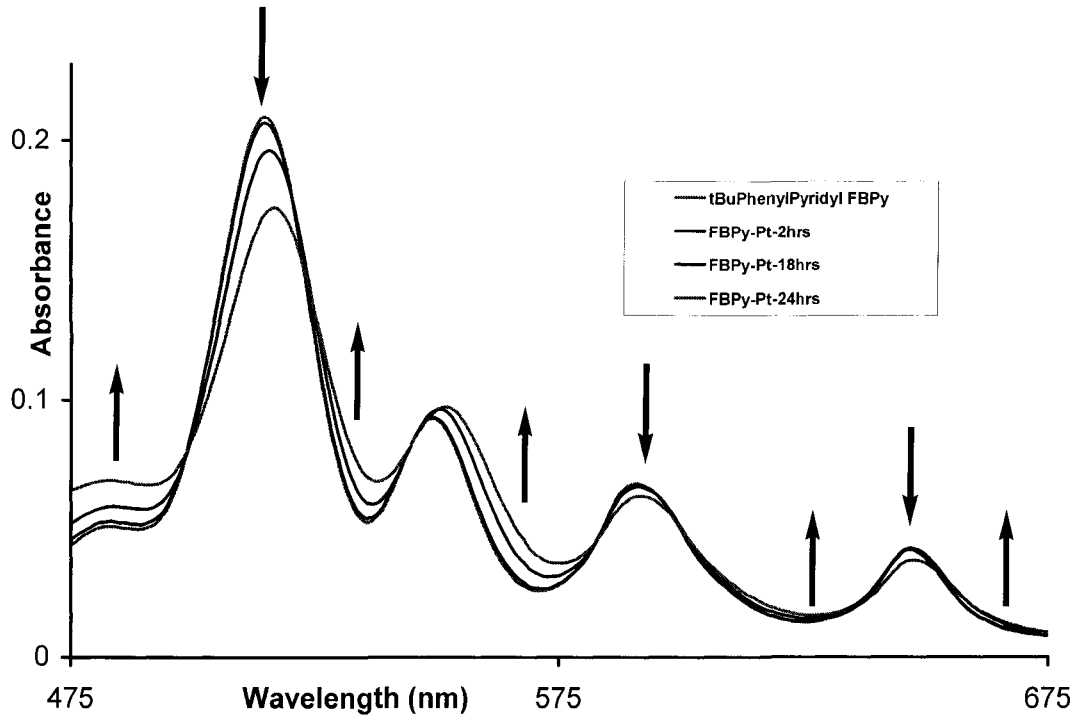

Figure 2.4.1. Formation of the Pt tape **5A** was monitored by UV-Visible spectroscopy. Several isosbestic points found in the Q band region indicate one product is formed.

The formation of Pt tape **5A** was monitored by UV-Visible spectroscopy (figure 2.4.1.). 2 nm red shift of the Soret band in the spectrum showed the binding of the platinum to the exocyclic pyridyl groups, and the several isosbestic points found in the Q band region that indicated the formation of only one species in solution. The proton NMR spectrum of the porphyrazine-porphyrin tetramer **6A** did not give the clear signals for structure determination because at the relatively high concentration of the sample (5-10 mM) the complex is poorly soluble and aggregates. We also investigated the formation of the tetramer **6A** through the UV-visible titration experiments in which four equivalents (in $5 \leq 10\mu L$ aliquots) of silver perchlorate, dissolved in dichloromethane, were titrated into a 5μM solution of Pt tape **5A** and free amino porphyrazine **3A** in toluene. The mixture was stirred at 25 ^{0}C for ~10 minutes and spectra were recorded at ~20 ^{0}C. Unfortunately, no clear isosbestic points were observed. One explanation of this result could be that the silver ions in the solution not only dechlorinated the Pt tape but also coordinated with the free amino Pzs. As a result, there may be formation of several species in solution. However, for the tetramer **6A** solution, the UV-visible spectra at low concentrations (~5μM in toluene) show a new peak at 700nm that neither belongs to the Pt tape **5A** nor the free amino-Pz **3A** nor **3A**·$PtCl_2$ (figure 2.4.2.).

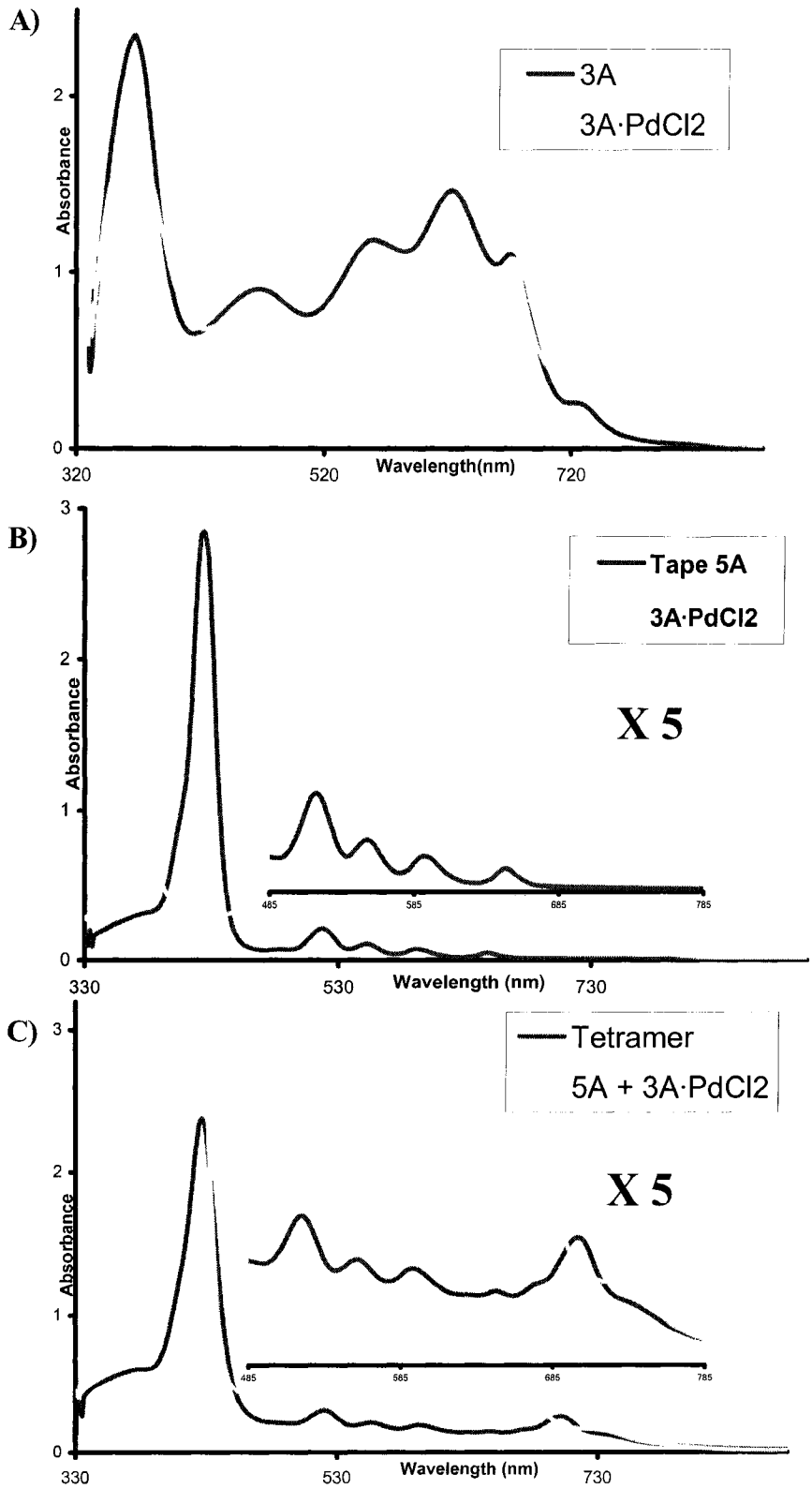

Figure 2.4.2. The UV-visible spectra of (A) **3A** and **3A**•$PdCl_2$; (B) tape **5A** and **3A**•$PdCl_2$; and (C) the tetramer **6A** (~5μM in toluene) and (B) shows a new peak at 700nm which neither belongs to the Pt tape **5A** nor **3A**•$PdCl_2$.

Fluorescence emission studies of the tetramer **6A** were performed in toluene solution. When the solution is excited at the highest energy porphyrin band (the Soret band of the porphyrin at 426nm where the porphyrin absorption is ~10X the porphyrazine absorption), it emits at 655nm and 730nm, which is about 3nm to the red of the emission of the Pt tape **5A** (emission at 652nm and 716 nm). When excitation is centered at 554nm where both the chromophores absorb (in this case the Pz absorbs ~5 times the porphyrin), the emission at 655nm diminished but another emission at 738nm is enhanced. The porphyrazine **3A** emission is at 736nm when excited at 563nm (figure 2.4.3.). The **3A**·$PdCl_2$ fluorescence is at 738nm when excited at 465nm. Importantly, there is large increase in the emission of 738nm compare with **3A** and **3A**·$PdCl_2$. The large change in the ratio of the emission peaks when the tetramer **6A** is excited with at the two different wavelengths (426nm and 554nm) may arise from several factors. There is energy transfer from the porphyrin tape to the Pz component as evidenced by the quenching of the porphyrin luminescence even when excited in the Soret band (426nm) (the emission is at 655nm and 730nm). Secondly, when the Pz is excited, preferentially over the porphyrin (554nm), we see that the emission at 655nm is diminished, and that at 738 increases. The excitation spectra reveal that the 655 peak arises largely from the porphyrin, half of the tetramer. Conversely, the peak at 738 arises largely from the porphyrazine.

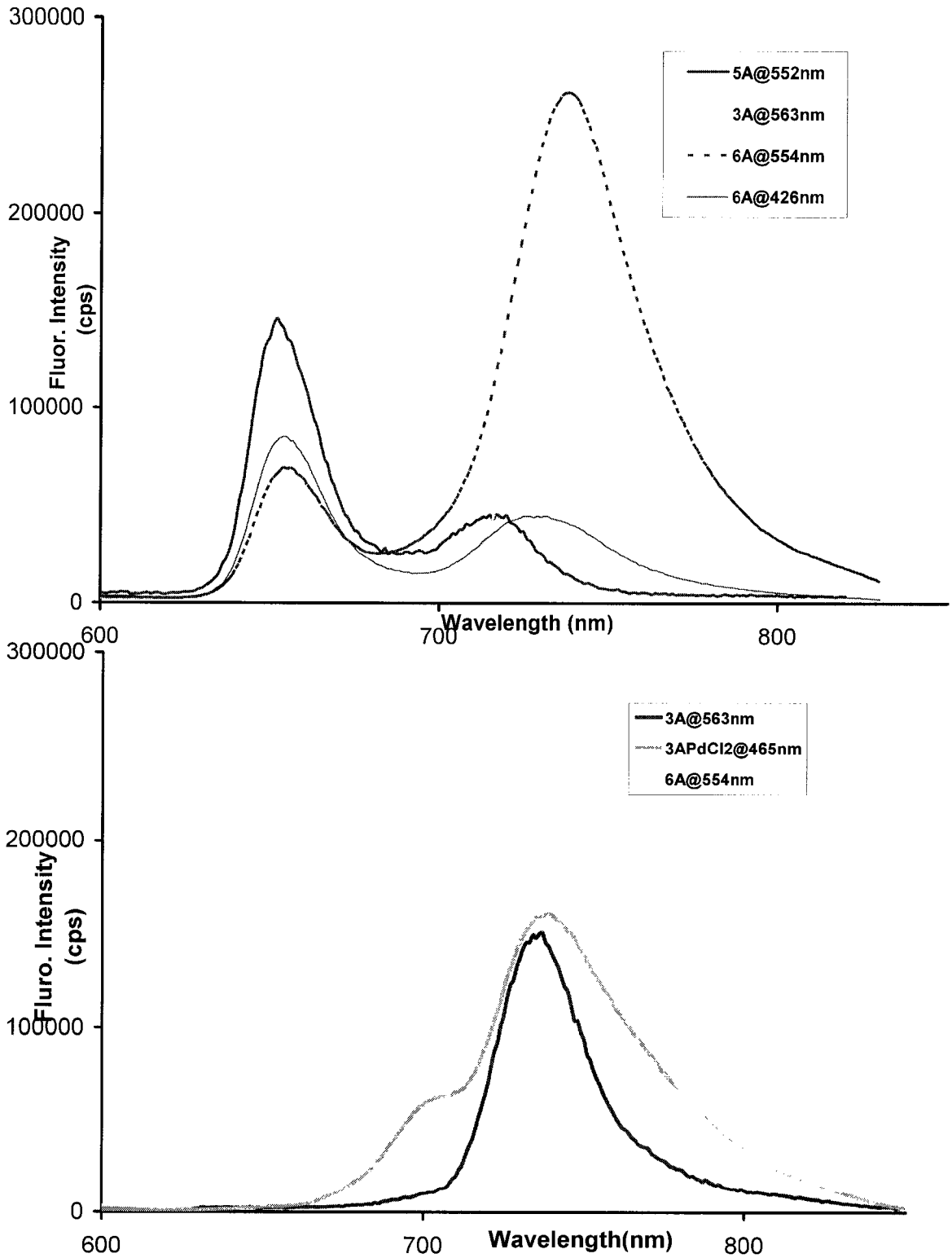

Figure 2.4.3. (Top) Fluorescence emission spectra of the tetramer **6A** indicate some energy transfers between the porphyrin and porphyrazine. (Bottom) Fluorescence emission spectra of **3A**, **3A**·PdCl2 and **6A** in toluene show the increasing in the Pz emission in the tetrameric array.

The structure of the tetramer **6A** was determined by MALDI mass spectroscopy in positive-ion mode. A broad peak at 4589 mass (m/z) is assigned to the tetramer **6A** with three perchlorate ions and one silver acetate salt (figure 2.4.5.).

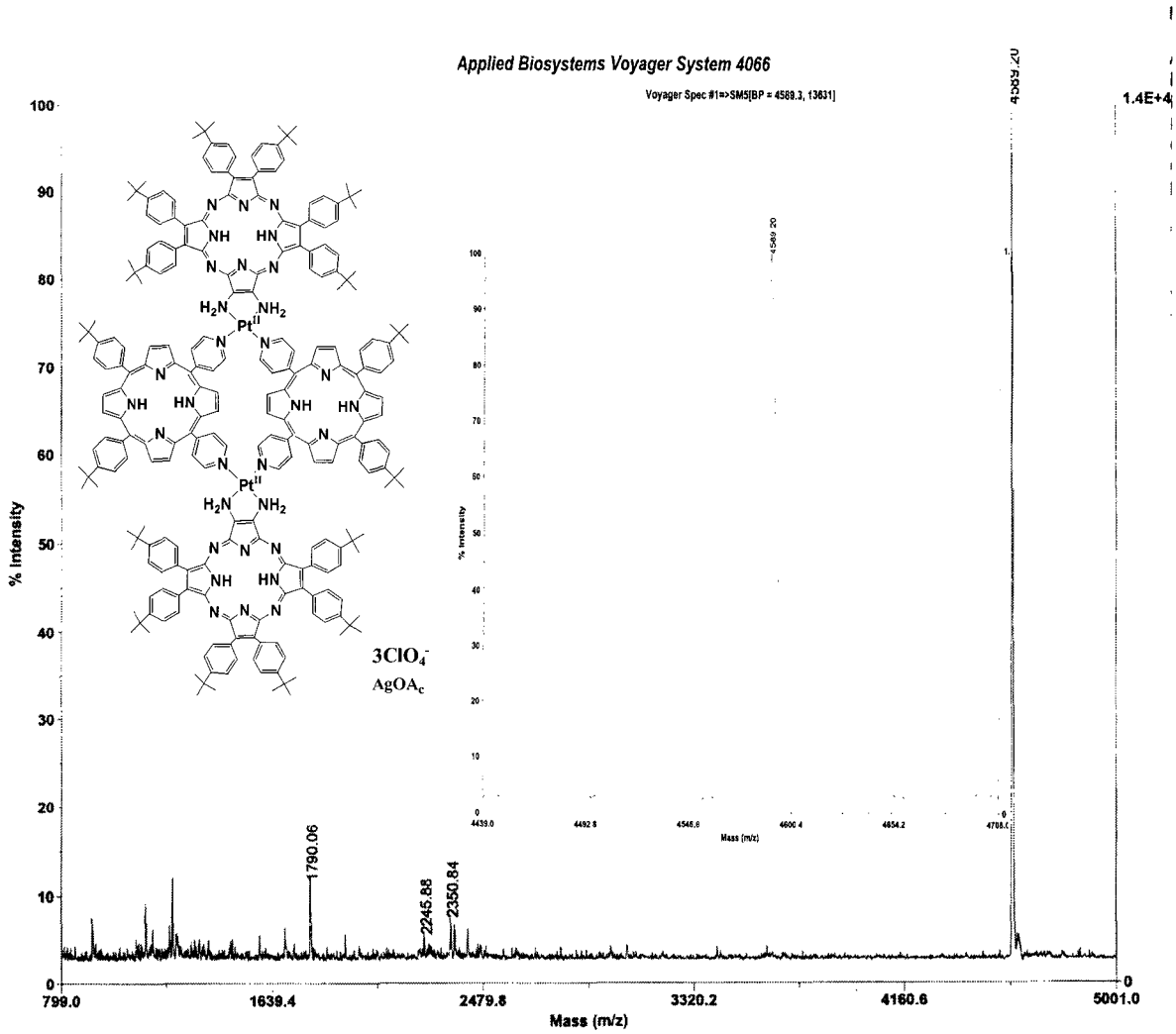

Figure 2.4.4. MALDI mass spectroscopy in positive-ion mode shows a broad peak at 4589 mass (m/z), which can be assigned as the tetramer **6A** with three perchlorate ions and one silver acetate salt. The calculated MS has an envelope of peaks from 4581 to 4598, which compare to the experimental MS envelope of 4581 to 4597.

We also self–assembled the porphyrazine-porphyrin tetramer **7A** with dimethylamino Pz **1A** (scheme 2.4.3.). With the dimethyl groups, yield of the tetrameric assembly is lower than the free amino-Pz assembly. The structure of the tetramer was determined by MALDI mass spectroscopy in positive-ion mode. A 2256 (m/z) peak in the spectrum is assigned to the tetramer **7A** with four perchlorate ions and two sodium ions. There are several small peaks at higher masses, which are assigned as the tetramer complex taking up different salts such as sodium chloride, silver chloride and silver perchlorate (figure 2.4.6.). We often observe that these large Pz-Py systems are associated with various salts in the mass spectra. The spectra presented are typical of several preparations.

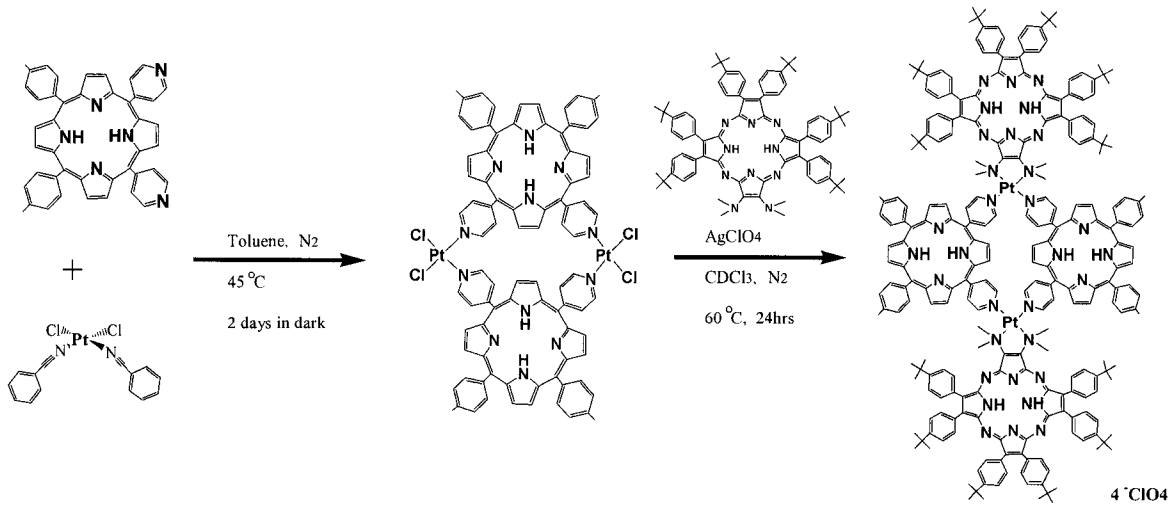

Scheme 2.4.3. Self–assembly the porphyrazine-porphyrin tetramer **7A** with **1A** and the tape **5B**.

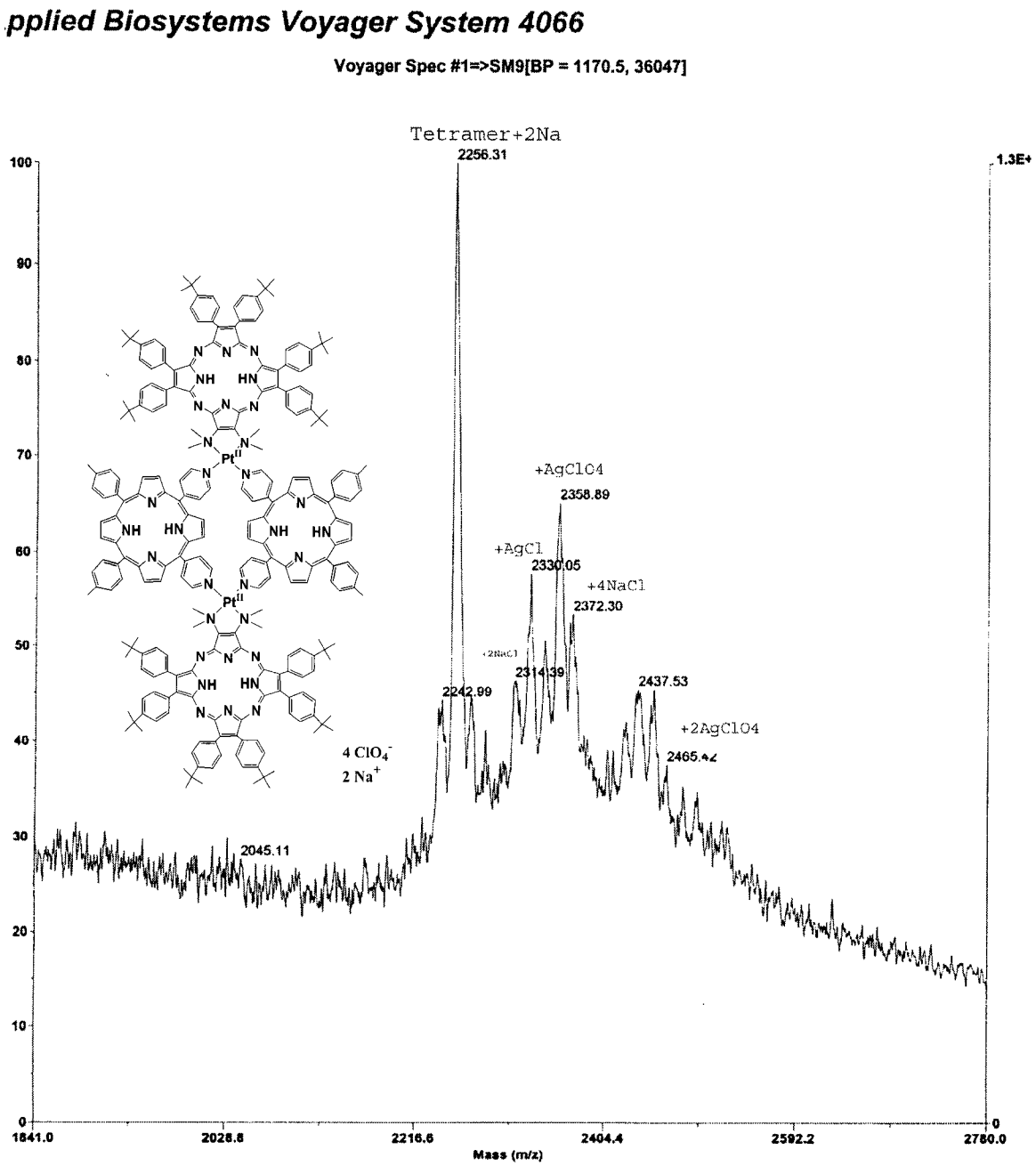

Figure 2.4.5. MALDI mass spectroscopy of the porphyrazine-porphyrin tetramer **7A** Pz **1A** and tape 5B shows a 2256 (m/z) peak that can be assigned as the tetramer with four perchlorate ions and two sodium ions. The other peaks are **7A** with various combinations of counter ions and salts.

B3.

Conclusion

Porphyrazine and porphyrin building blocks were synthesized and well characterized by ^{1}H NMR spectra and ESI-MS. The porphyrazine-porphyrazine dimers were also synthesized by coordination with the either Pd(II) or Pt(II) square planar linkers. The structures of the dimers were confirmed by UV-Vis, ^{1}H NMR and simple molecular dynamics calculations. We also synthesized two porphyrazine-porphyrin tetramers and studied their photophysical profiles by means of absorption and emission spectroscopy. Current data show that the steric hindrance among the dimethyl amino groups in the porphyrazines diminish the efficiency of the self-assembly of a rigid planar array, and the freebase porphyrin – free base porphyrazine palladium tetramer has some electronic communication among the chromophores. Again, our systematic approach is to make and understand the chemistry and photophysical properties of the dimers, the tetramers, and then use these results to design higher ordered structures and materials.

B4.

Experimental Section

4.1. Reagents and physical measurements

All solvents were distilled using standard methods. Silica gel (Baker, 60μm average particle size) and alumina (Fisher, 80-200 mesh) were used for column chromatography. The $CHCl_3$ was reagent grade and used directly. The methyl THF was of reagent grade and used as obtained. The THF was freshly distilled from Na and methanol was distilled from CaH_2. The other solvents were distilled either from CaH_2 or P_2O_5. Proton NMR spectroscopy was recorded on a Varian VXR-300 MHz instrument using chloroform-D solvent as internal reference. UV-visible spectra were recorded on a Varian Bio-100 spectrometer. Electrospray mass spectroscopy spectrum was performed on Hewlett-Packard HP-1100 LC/MS positive-ion mode. MALDI mass spectroscopy spectrum was performed on Applied Biosystems Voyager system 4066 in positive-ion mode as a service from the University Illinois at Urbana-Champaign.

In general for titration experiments, an aliquot of the solution containing the given metal ion was added to the porphyrazine solution, the mixture was stirred at room temperature for ~15 minutes and spectra were recorded at ~20 ^{0}C. Under the conditions described for the titrations, plots of either absorption intensity or chemical shifts versus

mole ratio indicate a 2:1 stoichiometry of the porphyrazine derivatives to the metal ion coordinated in the dimer unit.

4.2. Synthesis of compounds

Bis(dimethylamino)maleonitrile.[40] A solution of 13.5 g (0.125 mol) diamino maleonitrile (DAMN) in 75 mL glyme was added dropwise to a suspension of 25 g (0.75 mol) NaH in 250 mL glyme at –30 °C. Hydrogen gas was evolved. The reaction mixture was warmed to –10 °C and 60 mL (0.75 mol) of dimethyl sulfate was added over 1 hr. during the addition, hydrogen was produced. The reaction mixture was stirred for 1hr at –10 °C and then filtered. The unreacted NaH and sodium methyl sulfate was washed with 100 mL glyme and the combined filtrate was concentrated under vacuum. The residue was chromatographed on silica gel using dichloromethane as the eluent to separated the *cis* product and yield a pale yellow solid (9.0 g, 54%). ^{1}H NMR ($CDCl_3$) [δ (ppm)]: 2.78 (s, 12H) (Figure B1). ^{13}C NMR ($CDCl_3$) [δ (ppm)]: 42.2, 114.7, 117.8 (Figure B2).

(4-*tert*-butylphenyl)acetonitrile.[14] 4-*tert*-Butylbenzyl chloride (12.5 g, 0.068 mol), freshly ground NaCN (5 g, 0.1 mol), and NaI (105 g, 0.01 mol) were suspended in acetone (15 mL), and the solution was heated to reflux for 48 hrs. The reaction mixture was filtered hot, and the filtrate was concentrated under vacuum. The residue was taken up in $CHCl_3$, washed with hot water twice, and dried with $MgSO_4$. The $CHCl_3$ was rotary evaporated yielding yellow oil. The product was distilled under vacuum at 110 °C to

yield clear oil (10.8 g, 87%). ^{1}H NMR ($CDCl_3$) [δ (ppm)]: 7.42 (d, J=8.5Hz, 2H), 7.27 (d, J=8.5Hz, 2H), 3.73 (s, 2H), 1.34 (s, 9H) (Figure B3). ^{13}C NMR ($CDCl_3$) [δ (ppm)]: 23.4, 31.5, 34.8, 118.1, 126.1, 127.0, 127.7,151.2 (Figure B4).

Bis(4-*tert*-butylphenyl)fumaronitrile.[14] Freshly-cut Na (2.8 g, 0.123 mol) was added to MeOH (40 ml) cooled to 0 °C. The sodium methoxide was added dropwise over 20 mins to a solution of (4-*tert*-butylphenyl)acetonitrile (10.6 g, 0.061 mol) and I_2 (15.6 g, 0.061 mol) dissolved in diethyl ether (250 mL) at 0 °C. The dark brown color of the solution cleared (becoming pale yellow), and a white precipitate formed, which was collected, washed with MeOH, and dried under vacuum. The filtrate volume was reduced by half and placed in freezer overnight. A second crop of product was filtered out, washed, and dried under vacuum. Total yield (7.0 g, 67%). ^{1}H NMR ($CDCl_3$) [δ (ppm)]: 7.80 (d, J=8.5Hz, 4H), 7.55 (d, J=8.5Hz, 4H), 1.38 (s, 18H) (Figure B5). ^{13}C NMR ($CDCl_3$) [δ (ppm)]: 31.4, 35.4, 117.2, 124.5, 126.3, 128.6, 129.5, 155.4 (Figure B6).

3,4-Bis(4-*tert*-butylphenyl)pyrroline-2,5-diimine.[14] Bis(4-*tert*-butylphenyl) fumaronitrile (5 g, 0.015 mol) was suspended in ethylene glycol (300 mL) and heated to 115 °C. Two small chunks of Na (~30 mg) were added to the reaction. When the suspension reached 115 °C, gaseous NH_3 was bubbled through the suspension. After 1.5 hrs, the solution was filtered hot and filtrate was poured over ice water (700 mL). A yellow precipitate formed which was collect by filtration and washed with water. The solid was dissolved in $CHCl_3$, dried with Na_2SO_4, treated with activated charcoal, and filtered, and the solvent was removed under vacuum yielding a yellow powder (2.0 g,

26%). ^{1}H NMR ($CDCl_3$) [δ (ppm)]: 7.75 (d, J=8.5Hz, 4H), 7.51 (d, J=8.5Hz, 4H), 3.51 (s, 3H), 1.37 (s, 18H) (Figure B7). ^{13}C NMR ($CDCl_3$) [δ (ppm)]: 31.5, 35.0, 125.9, 127.1, 128.6, 129.3, 152.2, 166.8 (Figure B8).

2,3-bis(dimethylamino)-7,8,12,13,17,18-hexakis(4-(*tert*-butyl)-phenyl)porphyrazine.[14] Magnesium metal (0.22 g, 9.05 mmol) was stirred in a refluxing *n*-BuOH (50 mL) under N_2 for 24 hrs. 3,4-Bis(4-*tert*-butylphenyl)pyrroline-2,5-diimine (1.5 g, 4.17 mmol) and bis(dimethylamino)maleonitrile (1.1 g, 8.34 mmol) were added to the resulting magnesium butoxide under N_2 for 3 days. The BuOH was removed under vacuum, and the residue was dissolved in $CHCl_3$ and filtered. The residue was further washed with $CHCl_3$ until the washings were colorless. Solvent was removed by rotary evaporation and the residual crude solid was dried under vacuum. The solid dissolved in an excess of CF_3CO_2H (60 mL), and stored in dark for 1 hr. The dark purple slurry was poured over ice water (600 mL) and neutralized with concentrated NH_4OH. The purple solid was collected by filtration and washed with water and MeOH and dried under vacuum. The crude solid was chromatographed on silica gel using 50% hexanes/$CHCl_3$ as eluent. The desired porphyrazine was the second major band, which was collected and recrystallized from acetonitrile to yield 0.5 g product (10% yield). ^{1}H NMR ($CDCl_3$) [δ (ppm)]: 8.35 (d, J= 8.4 Hz, 4H), 8.31 (d, J= 8.4 Hz, 4H), 8.03 (d, J= 8.4 Hz, 4H), 7.63 (d, J= 8.4 Hz, 4H), 7.61(d, J= 8.4 Hz, 4H), 7.56 (d, J= 8.4 Hz, 4H), 3.68 (s, 12 H), 1.56 (s, 18H), 1.53 (s, 18H), 1.50 (s, 18H), -1.05 (br, 2H-internal) (Figure B9). UV/vis ($CHCl_3$): λ_{max} 363, 450, 636, 669, 738nm. ESMS: *m/z* 1193 ($M + H^+$).

[2,3-bis(dimethylamino)-7,8,12,13,17,18-hexakis(4-(*tert*-butyl)-phenyl)porphyrazinato]nickel(II).[14]

2,3-bis(dimethylamino)-7,8,12,13,17,18-hexakis(4-(*tert*-butyl)- phenyl)porphyrazine (0.1 g, 0.084 mmol), anhydrous $Ni(OAc)_2$ (0.15 g, 0.84 mmol), PhCl (10 mL), and DMF (5 mL) were heated to 100 °C under N_2 for 15 hrs. The solvent was removed under vacuum, and the solid was washed with 5% HCl in MeOH and then MeOH. Recrystallization from CH_3CN afforded 0.09 g product (90% yield). ^1H NMR ($CDCl_3$) [δ (ppm)]: 8.29 (d, J= 8.4 Hz, 4H), 8.21 (d, J= 8.4 Hz, 4H), 8.02 (d, J= 8.4 Hz, 4H), 7.63 (d, J= 8.4 Hz, 4H), 7.57(d, J= 8.4 Hz, 4H), 7.54 (d, J= 8.4 Hz, 4H), 3.60 (s, 12 H), 1.55 (s, 18H), 1.51 (s, 18H), 1.49 (s, 18H) (Figure B10). UV/vis ($CHCl_3$): λ_{max} 343, 457, 622, 670, 696nm. ESMS: *m/z* 1249 ($M + H^+$).

2,3-selenodiazole-7,8,12,13,17,18-hexakis(4-(*tert*-butyl)-phenyl)porphyrazine.[45] Magnesium metal (0.021 g, 0.88 mmol), and I_2 (1 small crystal) was stirred in a refluxing *n*-BuOH (10 mL) under N_2 for 24 hrs. 3,4-Bis(4-*tert*-butylphenyl)pyrroline-2,5-diimine (0.05 g, 0.14 mmol) and 3,4-dicyano-1,2,5-selenodiazole (0.05 g, 0.27 mmol) were added to the resulting magnesium butoxide under N_2 for 6 hrs. The BuOH was removed under vacuum, and the residue was dissolved in $CHCl_3$ and filtered. The residue was further washed with $CHCl_3$ until the washings were colorless. Solvent was removed by rotary evaporation and the residual crude solid was dried under vacuum. The solid dissolved in an excess of CF_3CO_2H (5 mL), and stored in dark for 1 hr. The dark purple slurry was poured over ice water (15 mL) and neutralized with $NaHCO_3$. The purple solid was collected by filtration

and washed with water and dried under vacuum. The crude solid was chromatographed on silica gel using $CHCl_3$ as eluent. The desired porphyrazine was the second purple band, which was collected and recrystallized from acetonitrile to yield 8.0 mg product (15% yield). ^1H NMR ($CDCl_3$) [δ (ppm)]: 8.32 (d, J= 8.1 Hz, 8H), 8.23 (d, J= 7.7 Hz, 4H), 7.74 (d, J= 8.4 Hz, 4H), 7.61 (d, J= 8.1 Hz, 8H), 1.54 (m, 54H), -1.72 (br, 2H-internal) (Figure B16). UV/vis (toluene): λ_{max} 364, 468, 578, 699 nm. ESMS: *m/z* 1213 ($M + H^+$) (Figure B21).

2,3-Bis(diamino)-7,8,12,13,17,18-hexakis(4-(*tert*-butyl)- phenyl)porphyrazine.[45]

1ml $CHCl_3$ saturated with H_2S (H_2S was bubbled through the solvent for 1min at 20 °C) was added to the 1ml $CHCl_3$ solution containing (2mg, 1.65μmol) 2,3-selenodiazole-7,8,12,13,17,18-hexakis(4-(*tert*-butyl)- phenyl)porphyrazine. To this solution was immediately added a pyridine (0.5 ml). The resulting mixture was stirred in dark for 15 min at 20 °C. the dark blue solution was concentrated to 0.5ml by rotary evaporation. To this blue solution was added acetonitrile (5ml). The mixture was cooled in an ice bath for 15 min and the precipitation was collected by a centrifuge and dried under a vacuum pump yielding a dark blue solid (1.8 mg, 95%). The product in solution is unstable under light and air, so it should be used immediately for the self-assembly. UV/vis (toluene): λ_{max} 366, 466, 560, 623, 669 nm. ESMS: *m/z* 1137 ($M + H^+$) (Figure B22).

B5.

Appendix

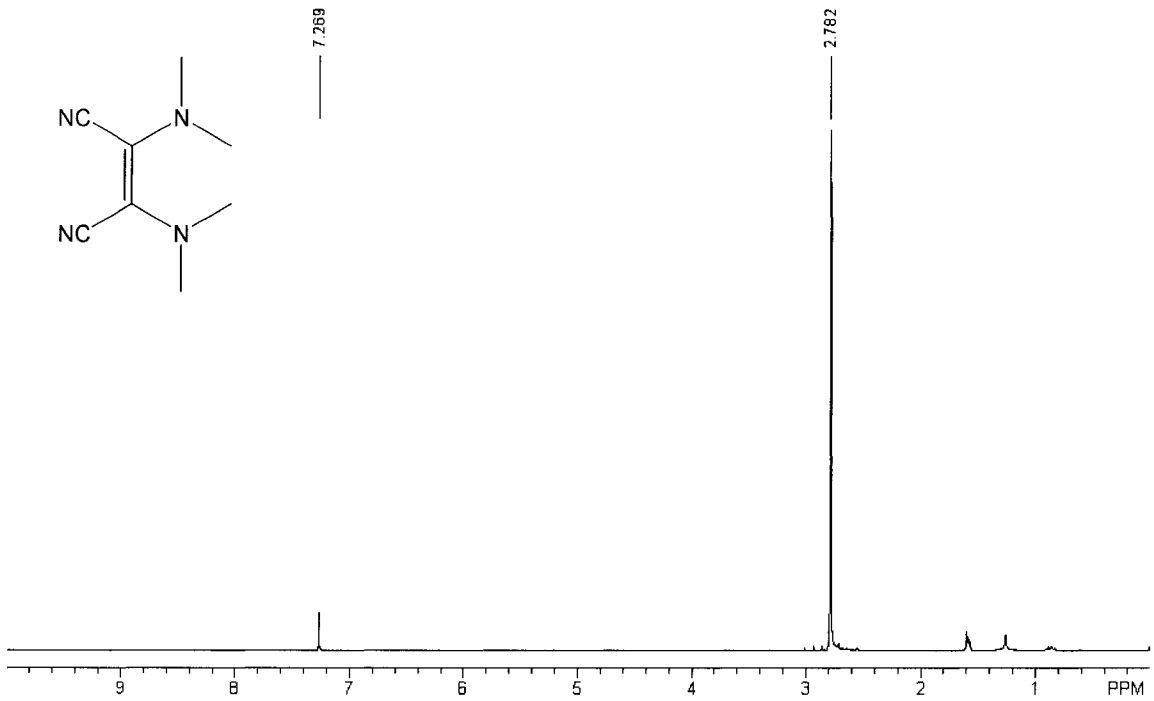

Figure B1. ^{1}H NMR (300 MHz, $CDCl_3$) of Bis(dimethylamino)maleonitrile.

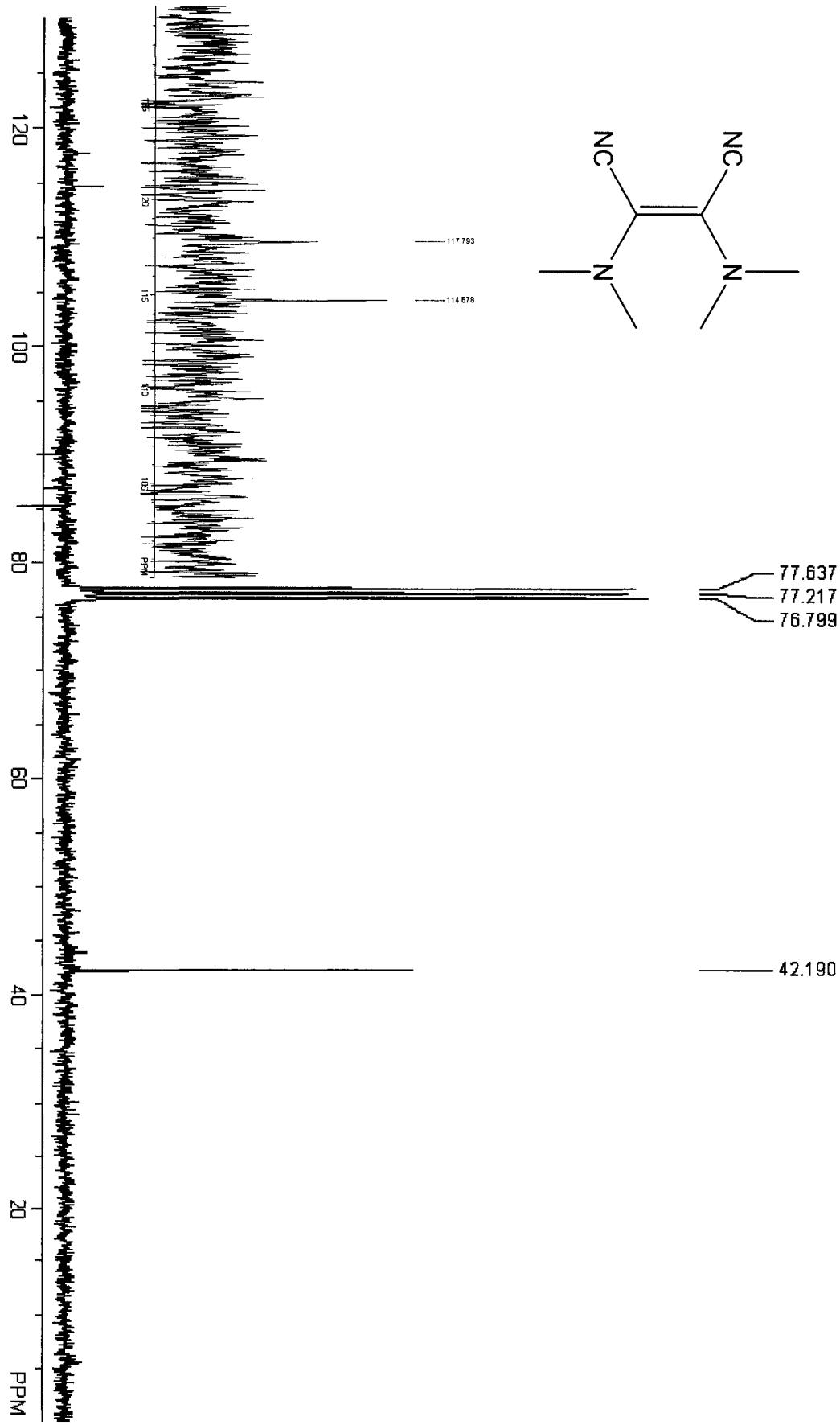

Figure B2. ^{13}C NMR (300 MHz, $CDCl_3$) of Bis(dimethylamino)maleonitrile.

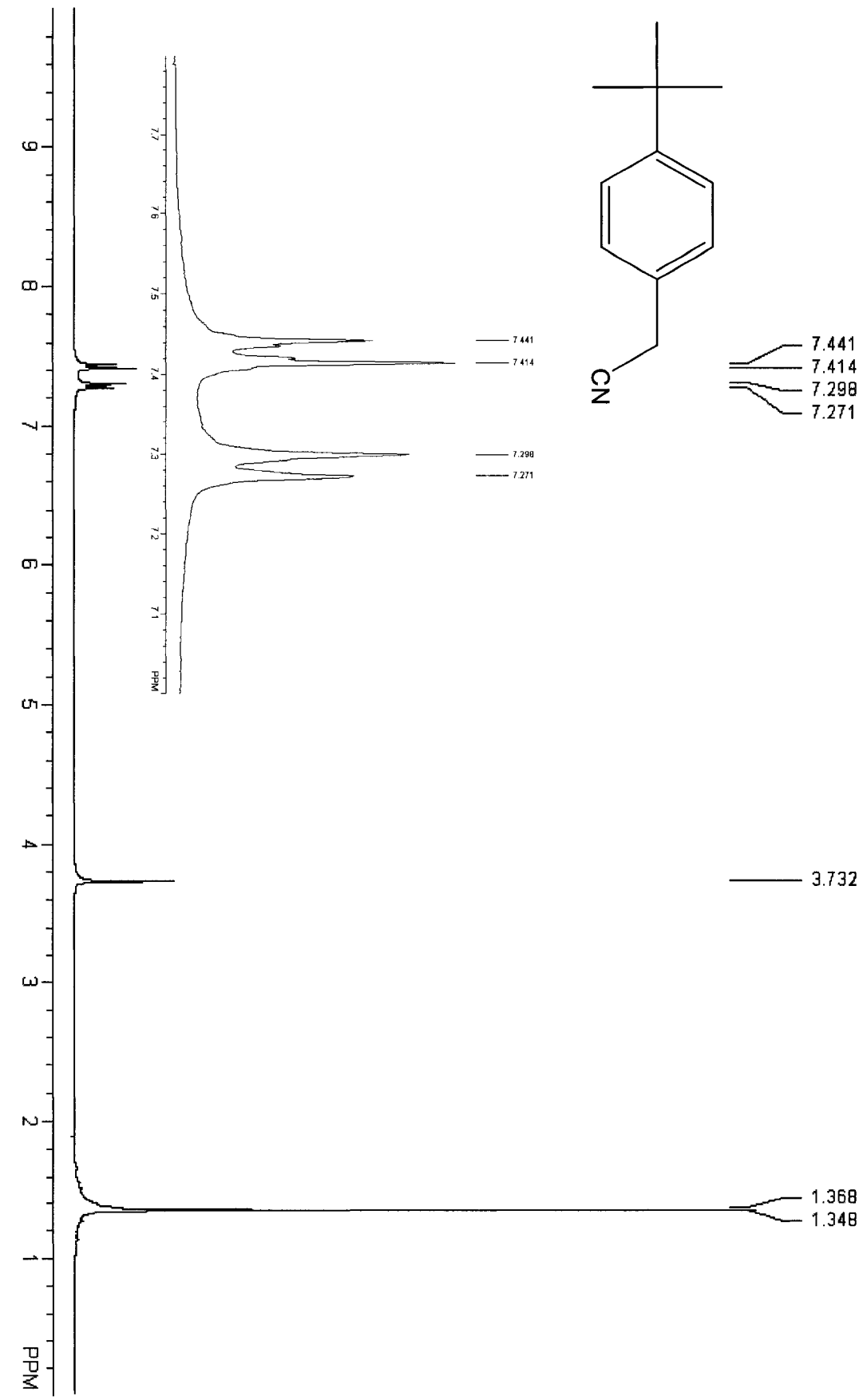

Figure B3. ^{1}H NMR (300 MHz, $CDCl_3$) of (4-*tert*-butylphenyl)acetonitrile.

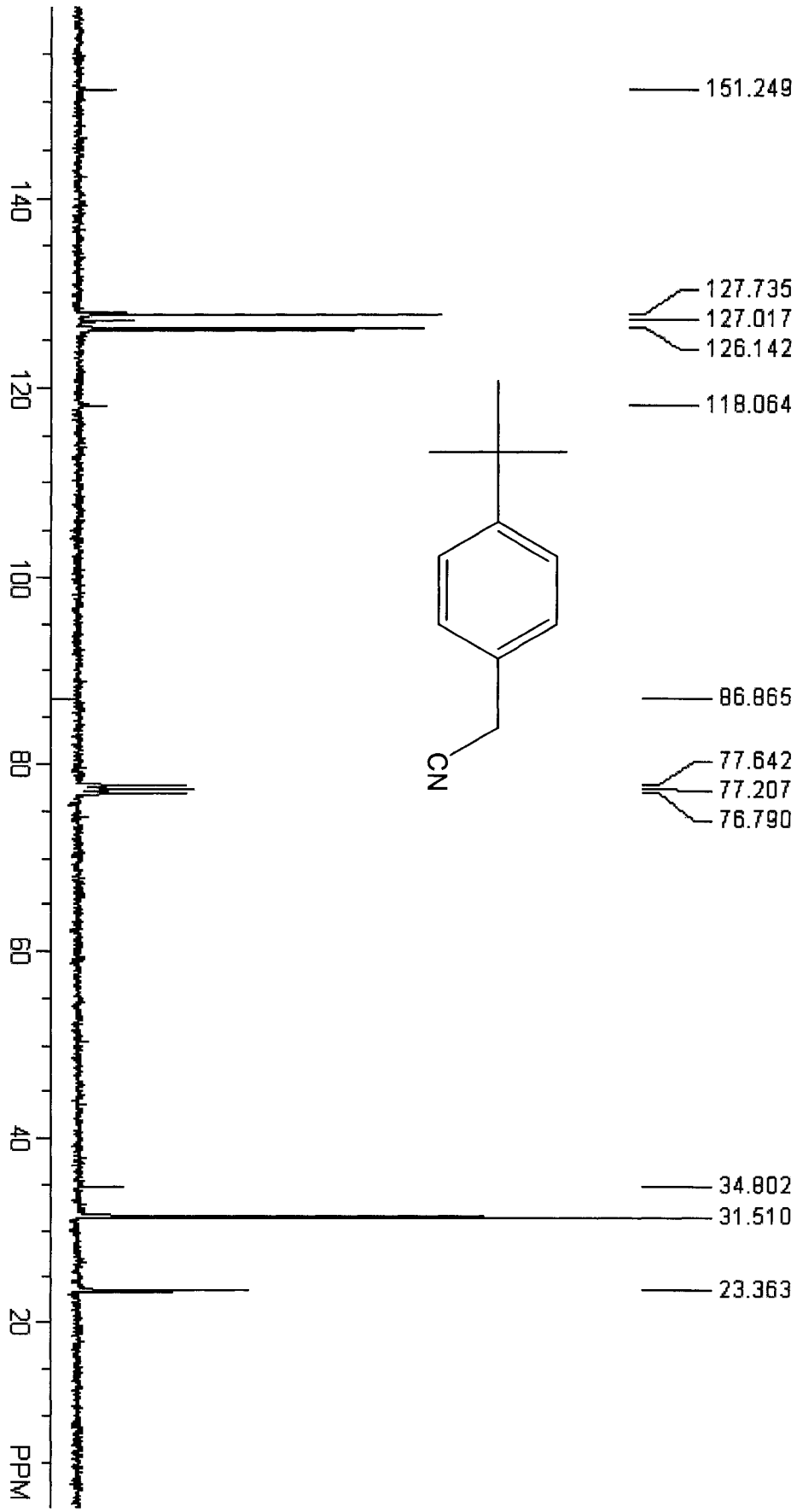

Figure B4. ^{13}C NMR (300 MHz, $CDCl_3$) of (4-*tert*-butylphenyl)acetonitrile.

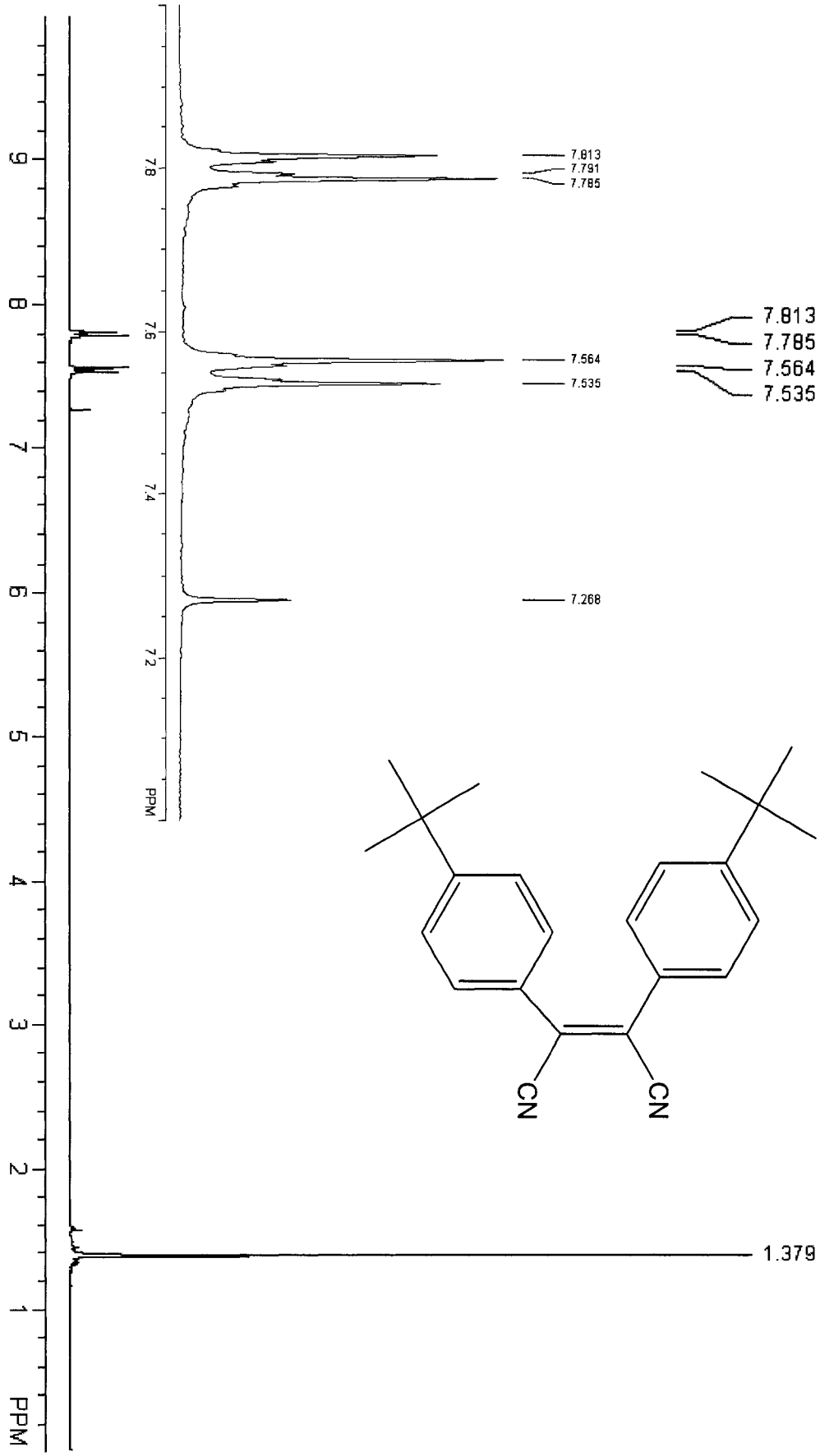

Figure B5. ^{1}H NMR (300 MHz, $CDCl_3$) of Bis(4-*tert*-butylphenyl)fumaronitrile.

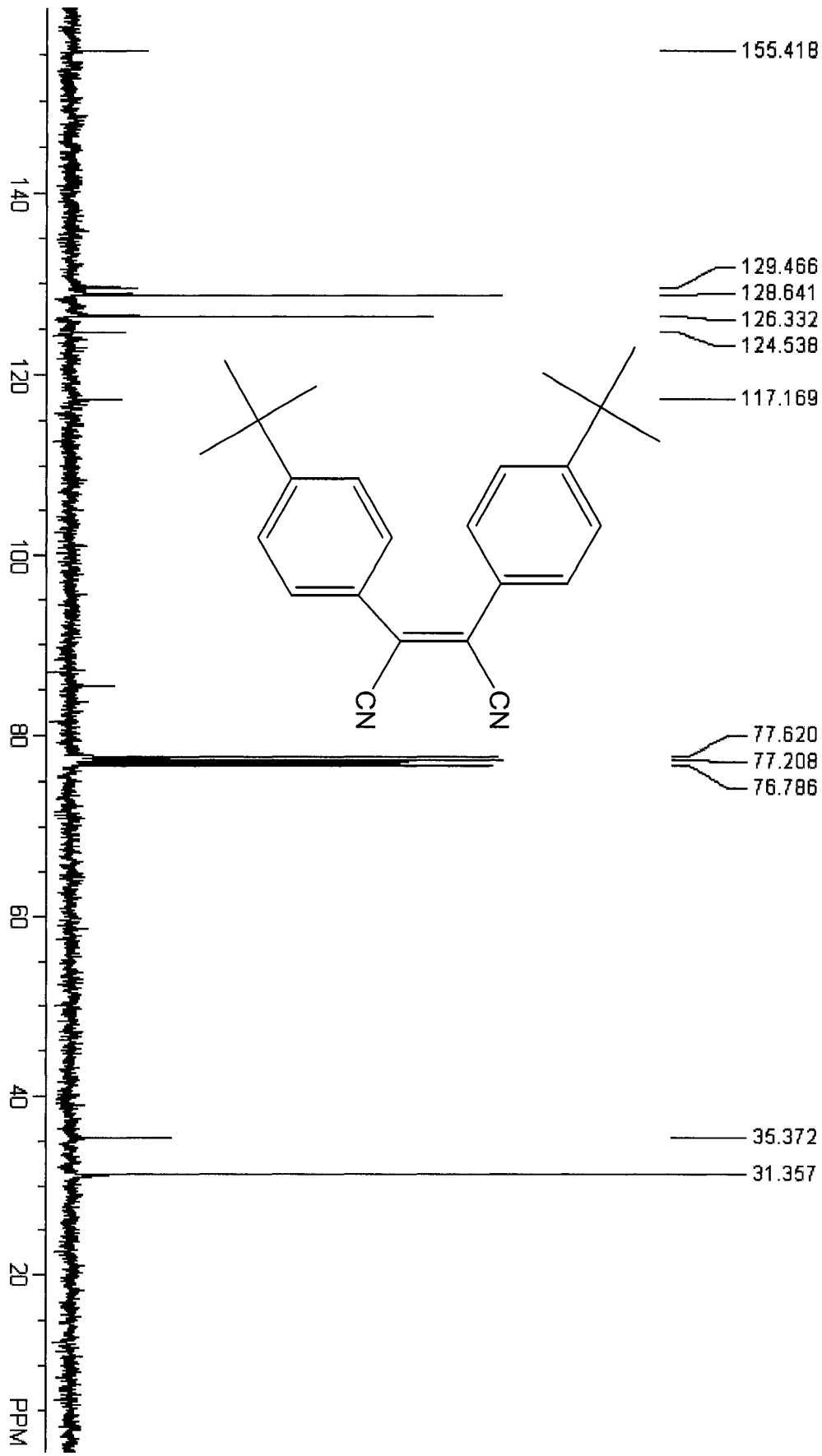

Figure B6. ^{13}C NMR (300 MHz, $CDCl_3$) of Bis(4-*tert*-butylphenyl)fumaronitrile.

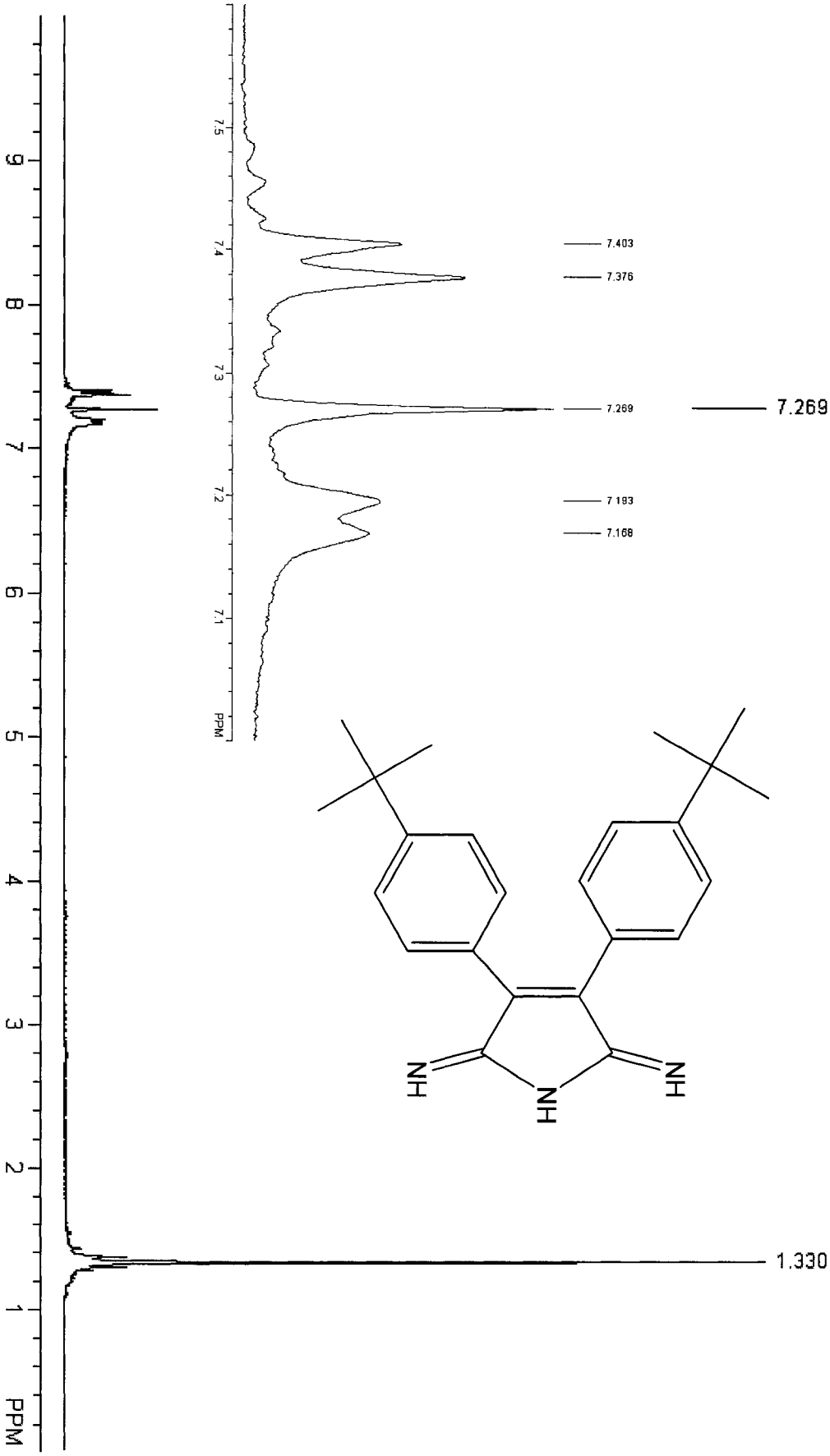

Figure B7. ^{1}H NMR (300 MHz, $CDCl_3$) of 3,4-Bis(4-*tert*-butylphenyl)pyrroline-2,5-diimine.

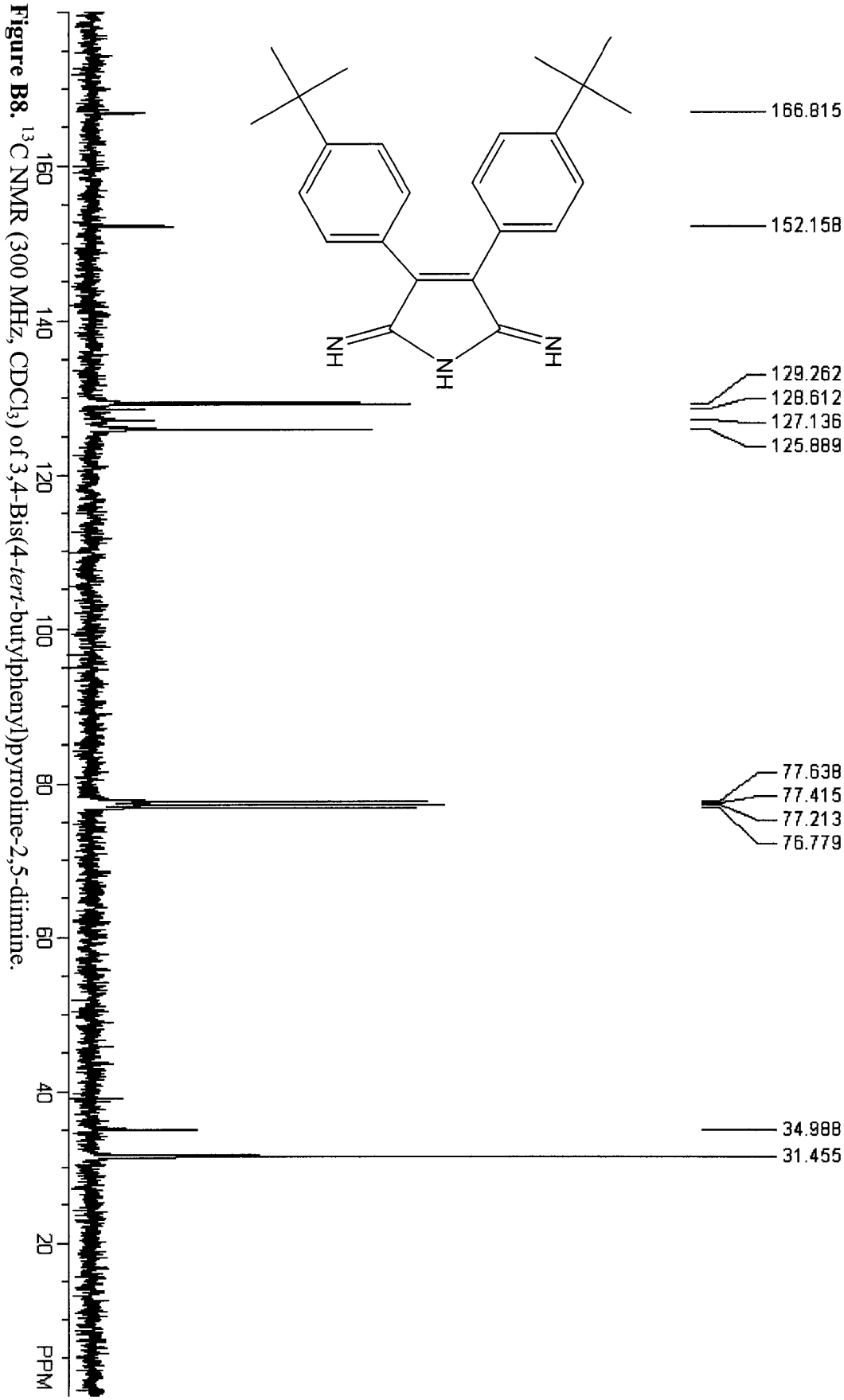

Figure B8. ^{13}C NMR (300 MHz, $CDCl_3$) of 3,4-Bis(4-*tert*-butylphenyl)pyrroline-2,5-diimine.

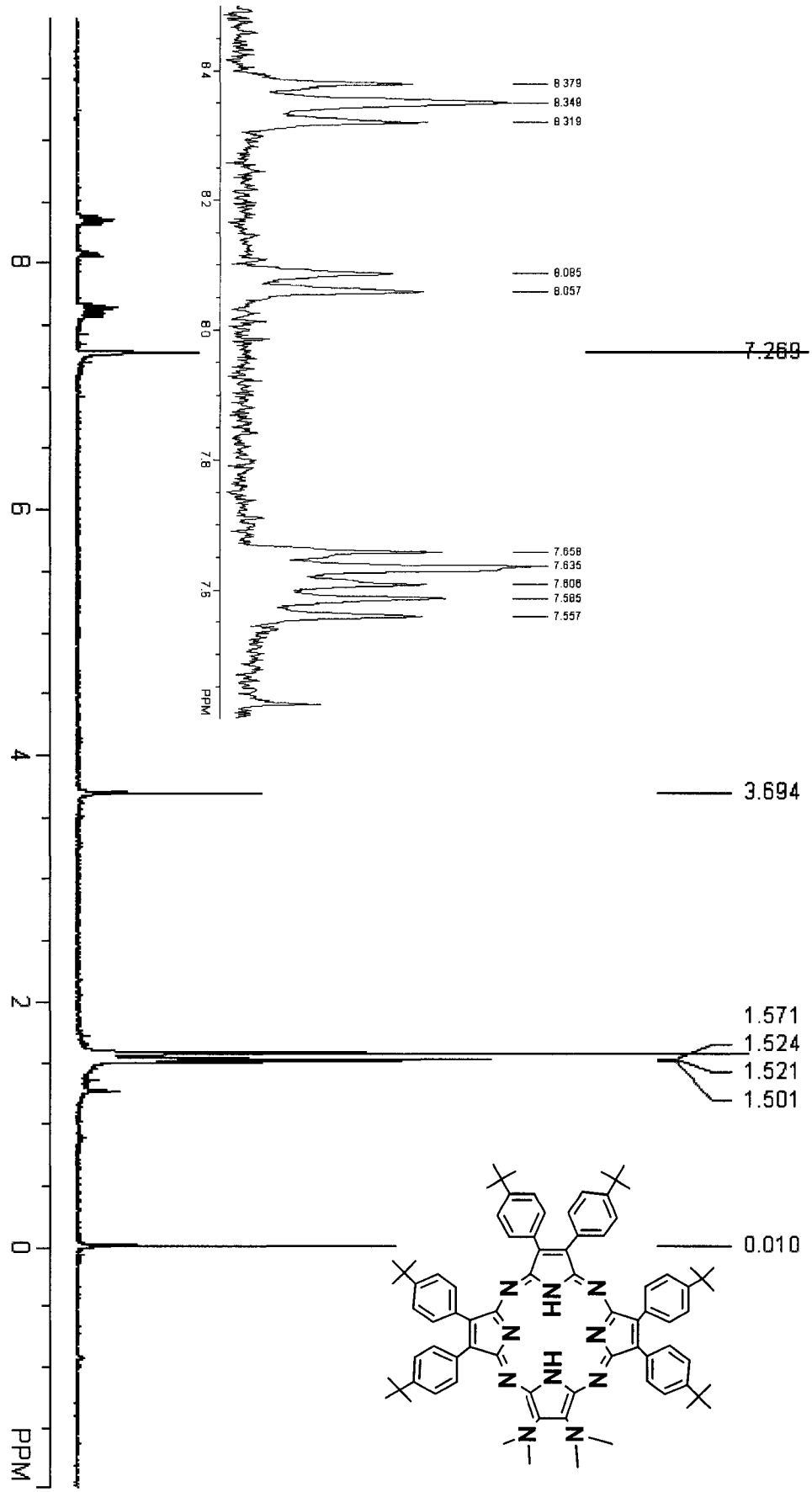

Figure B9. ^{1}H NMR (300 MHz, $CDCl_3$) of 2,3-bis(dimethylamino)-7,8,12,13,17,18-hexakis(4-(*tert*-butyl)- phenyl)porphyrazine.

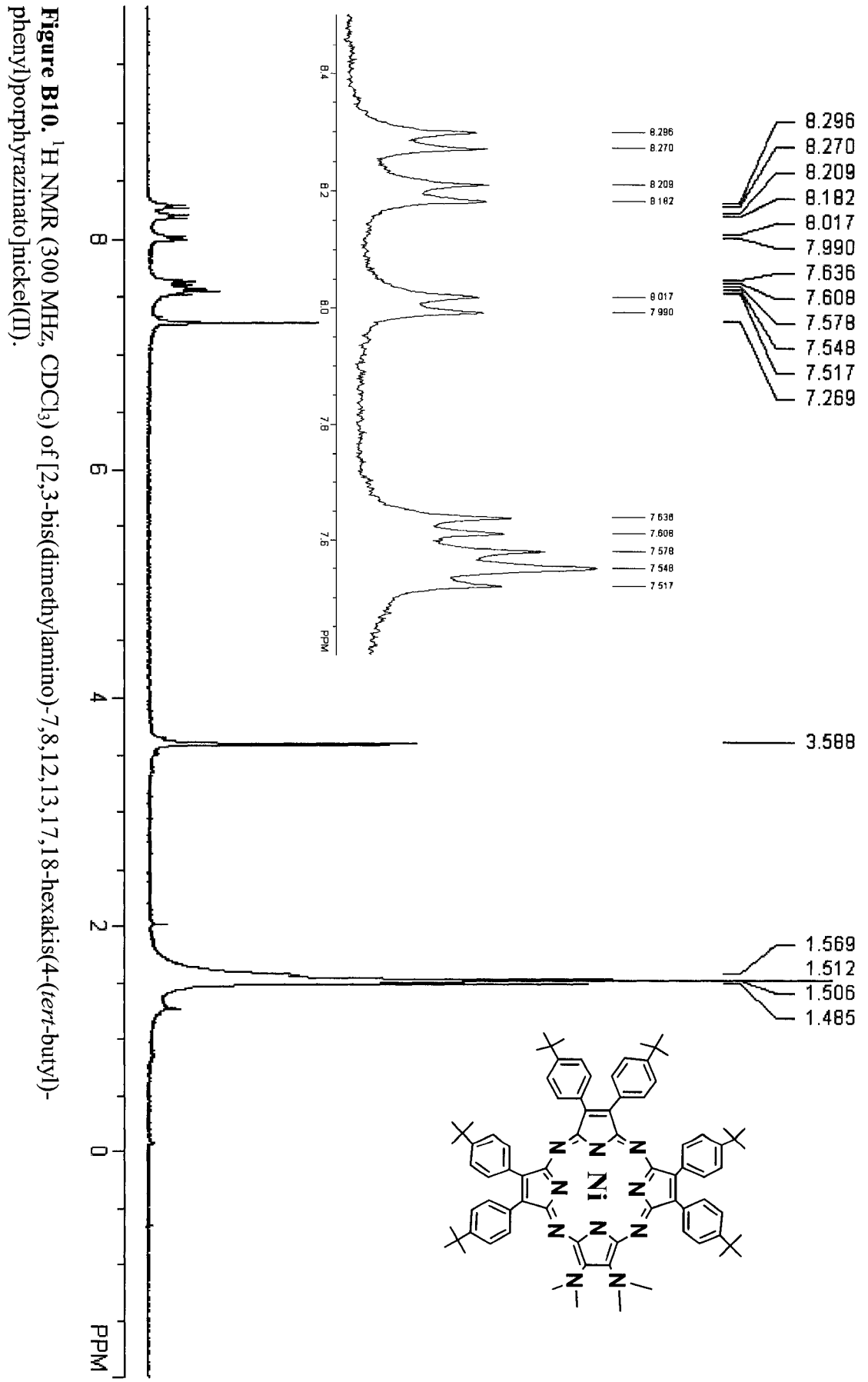

Figure B10. ^{1}H NMR (300 MHz, $CDCl_3$) of [2,3-bis(dimethylamino)-7,8,12,13,17,18-hexakis(4-(*tert*-butyl)-phenyl)porphyrazinato]nickel(II).

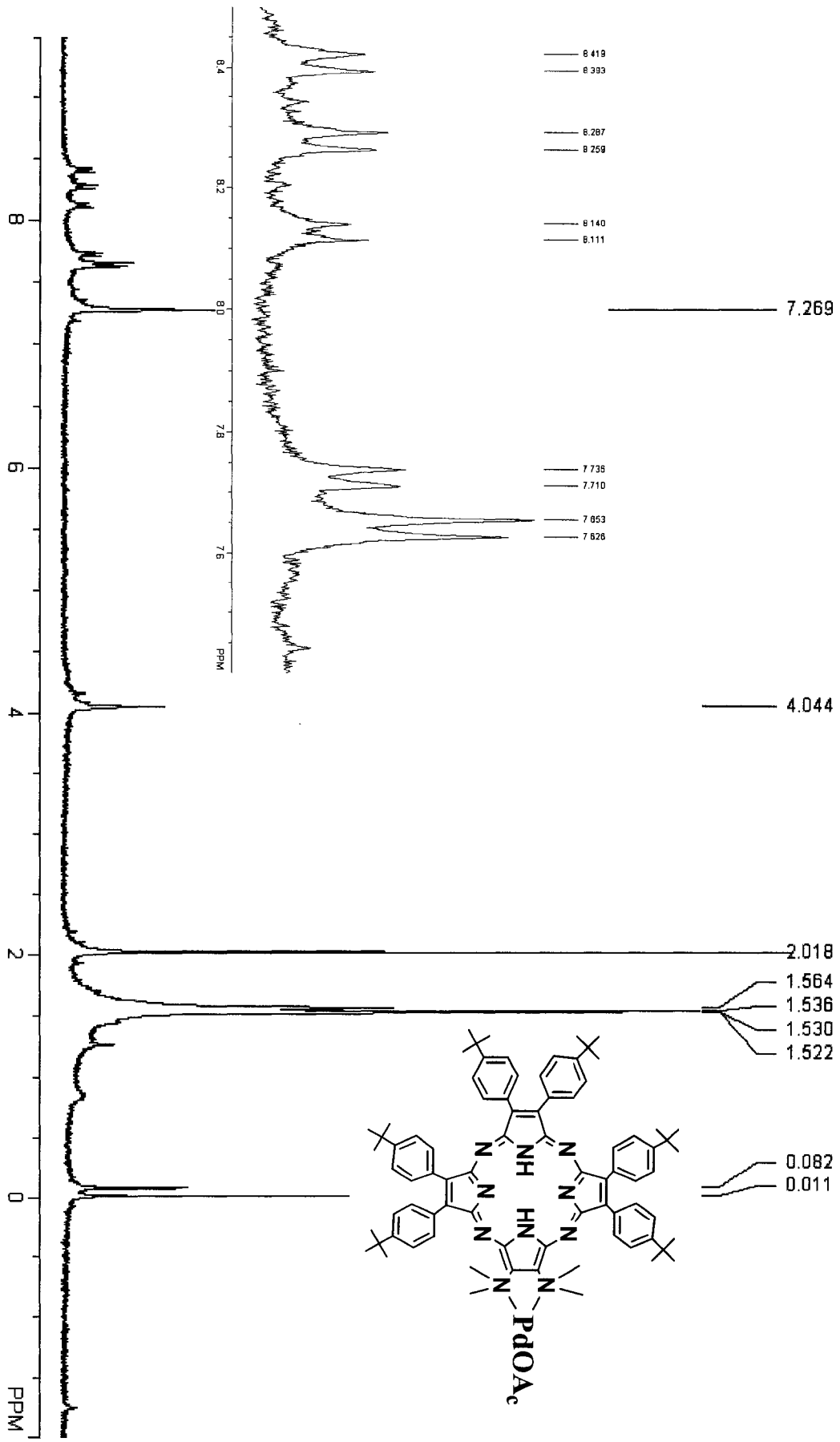

Figure B11. ^{1}H NMR (300 MHz, $CDCl_3$) of 2,3-bis(dimethylamino)-7,8,12,13,17,18-hexakis(4-(*tert*-butyl)- phenyl)porphyrazine-palladium(II) acetate monomer.

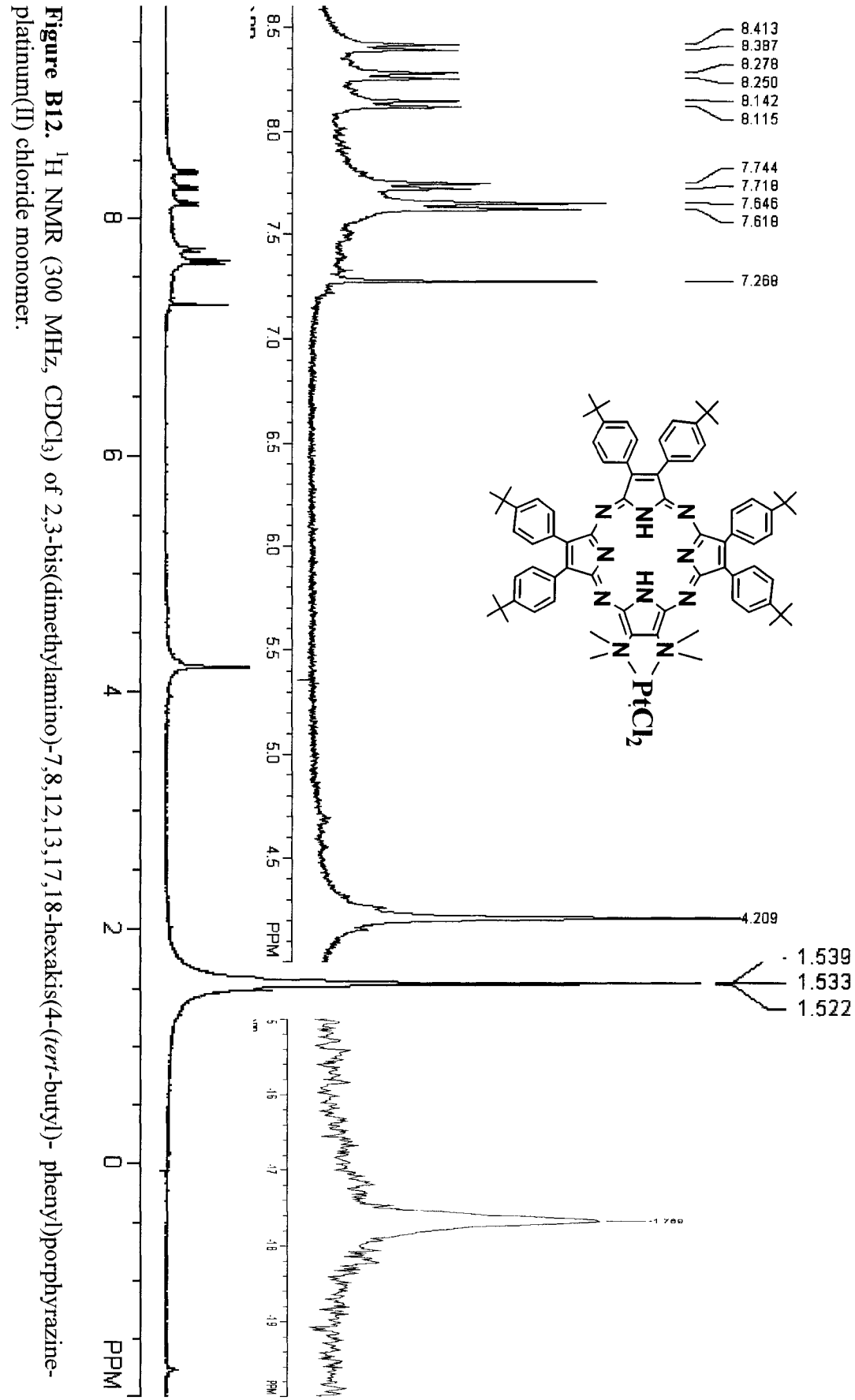

Figure B12. ^{1}H NMR (300 MHz, $CDCl_3$) of 2,3-bis(dimethylamino)-7,8,12,13,17,18-hexakis(4-(*tert*-butyl)- phenyl)porphyrazine-platinum(II) chloride monomer.

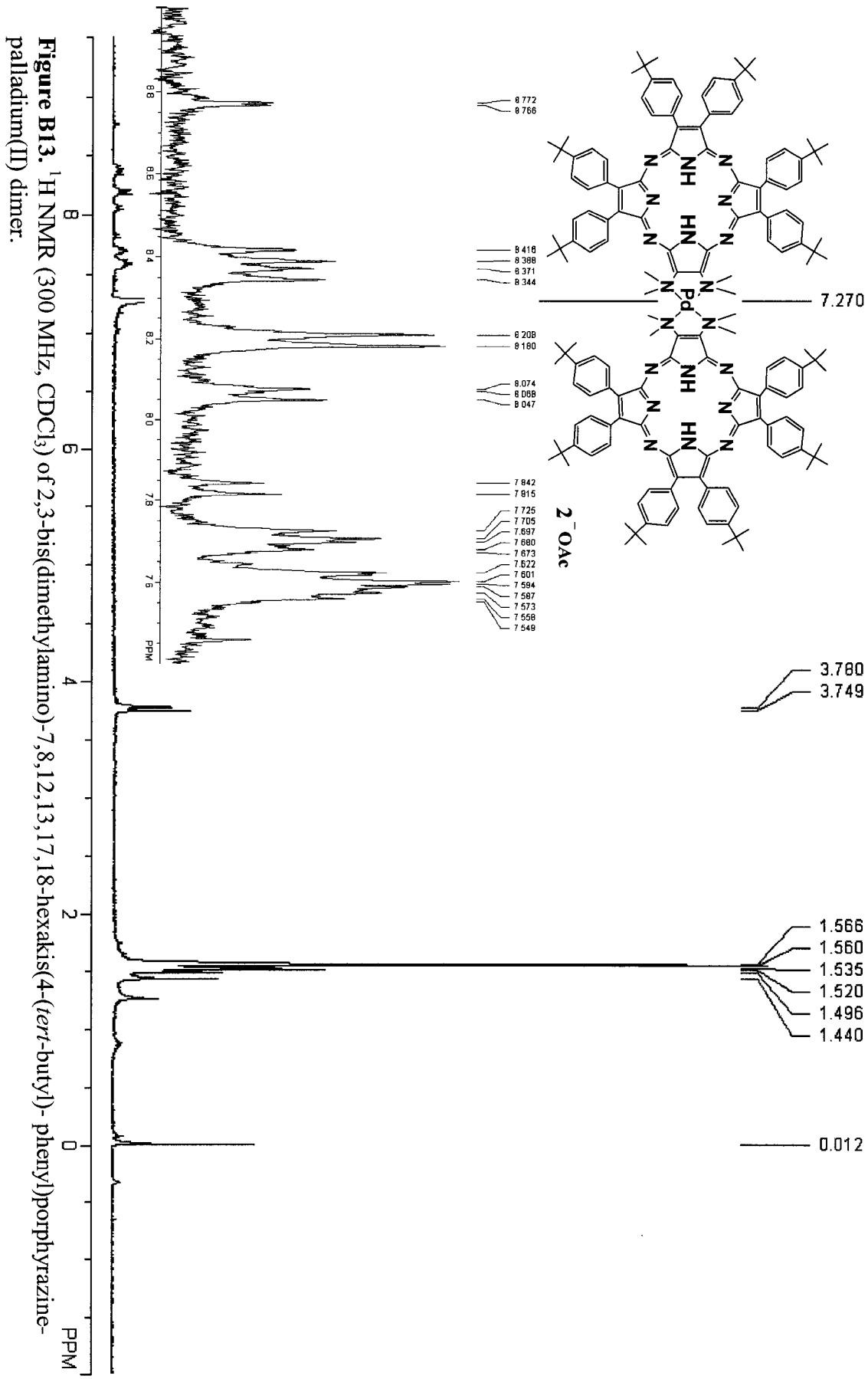

Figure B13. ^{1}H NMR (300 MHz, $CDCl_3$) of 2,3-bis(dimethylamino)-7,8,12,13,17,18-hexakis(4-(*tert*-butyl)- phenyl)porphyrazine-palladium(II) dimer.

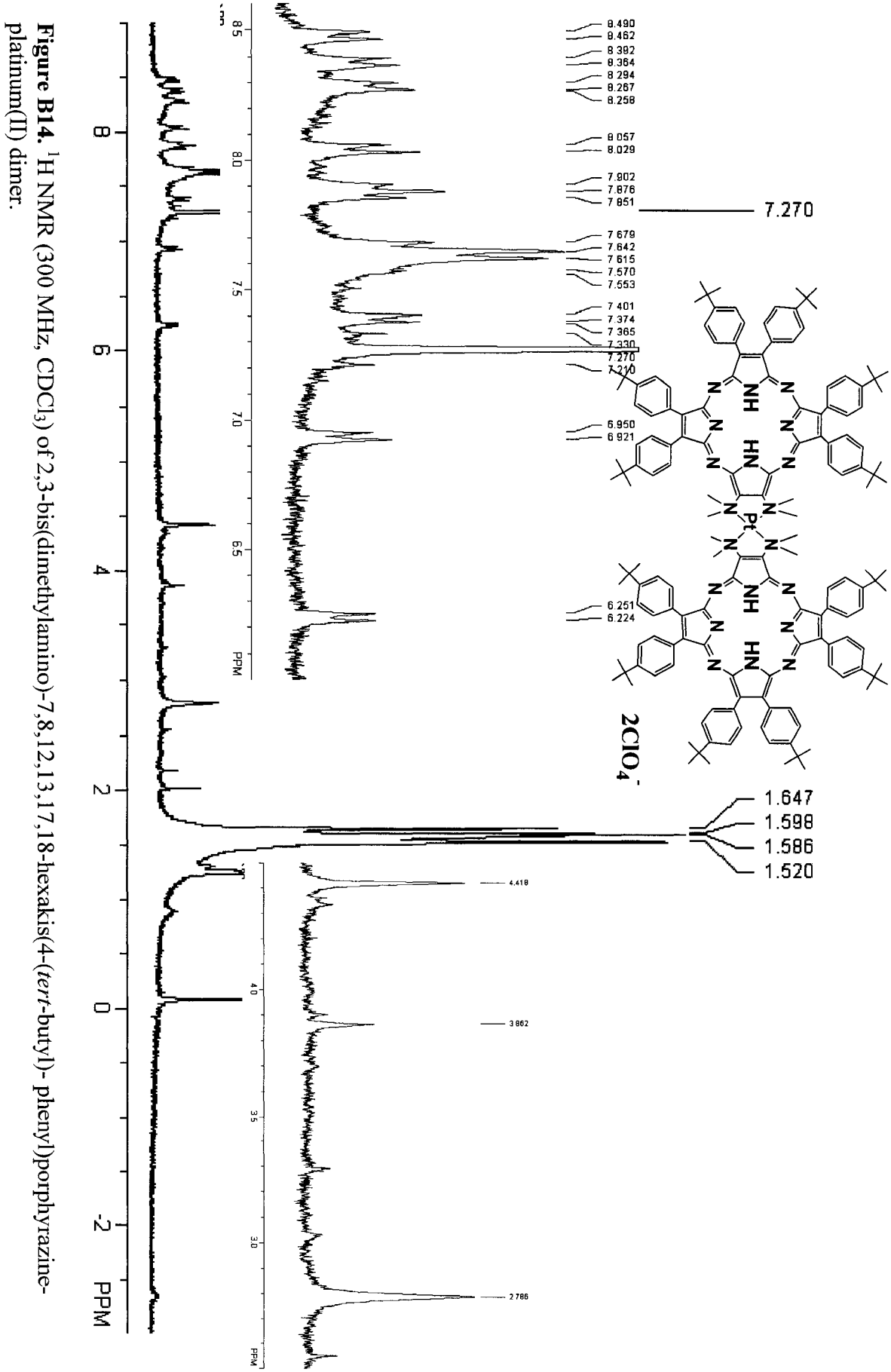

Figure B14. ^{1}H NMR (300 MHz, $CDCl_3$) of 2,3-bis(dimethylamino)-7,8,12,13,17,18-hexakis(4-(*tert*-butyl)- phenyl)porphyrazine-platinum(II) dimer.

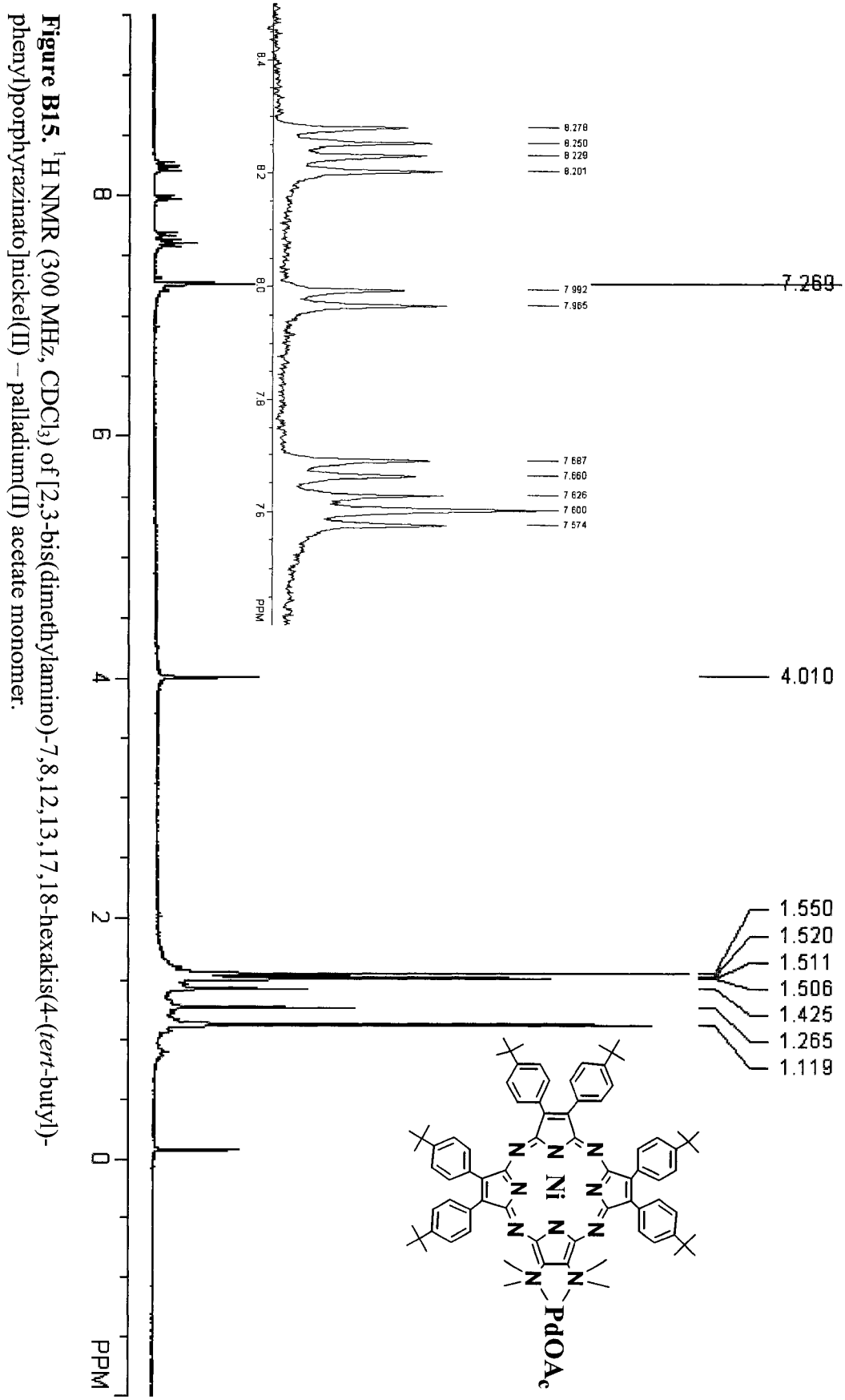

Figure B15. ^{1}H NMR (300 MHz, $CDCl_3$) of [2,3-bis(dimethylamino)-7,8,12,13,17,18-hexakis(4-(*tert*-butyl)-phenyl)porphyrazinato]nickel(II) – palladium(II) acetate monomer.

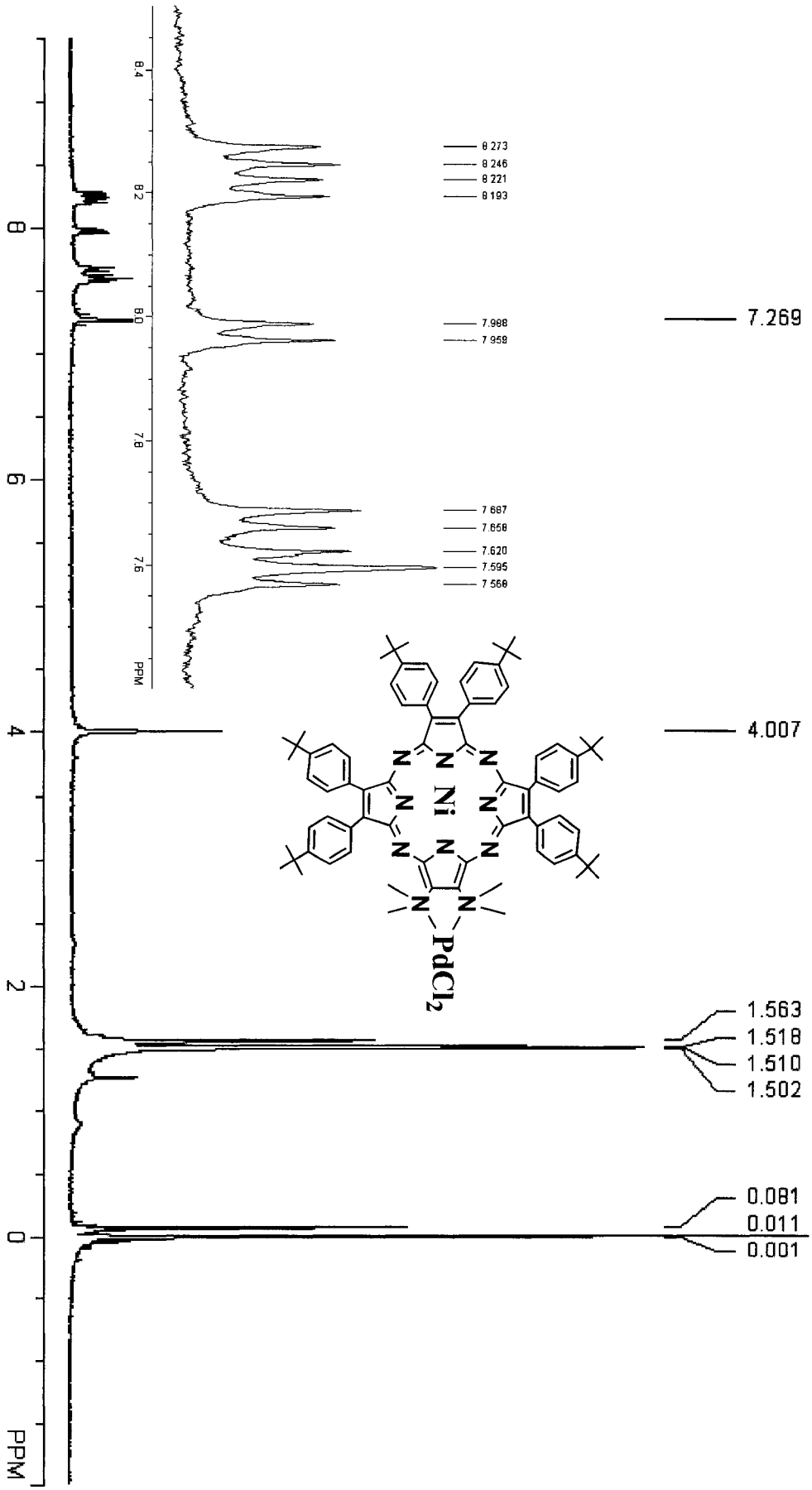

Figure B16. ^{1}H NMR (300 MHz, $CDCl_3$) of [2,3-bis(dimethylamino)-7,8,12,13,17,18-hexakis(4-(*tert*-butyl)-phenyl)porphyrazinato]nickel(II) – palladium (II) chloride monomer.

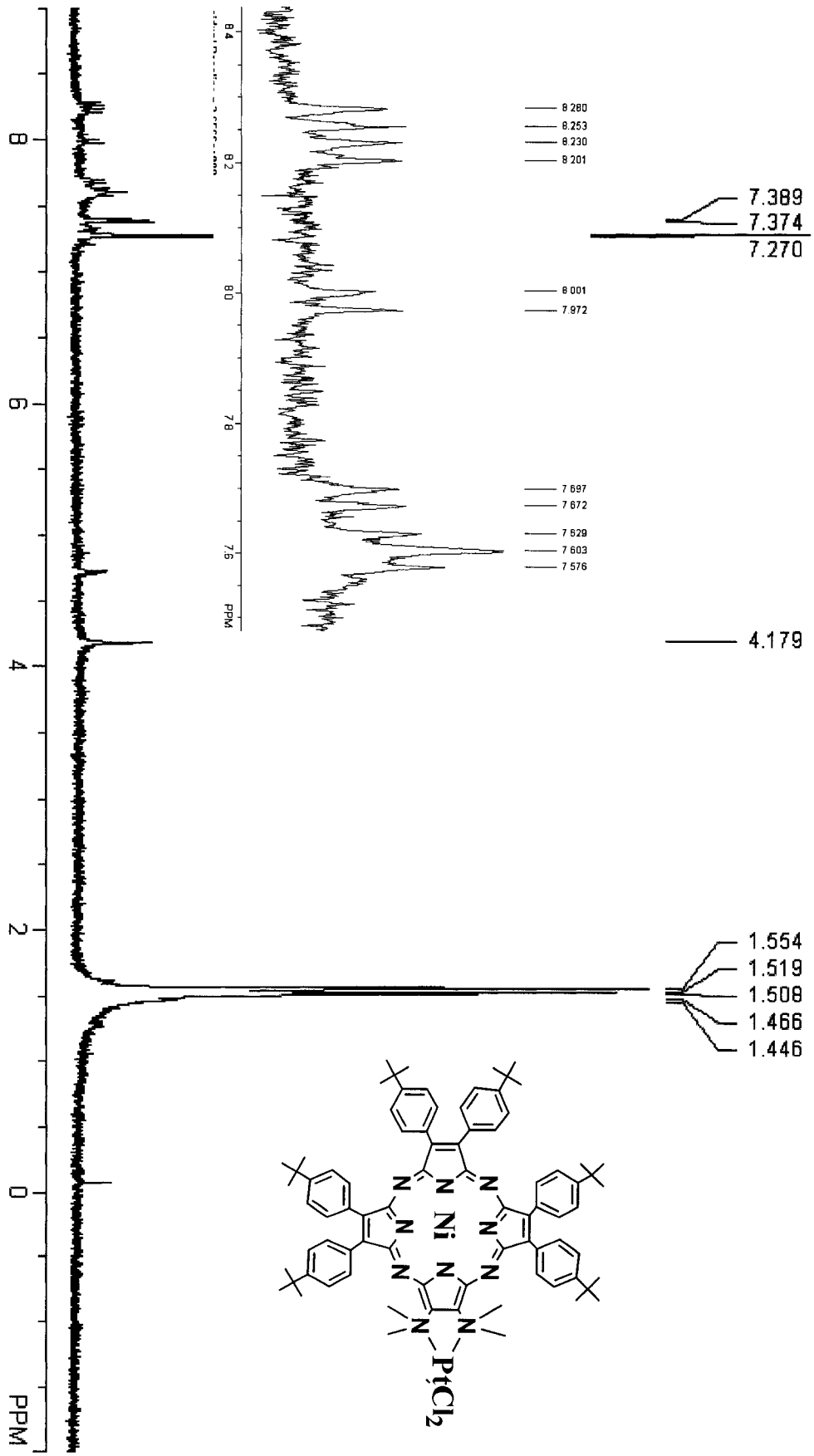

Figure B17. ^{1}H NMR (300 MHz, $CDCl_3$) of [2,3-bis(dimethylamino)-7,8,12,13,17,18-hexakis(4-(*tert*-butyl)-phenyl)porphyrazinato]nickel(II) – platinum (II) chloride monomer.

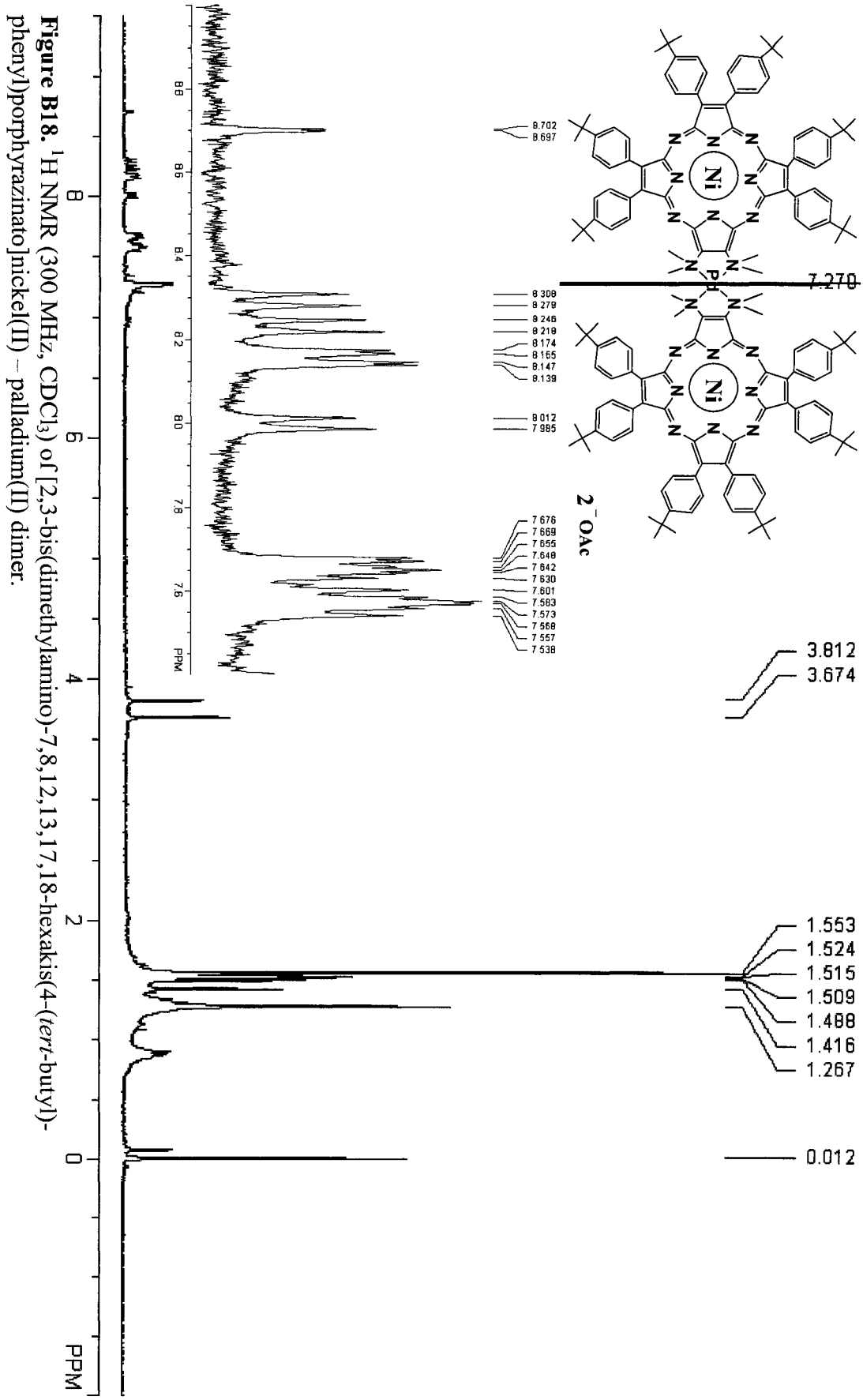

Figure B18. ^{1}H NMR (300 MHz, $CDCl_3$) of [2,3-bis(dimethylamino)-7,8,12,13,17,18-hexakis(4-(*tert*-butyl)-phenyl)porphyrazinato]nickel(II) – palladium(II) dimer.

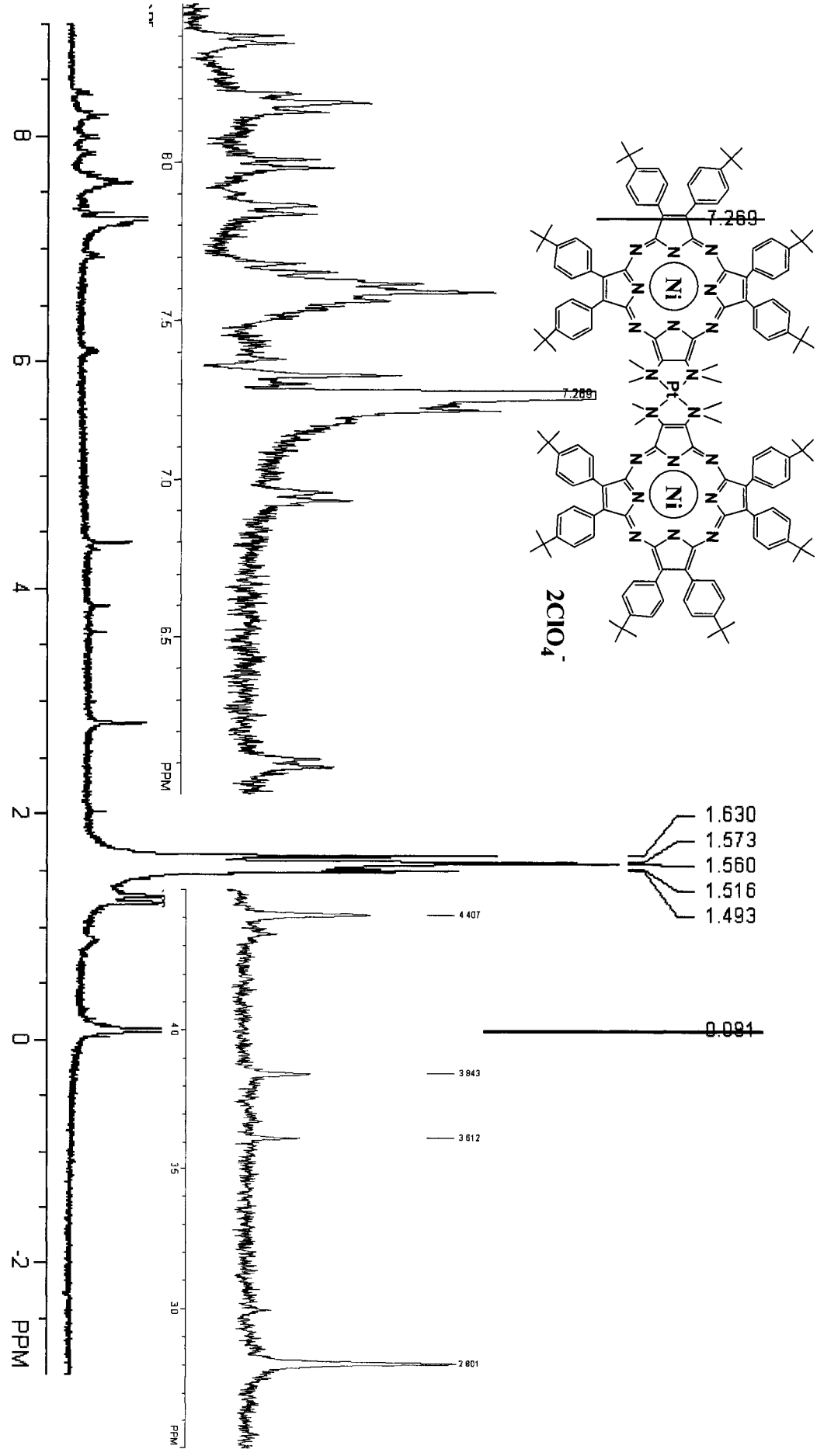

Figure B19. ^{1}H NMR (300 MHz, $CDCl_3$) of [2,3-bis(dimethylamino)-7,8,12,13,17,18-hexakis(4-(*tert*-butyl)-phenyl)porphyrazinato]nickel(II) – palladium(II) dimer.

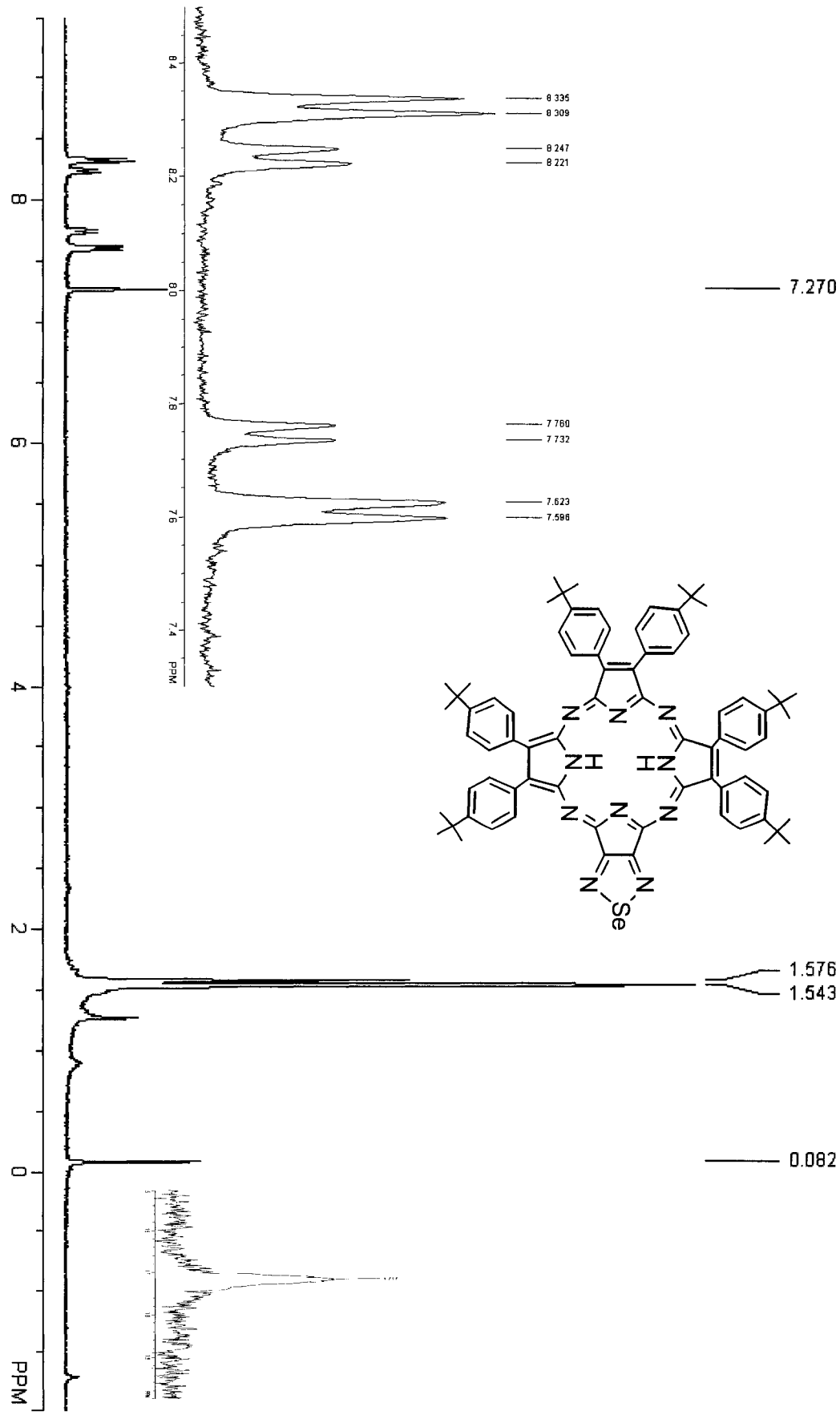

Figure B20. ^{1}H NMR (300 MHz, $CDCl_3$) of 2,3-selenodiazole-7,8,12,13,17,18-hexakis(4-(*tert*-butyl)- phenyl)porphyrazine.

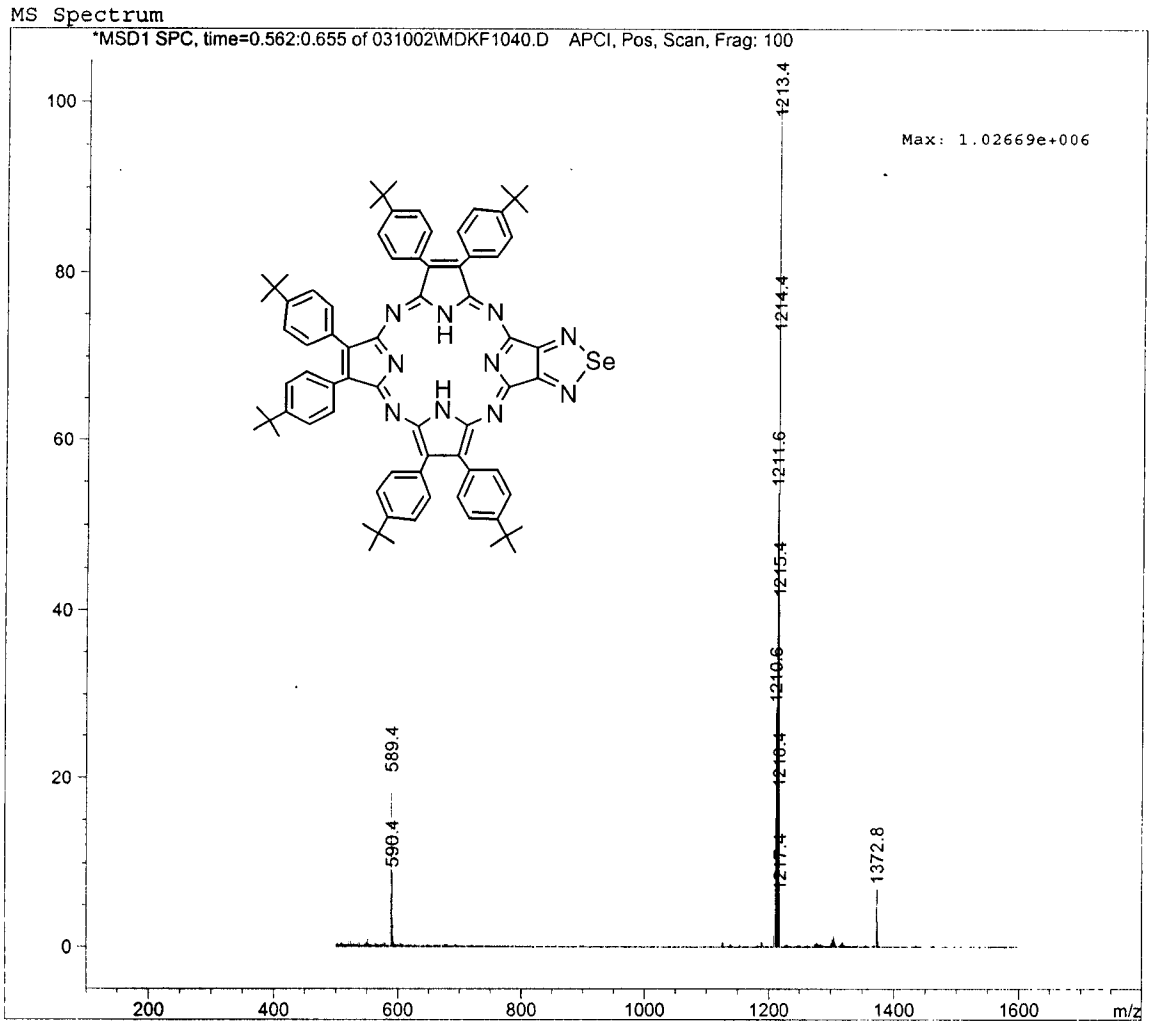

Figure B21. ESI-MS of 2,3-selenodiazole-7,8,12,13,17,18-hexakis(4-(*tert*-butyl)-phenyl)porphyrazine [*m/z* =1213 ($M + H^+$)].

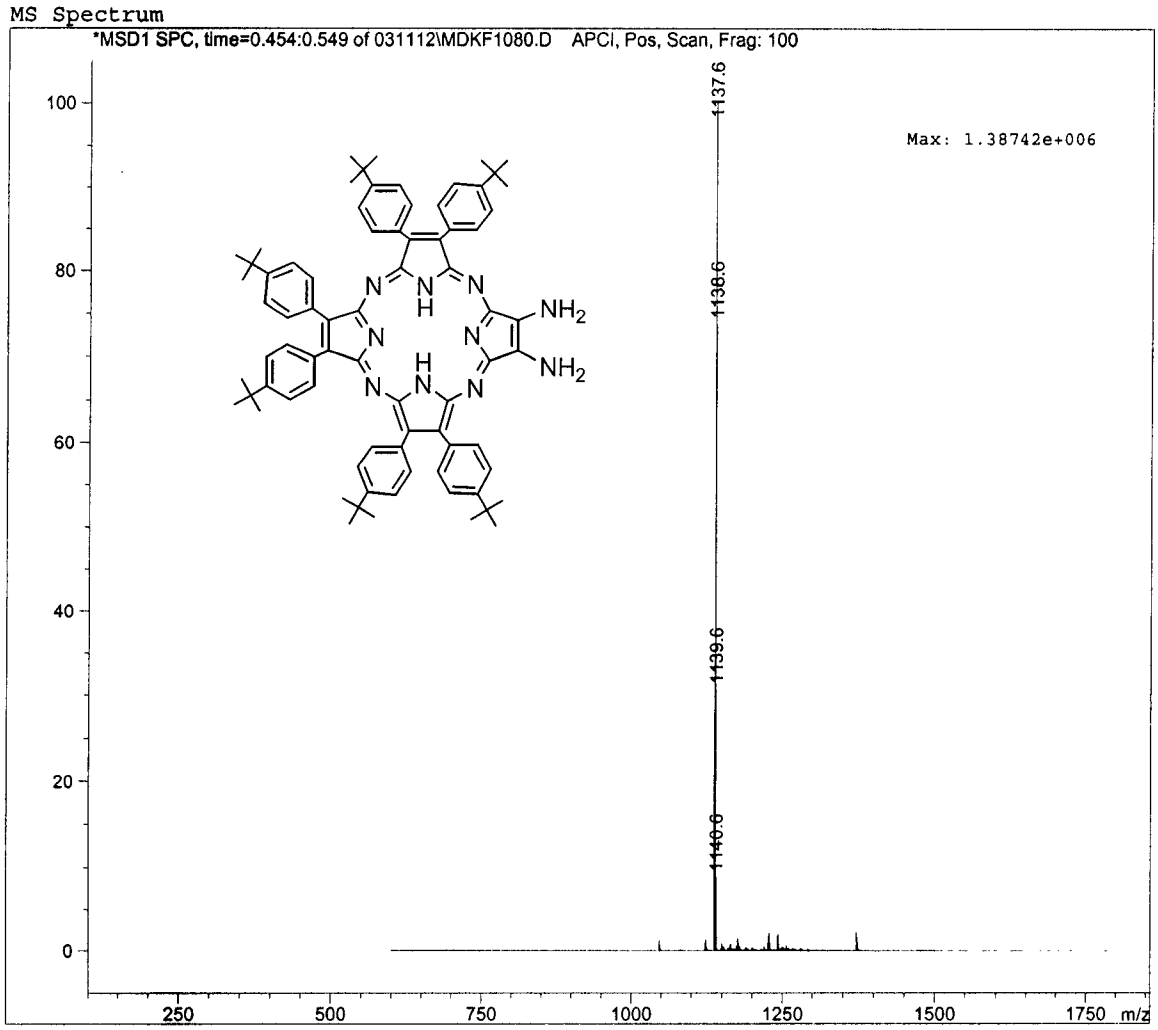

Figure B22. ESI-MS of 2,3-Bis(diamino)-7,8,12,13,17,18-hexakis(4-(*tert*-butyl)-phenyl)porphyrazine [m/z =1137 ($M + H^+$)].

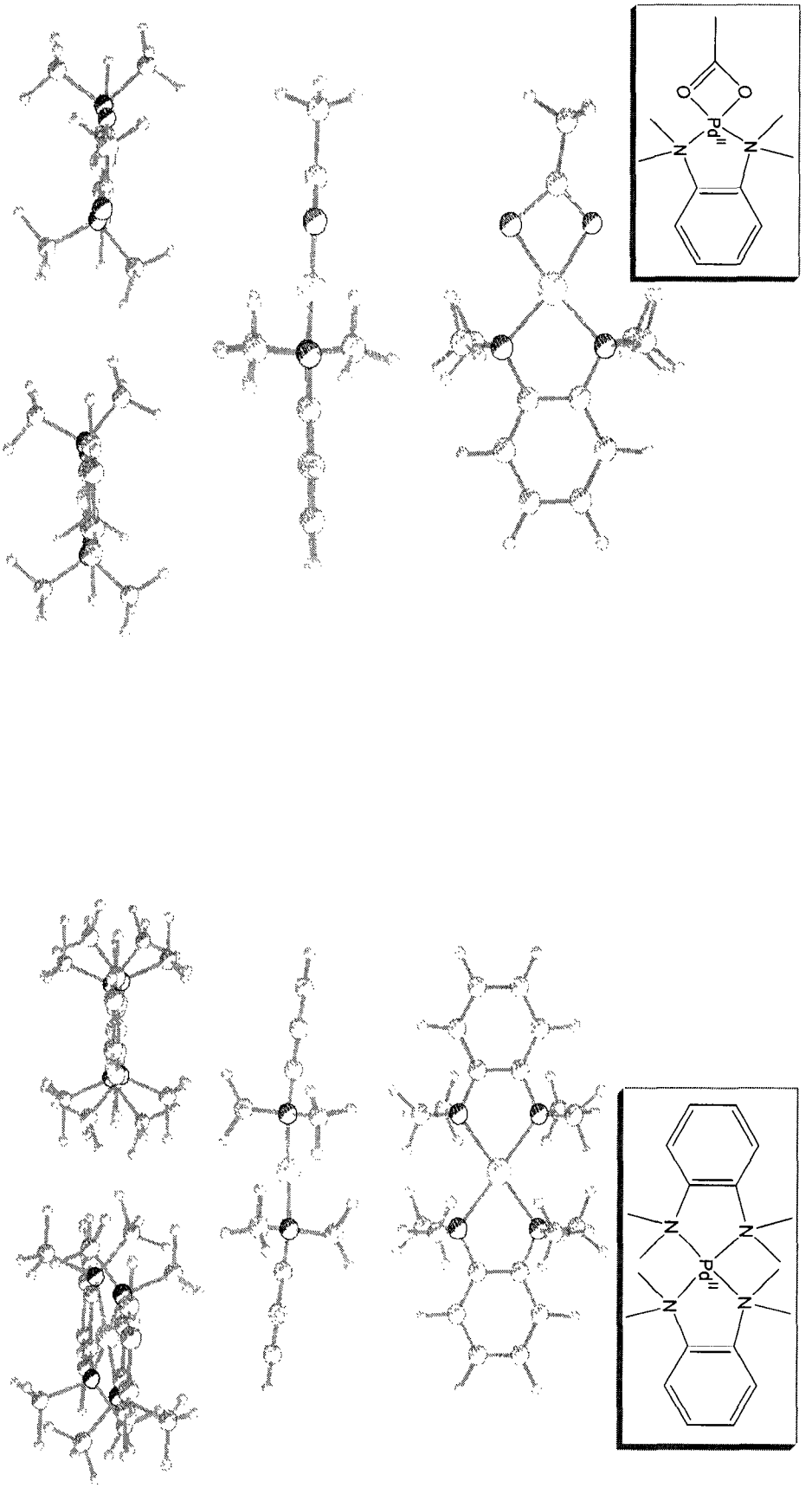

Figure B23. Simple molecular calculation in PC model on the ligand binding sites of the monomer and dimer of **1A**. (For simplification the chromophores were replaced by the benzene rings

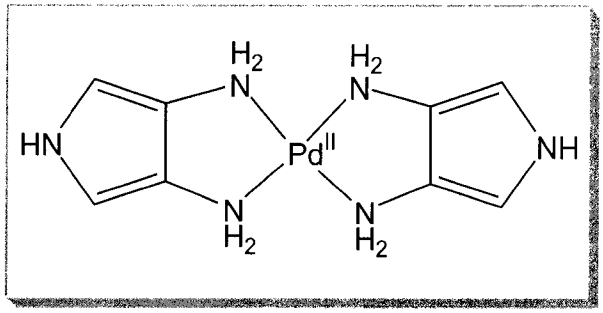

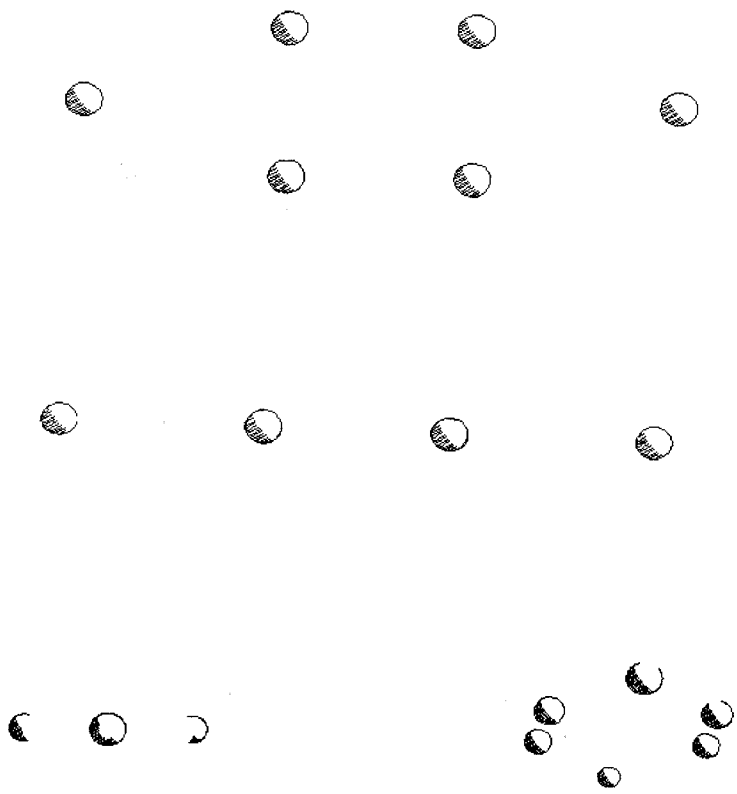

Figure B24. Simple molecular calculation in PC model on the ligand binding sites of the dimer of **3A**. (For simplification the chromophores were replaced by the pyrrole rings)

Figure B25. Formation of a porphyrazine-porphyrin heptamer via a sequence of reactions.

B6.

Bibliography

(1) Linstead, R. P.; Whalley, M. *J. Chem. Soc.* **1952**, 4839-4845.

(2) Bellec, N.; Montalban, A. G.; Williams, D. B. G.; Cook, A. S.; Anderson, M. E.; Feng, X.; Barrett, A. G. M.; Hoffman, B. M. *J. Org. Chem.* **2000**, *65*, 1774-1779.

(3) Skellariou, E. G.; Montalban, A. G.; Meunier, H. G.; Ostler, R. B.; Rumbles, G.; Barrett, A. G. M.; Hoffman, B. M. *J. Photochem. Photobiol., A* **2000**, *136*, 185-187.

(4) Nie, H.; Barrett, A. G. M.; Hoffman, B. M. *J. Org. Chem.* **1999**, *64*, 6791-6796.

(5) Anderson, M. E.; Barrett, A. G. M.; Hoffman, B. M. *Inorg. Chem.* **1999**, *38*, 6143-6151.

(6) Goldberg, D. P.; Montalban, A. G.; White, A. J. P.; Williams, D. J.; Barrett, A. G. M.; Hoffman, B. M. *Inorg. Chem.* **1998**, *37*, 2873-2879.

(7) Montalban, A. G.; Lange, S. J.; Beall, L. S.; Mani, N. S.; Williams, D. J.; White, A. J. P.; Barrett, A. G. M.; Hoffman, B. M. *J. Org. Chem.* **1997**, *62*, 9284-9289.

(8) Agirtas, S.; Ion, R.-M.; Berkaroglu, O. *Mater. Sci. Eng., C* **2000**, *7*, 105-110.

(9) Sun, Y.; Zhang, X.; Sun, C.; Wang, Z.; Shen, J.; Wang, D.; Li, T. *Chem. Commun.* **1996**, 2379-2380.

(10) Salabert, I.; Tran-Thi, T.-H.; Ali, H.; Van-Lier, J.; Houde, D.; Keszei, E. *Chem. Phys. Lett.* **1994**, *223*, 313-317.

(11) Hückel, W. *Z. Phys.* **1931**, *70*, 204.

(12) Hückel, W. *Z. Phys.* **1932**, *76*, 628.

(13) Hückel, W. *Z. Electrochem.* **1937**, *9*, 725.

(14) Baumann, T. F.; Barrett, A. G. M.; Hoffman, B. M. *Inorg. Chem.* **1997**, *36*, 5661-5665.

(15) Andersen, K.; Anderson, M.; Anderson, O. P.; Baum, S.; Baumann, T. F.; Beall, L. S.; Broderick, W. E.; Cook, A. S.; Eichhorn, D. M.; Goldberg, D.; Hope, H.; Jarrell, W.; Lange, S. J.; McCubbin, Q. J.; Mani, N. S.; Miller, T.; Garrido Montalban, A.; Rodriguez-Morgade, M. S.; Lee, S.; Nie, H.; Olmstead, M. M.; Sabat, M.; Sibert, J. W.; Stern, C.; White, A. J. P.; Williams, D., B. G.; ; Williams, D. J.; Barrett, A. G. M.; Hoffman, B. M. *J. Heterocyclic. Chem.* **1998**, *35*, 1013-1042.

(16) Gouterman, M. In *The Porphyrins*; Dolphin, D., ed.; Acadermic Press: New York: 1978; Vol. 3, p 1-165.

(17) Lever, A. B. P. *Adv. Inorg. Chem. Radiochem.* **1965**, *7*, 27-114.

(18) Sibert, J. W.; Baumann, T. F.; Williams, D. J.; White, A. J. P.; Barrett, A. G. M.; Hoffman, B. M. *J. Am. Chem. Soc.* **1996**, *118*, 10487-10493.

(19)Forsyth, T. P.; Williams, D. B. G.; Garrido Montalban, A.; Stern, C. L.; Barrett, A. G. M.; Hoffman, B. M. *J. Org. Chem.* **1998**, *63*, 331-336.

(20)Baumann, T. F.; Nasir, M. S.; Sibert, J. W.; White, A. J. P.; Olmstead, M. M.; Williams, D. J.; Barrett, A. G. M.; Hoffman, B. M. *J. Am. Chem. Soc.* **1996**, *118*, 10479-10486.

(21)Kobayashi, N.; Numao, M.; Kondo, R.; Nakajima, S.; Osa, T. *Inorg. Chem.* **1991**, *30*, 2241-2244.

(22)Cheng, K. F.; Drain, C. M.; Grohmann, K. *Inorg. Chem.* **2003**, *42*, 2075-2083.

(23)Lenzoff, C. C.; Lam, H.; Marcuccio, S. M.; Nevin, W. A.; anda, P.; Kobayashi, N.; Lever, A. B. P. *J. Chem. Soc., Chem. Commun.* **1987**, 699-701.

(24)Lelievre, D.; Bosio, L.; Simon, J.; Andre, J.-J.; Bensebaa, F. *J. Chem. Soc.* **1992**, *114*, 4475-4479.

(25)Prodi, A.; Keleverlaan, C. J.; Indelli, M. T.; Scandola, F.; Alessio, E.; Iengo, E. *Inorg. Chem.* **2001**, *40*, 3498-3504.

(26)Milic, T. N.; Chi, N.; Yablon, D. G.; Flynn, G. W.; Batteas, J. D.; Drain, C. M. *Angew. Chem. Int. Ed.* **2002**, *41*, 2117-2119.

(27)Drain, C. M.; Shi, X.; Milic, T.; Nifiatis, F. *Chem. Coummun.* **2001**, 287-288.

(28)Drain, C. M.; Nifiatis, F.; Vasenko, A.; Batteas, J. *Angew. Chem. Int. Ed.* **1998**, *37*, 2344-2347.

(29)Drain, C. M.; Batteas, J. D.; Flynn, G. W.; Milic, T.; Chi, N.; Yablon, D. G.; Sommers, H. *Proc. Natl. Acad. Sci., USA* **2002**, *99*, 6498-6502.

(30)Drain, C. M.; Chen, X. In *Encyclopedia of Nanoscience and Nanotechnology*; H.S. Nalwa ed.; American Scientific Press: 2004; Vol. 9, p 593-616.

(31)Drain, C. M.; Hupp, J. T.; Suslick, K. S.; Wasielewski, M. R.; Chen, X. *J. Porphyrins and Phthalocyanines* **2002**, *6*, 241-256.

(32)Adler, A. D.; Longo, F. R.; Finarelli, J. D.; Goldmacher, J.; Assour, J.; Korsakoff, L. *J. Org. Chem.* **1967**, *32*, 476-480.

(33)Shi, X.; Barkigia, K. M.; Fajer, J.; Drain, C. M. *J. Org. Chem.* **2001**, *66*, 6513-6522.

(34)Drain, C. M.; Lehn, J.-M. *J. Chem. Soc., Chem. Commun.* **1994**, 2313-2315.

(35)Fleischer, E. B.; Shachter, A. M. *Inorg. Chem.* **1991**, *30*, 3763-3769.

(36)Milgrom, L. R. *J. Chem. Soc., Perkin Trans. 1* **1984**, 1483-1487.

(37)Walker, F. A.; Balke, V. L.; McDermott, G. A. *Inorg. Chem.* **1982**, *21*, 3342-3348.

(38)Litter, R. G.; Anton, J. A.; Loach, P. A.; Ibers, J. A. *J. Heterocycl. Chem.* **1975**, *12*, 343-349.

(39)Cook, A. H.; Linstead, R. P. *J. Chem. Soc.* **1937**, 929-932.

(40)Begland, R. W.; Hartter, D. R.; Jones, F. N.; Sam, D. J.; Sheppard, W. A.; Webster, O. W.; Weigert, F. J. *J. Org. Chem.* **1974**, *39*, 2341-2351.

(41)Montalban, A. G.; Jarrell, W.; Riguet, E.; McCubbin, Q. J.; Anderson, M. E.; White, A. J. P.; Williams, D. J.; Barrett, A. G. M.; Hoffman, B. M. *J. Org. Chem.* **2000**, *65*, 2472-2478.

(42) Degener, E.; Petersen, S.; U.S. Patent 2, 292, July 4, 1961; *Chem. Abstr.* **1961**, *55*, 26456i.

(43) Kasha, M.; Rawls, H. R.; Ashraf EI-Bayoumi, M. *Pure. Appl. Chem.* **1965**, *11*, 371-392.

(44) Lange, S. J.; Nie, H.; Stern, C. L.; Barrett, A. G. M.; Hoffman, B. M. *Inorg. Chem.* **1998**, *37*, 6435-6443.

(45) Baure, E. M.; Ercolani, C.; Galli, P.; Popkova, I. A.; Stuzhin, P. A. *J. Porphyrins Phthalocyanines* **1999**, *3*, 371-379.

Part C:

Synthesis of a Covalent Base Pair of DNA

C1.

Introduction

The discovery of the double helical structure of DNA by Watson and Crick in 1953 has been regarded as one of the most significant breakthroughs in science[1] and has resulted in 50 years of research in nucleic acid biochemistry, biotechnology, gene therapy etc. The double helical structure of DNA arises from the complementary interactions of two polynucleotides which are held together by hydrogen bonding between the Watson-Crick base pairs.[1] The sugar-phosphate backbones of DNA and RNA;[2-4] the hydrogen bonding between the Watson-Crick base pairs[5,6] and the modification of the backbones and bases with a variety of shape analogues[7,8] have been well studied. A significant challenge for synthetic organic chemists in nucleic acid chemistry is to design and synthesize a covalent base pair that can replace a normal Watson-Crick base pair in a nucleic acid with minimal distortion of the structure of the double helix. A variety of strategies for the nonreversible cross-linking of nucleic acid strands have been reported in literature.[9-14] Recently, Orgel and coworkers proposed the design and synthesis of a covalent base pair reversibly cross-linked using a hydrazone bond between the two aromatic bases based on molecular modeling techniques (scheme 1.1.).[15,16] Through semiempirical calculations and dynamics simulations, they proposed that the geometry of the covalently joined base pair is very close to that found in the DNA double helix. They also suggested that a double helix containing this covalent base pair should be stable. However, the synthesis of these analogues and starting materials was only heuristically

outlined. Since these compound are of general interest to many working in the field of nucleic acid structure, the mechanisms of nucleic acid unwinding such as the helicases, transcription and translation, we report a detailed synthesis of these compounds.

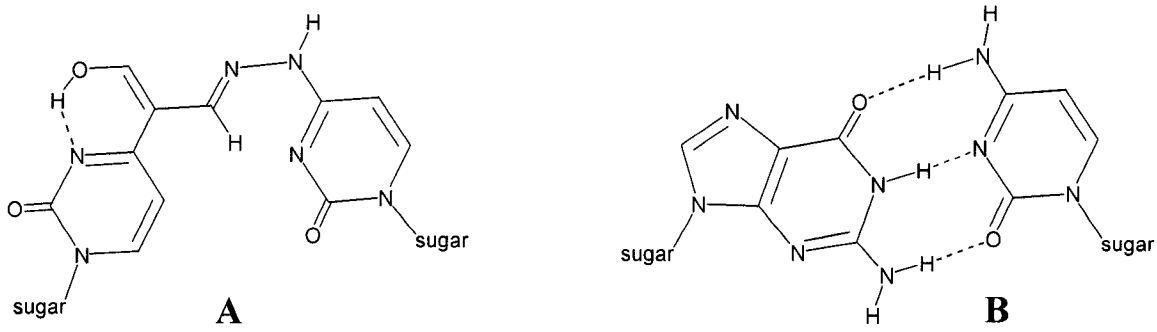

Scheme 1.1. (A) The structure of the proposed covalently bonded base pair. (B) The structure of a standard Watson-Crick base pair.

C2.

Synthesis

The target molecule **(7)** (scheme 2.1.) was synthesized from the condensation reaction of 4-(α-diformyl-methyl)-1-(β-D-ribofuranosyl)-2-pyrimidinone **(5)** and N^4-aminocytidine-5'-monophosphate **(6)** in 50mM, pH 5.23 ammonium acetate buffer. The reaction was performed at room temperature for 24 hours and then desalted on a Sep-Pak-C_{18} column. The product was identified by electrospray mass spectrometry

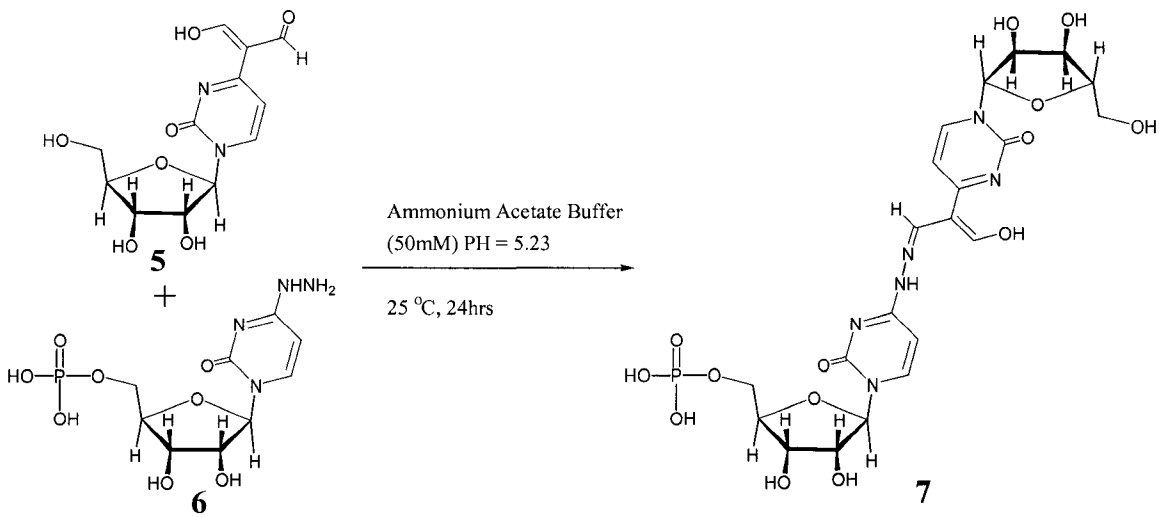

Scheme 2.1. Synthesis of the target molecule **(7).**

(ESI-MS): m/z = 619 [M + H^+] (figure C8). Compound **(6)** was synthesized from the commercially available cytidine-5'-monophosphate and using sodium bisulfite to

catalyze the reaction of hydrazine to give the N^4 hydrazine derivatives.[17,18] (scheme 2.2.). Cytidine-5'-monophosphate (0.39g, 1.2mmol) was dissolved in a 3mL reagent mixture

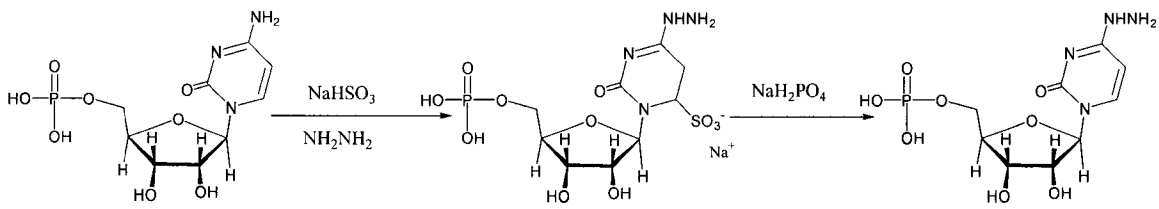

Scheme 2.2. Synthesis of the compound **(6).**

which was prepared by mixing 2mL hydrazine, 0.1g $NaHSO_3$, 0.15g NaH_2PO_4, 5mL water and neutralized to pH 7.0 with concentrated HCl. The resulting mixture was stirred at 60 °C in a warm water bath for 4 hours. The reaction was quenched by adding 10mL TET buffer (0.1M Tris·HCl/0.001M EDTA/0.01M triethylamine, pH 8.0) and desalted on a Sep-Pak-C_{18} column. The product **(6)** is unstable and decomposes slowly even at –20 °C. Hence, the freshly formed **(6)** must be condensed immediately with the aldehyde **(5)**. The freshly formed **(6)** is also identified by electrospray mass spectrometry (ESI-MS): m/z = 339 [M + H^+]. The aldehyde **(5)** was prepared from 2-Hydroxy-4-methylpyrimidine hydrochloride **(1)** and β-D-ribofuranose-1-acetate-2,3,5-tribenzoate **(2)**. Despite numerous trials based on a literature procedure,[16] which called for mixing **(1)** and **(2)** first in anhydrous acetonitrile and then adding $SnCl_4$, trimethylchlorosilane (TCS), and hexamethyldisilazane (HMDS) with careful exclusion of moisture, the desired product 1-(2,3,5-tri-O-benzoyl-β-D-ribofuranosyl)-4-methyl-2-pyrimidinone **(3)** was never formed in significant yields. The side products, determining by ^1H NMR and ESI-MS

data, are the β-D-ribofuranose-1-chloro-2,3,5-tribenzoate and some polymers (scheme 2.3.). A successful synthesis of the compound **(3)** can be accomplished by separating the reaction steps. Specifically, by protecting the alcohol groups on the pyrimidine with TMS before the coupling reaction with **(2)**, followed deprotection. 0.09g, 0.6mmol **(1)** and 0.26g, 0.5mmol **(2)** in a separated 10ml round-bottom flasks were dried under vacuum for three

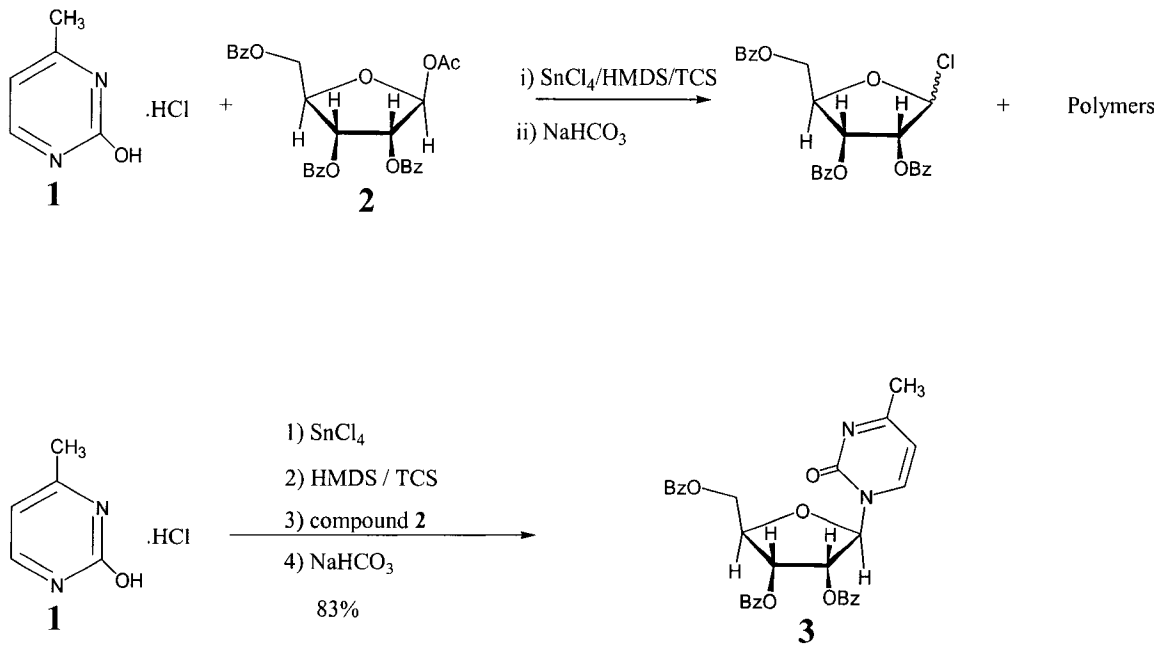

Scheme 2.3. The synthesis of the product **(3)** only success when use the modified procedure.

hours. After drying, the flasks were capped with a rubber septum with careful exclusion of moisture. 4mL and 3mL anhydrous acetonitrile were added to the flasks containing **(1)** and **(2)** respectively using a syringe. Then 0.12mL of $SnCl_4$ was added slowly to the mixture containing **(1)** under N_2 with vigorous stirring. After the suspension of **(1)** became a clear solution, 90 μL TCS and 90 μL HMDS were added to the pale yellow

solution. Then solution **(2)** was added dropwise for about 15 minutes. The resulting solution was allowed to stir under N_2 for 4 hours at room temperature. The reaction solution was rotary evaporated and the residual syrup dissolved in 5mL dichloromethane. The solution was neutralized with a saturated solution of sodium bicarbonate, and filtered with a pad of celite. The dichloromethane solution was washed with a 10mL saturated solution of NaCl and then a 10mL H_2O, dried ($MgSO_4$), rotary evaporated, and chromatographed ($CHCl_3$/MeOH 49:1) to give **(3)** (1.5g, 83%) as a pale yellow foam-like solid. The 4-(α-diformyl-methyl)-1-(2,3,5-tri-O-benzoyl-β-D-ribofuranosyl)-2-pyrimidinone **(4)** was obtained using a Vilsmeier reaction[19,20] that converted the methyl group on the pyrimidine to α-diformyl- methyl group (scheme2.4.). 0.11mL (1.18 mmol)

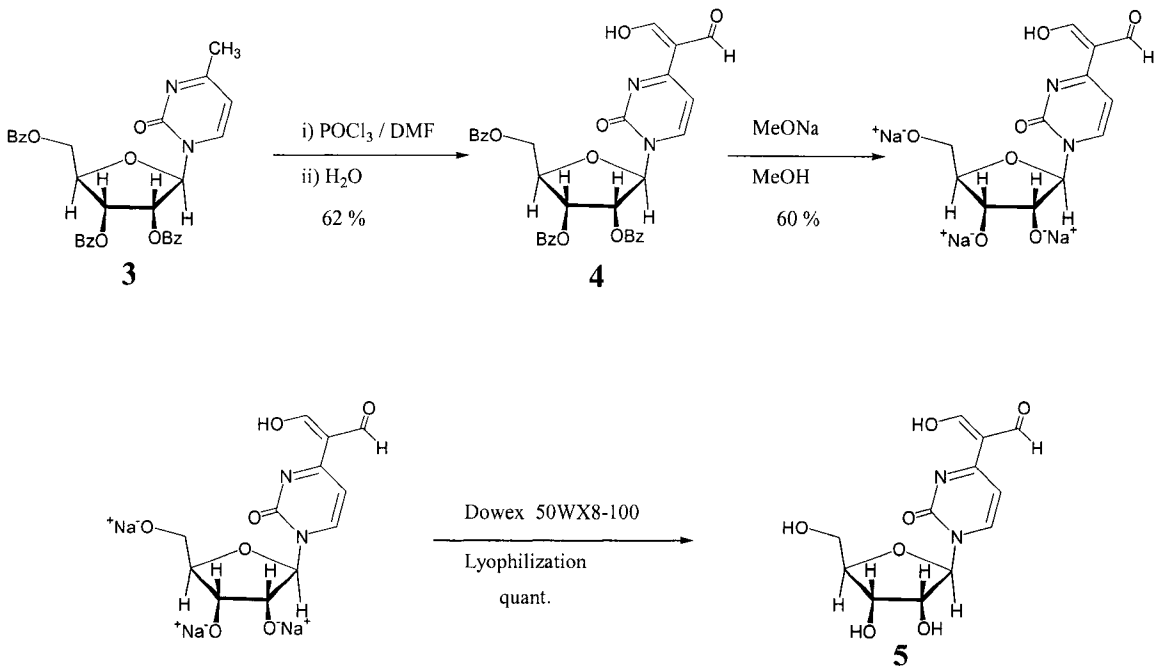

Scheme 2.4. Synthesis of the 4-(α-Diformyl-methyl)-1-(2,3,5-tri-O-benzoyl-β-D-ribofuranosyl)-2-pyrimidinone **(4)** and 4-(α-Diformyl-methyl)-1-(β-D-ribofuranosyl)-2-pyrimidinone **(5).**

phosphorous oxychloride ($POCl_3$) was added gradually to 0.36mL (4.65 mmol) DMF with vigorous stirring at 15 °C. **(3)** (0.2g 0.36mmol) dissolving in 0.36mL (4.65mmol) DMF was added dropwise to the $POCl_3$ solution keeping the temperature at 15 °C. The mixture was first warmed to room temperature with stirring for 30 mins and then at 60 °C for another 30 mins. After cooling to room temperature, the solution was poured onto ice water (10mL), the mixture stirred until it reached room temperature, whereupon it was neutralized with a saturated solution of sodium bicarbonate ($NaHCO_3$), and filtered. The precipitate was washed several times with H_2O, dried in air, and dissolved in 5mL chloroform. The resulting solution was washed with 3mL H_2O, dried ($MgSO_4$), rotary evaporated, and chromatographed ($CHCl_3$/MeOH 49:1) to give **(4)** (0.13g, 62%) as a syrup. The syrup was then dissolved in 5mL benzene-methanol (1:1 v/v), and 1.26mL of a 0.5M alcoholic solution of sodium methoxide was added. The mixture was allowed to stir at room temperature for 24 hours. The debenzoylated product was precipitated as a sodium salt by dilution of the reaction solution with 5mL benzene at 0 °C. The precipitate was collected and dissolved in 3mL water, passed over DOWEX® 50WX8-100 ion-exchange resin, filtered, and lyophilized to give 4-(α-Diformyl-methyl)-1-(β-D-ribofuranosyl)-2-pyrimidinone **(5)** (37mg, 59%) as a light yellow powder. The structure of compounds **(3)**, **(4)** and **(5)** were determined by ^1H NMR (figures C1, C2, C3 and C4) and ESI-MS in positive-ion mode (figure C8).

C3.

Experimental Section

3.1. Reagents and physical measurements

All solvents were distilled using standard methods.[21] Silica gel (Baker, 60μm average particle size) and alumina (Fisher, 80-200 mesh) were used for column chromatography. The $CHCl_3$ was reagent grade and use directly. The acetonitrile and methanol were freshly distilled from CaH_2. The other solvents were distilled either from CaH_2 or P_2O_5. Proton NMR spectroscopy was performed on QE 300 MHz using the residual protons in chloroform-D solvent as an internal reference. UV-visible spectra were recorded on a Varian Bio-100 spectrometer. Electrospray mass spectroscopy spectrum was performed on Hewlett-Packard HP-1100 LC/MS positive-ion mode.

3.2. Selected spectroscopic data of the compounds

Compound (3): ^{1}H NMR (300 MHz, $CDCl_3$): δ = 2.39(s, 3 H, CH_3), 4.68-4.90 (m, 3 H, H4+H5), 5.78 (t, 1 H, J = 5.5 Hz, H3), 5.91 (t, 1 H, J = 5.5 Hz, H2), 6.11 (d, 1 H, J = 7.0 Hz, H7), 6.48 (d, 1 H, J = 4.8Hz, H1), 7.35-7.56 (m, 9 H, Bz-H), 7.81 (d, 1 H, J = 7.0 Hz, H6), 7.93-8.00 (m, 4 H, Bz-H), 8.10 (d, 2 H, J = 7.0 Hz, Bz-H) (figure C1.). ESMS: m/z = 555 $[M + H^+]$.

Compound (4): ^{1}H NMR (300 MHz, $CDCl_3$): δ = 4.70-4.87 (m, 3 H, H4+H5), 5.77 (t, 1 H, J = 5.5 Hz, H3), 5.90 (t, 1 H, J = 5.5 Hz, H2), 6.34 (d, 1 H, J = 5.1Hz, H1), 7.26-7.65 (m, 9 H, Bz-H), 7.72 (s, 2 H, H6+H7), 7.93 (d, 2 H, J = 8.1Hz, Bz-H), 7.99 (d, 2 H, J = 8.1H, Bz-H), 8.10 (d, 2 H, J = 8.1 Hz, Bz-H), 9.59 (s, 1 H, H8), 9.64 (s, 1 H, H9) (figure C2.). ESMS: m/z = 611$[M + H^+]$.

Compound (5): ^{1}H NMR (300 MHz, DMSO-d_6): δ = 2.68-3.18(m, 5 H, H2,H3,H4,H5 4.81 (d, 1 H, J = 2.7 Hz, H1), 6.60 (d, 1 H, J = 7.4 Hz, H7), 7.59 (d, 1 H, J = 7.4Hz, H6), 8.59 (s, 2 H, H8 + H9) (figure C4). ESMS: m/z = 299 $[M + H^+]$(figure C8.).

C4.

Appendix

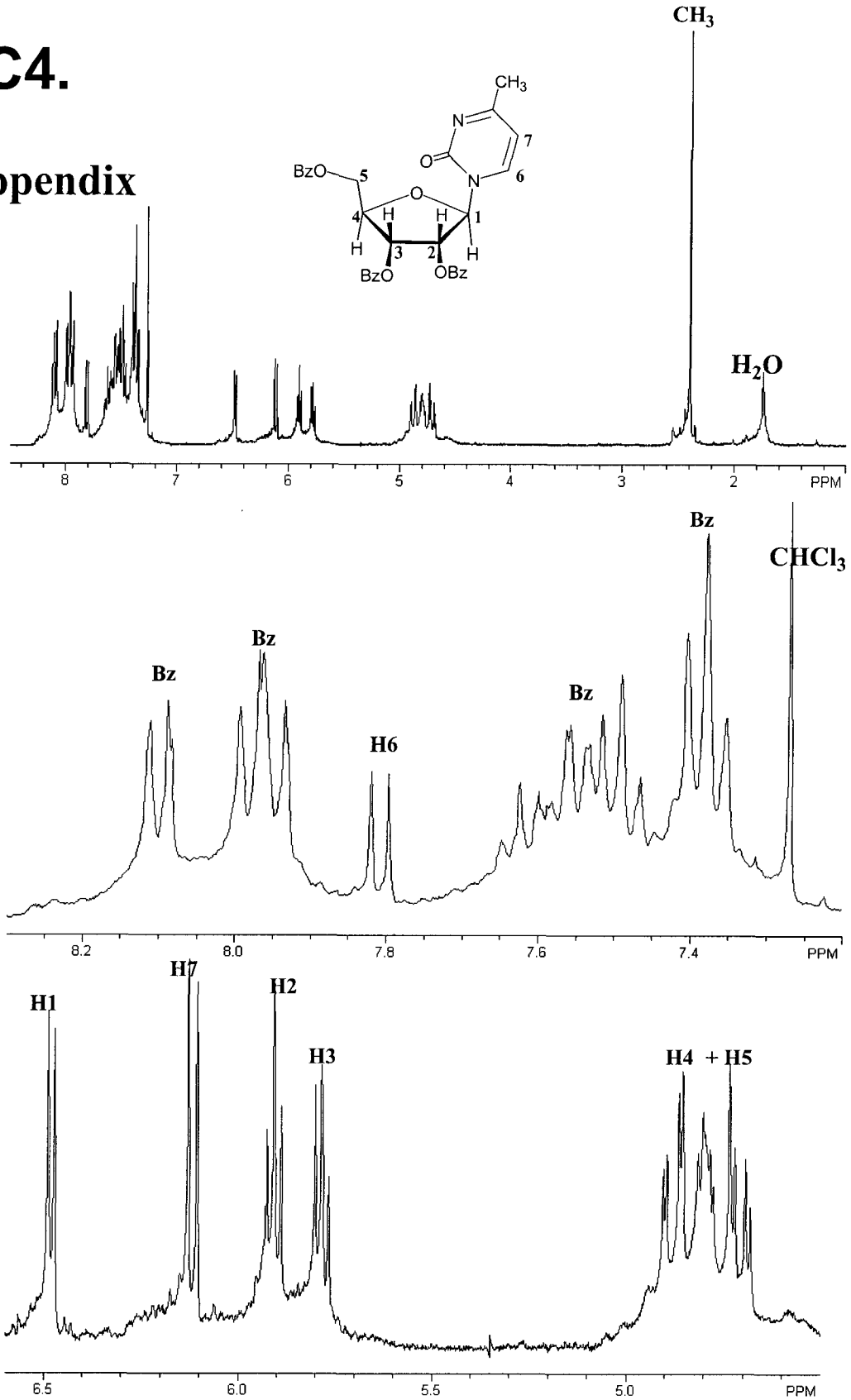

Figure C1. ^{1}H NMR (300 MHz, $CDCl_3$) of 1-(2,3,5-tri-O-benzoyl-β-D-ribofuranosyl)-4-methyl-2-pyrimidinone **(3)**.

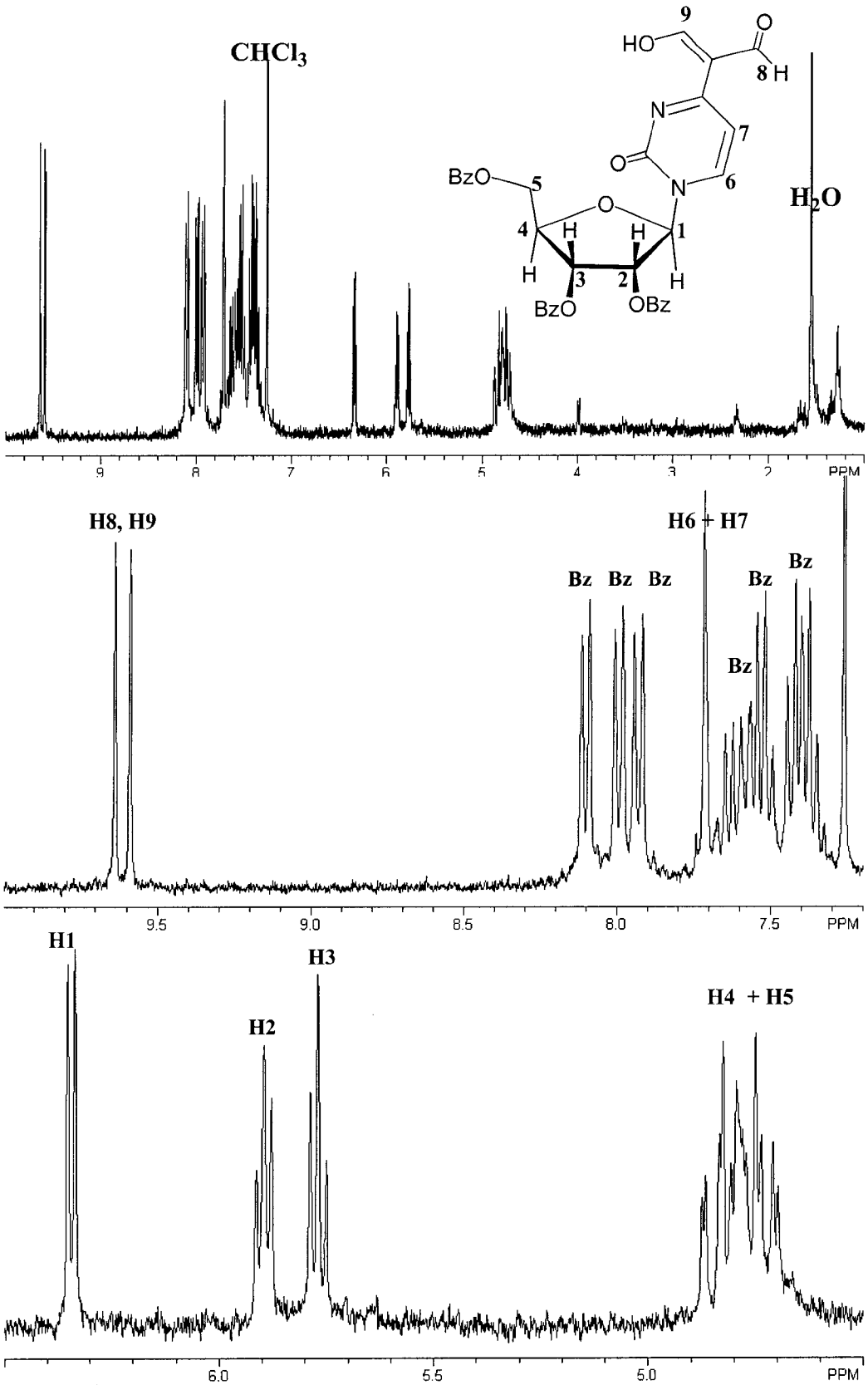

Figure C2. ^{1}H NMR (300 MHz, $CDCl_3$) of 4-(α-Diformyl-methyl)-1-(2,3,5-tri-O-benzoyl-β-D-ribofuranosyl)-2-pyrimidinone **(4)**

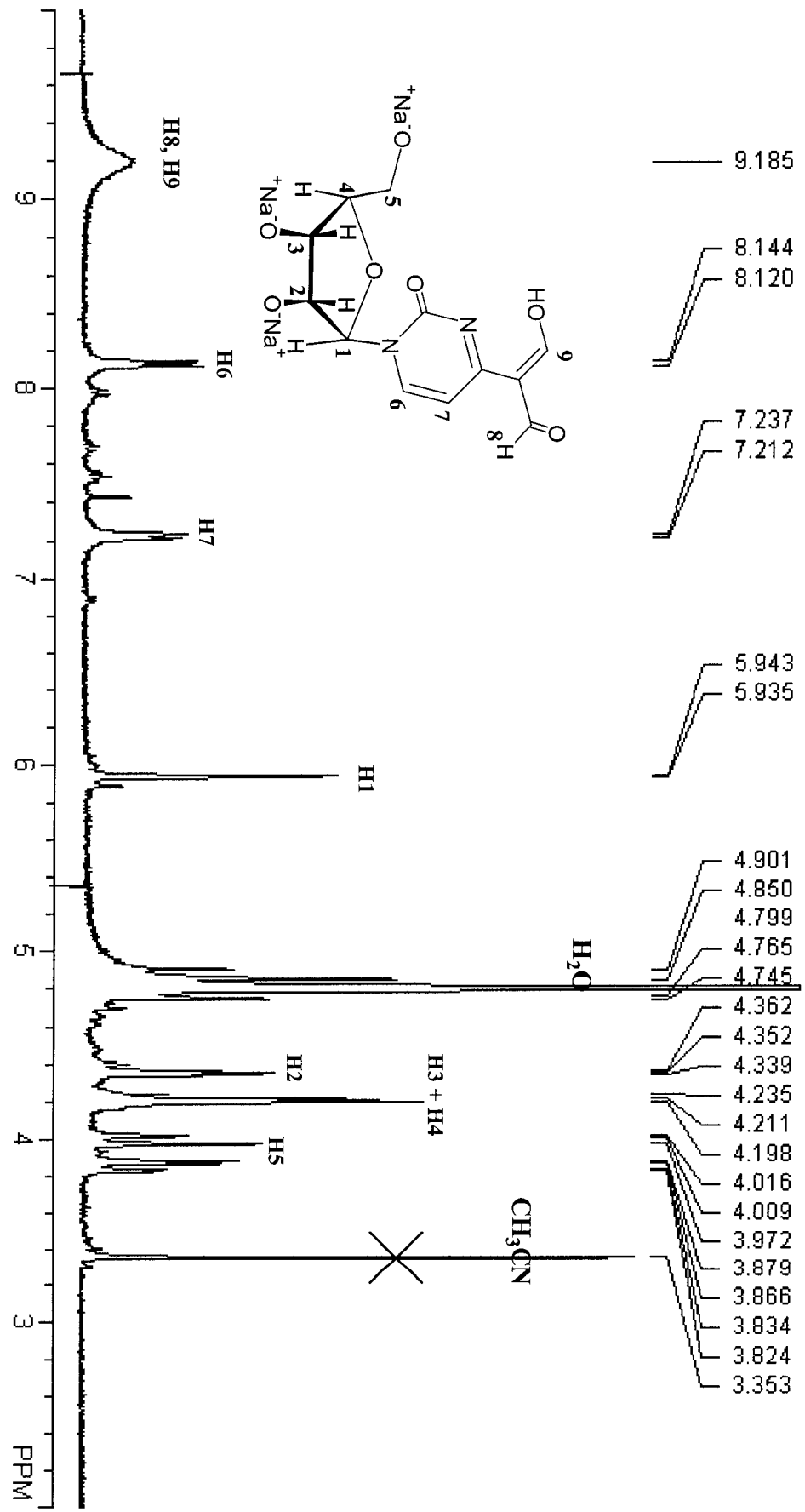

Figure C3. ^{1}H NMR (300 MHz, D_2O) of the sodium salt of 4-(α-Diformyl-methyl)-1-(β-D-ribofuranosyl)-2-pyrimidinone.

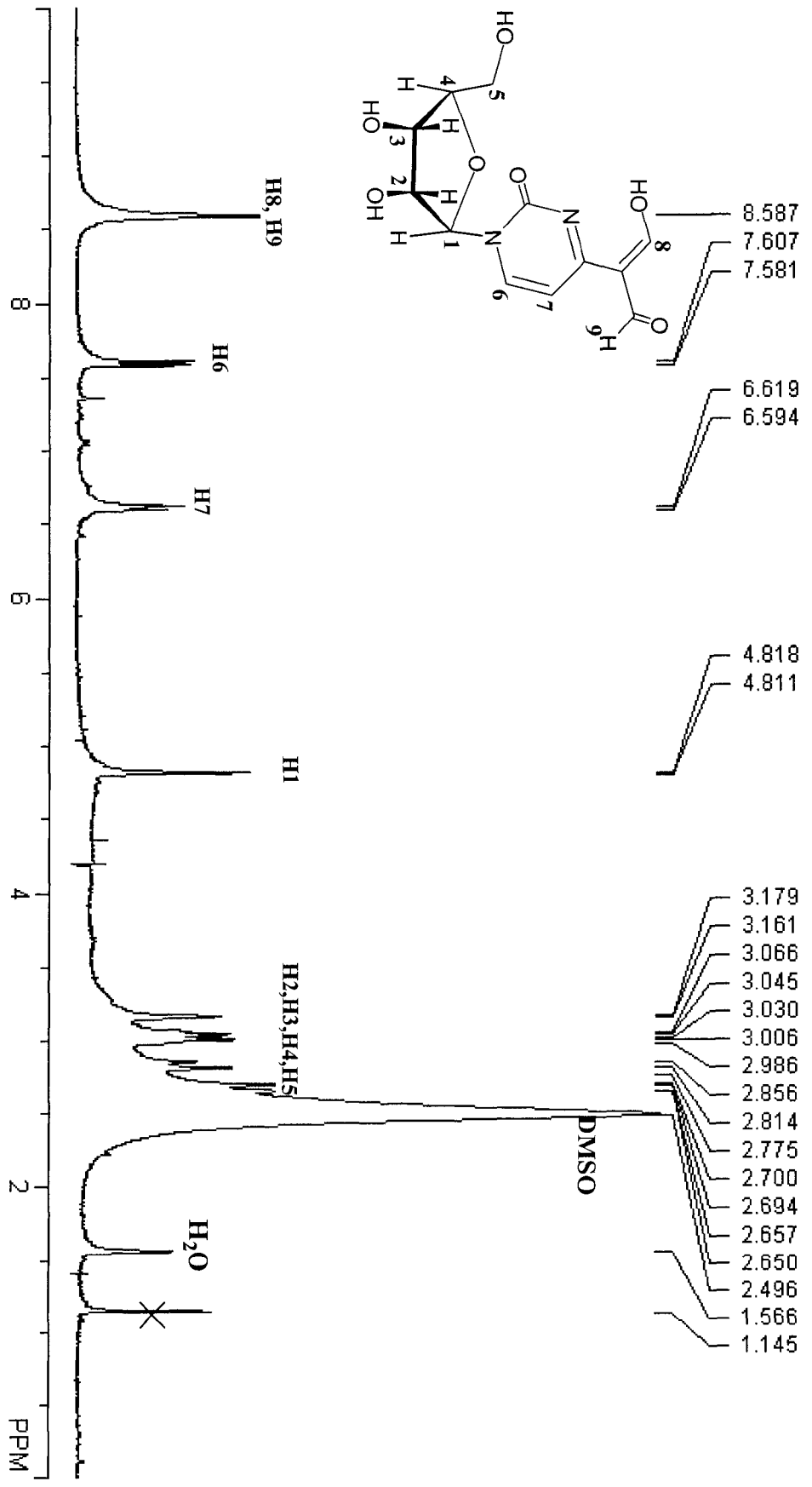

Figure C4. ^{1}H NMR (300 MHz, DMSO-d_6) of 4-(α-Diformyl-methyl)-1-(β-D-ribofuranosyl)-2-pyrimidinone.

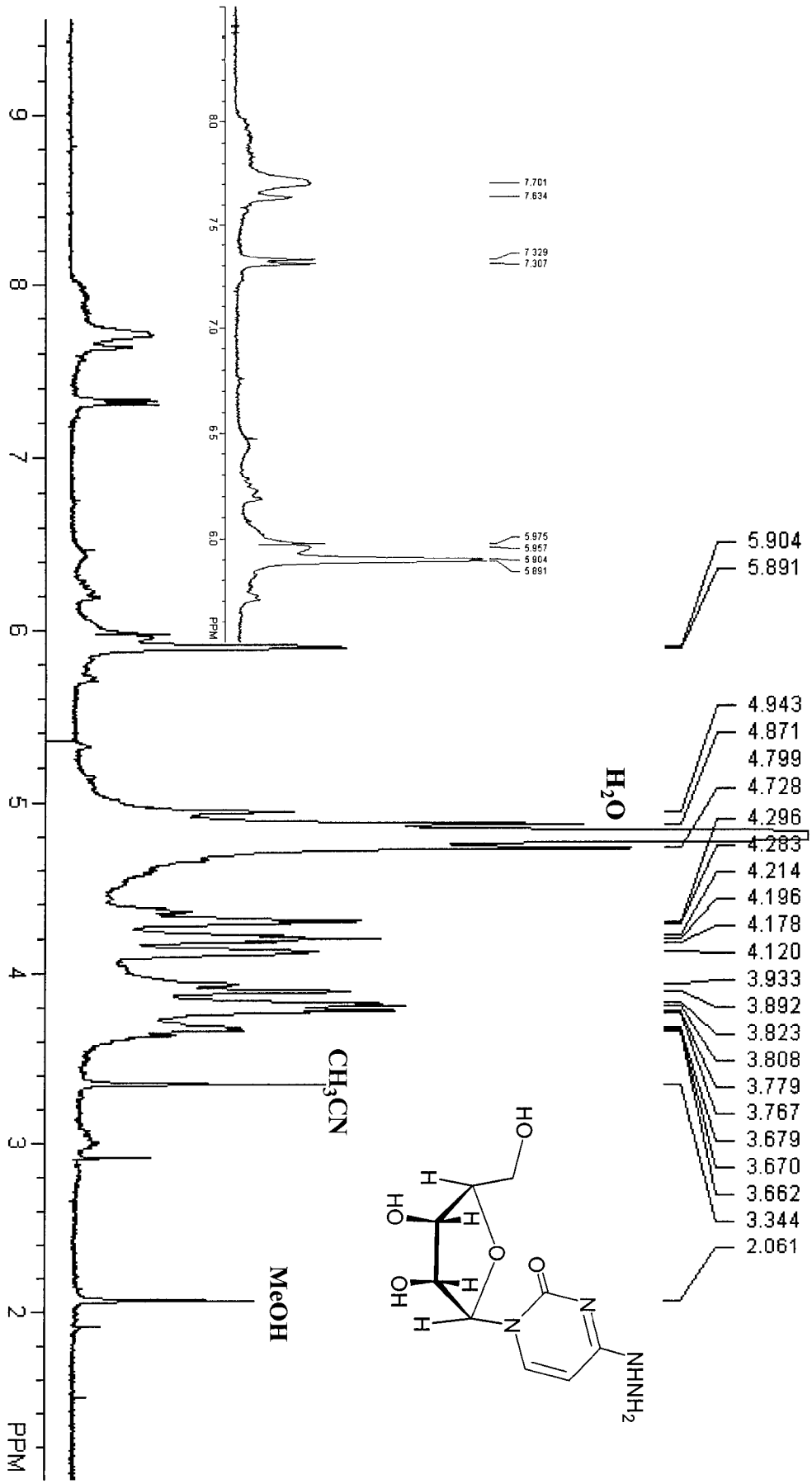

Figure C5. ^{1}H NMR (300 MHz, D_2O) of N^4-aminocytidine.

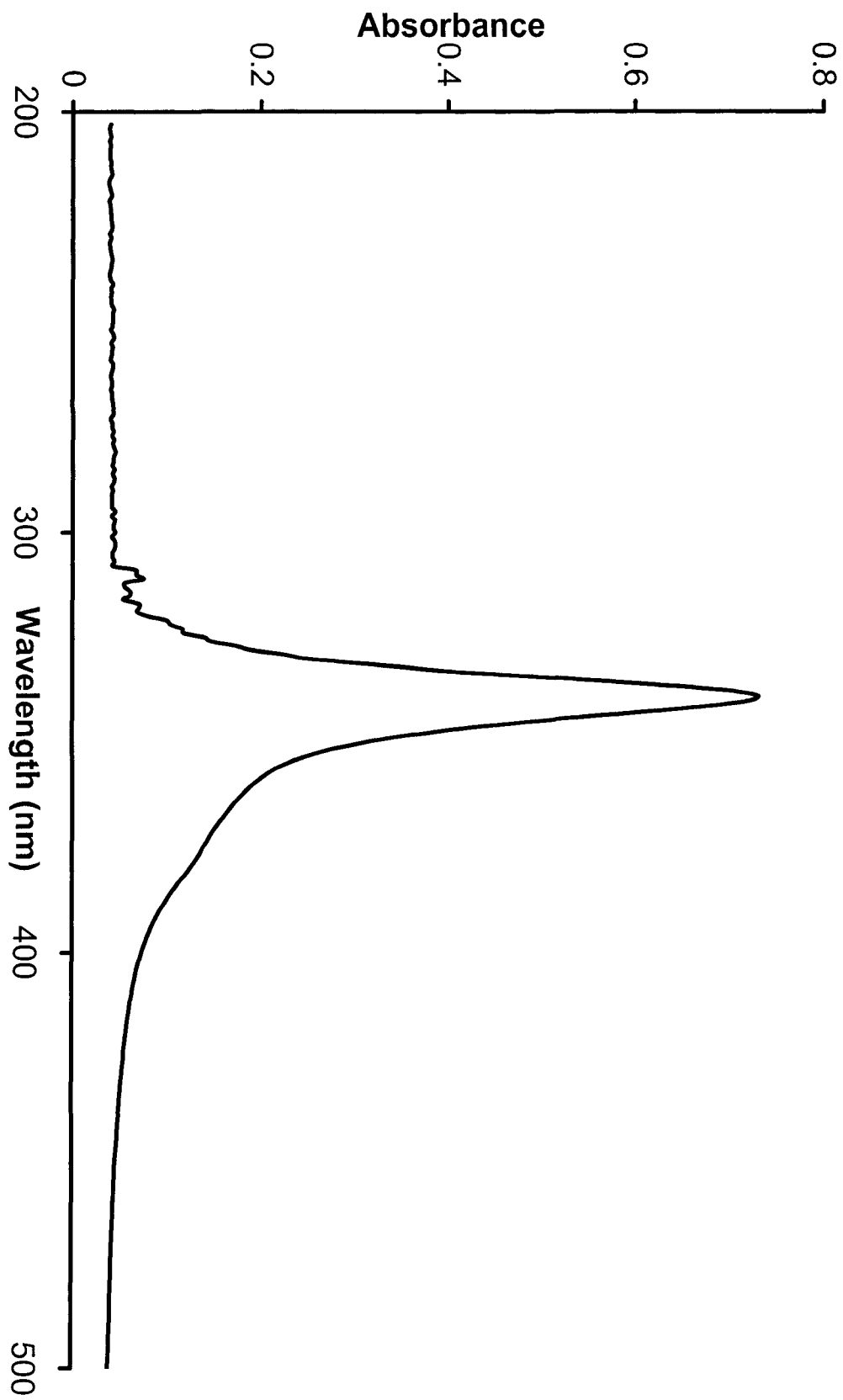

Figure C6. UV-visible spectrum of target molecule (7) in water with phosphate buffer pH=5.5.

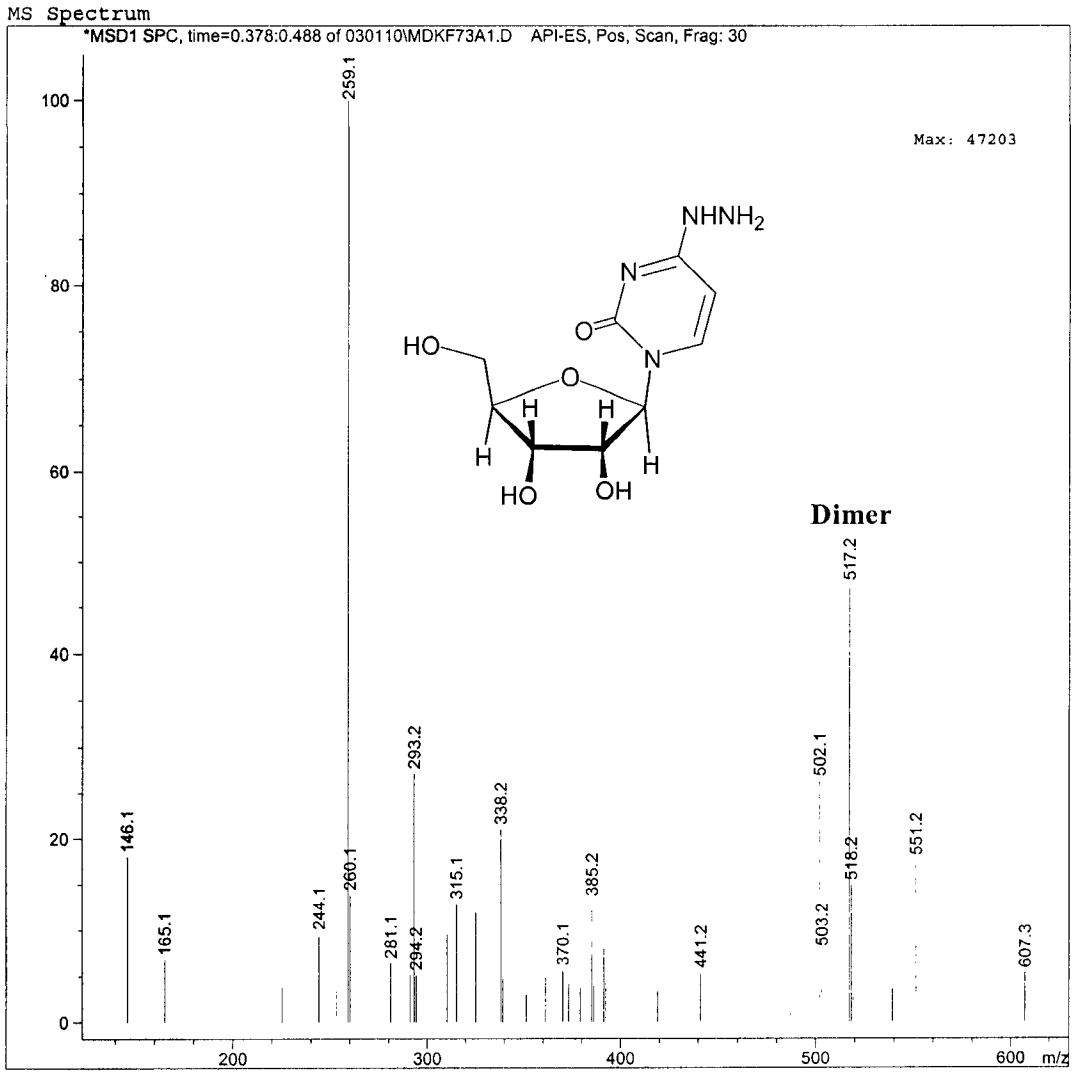

Figure C7. ESI-MS of N^4-aminocytidine [*m/z* =259 ($M + H^+$)].

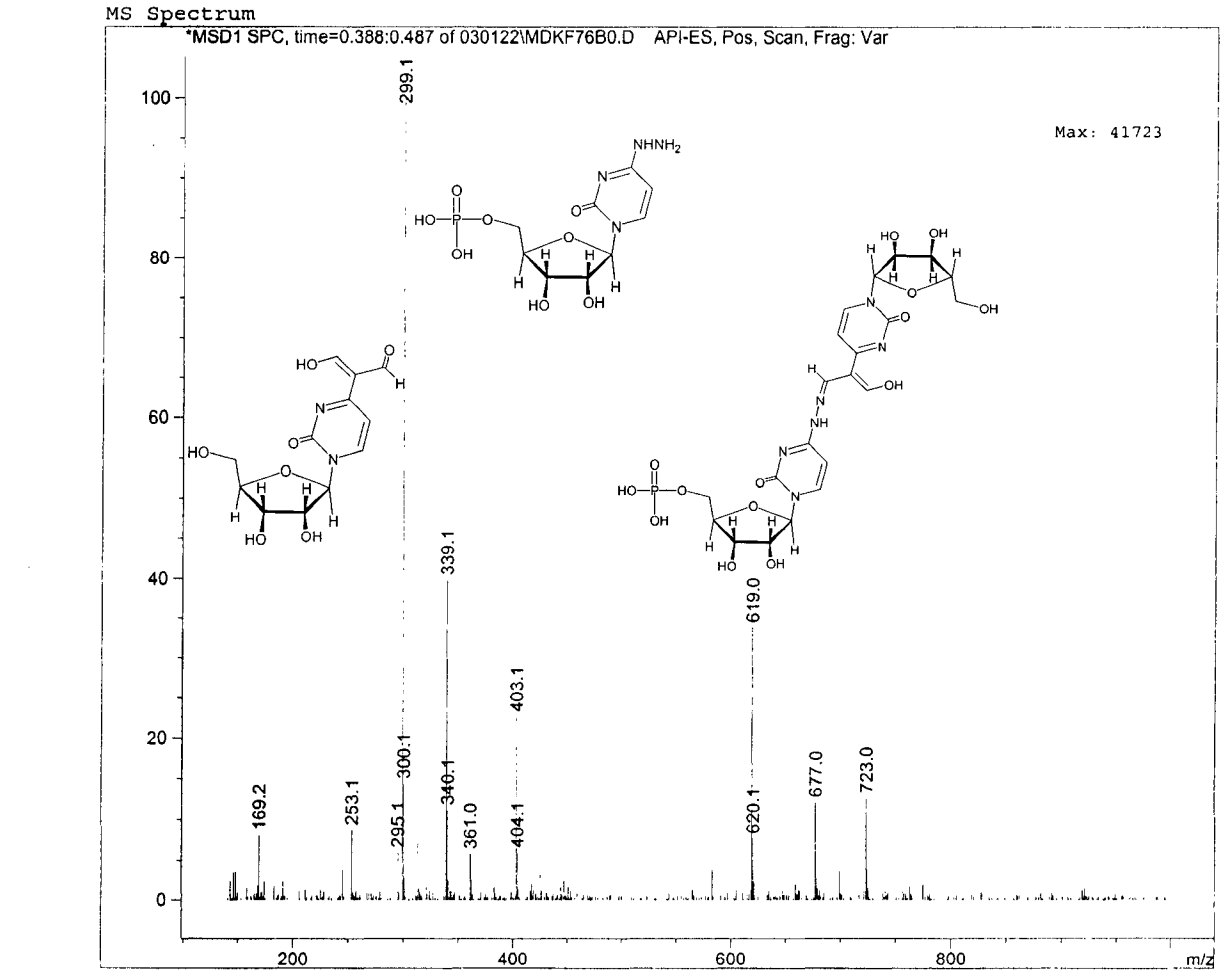

Figure C8. ESI-MS of target molecule **(7)** [*m/z* =619 ($M + H^+$)] together with the starting materials 4-(α-diformyl-methyl)-1-(β-D-ribofuranosyl)-2-pyrimidinone **(5)** [*m/z* =299 ($M + H^+$)] and N^4-aminocytidine-5'-monophosphate **(6)** [*m/z* =339 ($M + H^+$)].

C5.

Bibliography

(1) Watson, J. D. *The Double Helix*; 1st ed.; New York, Atheneum, 1968.

(2) Eschenmoser, A.; Leowenthal, E. *Chem. Soc. Rev.* **1992**, *21*, 1-16.

(3) Bolli, M.; Litten, J. C.; Schutz, R.; Leumann, C. *J. Chem. Biol.* **1996**, *3*, 197-206.

(4) Koshkin, A. A.; Nielsen, P.; Meldgaad, M.; Rajwanshi, V. K.; Wengel, J. *J. Am. Chem. Soc.* **1998**, *120*, 13252-13253.

(5) Lutz, M. J.; Held, H. A.; Hottiger, M.; Hubscher, U.; Benner, S. A. *Nucleic Acids Res.* **1996**, *21*, 1308-1313.

(6) Strobel, S. A.; Cech, T. R.; Usman, N.; Beigelman, L. *Biochemistry* **1994**, *33*, 13824-13835.

(7) Morales, J. C.; Kool, E. T. *Nat. Struct. Biol.* **1998**, *5*, 950-954.

(8) Guckian, K. M.; Krugh, T. T.; Kool, E. T. *Nat. Struct. Biol.* **1998**, *5*, 954-959.

(9) Knorre, D. G.; Vlassov, V. V. *Prog. Nucleic Acid Res. Mol. Biol.* **1985**, *32*, 291-320.

(10) Webb, T. R.; Matteucci, M. D. *Nucleic Acid Res.* **1986**, *14*, 7661-7664.

(11) Dong, Q.; Barsky, D.; Colvin, M. E.; Melius, C. F.; Ludeman, S. M.; Moravek, J. F.; Colvin, O. M.; Bigner, D. D.; Modrich, P.; Friedman, H. S. *Proc. Natl. Acad. Sci. USA* **1995**, *92*, 12170-12174.

(12) Huang, H.; Zhu, l.; Reid, B. R.; Drobny, G. P.; Hopkins, P. B. *Science* **1995**, *270*, 1842-1845.

(13) Coleman, R. S.; Pires, R. M. *Nucleic Acids Res.* **1997**, *25*, 4771-4777.

(14) Fagan, P. A.; Spielmann, P.; Sigurdsson, S. T.; Rink, S. M.; Hopkins, P. B.; Wemmer, D. E. *Nucleic Acids Res.* **1996**, *24*, 1566-1573.

(15) Gao, K.; Orgel, L. E. *Proc. Natl. Acad. Sci. USA* **1999**, *96*, 14837-14842.

(16) Gao, K.; Orgel, L. E. *Nucleotides & Nucleic Acids* **2000**, *19(5&6)*, 935-940.

(17) Shapiro, R.; Weisgras, J. M. *Biochem. Biophy. Res. Commun.* **1970**, *40*, 839-843.

(18) Negishi, K.; Kawakami, M.; Kayasuga, K.; Odo, J.; Hayatsu, H. *Chem. Pharm. Bull.* **1987**, *35*, 3884-3887.

(19) Bredereck, H.; Simchen, G. *Angew. Chem.* **1963**, *75*, 1102.

(20) Bergstrom, D. E.; Inoue, I.; Leonard, N. J. *J. Org. Chem.* **1972**, *37*, 3902.

(21) Perrin, D. D.; Armarego, W. L. F.; Perrin, D. R. *Purification of Laboratory Chemicals*; 2nd ed.; Pergamon Press, New York, 1980.